The electrophysiological and morphological characterisation of aminergic responsive neurones within the rat hypothalamic arcuate nucleus *in vitro*

Jasmeet K Virdee BSc Hons

A thesis written in partial fulfilment of the criteria set for the degree of Doctor of Philosophy

Clinical Sciences Research Institute
Warwick Medical School, November 2008

Table of Contents

Figures

Tables

Publications

Abstract:

J.K. Virdee, M. van den Top & D. Spanswick. (2008). Differential effects of noradrenaline on hypothalamic arcuate nucleus neurons *in vitro*. *Keystone Symposia: Neuronal mechanisms controlling food intake, glucose metabolism and body-weight: P329*

J.K. Virdee, M. van den Top & D. Spanswick. (2008). Noradrenaline differentially regulates neuronal excitability in hypothalamic arcuate nucleus neurones *in vitro. Themed meeting of The physiological society; Metabolism and Endocrinology; C3:PC13*

Acknowledgements

I would like to take this opportunity to thank everyone that has given me support and encouragement over the past four years to make this thesis possible. Firstly and most importantly I would like to thank my supervisor, Professor David Spanswick who gave me the opportunity to carry out this project, and for all his encouragement and advice throughout. Secondly, I would like to sincerely thank Dr Marco van den Top who has given me selfless advice, assistance and invaluable scientific training to carry out this project.

I would also like to thank all the people with whom I have had the pleasure of working with over the course of my PhD, in particular, Dawn Collins, Ross Jeggo, Andrew Whyment, Paul Giles, Ratchada Pattaranit, Tony Rush and David Lyons for their support, friendship and many a coffee mornings we have shared.
A special thank you to Louise Saker who has made the course of my PhD a lot of fun and for her continued friendship.

A final mention must go to all my friends and family, especially my parents for their continuous selfless support and love.

Declaration

I hereby declare that this thesis has been composed solely by myself and that it has not been accepted in any previous application for a degree. All work has been done by myself, with the exception of the electrophysiology in chapter 3 and the immunohistochemistry which was carried out in collaboration with Dr. Marco van den Top. All the sources used have been specifically acknowledged by means of a reference.

_____

Jasmeet K Virdee

Summary

1. The hypothalamic arcuate nucleus (Arc) is a key integrative centre of the central nervous system (CNS) involved in the control and maintenance of energy balance. Whole-cell patch clamp recording techniques were utilised, in isolated hypothalamic brain slice preparations, to investigate the electrophysiological and morphological properties of Arc neurones. Differential expression of subthreshold active conductances were identified and used to functionally classify Arc neurones into 8 electrophysiological clusters. This classification was based based upon differential expression of the following conductances: anomalous inward rectification (I_{an}); hyperpolarisation-activated non-selective cation conductance (I_h); transient outward rectification (I_a); T-type-like calcium conductance. Morphological analysis of recorded neurones, revealed retrospectively with biocytin staining, showed four populations based upon the orientation and number of primary dendrites. There were no obvious direct correlations between morphology and electrophysiological properties, suggesting considerable functional diversity of neurones and their associated circuits at the level of the Arc.

2. The physiological levels of glucose to which the brain is exposed are believed to be around 1-2.5 mM, and glucose-sensing neurones have been identified in the Arc. However, *in vitro* slice studies routinely use glucose around 10 mM in aCSF. The impact of this high level of glucose on fundamental properties and operation of hypothalamic circuits remains unclear. Here the effect of different ambient glucose levels (10 mM, hyperglycaemic and 2 mM, euglycaemic) on electrophysiological properties of Arc neurones was compared. Significant differences in passive and active subthreshold membrane properties of Arc neurones were observed, including: changes in neuronal input resistance, spontaneous activity and magnitude of I_h and I_a. Data from this study suggests a need to re-evaluate studies previously conducted in non-physiological levels of glucose.

3. The effects of noradrenaline (NA) on the neuronal excitability of hypothalamic Arc neurones were studied. Application of NA induced a membrane depolarisation and increase in electrical excitability in 51% of Arc neurones, including orexigenic NPY/AgRP neurones, a response that persisted in the presence of TTX indicating a direct effect. NA-induced depolarisation was mediated through α_1-ARs, in particular through α_{1A}-ARs, and associated with multiple ionic mechanisms including: closure of a potassium conductance, activation of a non-selective cation conductance, or a combination of the two.

4. NA also induced a membrane hyperpolarisation in a sub-population of Arc neurones (15%) including 4/9 putative anorexigenic CART-expressing neurones, the remaining CART neurones responded with a NA-induced excitation. NA-induced hyperpolarisation, mediated via α_2-ARs and activation of one or more potassium conductances, persisted in the presence of TTX indicating a direct effect on Arc neurones. 7.5% of neurones responded to NA with biphasic inhibitory/excitatory responses. Taken together, these data suggest that NA, at least in part, excites a subpopulation of NPY/AgRP neurones and inhibits a population of CART expressing neurones which may serve an orexigenic role at the level of the Arc.

5. Histamine induced membrane depolarisation in a population of Arc neurones (65%), most likely through H_1 receptors, via a direct effect on the postsysnaptic membrane. Histamine induced depolarisation through multiple ionic mechanisms, including closure of a potassium conductance or activation of an electrogenic pump.

Abbreviations

ABC	Avidin-Biotin-Peroxidase-Complex
aCSF	Artificial cerebrospinal fluid
ACTH	Adrenocorticotropin hormone
AgRP	Agouti-related peptide
AHP	after-hyperpolarisation potential
α-MSH	α-melanocyte stimulating hormone
ANS	Autonomic nervous system
AR	Adrenoceptor
Arc	Arcuate nucleus
ATP	Adenosine triphosphate
Ba^{2+}	Barium
$BaCl_2$	Barium chloride
BBB	Blood brain barrier
BMI	Body mass index
cAMP	Cyclic adenosine-mono-phosphate
CART	Cocaine and amphetamine regulated transcript
CCK	Cholecystokinin
CNS	Central nervous system
CORT	Corticosterone
CRF	Corticotrophin releasing factor
DAB	3,3-diaminobenzidine
DAG	Diacylglycerol
DAT	Digital audio tape
DMH	Dorsal medial hypothalamus
DMSO	Dimethylsulphoxide
EGTA	Ethylene glycol-bis(2-aminoethylether)-N,N,N',N'-tetraacetic acid
EPSC	Excitatory post-synaptic current
EPSP	Excitatory post-synaptic potential
GABA	γ-aminobutyric acid
GAD	Glutamic acid decarboxylase
GALP	Galanin-like peptide
GE	Glucose-excited

GH	Growth hormone
GHSR	GH secretagogue receptor
GI	Glucose-inhibited
GIRK	G-protein inwardly rectifying potassium
GK	Glucokinase
GPCRs	G-protein-coupled receptors
GR	Glucose responsive
GS	Glucose sensitive
GT	Gastrointestinal tract
GLUT	Glucose Transporter
HDC	L-histidine decarboxylase
HEPES	4-(2-hydroxyethyl)piperazine-1-ethanesulfonicacid
HVACC	High-voltage activated calcium channel
I_a	A-like outward rectifier
I_{an}	Anomalous inward rectifier
I_h	Hyperpolarisation-activated non-selective cation channel
IP3	Inositol triphosphate
IPSC	Inhibitory post-synaptic current
IPSP	Inhibitory post-synaptic potential
IRS	Insulin receptors substrate
I/V	Current-voltage relationship
JAK-STAT	Janus-Kinase-Signal transducer and activator of transcription
K_{ATP}	ATP-sensitive potassium channel
LC	Locus coerulus
LH	Lateral hypothalamus
LHA	Lateral hypothalamic area
MCH	Melanin concentrating hormone
MCR	Melanocortin receptor
ME	Median eminence
mRNA	Messenger ribonucleic acid
γ-MSH	γ-melanocyte stimulating hormone
NA	Noradrenaline
NBQX	6-nitro-7-sulphamoylbenzo(*f*)-quinoxaline-2,3-dione
NDS	Normal donkey serum

NGF	Nerve growth factor
NGS	Normal goat serum
NMDA	N-methyl-D-aspartate
NPY	Neuropeptide Y
NSCC	Non-selective cation channel
NTS	Nucleus of the tractus solitarius
PCR	Polymerase chain reaction
PFA	Perifornical hypothalamus
PNS	Parasympathetic nervous system
PI3K	Phosphatidylinositol 3-kinase
PLC	Phospholipase C
POA	Preoptic area
POMC	Pre-pro-opiomelanocortin
PVN	Paraventricular nucleus
PYY	Peptide tyrosine tyrosine
RT-PCR	Reverse transcription polymerase chain reaction
SEM	Standard error of the mean
SCN	Suprachiasmatic nucleus
SNS	Sympathetic nervous system
SPN	Sympathetic preganglionic neurones
SUR	Sulphonylurea
Tau	Membrane time constant
TASK	Tandem-pore acid sensitive potassium channel
TBS-T	Tris-buffered saline containing 1% Triton X-100
TM	Tubermammillary
TTX	Tetrodotoxin
VMN	Ventromedial nucleus
VMH	Ventromedial hypothalamus
Vp	Vasopressin
WHO	World Health Organisation

Chapter 1

General Introduction

1.1 The autonomic nervous system

The autonomic nervous system (ANS) acts as a control system that provides a steady homeostatic state for the internal environment of the individual. Often termed the visceral nervous system, it is this part of the central nervous system (CNS) that innervates virtually all internal organs with the exception of skeletal muscle to provide a constant environment. The ANS can be divided into three principal divisions; the enteric nervous system, the parasympathetic nervous system (PNS) and the sympathetic nervous system (SNS). The SNS and the PNS function in a complementary manner controlling most internal organs. The enteric nervous system however independently regulates gastrointestinal motility secretions by innervating the gastrointestinal tract (GT), the pancreas and gall bladder. The SNS and PNS exert control through two sets of neurones; preganglionic neurones originating in the CNS that synapse with postganglionic neurones situated within the periphery. Both branches of the ANS use acetylcholine as a neurotransmitter at the pre-post ganglionic synapse. There are however anatomical differences between the PNS and the SNS in terms of the location of the preganglionic neurones in the CNS and the neurotransmitters released from postganglionic neurones. Parasympathetic preganglionic neurones originate in brainstem nuclei or in the sacral spinal cord whereas the somata of sympathetic preganglionic neurones (SPNs) are located in the thoracic and lumbar regions of the spinal cord (Loewy, 1991). The parasympathetic postganglionic neurones release acetylcholine in contrast to the sympathetic postganglionic neurones which release noradrenaline (NA) from their terminals. The ANS is a complex system that maintains and establishes homeostasis with a number of feedback loops i.e. sensory feedback neurones signal information back to the CNS regarding the state of the target tissue. A major component of this feedback loop is the hypothalamus which is heavily

involved in the central control of a large number of autonomic processes, including energy homeostasis.

1.2 Energy homeostasis

Energy homeostasis is defined as the balance and the precise regulation of food intake in order to sustain a stable and constant internal environment, thus maintaining suitable energy stores as a safeguard against food deficit or a change in metabolic demand. In reality, caloric intake and energy expenditure are meticulously controlled parameters in that net energy balances are maintained within 1% per day (Rink, 1994). From an evolutionary perspective there is however an intrinsic bias towards positive energy balance as energy deficit is most likely to compromise survival (Beales & Kopelman, 1996).

The hypothalamus and brainstem are reciprocally connected and play an important role in the central control of energy homeostasis by assessing the metabolic status of the body and engaging the ANS to produce an appropriate output. Peripheral signals regarding the energy status of the body relay information directly via the vagal afferent pathway to the brainstem or act directly on the hypothalamus. The involvement of the CNS and in particular the involvement of the hypothalamus in integrating and processing information regarding the energy status of the body has been known for decades. Previously, it was thought that feeding was regulated by two core hypothalamic areas: the lateral hypothalamus (LH) and the ventromedial hypothalamus (VMH; Hetherington & Ranson, 1940; Anand & Brobeck, 1951). This was described as the 'dual feeding centre' hypothesis. A combination of electrolytic lesion and electrical stimulation studies within the LH resulted in fatal anorexia and increased food intake, respectively, thus it was considered the 'feeding' centre. The VMH was termed the 'satiety' centre as lesions in this area resulted in obesity associated with hyperphagia

(Hetherington & Ranson, 1940; Anand & Brobeck, 1951). Although it is now apparent that other hypothalamic nuclei are involved in the regulation of energy homeostasis, these initial rather rudimentary lesion experiments provided the foundations for the 'lipostatic hypothesis' and the 'glucostatic hypothesis' proposed in the 1950s, and for our knowledge and work today.

The 'glucostatic hypothesis' proposed by Mayer in 1955 suggested that glucose serves as a physiological satiety factor, in that post-prandial increases in plasma glucose cause meal termination and that eating is initiated when blood glucose of the brain is reduced (Mayer, 1953, 1955). This theory however did not deal with the long-term regulation and precision of body-weight control. The 'lipostatic theory' was proposed by Kennedy in 1953 and it provided a better understanding of the long-term control of energy balance (Kennedy, 1953; Schwartz *et al.*, 2000). He proposed that (a) circulating signals generated in proportion to body fat stores interacted with the hypothalamus to influence food intake and energy expenditure in a coordinated manner to regulate body weight. Parabiosis experiments further substantiated the idea that circulating factors could regulate food intake (Hervey, 1959). For general reviews on the central control of energy homeostasis see Schwartz *et al.*, 1999; Schwartz *et al.*, 2000; Gao & Horvath, 2007.

1.3 The hypothalamus

The hypothalamus, a small cone shaped structure, is situated in the middle of the base of the brain and surrounds the third ventricle. It plays an essential role in coordinating vital autonomic processes such as body temperature, blood pressure, fluid balance and reproduction, amongst many others. It achieves homeostasis by core circuitry within the hypothalamus interacting with key regions within the brainstem and spinal cord, as well as integrating signals from the periphery and the external environment. Directly underneath the

hypothalamus is the (anterior and posterior) pituitary gland that secretes protein hormones into the circulation under the direct control of the hypothalamus.

The present study focuses on the central control of energy homeostasis and in this case circulating leptin and insulin amongst others which provide peripheral signals, whilst external signals include food availability and /or social cues to the hypothalamus.

Previous research has identified that nuclei within the hypothalamus have clusters of neurones with specific functional roles within feeding. These discrete nuclei integrate a number of chemical and electrical signals whilst interacting with each other. Key nuclei implicated in the maintenance of energy homeostasis include the arcuate nucleus (Arc), LH, paraventricular nucleus (PVN), ventral medial nucleus (VMN) and the dorsal medial hypothalamus (DMH). These nuclei are under the control and influence of higher structures such as the amygdala and orbitofrontal cortex as well as circulating factors (Rolls, 1984; LeDoux *et al.*, 1988). These higher centres bring in cognitive, motivational and emotional cues, such as the desire for palatable food.

1.4 The arcuate nucleus

The Arc is considered to be the key integrative centre in regulating energy homeostasis. This nucleus is an aggregation of densely packed cell bodies located at the base of the hypothalamus surrounding the third ventricle (Chronwall, 1985; Schwartz *et al.*, 2000). It lies directly above the median eminence (ME) which is a neurohemal region (Knowles & Bern, 1966) characterised by having a compromised blood brain barrier (BBB). The ME is termed a circumventricular organ; therefore it has a higher rate of endocytosis, pinocytosis and transcytosis due to a lack of tight junctions (Davson & Segal, 1996). The close proximity of the Arc to the ME is thought to allow the Arc to sense and process

peripheral factors concerning the body's energy state. These peripheral factors include insulin, leptin, ghrelin and glucose among others. It has been shown that both insulin and leptin receptors are found abundantly within the Arc (van Houten *et al.*, 1980; Baskin *et al.*, 1988; Mercer *et al.*, 1996a; Cheung *et al.*, 1997). Leptin appears to be transported into the CNS by a saturable receptor mediated process (Banks *et al.*, 1996). Leptin and insulin activate the long form of the leptin receptor (Ob-Rb) and the insulin receptor, respectively, both of which are expressed on the cellular membrane of Arc neurones and act to modulate electrical activity (Mercer *et al.*, 1996b; Spanswick *et al.*, 1997; Elmquist *et al.*, 1998; Spanswick *et al.*, 2000; Cowley *et al.*, 2001; see section 1.9). Ghrelin released from the stomach increases appetite and leads to hyperphagia. Its receptor, the growth hormone secretogue receptor (GHS-R) is found in high levels within the Arc (Guan *et al.*, 1997b). The apparatus for glucose sensing is also found within the Arc (Ashford *et al.*, 1990; Spanswick *et al.*, 1997; Ibrahim *et al.*, 2003; van den Top *et al.*, 2007), which further substantiates the importance of the Arc in the control of energy homeostasis. See Figure 1.1 for an overview of the central control of energy homeostasis.

The Arc is an extremely complex nucleus with heterogeneity of neuronal inputs, targets and chemical phenotypes. It is innervated by other hypothalamic nuclei involved in energy homeostasis, including the lateral hypothalamic area (LHA), suprachiasmatic nucleus (SCN), and PVN (see Figure 1.2; Chronwall, 1985; Cone *et al.*, 2001; Williams *et al.*, 2001). Neuropeptides and neurotransmitters contained in nerve terminals innervating the Arc include orexin from the LH, serotonin and noradrenaline (NA) from the brainstem (Swanson & Sawchenko, 1983; Sawchenko, 1998) and the fast neurotransmitters γ-aminobutyric acid (GABA) and glutamate (Chronwall, 1985; Horvath *et al.*, 1997). The efferent targets are just as diverse and include outputs to the ME, PVN, nucleus tractus solitarius (NTS), and the LHA (see Figure 1.2; Chronwall, 1985; Baker & Herkenham, 1995) which provide behavioural,

neuroendocrine and autonomic outputs to ensure a homeostatic balance for ingestion, energy expenditure and storage. Neuropeptidergic expression reveals that within the Arc there is an extremely diverse chemical phenotype. Neuropeptide expression includes neuropeptide Y (NPY), pro-opiomelanocortin (POMC), agouti-related peptide (AgRP), neuromedin U, urocortin II, galanin, dopamine, prolactin and cocaine and amphetamine- related transcript (CART; Chronwall, 1985; Howard *et al.*, 2000; Reyes *et al.*, 2001).

1.5 Leptin & insulin; long term signals relating to energy stores

Energy homeostasis is accomplished through a highly integrated neurohumoral system that minimises the impact of short term fluctuations in energy balance on fat mass. Critical elements of this meticulously controlled system are hormones secreted in proportion to body adiposity, including leptin and insulin.

The lipostatic hypothesis gave rise to the idea of a circulating factor involved in integrating peripheral signals indicating energy status, with integration of these signals at the level of the hypothalamus in relation to satiation. Experiments, inspired by Hervey, undertaken by Douglous Coleman included parabiosis experiments on naturally occurring obese mouse models, obese (ob/ob) and diabetic (db/db), which subsequently identified the existence of a satiety signal. These parabiotic experiments revealed that ob/ob mice were deficient in a circulating factor and the resulting hyperphagia could be restored via blood circulation originating from the normal mouse (Hausberger, 1959). In contrast parabiosis experiments carried out between a db/db mouse and a lean control mouse resulted in feeding inhibition in the normal mouse, but did not result in normalisation of body weight in the db/db mouse. Thus, this suggested that the db/db mouse had high levels of Hervey's 'circulating satiety factor' but was defective in its ability to respond to it through a mutation preventing its correct transduction (Coleman, 1973). However, despite these early studies supporting the idea of a

satiation signal it was not until 1994 that the protein product of the Ob gene, leptin, was discovered by the Friedman laboratory (Zhang *et al.*, 1994). It was found that leptin deficient animals were obese, and subsequently the administration of leptin both centrally and periphery to these animals reversed their hyperphagia and their neuroendocrine abnormalities (Friedman & Halaas, 1998). Leptin is predominately secreted from white adipose tissue in proportion to the amount of body fat mass, thus as adipocytes increase in size due to a build up of triglycerides they produce larger quantities of leptin, which gives an indication of the body's nutritional status (Bagdade *et al.*, 1967). Leptin has been shown to signal via a single-transmembrane domain receptor of the cytokine receptor family. Alternative mRNA splicing and post-translational processing results in multiple isoforms of the receptor (Ob-R). It is the long form Ob-Rb that is expressed widely within the hypothalamus and in particular the Arc, PVN, DMH and the LHA (Tartaglia *et al.*, 1995; Lee *et al.*, 1996; Mercer *et al.*, 1996b; Guan *et al.*, 1997a). This receptor possesses a long intracellular domain that binds to Janus- kinases (JAK) and STAT 3 transcription factors resulting in signal transduction and leptin's effects on food intake (Tartaglia *et al.*, 1995; Fruhbeck, 2006). Circulating leptin's abiltity to cross the BBB via a saturable process (Banks *et al.*, 1996) means that it is able to provide the brain with an indication of energy storage for the purpose of regulating appetite and metabolism. The binding of leptin to its receptor within the hypothalamus initiates a signalling cascade that results in the inhibition of several orexigenic peptides whilst stimulating several anorexigenic peptides.

Since leptin's discovery, it is now well known as a long-term adiposity signal that regulates the activity of central neural elements and pathways which form the circuits maintaining energy homeostasis (Schwartz *et al.*, 1999). In addition to insulin's classical role in the peripheral maintenance of glucose homeostasis, it is also a well known long-term adiposity signal that works in tandem with leptin. Insulin is secreted from pancreatic β-cells in

basal proportions that correlate with body adiposity, thus plasma insulin levels increase at times of positive energy balance and decrease at times of negative energy balance (Woods *et al.*, 1974). The insulin receptor is composed of a disulphide-bonded dimer of an α subunit and β subunit. Upon insulin binding to its receptor, it induces activation of an intrinsic tyrosine kinase resulting in receptor autophosphorylation. This subsequently recruits one of a family of insulin receptor substrate molecules (IRS) to the receptor where it becomes activated by tyrosine phosphorylation. IRS consequently binds to and activates further downstream targets such as the enzyme phosphatidylinositol 3- kinase (PI3K). IRS-2 is most abundantly expressed within the Arc; its knockout is associated with increased food intake and increased fat stores (Burks *et al.*, 2000).

The long term adiposity hormones insulin and leptin exert their effects via actions on specific neurones of the hypothalamus to produce an overall anorexigenic effect (discussed in section 1.6). It has been suggested that these key hormones involved in energy homeostasis share common intracellular pathways via IRS and PI3K resulting in downstream signal transduction (Niswender *et al.*, 2003; Niswender & Schwartz, 2003; Spanswick *et al.*, 2000). To be able to delineate key events in leptin and insulin signalling in brain areas such as the Arc at the cellular level would be an advance in our understanding of how these peripheral signals are involved in energy balance.

1.6 NPY/AgRP, POMC/CART neurones in the control of energy homeostasis

The chemical phenotype of the Arc is diverse; however in the maintenance of energy homeostasis the main focus is on two neuronal populations differentially expressing NPY/ AgRP and POMC/CART, which are the best characterised metabolic sensing neurones. Within the Arc they reside in discrete areas, with NPY/AgRP neurones predominately located

in the ventromedial Arc (Chronwall, 1985; Allen *et al.*, 1986) and POMC/CART located more laterally (Bloch *et al.*, 1978; Bloom *et al.*, 1978). These two sets of neuronal populations are anatomically adjacent and work in an antagonistic fashion as parallel but opposing pathways to maintain a balanced energy state. They are differentially regulated by circulating factors that ultimately determine the Arc outflow and hence change the overall energy status (Schwartz *et al.*, 2000).

NPY is a 36 amino acid potent orexigenic neuropeptide (Williams *et al.*, 2000). It is widely expressed throughout the brain (Adrian *et al.*, 1983), with strong expression within the Arc (Chronwall *et al.*, 1984). NPY/AgRP has strong projections to the brain-stem, specifically the NTS. Its orexigenic effects are mediated through G-coupled receptors, mainly Y_1, Y_2 and Y_5 (Gerald *et al.*, 1996; Broberger *et al.*, 1997). NPY however has 6 known receptors, Y_6 being specific to mouse (Beck *et al.*, 2001). NPY has not only a stimulatory effect on food intake (Stanley *et al.*, 1993) but it also decreases energy expenditure (Menendez *et al.*, 1990) subsequently favouring fat deposition. Hyperphagia is accompanied by inhibition of SNS outflow to brown adipose tissue and other thermogenic tissues thus leading to a fall in energy expenditure and favouring weight gain (Egawa *et al.*, 1991). NPY mRNA within the Arc increases in states of negative energy balance or food deprivation compared to that of controls (Schwartz *et al.*, 1991b; Guan *et al.*, 1998a; Lin *et al.*, 2000). Low body fat stores activate the Arc-PVN NPY pathway which is integral to the control of energy balance (Sahu *et al.*, 1988). Central administration of NPY enhances food intake and increases body weight in rodents, with repeated application resulting in obesity (Stanley *et al.*, 1986; Billington *et al.*, 1994).

Within the Arc, Ob-Rb mRNA is expressed on neuronal groups expressing NPY (Hakansson *et al.*, 1996; Mercer *et al.*, 1996a; van den Top *et al.*, 2004). Leptin inhibits the activity of NPY neurones and reduces its expression (Erickson *et al.*, 1996; Smith *et al.*, 1998;

Stanley *et al.*, 2005). Thus, in times of low circulating leptin, NPY expression is unregulated which results in a shift towards equilibrium. Insulin, another adiposity signal, also inhibits hypothalamic expression of NPY (Benoit *et al.*, 2002). It has been reported that administration of insulin during food deprivation in rats prevents the fasting-induced increase in NPY mRNA within the Arc (Schwartz *et al.*, 1992).

Co-expressed with NPY in the medial aspects of the Arc is Agouti- related protein (AgRP), the agouti homolog in the brain. AgRP is exclusively expressed within the hypothalamus and is secreted with NPY from the axonal terminals to hypothalamic and extrahypothalamic areas (Broberger *et al.*, 1998; Hahn *et al.*, 1998) to increase feeding. Ablation of AgRP neurones results in acute reduction of feeding showing that they are critical in energy homeostasis (Gropp *et al.*, 2005). The ablation of NPY/AgRP in adult mice but not neonates results in starvation (Luquet *et al.*, 2005). It is thought that the ability of neonates to deal with such a loss is due to them lacking functional connections which thus promote compensatory mechanisms (Luquet *et al.*, 2007).

Leptin inhibits the release of AgRP (Hoggard *et al.*, 2004a; Hoggard *et al.*, 2004b). As with NPY expression, AgRP is unregulated in leptin deficient rodents due to fasting or a mutation (Hahn *et al.*, 1998). AgRP administered intracerebroventricularly (I.C.V) increases food intake with a single injection, showing its potent orexigenic effects over long periods of time (Rossi *et al.*, 1998). AgRP has also been found to act as an endogenous antagonist / inverse agonist of the melanocortin 3 and 4 receptors (MC_3-R and MC_4-R) by competing with α-melanocyte stimulating hormone (α-MSH), a natural agonist of the above receptors (Cowley *et al.*, 1999). Suppression of the activity of the MC_4-R by ectopic agouti over expression in the A^y mouse mutant (lethal yellow; a gain of function mutation in the agouti gene locus) leads to obesity. These mice also display characteristic yellow fur due to the loss of MC_1-R receptor signalling (for review see Adan & Kas, 2003). α-MSH inhibits feeding and induces weight loss.

The unique colocalisation of mRNA AgRP with NPY makes a distinctive subset of neurones that are capable of increasing food intake via two different mechanisms; by increasing NPY signalling and by decreasing melanocortin signalling.

Proopiomelanocortin (POMC) is a precursor polypeptide for the catabolic melanocortins, which include adrenocorticotrophic hormone (ACTH) and α-MSH which has the most apparent importance within feeding. Within the CNS, POMC and its derivatives are located exclusively within the NTS and the Arc (Jacobowitz & O'Donohue, 1978; Watson & Akil, 1979). Melanocortins mediate their effects through the G-protein coupled melanocortin receptors (MC_1R- MC_5R). Two melanocortin receptors, MC_4-R and MC_3-R are widely expressed within hypothalamic regions (Roselli-Rehfuss *et al.*, 1993; Mountjoy *et al.*, 1994) including the Arc and ME (Harrold *et al.*, 1999). The binding of the melanocortins to the above receptors inhibits food intake and promotes weight loss (Cone, 1999). The injection of an α-MSH homologue leads to suppression of food intake (Fan *et al.*, 1997). Disruption in POMC expression or in signalling of the POMC peptides leads to obesity in both mice and humans (Spiegelman & Flier, 2001). Genetic deletion of MC_4-R in mice and humans results in severe hyperphagic obesity (Huszar *et al.*, 1997; Coll *et al.*, 2004). A common monogenic cause of obesity within humans has been identified to be due to the disrupted MC_4-R signalling (Yeo *et al.*, 1998). MC_4-R-/- null mice are severely obese and have severe hyperphagia, an identical phenotype of that seen in an agouti lethal yellow mutant (ectopic expression of the agouti protein; a homologue of AgRP; Miller *et al.*, 1993; Huszar *et al.*, 1997). As discussed previously, agouti has been shown to be a natural antagonist of the MC_4-R; these studies further substantiating the idea that POMC has an anorexigenic role within feeding.

The Ob-Rb receptor has been shown to be expressed by POMC neurones and they have been shown to be directly activated by leptin via activation of a non-selective cation

channel, involving a PI3K-dependent downstream signalling pathway (Elias *et al.*, 2000; Cowley *et al.*, 2001; Hill *et al.*, 2008; Rother *et al.*, 2008). When neuronal input from leptin is reduced, POMC neurones are inhibited resulting in positive energy balance (Cone, 1999). Within the Arc, POMC is co-localised with CART, also an anorexigenic peptide (Elias *et al.*, 1998). CART neurones are also upregulated by leptin. CART mRNA levels decrease at times of low leptin levels, such as starvation and reverse following administration of leptin (Kristensen *et al.*, 1998). Interestingly, insulin has been shown to hyperpolarise and decrease the firing rate of a subset of Arc neurones (Spanswick *et al.*, 2000). Insulin has been shown to inhibit POMC neurones through the PI3K pathway (Hill *et al.*, 2008).

There is also interplay between the two main opposing neuropeptides within the Arc. The orexigenic NPYAgRP neurones innervate the anorexigenic POMC/CART neurones within this nucleus. POMC/CART neurones receive spontaneous GABAergic inputs which partially originate from NPY terminals synapsing on these neurones (Cowley *et al.*, 2001). NPY has been shown to inhibit POMC mRNA expression via the Y_2 receptor (Garcia de Yebenes *et al.*, 1995) and has also been shown to directly hyperpolarise POMC neurones through the Y_1 receptor, mediated via the activation of G-protein inwardly rectifying potassium (GIRK) channels (Broberger *et al.*, 1997; Roseberry *et al.*, 2004). The neonatal ablation of NPY/AgRP neurones results in an increase in ACTH/αMSH, as would be expected due to the loss of an inhibitory input from NPY/AgRP neurones (Luquet *et al.*, 2007).

1.7 Other neuropeptides implicated in the control of energy balance

1.7.1 Orexin

The Arc receives extensive afferent and efferent projections. In particular POMC and NPY neurones within the Arc project to the LH, the PVN and the DMH (Chronwall, 1985; Bagnol *et al.*, 1999) and these connections are reciprocal.

The LH contains neurones that express the orexins and melanin-concentrating hormone (MCH) which are implicated heavily within feeding and act as downstream targets for the Arc. Orexins A and B (also known as hypocretin 1 and 2) are exclusively located within the LH in the CNS (Date *et al.*, 1999) and are endogenous ligands for previous orphan G-protein-coupled receptors, OX_1R and OX_2R (Sakurai *et al.*, 1998).They project throughout the neuronal axis including projections within the hypothalamus incorporating the Arc. The orexins are essential to maintain an appropriate state of arousal, illustrated by the occurrence of narcolepsy in the absence of orexin signalling (Hara *et al.*, 2001; Taheri *et al.*, 2002). The injection of orexin into the hypothalamus stimulates feeding (Sakurai *et al.*, 1998; Willie *et al.*, 2001) and thus suggests it to be important for appetite control. Their suggested role has been to ensure that the body is alert at times when food resources are low and thus the need to seek food is high (Willie *et al.*, 2001; Sakurai, 2003). Arc NPY neurones express the orexin receptors (OX_1R and OX_2R) and have been shown to mediate the induction of oscillations in a subpopulation of Arc neurones which are functionally thought to be acting as conditional pacemakers (van den Top *et al.*, 2004). Orexin neurones have also been shown to indirectly inhibit the activity of POMC neurones (Ma *et al.*, 2007). In addition through the OX_2R, orexin directly decreases intracellular calcium through a pertussis toxin (PTX) sensitive pathway

(Muroya *et al.*, 2004). Leptin administration also decreases orexin expression further suggesting that this peptide has an orexigenic role within feeding (Yamanaka *et al.*, 2003).

1.7.2 Melanin-concentrating hormone

Melanin-concentrating hormone (MCH) has also been shown to have an orexigenic role in feeding. It exerts its effects through two types of G-protein-coupled receptors, MCH-1 and MCH-2. Injection of MCH into the brain (lateral ventricles) increases food intake (Qu *et al.*, 1996) and mice lacking MCH are hypophagic and lean (Shimada *et al.*, 1998). It also has a role in arousal; decreasing energy expenditure and increasing food intake simultaneously when injected intracerebroventrically (Cvetkovic *et al.*, 2003). MCH is also involved in the downstream effects of leptin, shown by increased expression of MCH within the hypothalamus after 48 hour fasting (Kokkotou *et al.*, 2001). Interestingly, MCH co-localises with CART within the LH, therefore leading to a neuronal group which contains both anorexigenic and orexigenic peptides (Broberger, 1999).

1.7.3 Corticotrophin releasing hormone

Second order neurones such as those found in the LH are also present within the PVN; so called due to their indirect contact with peripheral satiety factors, the Arc neurones being termed ‘first order’ neurones. The PVN is the main site for production of corticotrophin releasing hormone (CRF) and thyrotrophin releasing hormone (TRH) which have been implicated to have a role in feeding. CRF is best known as the regulator of ACTH release and has a key role in integrating signals of energy status with the hypothalamic–pituitary-adrenal axis (HPA; Neary *et al.*, 2004). Injection of CRF into the brain decreases feeding and chronic

administration causes anorexia and sustained weight loss (Levine *et al.*, 1983; Krahn *et al.*, 1988). In contrast, administration of CRF antagonists within the hypothalamus enhances NPY expression, thus suggesting that CRF has a role in tonically inhibiting an orexigenic signal (Hanson & Dallman, 1995; Arora & Anubhuti, 2006).

1.8 Short-term signals regarding energy status originating from the periphery

To regulate food intake the brain must modulate satiety signals and this is achieved by the regulation of the gut-brain axis. The hindbrain receives inputs from short-acting satiety signals which are transmitted both neurally, through vagal afferents projecting to the NTS and also hormonally, where gut peptides act directly either on the area postrema or the Arc. Amongst inputs of central origin, the hypothalamus also receives afferent inputs from the periphery; insulin and leptin which have already been mentioned but short term signals regarding energy status are also implicated such as ghrelin and peptide YY_{3-36} (PYY_{3-36}).

1.8.1 Ghrelin

Ghrelin is a potent orexigen released and synthesised by the oxyntic cells within the stomach, and was initially identified as the endogenous ligand of the growth hormone secretagogue receptor (GHS-R; Kojima *et al.*, 1999). Its plasma concentration increases pre-prandially and falls post-prandially thus proposing a function as a short-term signal initiating feeding (Tschop *et al.*, 2000; Cummings *et al.*, 2001). Central continual administration of ghrelin causes obesity in mice by increasing food consumption and reducing fat utilisation (Tschop *et al.*, 2000; Wren *et al.*, 2001a; Wren *et al.*, 2001b; Lawrence *et al.*, 2002; Wang *et al.*, 2002; Faulconbridge *et al.*, 2003; Currie *et al.*, 2005). It also has the ability to abolish

leptin-induced anorexia (Shintani *et al.*, 2001). This gut peptide has the ability to cross the BBB and thus has the ability to exert its actions upon the neurones of the Arc

Furthermore the vagal efferent pathway has also be shown to be an important route for conveying peripheral orexigenic ghrelin signals to the hindbrain which in turn transmits signals through the noradrenergic pathway to the Arc (Date *et al.*, 2006). Arc neurones express the GHS-R, and 94% of orexigenic NPY neurones express this receptor (Willesen *et al.*, 1999; Zigman *et al.*, 2006). High levels of the receptor are also expressed within the VMN and brainstem (Bennett *et al.*, 1997; Guan *et al.*, 1997b). Administration of ghrelin in the Arc increases mRNA content, C-FOS and electrical activity of NPY neurones (Kamegai *et al.*, 2001; Nakazato *et al.*, 2001). Antibodies of NPY and AgRP and NPY Y_1 receptor antagonists have all been shown to abolish ghrelin-induced feeding (Kamegai *et al.*, 2000, 2001). Furthermore ghrelin has also been shown to directly excite a subpopulation of NPY neurones within the Arc that are directly inhibited by the anorexigen leptin (van den Top *et al.*, 2004). Neonatal ablation of NPY/AgRP reveals there is also a loss of ghrelin signalling, thus indicating that NPY/AgRP neurones are critical for mediating the ghrelin response. It also shows that there are no compensatory mechanisms to mediate this hormone's effects (Luquet *et al.*, 2007). Thus, this substantiates that the Arc is a key intrinsic site of action for ghrelin and its downstream effects within feeding, importantly acting on the orexigenic NPY/AgRP neurones. For a general review on ghrelin see Kojima & Kangawa, 2005.

1.8.2 Peptide YY

Peptide YY (PYY) belongs to the pancreatic polypeptide family which includes NPY. It is secreted postprandially from endocrine cells of the gut, in proportion to caloric intake (Stanley et al, 2005). Two main forms of PYY are released into the circulation; PYY_{1-36} and

PYY $_{3-36}$ which bind with differential specificity to the Y- receptors. PYY $_{3-36}$ binds specifically to the Y_2 receptors (Keire *et al.*, 2000; Batterham *et al.*, 2002; Keire *et al.*, 2002). Peripheral administration of PYY $_{3-36}$ has been shown to delay gastric acid secretion and gastric emptying and to reduce food intake and body weight (Batterham *et al.*, 2002). Its proposed action within the Arc involves acting on pre-synaptic Y_2 receptors of NPY neurones to reduce expression and therefore stop the tonic inhibition of POMC neurones which in turn reduces feeding (Broberger *et al.*, 1997; Batterham *et al.*, 2002). However, peripheral administration of PYY_{3-36} and its effects are in contrast to central administration of the peptide which stimulates feeding in rats (Stanley *et al.*, 1985; Hagan *et al.*, 1998).

There are a plethora of neuropeptides and hormones implicated in the control of energy homeostasis, several of which have been discussed so far. However, to discuss each individual in detail would be beyond the scope of this project, and therefore for simplicity a comprehensive list of these peptides is presented in Table 1.1.

Table 1.1 Neuropeptides and hormones implicated in the control of energy homeostasis

Orexigenic	**Anorexigenic**
Agouti-related protein	Adiponectin
Dynorphin	α-Melancyte stimulating hormone
Galanin	Amylin
Ghrelin	Bombesin
Growth Hormone-Releasing Hormone	Cholecystokinin
Melanin Concentrating Hormone	Cocaine-amphetamine regulated transcript
Neuropeptide Y	Cortciotrophin releasing factor
Orexin A/Hypocretin A	Glucagon-like peptide 1

Orexin B/Hypocretin B	Insulin
	Leptin
	Neuromedin U
	Oxyntomodulin
	Oxytocin
	Peptide YY $_{3-36}$
	Pro-opiomelanocortin
	Serotonin
	Somatostatin
	Thyrotropin releasing factor
	Urocortin II

1.9 Glucose

Glucose, a monosaccharide, is a vitally important carbohydrate as it provides the brain's main fuel source. Its metabolism accounts for up to 50% of the total body's glucose utilisation (Owen *et al.*, 1967). Glucose control is imperative as the brain becomes irreversibly damaged even if deprived of glucose for a few minutes, and therefore the body maintains glucose levels within a narrow range via both central and peripheral mechanisms. Blood glucose concentrations directly control the release of the pancreatic hormone glucagon and insulin. However, fluctuations in plasma glucose also cause the brain to initiate compensatory responses by activating the SNS to maintain glucose homeostasis (Hoffman *et al.*, 1999). Thus the brain has developed the ability to mechanistically sense changes in plasma glucose and restore homeostasis. If glucose levels fall in a healthy individual an endocrine response occurs with increased levels of glucagon (released from α- cells of the pancreas), adrenaline,

NA and cortisol, this release being under the control of the ANS. This hormonal increase in combination with decreased glucose levels increases glucose production by the liver and limits glucose utilization by the body's tissues. Disruption of this intricate network occurs in type 2 diabetes mellitus which commonly is a result of those who are obese. Circulating levels of glucose are detected by both the periphery and the brain and work in synergy to regulate homeostasis.

Signals regarding blood glucose levels are detected by specialised cells within the mesenteric and hepatoportal veins termed enteric glucose sensors and are communicated to the brain-stem via the vagus nerve (Adachi *et al.*, 1984; Knauf *et al.*, 2008). These signals regarding blood glucose level changes are subsequently relayed to hypothalamic nuclei (Adachi, 1981). The brain also detects circulating glucose levels directly. Within the brain the neurones of the VMH which includes the VMN and the Arc, are well positioned to detect circulating glucose levels due to being in close proximity to a vascularised structure and fenestrated endothelial cells (Ganong, 2000). Neurones within this area use glucose (and insulin and leptin) as a signalling molecule to regulate electrical excitability and consequently neuronal firing (Anand *et al.*, 1964; Oomura *et al.*, 1964; Spanswick *et al.*, 1997; Spanswick *et al.*, 2000). The addition of glucose to the VMH has been shown to increase the firing rate of SNS nerves and to increase energy expenditure through the activation of brown adipose tissue (Rothwell & Stock, 1978; Sakaguchi & Bray, 1987). Conversely ablation of this area reduces sympathetic activity, including SNS innervation of the pancreas, thus leading to a decrease in insulin release and glucose utilisation.

It has been proposed that are two main groups of glucose-sensing neurones that exist within the VMH; glucose responsive (GR) and glucose sensitive (GS). GR neurones are those that increase their firing rate as brain glucose levels rise, also termed glucose excited neurones (GE). Conversely, GS neurones decrease their firing rate as glucose levels rise,

also termed glucose inhibited (GI) neurones. The physiological levels of glucose will be discussed in detail in chapter 4. It has been shown that GR neurones sense changes in glucose levels in a manner similar to that of a pancreatic β-cell to modulate membrane potential i.e. use ATP- sensitive potassium channels ($K_{ATP)}$ to sense glucose (Ashford *et al.*, 1990; Spanswick *et al.*, 1997; Spanswick *et al.*, 2000; Ashcroft, 2005). Glucose is thought to enter the cell predominantly via the GLUT 2 or the GLUT 3 transporter within the neurones of the pancreas and brain respectively (Pessin & Bell, 1992; Levin, 2001; Bady *et al.*, 2006) where it is phosphorylated by glucokinase and processed (glycolysis) resulting in an increase in the cytosolic ATP/ADP ratio. This causes the K_{ATP} channel to close within the membrane which raises intracellular potassium levels resulting in a membrane depolarisation and Ca^{2+} influx (Levin *et al.*, 2001; Dunn-Meynell *et al.*, 2002; Kang *et al.*, 2004; Yang *et al.*, 2007). Within the pancreas this leads to an increase in the release of insulin and glucose utilisation. Other mechanisms for how GR neurones sense glucose have been proposed which suggest a K_{ATP} independent mechanism, involving a non-selective cationic conductance mediating a depolarisation at high glucose levels (Fioramonti *et al.*, 2004).

The mechanism by which GS neurones respond to changes in extracellular glucose is less clear. Ideas suggest the activation of a hyperpolarising chloride current (Song *et al.*, 2001; Routh, 2002; Fioramonti *et al.*, 2007) and a mechanism involving the reduction in the depolarising activity of the electrogenic Na^+/ K^+ pump within the LH (Oomura *et al.*, 1974).

K_{ATP} channels are octameric proteins (Shyng & Nichols, 1997) and are composed of two distinct subunits: a pore forming subunit (Kir 6.2) for K^+ (Trapp *et al.*, 1997) and a sulphonylurea binding site (SUR) that are arranged in a 4:4 stoichiometry. Predominately within the hypothalamus, glucose sensing neurones sense changes in levels of glucose via a Kir 6.2 SUR 1 mechanism (Ashford *et al.*, 1990; Levin *et al.*, 1996; van den Top *et al.*, 2007). However the expression of Kir 6.1 SUR 1 has also been reported within the VMH (Lee *et al.*,

1999). Studies have shown however that Kir 6.2 deficient mice (Kir 6.2 -/-) have non-functional K_{ATP} channels and GR neurones within the VMH. This therefore suggests that the Kir 6.2 forms the pore of the K_{ATP} channel in hypothalamic GR neurones and is essential for neuronal glucose sensing particularly for the stimulation of glucagon secretion and food intake when brain glucose levels are low (Miki *et al.*, 2001). These results are in accordance with immunocytochemistry studies which show the VMH and the Arc display strong Kir 6.2 immunoreactivity only, again suggesting that Kir 6.2 is a critical subunit of the K_{ATP} channels in GR neurones (Thomzig *et al.*, 2005).

Approximately 70% of neurones in the Arc have been shown to express functional K_{ATP} channels, including both opposing populations of neurones with the Arc; the anorexigenic POMC/CART and orexigenic NPY/AgRP neurones (Ibrahim *et al.*, 2003; van den Top *et al.*, 2007). K_{ATP} channels are also expressed by neurones that are sensitive to leptin and insulin. High levels of insulin and leptin, and hypoglycaemia represent contrasting physiological states; however both states inhibit Arc neurones through the opening of K_{ATP} channels. Thus, K_{ATP} channels are expressed on functionally antagonistic populations within the Arc but how they sense and signal changes in energy status in a functional context are unclear. It has been suggested that the long-term anorectic effects of leptin may not be dependent on K_{ATP}, and that K_{ATP} channels may only be involved in short-term regulation of food intake, by coupling glucose levels to appetite (Miki *et al.*, 2001).

Studies using 2-deoxy–glucose which produces glucoprivation show that NPY/AgRP peptides are up regulated in states of energy deficiency (Akabayashi *et al.*, 1993). Furthermore studies using real-time quantitative PCR and in situ hybridization show that peripheral administration of glucose significantly suppresses the expression of both NPY and AgRP within the Arc (Chang *et al.*, 2005). The role of POMC neurones in glucose sensing is less clear. Fioramonti *et al.*, 2007 mimicked a hyperglycaemic state within the Arc and found

that POMC neurones were not activated, suggesting that POMC neurones are not directly glucose sensitive and they are involved downstream in the regulation of glucose homeostasis. On the contrary, Ibrahim found that POMC neurones are glucose responsive mediated by the K_{ATP} channel (Ibrahim *et al.*, 2003).

The phenomenon that there are functionally opposing populations of neurones within the hypothalamus that respond differentially to glucose is not confined to the Arc. Within the LH, MCH and orexin expressing neurones have been shown to be differentially regulated by glucose. MCH neurones have been reported to be excited and increase their firing rate in response to an increase in glucose concentration, conversely subpopulations of orexin neurones are hyperpolarised with an increase in glucose (Burdakov *et al.*, 2005). Functionally this is advantageous as post-prandially (i.e. high glucose levels) MCH neurones will be activated which promote rest and energy conservation. Conversely, in times of low glucose, decreased excitability of MCH neurones suppresses the desire to sleep and promotes activity which is advantageous when seeking for food (Burdakov & Alexopoulos, 2005; Burdakov *et al.*, 2005).

1.10 Noradrenaline

Noradrenaline (NA), a bioamine synthesised in a series of steps from tyrosine, is released as a hormone from the adrenal medulla where it underlies the "fight or flight" response in times of stress. It is however also a neurotransmitter within CNS where it plays a large role in sleep, arousal, mood, appetite and autonomic outflow. Thus NA has multiple roles within the body and the individual systems utilising NA react rapidly to environmental changes. The receptors which recognise the chemical signals are distributed throughout both the CNS and periphery.

NA fibres in the brain arise from brainstem nuclei with the majority coming from NA-containing neurones originating in the locus coeruleus (A6; Dahlstrom & Fuxe, 1964). NA-containing fibres innervate all areas of the brain, including the hypothalamus which is essential in controlling a variety of homeostatic responses (see Figure 1.3; Sawchenko & Swanson, 1981). NA is believed to act upon hypothalamic alpha-adrenoceptors (α-ARs) to stimulate food intake, by interacting closely with circulating hormones and nutrients, and affecting metabolic processes, consequently serving a role within energy homeostasis. Application of NA directly into the brain can either increase or decrease feeding depending on the site of application (Leibowitz *et al.*, 1983).

Neurones of the Arc are innervated by noradrenergic fibres originating from the NTS (A2) and the locus coeruleus (A6; Sawchenko & Swanson, 1981). The PVN, another essential hypothalamic nucleus implicated within feeding, is heavily innervated by noradrenergic neurones and it is this interaction that has been most extensively studied.

Injection of NA into the hypothalamus specifically within the PVN has multiple effects. These include changes in feeding behaviour, water intake (Leibowitz, 1978; Leibowitz & Brown, 1980), energy metabolism (Siviy *et al.*, 1989) and also the release of corticosterone (CORT), vasopressin (Vp) and glucose (Benetos *et al.*, 1986; Chafetz *et al.*, 1986; Leibowitz *et al.*, 1988). The PVN, not only being a site for convergence of several neuronal pathways concerned with feeding, also sends efferent projections to the ME, pituitary and caudal brainstem (Swanson & Sawchenko, 1980). Thus, the effect of NA within this nucleus has a crucial role in a number of homeostatic processes.

The injection of NA into the perifornical region of the anterior hypothalamus (most specifically the PVN) elicits vigorous bouts of eating and drinking within satiated rats (Leibowitz, 1978). This effect was antagonised by α- AR receptor blockers, thus suggesting that α- ARs mediate the NA induced feeding response. The initial short period of intense

eating is also accompanied by intense drinking; however even though the eating may continue there is a long-term depression of drinking upon injection of NA. This has been shown to be also mediated through α- ARs. Thus, the study showed that NA not only had an effect on feeding but also water consumption which was dose-dependent and which effects were reversed in the presence of α- AR antagonists (Leibowitz, 1978) This study also concluded that β- AR in the PVN are not involved in NA induced feeding. The subtype of the AR was later considered, and it was found that intra-PVN injection of clonidine, a selective α_{2}- AR agonist stimulated feeding (Leibowitz, 1988). Furthermore these effects were reversed with pre-treatment with a selective α_{2}- AR antagonist (Goldman *et al.*, 1985).

α_{2}- AR expression has been shown to peak at the onset of the nocturnal cycle within the rat (Jhanwar-Uniyal *et al.*, 1986; Stanley *et al.*, 1989). It is at this time that the rats are most active and their feeding behaviour is at its highest. This peak also coincides with the rise in circulating CORT levels, and it has been shown that the depletion of hypothalamic NA would also result in a loss of the circadian rhythms for CORT and ACTH (Szafarczyk *et al.*, 1985; Leibowitz *et al.*, 1989). Thus NA has been shown to play an intricate role in the hypothalamic- pituitary-adrenal (HPA) axis; stimulation of the PVN noradrenergic system which exhibits a peak in its activity, simultaneous to the rise of CORT, acts through local CRF neurones which ultimately stimulate pituitary release of ACTH (Leibowitz *et al.*, 1988). The effects of NA on CORT release is correlated with NA effects on vasopressin (Vp) release; an antidiuretic hormone which presumably has a role in the secretion of ACTH (Leibowitz *et al.*, 1988).

Glucose levels decline after a period of food deprivation, which has been shown to be correlated with the magnitude of compensatory feeding (Larue-Achagiotis & Le Magnen, 1983). Studies show that with the decline in blood glucose levels there is also a decline in the expression of α_{2}- AR which is reversed with a brief application of peripheral glucose or re-

feeding (Jhanwar-Uniyal *et al.*, 1988). Injection of NA within the PVN increases blood glucose levels (Chafetz *et al.*, 1986) through the ANS. The link between glucose and α_2- AR mechanisms is consistent with the findings that increases in blood glucose are prevented by α- AR antagonists (Leibowitz, 1988; Steffens *et al.*, 1988). This is further substantiated when levels of CNS glucose are low; NA levels increase within the hypothalamus which subsequently increases circulating blood glucose levels (McCaleb *et al.*, 1979; Smythe *et al.*, 1984) via direct action of the ANS.

In many brain areas such as the VMH, activation of α_1- ARs generally excites and α_2- AR activation inhibits neuronal firing (Kow & Pfaff, 1987). Both receptors can exist on the same neurone but have opposing effects (Wellman *et al.*, 1993). Thus the ratio of α_2- AR to α_1- AR on a given neurone can determine its intrinsic response to NA.

NA is thought to increase feeding within the PVN by inhibiting descending satiety signals through activation of α_2- ARs. To summarise, PVN neurones are tonically active with descending outputs to brainstem nuclei producing an overall inhibition of feeding. This tonic activation is thought to be through the activation of the α_1- AR by an endogenous α_1- AR agonist. The increase of NA at times when food is low and the increase of the α_2- AR at the onset of the dark phase suggests that the activation of the antagonistic α_2- ARs inhibits the neurone thereby inhibiting the satiety signal and increasing food intake (Levin & Planas, 1993; Wellman *et al.*, 1993; Levin *et al.*, 1998).

Within the LH, NA has been shown to both directly increase and decrease the activity of orexin-expressing neurones (Bayer *et al.*, 2005; Li & van den Pol, 2005; Yamanaka *et al.*, 2006). Thus, NA again within hypothalamic nuclei has differential effects on populations of neurones that express common transmitters (Nakamura *et al.*, 1984).

Leptin and insulin, two major long-term signals implicated in food intake, have also been studied for their effects on NA signalling within the brain. Insulin has been shown to down-regulate the expression of α_2- AR. How this affects food intake is not yet known, however, it is thought within the Arc, down-regulation of the receptor increases synaptic NA, and has a role with NPY to alter feeding (Levin *et al.*, 1998). Studies have shown that NPY increases NA levels and thus, NPY may 'use' NA in facilitating its stimulatory role within feeding (Hastings *et al.*, 1997).

Leptin has been shown to inhibit depolarisation-induced NA release, thus leptin's anorectic effects may be partly though inhibiting NA fibres within the hypothalamus (Brunetti *et al.*, 1999).

The role of central NA and its link to the digestive tract has also been reported. The effect of ghrelin, a potent orexigen released from the stomach, has been shown to have no effect on the release of NA within the hypothalamus and thus does not modulate NA stimulatory effects associated with feeding (Brunetti *et al.*, 2002). This is contrary to a later study which has found that ghrelin stimulates the noradrenergic pathways from the hindbrain to the Arc (Date *et al.*, 2006).

To date, there have been no studies on the effects of NA within the Arc and its role in feeding. Thus, this study in part has attempted to address the issue of the effects of NA on the electrical activity of Arc neurones.

1.10.1 Adrenergic receptors

The adrenergic receptors are part of the superfamily of G-protein coupled receptors (GPCRs), which contain seven putative transmembrane spanning domains that bind the endogenous agonists, NA and adrenaline (Cotecchia *et al.*, 1998; Tanoue *et al.*, 2002).

Based on different responses to a variety of agonists, adrenergic receptors were initially divided into two separate groups; α- AR and β- AR by Alquist in 1948 (Liggett & Raymond, 1993). He observed opposing effects of NA on smooth muscle cells and proposed that α ARs were responsible for the excitatory actions and that β- ARs were responsible for inhibitory actions. Subsequently, molecular cloning (Bylund *et al.*, 1994) and advances in pharmacological affinities for adrenergic agonists and antagonists (U'Prichard & Snyder, 1979) has further classified these receptors. Presently there are nine adrenoceptors identified; three α_1- AR subtypes ($\alpha_{1a,}$ $\alpha_{1b,}$ α_{1d}), three α_2- AR subtypes ($\alpha_{2a,}$ $\alpha_{2b,}$ α_{2c}), and finally three β- AR subtypes ($\beta_{1,}$ $\beta_{2,}$ β_3; Cotecchia *et al.*, 1998). It was thought that there existed a fourth α_{2-} AR (α_{2d}), but subsequent studies showed it to be a species variant of the α_{2a} receptor (Bylund *et al.*, 1992).

α_{1-} ARs are coupled to Gq/11- signalling pathways, which involve the activation of phospholipase C (PLC), generation of the second messengers inositol triphosphate (IP3) and diacylglycerol (DAG), and the mobilisation of intracellular calcium stores (Zhong & Minneman, 1999; Koshimizu *et al.*, 2007). Of sympathetically innervated tissue, the cardiovascular system is the most characterised with its effects and expression of the α_{1-} AR. Stimulation of this receptor has a major role in contraction and growth of vascular smooth muscle cells and the regulation of basal blood pressure (Zhong & Minneman, 1999; Piascik & Perez, 2001). Little is known of the contribution this receptor subtype makes within the CNS. It is however abundantly found within the brain (Tanoue *et al.*, 2002; Papay *et al.*, 2006). The α_{1-} AR subtypes have also shown a differential distribution within the brain. For example, within the Arc the α_{1a-} ARs are the most abundant AR subtype, whereas the α_{1d-} AR is undetectable, as determined by *in situ* hybridisation studies (Day *et al.*, 1997). Within the cerebral cortex the activation of the α_{1-} ARs can increase excitations mediated by glutamate (Mouradian *et al.*, 1991) and enhance neurotransmitter release from glutamatergic terminals (Marek &

Aghajanian, 1999; Papay *et al.*, 2006). Knock-out studies show the importance of these receptors in the modulation of behaviour, attention and memory (Spreng *et al.*, 2001; Drouin *et al.*, 2002).

α_{2-} ARs are coupled to Gi/o signalling pathways, the activation of which leads to the inhibition of adenylyl cyclase, thus resulting in decreased cAMP levels. It also is an important regulator of neuronal function by inhibiting voltage-gated Ca^{2+} channels and activating GIRK K^{+} channels (Rogawski & Aghajanian, 1982; Limbird, 1988; Hein, 2006). It was initially thought that the discriminating factor between α_{1-} AR and α_{2-} AR were that α_{1-} ARs were located post-synaptically and α_{2-} ARs were located pre-synaptically (Langer, 1974). However this was later found to be incorrect, as α_{2-} AR are located both pre- and post-synaptically. Postsynaptic α_{2-} ARs are generally inhibitory whereas presynaptic α_{2-} AR provide negative feedback which inhibits presynaptic release of NA (Rogawski & Aghajanian, 1982; Wellman *et al.*, 1993). It is the α_{2A-} AR which is thought to be involved in the feedback regulation of NA release (Altman *et al.*, 1999). Non-neuronal functions of this receptor subtype include modulation of insulin secretion from the pancreas and regulation of the cardiovascular system. In regards to energy homeostasis, it has been shown that application of clonidine (a α_{2-} AR agonist) or NA, into the PVN elicits feeding. These receptors seem postsynaptic in nature, since their sensitivity to noradrenergic stimulation is unaffected or even enhanced by drug manipulations that destroy the presynaptic terminals or block neurotransmitter synthesis (Goldman *et al.*, 1985). Within the hypothalamus these receptors have been shown to be involved in the release of growth hormone, prolactin release and cause bradycardia (Li *et al.*, 1996). Within the CNS, α_{2-} ARs are also involved in the regulation of pain perception and behaviour (Hunter *et al.*, 1997; Hein, 2006). α_{2-} ARs are also termed heteroreceptors, as they have the ability to regulate other neurotransmitters, namely serotonin and dopamine, also monoamines (Scheibner *et al.*, 2001; Bucheler *et al.*, 2002).

It has been found that NA is less potent in activating β- ARs than adrenaline (Molinoff, 1984). β - ARs are classified in their responsiveness to the selective antagonist, propranolol, which is clinically used today to treat migraines, glaucoma and most commonly hypertension (Turner, 1984; Kostic, 1992). They are well known for their role in peripheral metabolic functions, their role in mediating sympathetically-driven thermogenesis and their role in cardiovascular functions (Lowell & Bachman, 2003; Hein, 2006). For summary, see Figure 1.4.

1.11 Histamine

The projections of the noradrenergic system represent only one of four aminergic systems present within the mammalian brain. The others are the serotonergic, dopaminergic and histaminergic systems. These systems are unique in that their projections cover the majority of the brain and thus play a major role in modulating neuronal function (Brown *et al.*, 2001). Here, the histaminergic system is discussed.

The Arc receives direct histaminergic projections from the tuberomammillary nucleus (TM). The TM comprises of approximately 2000 histamine containing neurones which reside within the posterior hypothalamus (Haas *et al.*, 1989; see Figure 1.5). The histaminergic TM system is involved in arousal including hibernation (Kiyono *et al.*, 1985), the control of energy balance, fluid balance and cardiovascular regulation (Leibowitz, 1973; Sakata *et al.*, 1988b; Schwartz *et al.*, 1991a; Wada *et al.*, 1991).

The effect on feeding behaviour induced by histamine was first recognised by the use of both antidepressants and antipsychotics which had side-effects in the form of weight gain via appetite stimulation and acted directly on the histaminergic system (Kalucy, 1980). The increase in food intake was determined to be through the antagonism of the H_1 receptor (Hill & Young, 1978) revealed by binding assays. The administration of histamine centrally has since

been shown to reduce body-weight in both genetically obese mice and diet-induced obese mice. This is by the alteration of energy expenditure, food intake and increase in lipolysis, with a great reduction in visceral fat deposition most likely through the activation of the SNS (Masaki *et al.*, 2001a, b), thus showing the complexity of histamine's neuronal actions. Furthermore, obese Zucker rats have been shown to have lower histamine levels than their lean litter mates (Sakata *et al.*, 1991).

The H_1 receptor has been implicated in histamine's anorexigenic effects within the control of energy homeostasis. Nuclei involved in food intake, such as the PVN and the VMH have been shown to be rich in H_1 receptors (Palacios *et al.*, 1981) and injections of H_1 antagonists into these sites has been shown to increase food intake (Ookuma *et al.*, 1989).

H_1 knock-out mice (H_1 KO) show age-related obesity with increased fat deposition. They interestingly also show an altered circadian rhythm (abnormal circadian feeding rhythms have been linked to the onset of obesity; Murakami *et al.*, 1995) which may contribute to the obese phenotype, as scheduled feeding of an obese H_1KO mouse attenuates an increase in body mass (Masaki *et al.*, 2004). Therefore, it is hypothesised that an altered circadian rhythm in H_1 receptor deficient mice affects their feeding behaviour and most probably alters their energy expenditure resulting in development of obesity (Masaki & Yoshimatsu, 2006). Studies also suggest that neuronal histamine modulates the feeding circadian rhythm within the hypothalamus, with higher neuronal histamine levels in the early light period (when feeding is low), and lower histamine levels at the early dark period (when feeding is high; Orr & Quay, 1975).

Leptin, has been suggested to have an effect on feeding behaviour through the activation of the central histaminergic system and the H_1 receptor (Morimoto *et al.*, 1999). Leptin has been shown to directly increase neuronal release of histamine, and thus the histaminergic system may act as a downstream target for leptin-induced anorectic effects

(Morimoto *et al.*, 2000). However, it is not yet clear by which mechanism through which leptin affects the histamine system (Morimoto *et al.*, 2000). Studies carried out by Ishizuka and colleagues considered the involvement of the histaminergic system and the control of orexigenic peptides. They found that the injection of ghrelin had no effect on histamine release, and ghrelin exerted its effects even in H_1KO mice thus suggesting that ghrelin increases food intake in a histamine-independent manner (Ishizuka *et al.*, 2006). Furthermore the effects of histamine on NPY have also been studied. Histamine has been shown to have an inhibitory tone on NPY synthesis, as shown by the suppression of neuronal histamine by α-fluoromethylhistidine (FMH); a specific and irreversible inhibitor of histidine decarboxylase (HDC; Ookuma *et al.*, 1990), which enhances NPY mRNA expression (Toftegaard *et al.*, 2003). It is suggested that the histaminergic system acts as a feedback signal downstream of NPY, so that when feeding is high through NPY this is terminated by histamine (Ishizuka *et al.*, 2006). POMC neurones, which also like NPY form part of the leptin signalling pathway, do not interact with the histaminergic system to reduce bodyweight (Yoshimatsu, 2006).

With the use of agouti yellow obese mice (A^y) which show suppression of the activity of the MC_4-R by ectopic *agouti* over expression, histamine H_1-R signalling in regulating food intake, energy expenditure and adiposity was shown to be through a pathway independent of the POMC/AgRP MC_4-R signalling pathway (Yoshimatsu, 2006).

Another orexigen that interacts with the histaminergic system is orexin. Orexin-containing fibres innervate the TM (Peyron *et al.*, 1998), and orexin receptors are present within the TM (Eriksson *et al.*, 2001; Marcus *et al.*, 2001). Studies show that orexin (A) increases histamine release (Huang *et al.*, 2001; Ishizuka *et al.*, 2006) which increases wakefulness and locomotor activity which is dependent on the H_1 receptor (Masaki *et al.*, 2004; Masaki & Yoshimatsu, 2006), but has no effect on food intake. Based on these findings and as mentioned above both orexin and histamine are also involved in arousal (Kiyono *et al.*,

1985; Hara *et al.*, 2001; Taheri *et al.*, 2002), and therefore it is unlikely that the activation of the histaminergic system by orexin is involved directly in the control of feeding but plays a larger part in wakefulness.

So far only the H_1 receptor has been discussed within the role of feeding; however H_2 and H_3 have also been implicated. The H_2 receptor is least involved within the regulation of feeding. Unlike with the use of H_1 agonists which decrease food intake (Sakata *et al.*, 1988a), H_2 agonists have no effect (Lecklin *et al.*, 1998) nor do H_2 antagonists (Doi *et al.*, 1994; Lecklin & Tuomisto, 1998). This is in contrast to other reports that suggest H_2 receptors are involved in the regulation of food intake in the VMH (Magrani *et al.*, 2004). Thus, the involvement of the H_2 receptor in energy homeostasis is unclear.

The H_3 receptor is an autoreceptor that provides negative feedback to restrict histamine synthesis and release. Thioperamide, an antagonist at the H_3 receptor (which has also been reported as an inverse agonist) has been shown to decrease both feeding and drinking in spontaneous, fasted-induced and NPY induced-feeding due to the increase in histamine release (Lecklin *et al.*, 1998; Ito *et al.*, 1999). Interesting H_3 KO mice show hyperphagia and late on-set obesity, similar to the phenotype of H_1 KO mice (Takahashi *et al.*, 2002; Tokita *et al.*, 2006). However, this is not what one would expect. The knockout of this receptor would increase histamine release that ultimately decreases food intake and increase energy expenditure. One theory for this paradoxical theory is that the lack of H_3 receptor may alter neural circuitry, or that the increase in histamine may desensitise/ down regulate both H_1 and H_2 receptors and thus block histamine-mediated effects (Takahashi *et al.*, 2002; Tokita *et al.*, 2006).

1.11.1 Signalling of the histamine receptors

Histamine exerts its effect through four GPCRs, designated H_1, H_2, H_3, and H_4 (Teuscher *et al.*, 2007). Only three of the four identified histamine receptors (H_1-H_3) are expressed in the CNS, whereas the fourth (H_4) receptor is detected predominately within the periphery, for example in bone marrow and leukocytes (Liu *et al.*, 2001; Shin *et al.*, 2002).

H_1 receptor

The H_1 receptor is widely distributed throughout the brain with highest receptor concentrations in the limbic system, including the VMN, and areas involved in arousal such as the thalamus and cortex (Palacios *et al.*, 1981). Histamine binds to the H_1 receptor and activates $G_{q/11}$ and PLC which subsequently leads to the formation of two second messengers, DAG and IP3. IP3 releases Ca^{2+} from internal stores that can go on to activate a number of other processes. These include the opening of a cation channel, the activation of a Na^{+}- Ca^{2+} exchanger, and a block of a leak potassium conductance, all of which cause a strong depolarisation (Brown *et al.*, 2001; Haas & Panula, 2003).

H_2 receptor

The H_2 receptor, like the H_1 receptor has been shown to have high expression in the spinal cord and parts of the brain. However, unlike the H_1 receptor that has high expression in the hypothalamus, the H_2 receptor here is found in low densities (Brown *et al.*, 2001). H_2 receptors are coupled to G_S and adenylyl cyclase and generally have excitatory actions on neuronal membranes thus having similar physiological functions within the brain as H_1 (Haas

& Panula, 2003; Yanai & Tashiro, 2007). Histamine blocks a Ca^{2+} dependant K^{+} conductance which causes a long lasting after-hyperpolarisation and a subsequent increase in firing.

H_3 receptor

H_3 receptors are found only moderately within the hypothalamus with high densities found in the nucleus accumbens, olfactory and the substantia nigra. As previously mentioned H_3 receptors are auto-receptors and therefore they regulate the release and synthesis of histamine (Arrang *et al.*, 1983). They have also been termed heteroreceptors and have been shown to inhibit the release of other transmitters such as GABA, glutamate, noradrenaline and serotonin amongst others (Schlicker *et al.*, 1988; Schlicker *et al.*, 1989; Brown & Reymann, 1996; Garcia *et al.*, 1997; Brown *et al.*, 2001). The H_3 receptor is coupled to G_i/ G_o that inhibits adenyl cyclase, and thus the production of cAMP is depressed. The activation of H_3 receptors on TM neurones leads to the inhibition of high-voltage activated calcium channels (HVACCs) which within the presynaptic terminal results in the inhibition of transmitter release (Takeshita *et al.*, 1998; Brown *et al.*, 2001).

Table 1.2 Summary of the characteristics of histamine receptors

Receptor	**Location**	**Responses (Cellular and membrane responses)**
Histamine H_1	• Smooth muscle • Endothelial cells • Adrenal medulla • Heart • CNS	• Muscle contraction • Stimulation of Nitric Oxide • Endothelial cell contraction • Stimulation of hormone release • Depolarisation and increase in firing via 1) Calcium cation channel 2) Activation of a Na^{+}- Ca^{2+} exchanger 3) A block of a leak K^{+} conductance • IP3 hydrolysis leading to calcium

		mobilisation • Phosphorylation of the glutamate NMDA receptor by PKC-thus weaker Mg^{2+} block
Histamine H_2	• Gastric parietal cells • Vascular smooth muscle • Suppressor T-cells • Neutrophils • CNS • Heart	• Stimulation of gastric acid secretion • Smooth muscle relaxation • Block of Ca^{2+} dependent K+ conductance • Block of slow AHP and accommodation of firing • cAMP dependent shift of activation threshold of Ih • Inhibition of lymphocyte function
Histamine H_3	• CNS • Peripheral nerves	• Inhibition of neurotransmitter release • Inhibition of firing of TM neurones • Increase in smooth muscle voltage-dependent Ca^{2+} current

(Adapted from Hill *et al.*, 1997; Brown *et al.*, 2001)

1.12 Obesity

Disruption within the tightly controlled regulation of energy homeostasis can result in a number of medical conditions, of which obesity is the most common. Obesity is fast becoming a major health and economic burden in both developing and developed societies. The increases in availability of high caloric food in combination with a decline in daily physical activity are major factors leading to increased prevalence. The world health organisation (WHO) estimates that by 2015 approximately 2.3 billion adults worldwide will be overweight and more than 700 million will be obese. Generally people are considered to be obese if they have a body mass index (BMI; weight (kg)/ height (m^2)) that is greater than 30 kgm^2. Obesity occurs when there is an imbalance between calories consumed and exhausted and when there is a bias towards positive energy balance, thus leading to excess body fat. Of great

concern is the pathology related to obesity which can include the development of type 2 diabetes mellitus, cardiovascular disease, musculoskeletal disorders and the development of certain forms of cancers. The risks of the above health consequences as result of obesity increase as the BMI increases. The financial, political and social pressures of obesity are evident in today's society and thus it is imperative that a pharmaceutical intervention is found.

Currently, the most effective treatment for the obese, when a well balanced diet, exercise and drug treatments are all options that have been exhausted, is bariatric surgery. This involves the modification of the GT to reduce the uptake and absorption of nutrients and increase satiety levels. However, this procedure is only carried out in extreme cases. Thus, drug treatment is often important within those individuals where weight loss regimes are short-lived.

Anti-obesity drugs currently used today include, sibutramine® and orlistat® (Rubio *et al.*, 2007) and until very recently, rimonabant®, which was recently withdrawn from the market due to adverse side effects. The aminergic systems are often attractive drug targets for the treatment of obesity. For example, sibutramine is a noradrenaline and serotonin reuptake inhibitor which leads to enhanced satiety and decreased food intake (Jackson *et al.*, 1997). The H_3 receptor is also attractive as a CNS drug target, as it has limited expression in the periphery, it acts as an autoreceptor modulating its own release, and also is a neurotransmitter which has a role within energy homeostasis (Esbenshade *et al.*, 2006).

To be able to understand and delineate key pathways and ionic mechanisms that are involved within the control of energy homeostasis within systems such as the central aminergic system will help us develop an effective pharmacological intervention for obesity.

1.13 Project aims

The aim of this study was to investigate the effects of noradrenaline, histamine and differential concentrations of glucose on the electrophysiological properties, function and operation of hypothalamic Arc neurones.

Accordingly, whole-cell patch-clamp recording techniques, biocytin staining and immunohistochemistry were employed to record the electrical activity and record morphological features, respectively, of neurones located within the Arc. Specific aims included:

1. The identification of neuronal subpopulations within the Arc based on the expression of subthreshold active conductances and morphological properties that identify functionally distinct neuronal populations.
2. To describe the effects of differing concentrations of external glucose on the active membrane conductances and functional operation of Arc neurones (mimicking either a hyperglycaemic state or euglycemic state).
3. To investigate the effects of noradrenaline on the excitability of orexigenic and anorexigenic Arc neurones and establish the receptors involved.
4. To investigate the effects of histamine on the excitability of Arc neurones and determine the receptors involved.

Figure 1.1 **The central control of energy homeostasis**

A: Leptin released from adipose tissue, insulin released from the pancreas, glucose from the liver, and peptides such as ghrelin and PYY released from the gastrointestinal tract (GT) regulate energy intake through the modulation of meal size. The NTS receives peripheral vagal and sympathetic afferent inputs related to energy balance, which integrate with descending hypothalamic inputs. Within the arcuate nucleus (Arc), peripheral hormones differentially activate the anabolic or catabolic pathway; neuropeptide Y (NPY) or pro-opiomelanocortin (POMC) neurones. These neurones projects to second order neurones in the paraventricular nucleus (PVN) and the lateral hypothalamus area (LHA), where they synapse with neurones that project to the brainstem. The hypothalamus and brainstem contain reciprocal connections to produce a coordinated response to bring about changes in feeding and energy homeostasis

Figure 1.2 **Connective reciprocity between the Arc and other hypothalamic areas involved in the control of energy homeostasis**

A: Schematic drawing of the hypothalamus showing the location of the nuclei that are involved in energy homeostasis. These include the arcuate nucleus (ARC) situated at the base of the brain, the lateral hypothalamus (LH), ventromedial nucleus (VMN), paraventricular nucleus (PVN), and the dorsomedial nucleus (DMH). There are reciprocal connections between many of the nuclei that enable them to bring about a coordinated response to energy homeostasis.

Figure 1.3 **The Noradrenergic system in the rat brain**

A: A sagittal schematic of the noradrenaline system in the rat brain. Noradrenaline containing neurones present within brainstem nuclei project to all parts of the brain (blue arrow) and to the hypothalamic Arc (red arrow).

(Adapted from Guyton & Hall, 2006)

Figure 1.4 **Signal transduction pathways of the adrenoceptors (ARs)**

A: The AR family can be divided in to three main classes the α_1, α_2, and β_1- AR. These classes can be further subdivided. The α_{1-} ARs signal through the Gq/11 pathway to increase intracellular calcium. The α_{2-} ARs signal through the Gi pathway to inhibit adenyly cyclase. The β_1- ARs signal though the Gs pathway to stimulate adenyly cyclase. Thus each AR acts in a different G- protein to activate different second messenger pathways.

(Adapted from Zhong & Minneman, 1999; Hein, 2006)

Figure 1.5 **The histaminergic system in the rat brain**

A: A sagittal schematic of the histaminergic system in the rat brain. Histamine containing neurones present within the TM project to all parts of the brain (red arrows) including to the hypothalamic Arc (blue arrow).

(Adapted from Wada *et al.*, 1991)

Chapter 2

Experimental Procedures

2.1 Whole-cell patch-clamp: The Arcuate Nucleus

2.1.1 Slice Preparation

Hypothalamic slice preparations containing the arcuate nucleus (Arc) were obtained from male Wistar rats older than 5 weeks. Animals were housed under a 12/12 hour light/dark cycle and food and water were provided *ad libitum.* Animals were decapitated following cervical dislocation or were given a lethal dose of anaesthetic (isoflurane) in line with national guidelines. Following decapitation the brain was immediately removed from the cranial cavity and placed in freshly prepared oxygenated (95% O_2, 5% CO_2) ice cold (2°C - 4°C) artificial cerebrospinal fluid (aCSF). The composition of aCSF is shown in table 2.1. For experiments where 2 mM glucose-containing aCSF was used rather than 10 mM glucose-containing aCSF, glucose was replaced in equimolar quantities by D-mannitol to maintain osmolarity. The brain was trimmed to a hypothalamic block which was subsequently glued onto the tissue plate of a vibratome (Intracel series 1000, Royston, UK or Leica VT1000S, Leica Microsystems Nussloch GmbH, Nussloch, Germany) where transverse slices of 300 μm-400 μm thickness were cut. Within the slices, the Arc was defined as the area directly above the median eminance (ME) on both sides and directly adjacent to the 3rd ventricle. Slices were maintained for at least one hour at room temperature in oxygenated aCSF prior to whole cell recording.

2.1.2 Solutions

Experiments required the daily preparation of aCSF, of the following composition:

Table 2.1: aCSF composition

	10mM glucose aCSF (mM)	2mM glucose aCSF (mM)
NaCL	127	127
KCL	1.9	1.9
KH_2PO_4	1.2	1.2
$NaHCO_3$	26.0	26.0
Glucose	10	2
$CaCl_2$	2.4	2.4
$MgCl_2$	1.3	1.3
D-Mannitol	0	8

The osmolarity of the aCSF was 300-315 $mOsm.kg^{-1}$ and pH 7.3- 7.4.

Pipette solution was prepared on the day of each experiment as a 1 ml volume, from stock solutions. Solutions were prepared in advance as 10x stocks and kept at 4 °C with the exception of biocytin and Na_2-ATP which were stored at -20 °C.

Table 2.2: Standard recording pipette Solution

	(mM)
K-gluconate	140
Hepes	10
EGTA	1
KCL	10
Na_2ATP	2
Biocytin	5
Alexa 633	0.1

The pH of the resulting solution was adjusted with KOH to 7.4. The osmolarity of the pipette solution was within 5-10 mOsm kg^{-1} of the aSCF and was adjusted for hypo-osmolarity with sucrose.

2.2 Drugs

The following drugs were used in the present study: tetrodotoxin (TTX) obtained from Alomone Labs, Jerusalem, Israel. Bicuculline methochloride (BMC), 6-nitro-7-sulphamoybenzo(*f*)- quinoxaline-2,3-dione (NBQX), prazosin hydrochloride, isoproterenol, L-norepinephrine bitartate salt (monohydrate), R-phenylephrine hydrochloride, histamine-trifluromethyl-toluidine (HTMT), dimaprit dihydrochloride and imetit dihydrobromide from Tocris Cookson Ltd, UK. Idazoxan HCl, mepyramine maleate, RS100329 hydrochloride and histamine were from Sigma Aldrich, UK. UK-14,304 was from Research Biochemical

International (RBI), Ghrelin (rat) was obtained from Bachem, UK and 02484100 was a kind donation from Eli-Lilly, UK.

Those drugs (NBQX, UK-14, 304 and prazosin) that were insoluble in water were dissolved in 100% dimethylsulphoxide (DMSO) and then further diluted to the final concentration in aCSF on the day of experimentation. Final DMSO concentrations did not exceed 0.1% and appropriate vehicle controls were performed.

All drugs were bath applied to the slice by a gravity feed perfusion system from a series of 60 ml syringes with manually operable three-way taps connected with the main aCSF reservoir.

2.3 Recording procedure and data analysis

To conduct electrophysiological recordings, hypothalamic slices containing the Arc were individually transferred to the recording chamber and secured between two nylon grids. The system was constantly superfused through a gravity-fed system at a flow rate of 5-10 $ml.min^{-1}$ with oxygenated aCSF. Recording electrodes were pulled using a horizontal puller (P-97, Sutter Instrument Co, Novato, CA, USA) from borosilicate filamented thin-walled glass capillaries (GC150TF-10, Harvard apparatus LTD, Edenbridge, Kent, UK) and had resistances between 4-7 MΩ when filled with intracellular recording solution.

The 'blind' patch-clamp recording method was employed for whole-cell recordings (both current-clamp and voltage–clamp) using an Axopatch-1D amplifier (Axon Instruments, Foster City, CA, USA), in which recordings were obtained with series resistance in the range of 8-20 MΩ. Series resistance compensation was carried out as appropriate. A digital oscilloscope (Gould DS01602) was used to display the current traces online which were

sampled at 5 kH_Z and directly stored on Digital Audio Tapes (DAT, Biologic DTR-1205, Intracel, Royston, UK).

In cases where current traces were directly recorded and stored on the computer they were sampled at 10 kHz. For later offline analysis, pClamp 9 software (Axon Instruments) was used where the signal was digitised at 20 kHz. Subsequently, current-voltage relationships were produced with Clampex 9, sampled at 20 kHz. Data were filtered at 1-5 kHz for voltage-clamp studies.

Clampfit 9 (Axon Instruments) was used off-line to establish the resting membrane potential of silent and slowly active cells. In these cells there was a sufficient period of quiescence where the accurate measurement of the neuronal resting membrane potential could be obtained without interference of the activation of current associated with action potential firing. However, for a minority of cells that were too active this was impossible and therefore the low-pass readout of the recording amplifier was used (Axopatch 1D, Axon Instruments). Input resistances were calculated at steady-state membrane potential using the smallest negative current injection in the current-voltage protocol (step: amplitude 5-20 pA, duration 1200 ms, 0.2 Hz), and was calculated using Ohm's law, V=I R.

Membrane time-constants (tau) were calculated by performing a bi-exponential fit to the first membrane voltage response to a negative current step. Care was taken to perform the fits on steps in the linear portion of the current-voltage relationship.

2.4 Biocytin staining

Visualisation of whole-cell patched neurones filled with intracellular solution containing 5 mM biocytin, required the hypothalamic slices to be fixed following recording for 1-3 hours in 4% paraformaldehyde (pH 7.4) in phosphate buffered saline (PBS). The

composition of PBS is shown in table 2.3. Slices were then washed thoroughly to remove all traces of the fixative in 0.05 Tris buffer with 1% triton (Tris-Triton) and stored in the buffer for up to 2 weeks or until the day of processing. To analyse slices, they were first placed in a solution comprised of 3 % H_2O_2, 10% methanol in Tris for 30 minutes. Slices were then washed and rehydrated in Tris-Triton buffer. Consequently, the VECTASTAIN® ELITE® Avidin and Biotinylated horseradish-peroxide macromolecular complex (ABC) system was used in accordance with the manufacture's guidelines (Vector Laboratories Ltd., Peterborough, England).Staining was completed using 3,3-diaminobenzidine (DAB) and Nickel as a chromogen/ peroxide substrate that gave a black appearance to the stained neurones, according to the manufactures instructions. The slices were then dehydrated in progressive ethanol concentrations (10, 30, 50, 70, 100%) prior to clearing in methyl salicylate for at least 2 hours (majority of times slices were left overnight) in glassware before visualization of neurones. Visualisation was achieved under a microscope connected to a Zeiss AxioCam MRc camera (Zeiss Axioskop, Carl Zeiss Ltd., Welwyn Garden City, UK) which was attached to a computer running Axiovision 4.1 imaging software (Carl Zeiss Vision). Images were taken of stained neurones with different magnification powers. Using the water 40x lens photographs were taken in different focal planes and subsequently the neurones were reconstructed using CorelDraw 11 and Corel Photo Paint 11 software to reveal the full dendritic tree.

Table 2.3: Standard composition of Phosphate buffered saline

	(mM)
NaCL	137
KCl	2.7
Na_2HPO_4	8.1
KH_2PO_4	1.5

2.5 Double immunofluorescence staining for CART and Alexa 633

Recordings were obtained utilising an intracellular solution containing the fluorescent dye Alexa 633 hydrazide (100 μM; Invitrogen LTD, Paisley, UK). Post-recording, slices were fixed overnight in 0.1 M PBS containing 4% paraformaldehyde (pH 7.4) and were consequently rinsed thoroughly in Tris-buffered saline containing 1% Triton X-100 (TBS-T). Subsequently, slices were incubated in TBS-T and 4% normal goat serum (NGS; Stratech Scientific Ltd. Suffolk, UK) for 1 h under agitation. Slices were incubated overnight at 4 °C in rabbit anti-CART (55-102, Rat) serum, the primary antibody (Phoenix Pharmaceuticals, 1:1000 in TBS-T) in the presence of 2% NGS and rinsed prior to incubation in goat anti-rabbit antibody conjugated to a fluorophore Cy2 (absorption peak 492mm, emission peak 510nm), the secondary antibody (Jackson ImmunoResearch Laboratories 1:200). Finally, slices were washed in TBS before being mounted and covered with Prolong® Antifade (Molecular Probes). The sections were examined using a confocal laser scanning microscope (Leica SP2 linked to a Leica DM RE7 upright microscope).

The current antibodies have been previously been used, see Dun *et al*, 2000; van den Top *et al*, 2007. The appropriate controls were carried out, omitting both primary and then secondary antibodies. Lasers were switched off on each channel to exclude the possibility of 'bleed' through.

2.6 Statistical Analysis

Statistical analysis was performed using Excel 2003 (Microsoft) and Instat (Graphpad Software Inc., San Diego, CA, USA) with all values being expressed as a mean ± SEM. Numbers of observations are stated as *n* values .Statistical significance was determined using

either student's two-tailed t-tests, paired or unpaired as appropriate or one-way ANOVA's. The post-hoc test performed was the Dunn test followed by the Friedman test which is a non-parametrical statistical test.

Chapter 3

The electrophysiological and morphological properties of rat hypothalamic arcuate nucleus neurones *in vitro*

3.1 Introduction

The hypothalamic arcuate nucleus (Arc) is an essential nucleus implicated in forebrain pathways which regulate a variety of homeostatic circuits and neuroendocrine functions (Beck *et al.*, 2001; Bouret *et al.*, 2004). These include the regulation of energy metabolism (Williams *et al.*, 2000; Cone *et al.*, 2001; Williams *et al.*, 2001), reproduction (Gottsch *et al.*, 2004) and the body's adaptation to stress (Bell *et al.*, 2000) amongst other functions.

Neurones of the Arc are innervated by a number of afferent inputs from multiple hypothalamic nuclei, including the suprachiasmatic nucleus (SCN), paraventricular nucleus (PVN), lateral hypothalamic area (LHA) and dorsomedial nucleus (DMN; Chronwall, 1985). Some of the neuropeptides and neurotransmitters contained in the nerve terminals innervating the Arc include orexin, serotonin, γ-aminobutyric acid (GABA), glutamate and noradrenaline (NA; Sawchenko & Swanson, 1981; Chronwall, 1985; Elias *et al.*, 1998; Hentges *et al.*, 2004; Horvath *et al.*, 2004). The efferent targets are equally as diverse and include outputs to the median eminance (ME), PVN, nucleus of the tractus solitarius (NTS), and the LHA (Chronwall, 1985; Baker & Herkenham, 1995). Furthermore, neuropeptidergic expression within the Arc reveals an extremely diverse chemical phenotype. Neuropeptides include neuropeptide Y (NPY), pre-pro-opiomelanocortin (POMC), agouti-related peptide (AgRP), cocaine and amphetamine regulated transcript (CART), urocortin, galanin and ghrelin, amongst others (Chronwall, 1985; Melander *et al.*, 1986; Koylu *et al.*, 1997; Reyes *et al.*, 2001; Lu *et al.*, 2002).

The Arc, being situated directly above the ME, lies in close proximity to a compromised blood brain barrier (BBB) and is therefore accessible to circulating peripheral signals (Broadwell *et al.*, 1983; Ganong, 2000) thus forming a site for convergence of both central and peripheral signals (Cone *et al.*, 2001). However, despite this knowledge of the

functional organisation of the Arc, it is yet to be elucidated how the neuronal network at a cellular level within the Arc functions to detect, integrate and generate appropriate output and behavioural change to counteract perturbations in energy status, both in the short and long term.

A study of Arc neurones and their biophysical mechanisms that ultimately control electrical excitability and neurotransmitter/neuropeptide release is yet to be undertaken. Active and passive membrane properties of a neurone shape its function, integration and computational capability. Passive membrane properties of a neurone can be useful in indicating the size of a neurone by studying its membrane time-constant (tau). Voltage-dependent conductances can contribute to non-linearity in the current-voltage relation of neurones that strongly modify their responsiveness with important functional consequences. It has been suggested that subthreshold currents (i.e.currents with activation thresholds below that of the voltage-gated Na^+ channel) shape electrical activity, that is changes in spontaneous firing and the membrane potential of individual neurones (Gulledge *et al.*, 2005). Such a subthreshold active conductance that contributes to the neuronal output is the hyperpolarisation-activated cation conductance (I_h). This current has been suggested to be involved in establishing the resting membrane potential of hypothalamic neurones (Akasu *et al.*, 1993). It has also been shown to act as a pacemaker potential to time action potential firing (Pape & McCormick, 1989) and hence ultimately contribute to the neurone's output. Evidently, examining and understanding the expression of active (ionic) conductances expressed by Arc neurones would be a critical step towards understanding the functional operation of its circuits.

Investigating the morphology of Arc neurones gives an indication of soma location, size and dendritic number and length. Shapes and sizes of dendrites of different neurones are extremely diverse (Ramon-Moliner, 1967). Arc neurones have been shown to have a simple dendritic tree (Bodoky & Rethelyi, 1977; van den Pol & Cassidy, 1982). Dendritic

arbores give an indication of the neurones receptive field and projection targets and ultimately detect circulating factors and hence form the neurone's inputs.

Examining both subthreshold active conductances and morphological features of Arc neurones, this study has attempted to develop a functional classification of hypothalamic Arc neurones which will ultimately be used as a basis for further studies exploring the functionality of these neurones.

Several investigations (Tasker & Dudek, 1991; Armstrong, 1995; Pennartz *et al.*, 1998; Stern, 2001) have used electrophysiological recording techniques in an attempt to characterise and hence classify neuronal populations in distinct and complex hypothalamic nuclei including the SCN, PVN and the supraoptic nucleus (SON). In combination with electrophysiology they have also studied the morphology of the neurones and their dendritic configuration (Armstrong, 1995; Pennartz *et al.*, 1998; Stern, 2001) in order to provide a more comprehensive classification of the respective nuclei However, these classifications have described a very limited number of neuronal populations, the functional significance of which is unclear. One would assume that with the diversity of expression of neuropeptides and the heterogeneity of inputs and outputs within the Arc that this could be reflected in diverse electrophysiological characteristics. Thus, does neuropeptidergic heterogeneity imply electrophysiological and/or morphological heterogeneity?

Burdakov has previously attempted to electrophysiologically classify the neurones of the Arc within the mouse and described 3 distinct neuronal subtypes based solely on electrophysiology (Burdakov & Ashcroft, 2002). Fioramonti *et al.*, (2004), observed five different electrophysiological cell types within the mouse and again did not correlate this with morphological phenotypes.

This present study established the main subthreshold active conductances expressed by Arc neurones and used these as criteria to group neurones. Electrophysiology is an

important tool which will be used as a parameter to classify the heterogeneity of Arc neurones based on their expression of subthreshold active conductances. The membrane conductances that ultimately determine the pattern and level of activity in rat Arc neurons have not yet been described. The release of neuropeptides from the Arc could be dependent upon the electrical activity of these neurones as described for the release of vasopressin (Vp) from hypothalamic magnocellular neurones (Dutton & Dyball, 1979). Arc neurones have also been previously characterised according to their morphological appearances (Bodoky & Rethelyi, 1977; van den Pol & Cassidy, 1982) and studies have analysed neurones based upon their location and dendritic branching.

Heterogeneity of neuropeptidergic expression, inputs and outputs to and from the Arc is to be expected. However, to-date, no study has been undertaken at the level of the Arc where both electrophysiological and corresponding morphological properties have been characterised and attempts made to correlate these fundamental properties in creating a functional classification of rat hypothalamic Arc neurones. This project set out to address this issue. This characterisation of Arc neurones builds on previous work carried out by van den Top (2002).

3.2 Results

3.2.1 General electrophysiological membrane properties

In the present study the electrophysiological properties of 254 Arc neurones were obtained that were subsequently studied for their morphology with the use of biocytin labelling. The nucleus of each individual neurone resided within the Arc which was confirmed by morphological analysis. Figure 3.1Ai shows a schematic representation of the location of all Arc neurones recorded. Evaluation of general properties of the Arc neurones included analysing action potential spike threshold, amplitude and duration. How these properties were calculated is described in Figure 3.1Bi. A summary of the basic membrane properties of all 254 neurones recorded are presented in Table 3.1. The corresponding frequency distribution histograms are represented in Figure 3.2.

The mean resting membrane potential and input resistance were -46.7 ± 0.4 mV (range -36 to -66 mV) and 1669 ± 52 MΩ (range 415 to 4667 MΩ) respectively (n=254). The membrane time constant (tau) was calculated to be -48.5 ± 1.8 ms (range 7.3 to 142 ms). The tau value was obtained by carrying out bi-exponential fits to the membrane voltage charging curves induced by a hyperpolarising rectangular current step, with the use of Clampfit 9 (Axon instruments). At first sight, the frequency histogram summarising the distribution of the different time-constants skews to the right showing a large tail which may represent different populations thus Arc neurones may not be homogeneous in their morphological properties. The mean absolute action potential threshold and spike amplitude amounted to -29.9 ± 0.3 mV (range -17 to -46 mV) and 90.1 ± 0.9 mV (range 54 to 119 mV) respectively with an average spike duration at threshold of 3.2 ± 0.0 ms (range 1.6 to 7 ms).

Table 3.1: Membrane properties of Arc neurones: A Table summarising the general electrophysiological membrane properties of the recorded neurones used within this study

Table 3.1 Passive and active membrane properties of Arcuate nucleus neurones			
Parameter	**Mean ± SEM**	**Max**	**Min**
Resting membrane potential (mV)	-46.7±0.4	-36	-66
Input resistance (MΩ)	1669±52	4667	415
Membrane time constant (ms)	48.5±1.8	142	7.3
Action potential spike threshold *	-29.9 ± 0.3	-17	-46
Action potential spike amplitude (mV) *	90.1 ± 0.9	119	54
Action potential spike duration (ms) *	3.2 ± 0.0	7	1.6
n= 254 ; * n=243			

3.2.2 Subthreshold Active conductances expressed by Arc neurones

This study focused in detail on the expression of subthreshold active conductances to characterise and thus classify Arc neurones. In order to explore the active conductances expressed by Arc neurones, current-voltage relationships (I/V) were carried out on each individual neurone. This was shown as superimposed traces of membrane responses to hyperpolarising and depolarising current injections of constant increment. It became apparent that Arc neurones expressed a range of active conductances, some expressing more than one. In the absence of any subthreshold active conductance, the injection of hyperpolarising current injection pulses induced membrane potential responses directly proportional to the amount of current injected, thus showing a linear relationship. The identification, characterisation and analysis of the active conductances of Arc neurones are described in Figure 3.3.

3.2.2.1 I_{an} - Anomalous inward rectification

118/254 (46%) of Arc neurones exhibited a decrease in membrane responses (Figure 3.3Ai) compared to those that expressed no active conductance and showed a linear relationship. The decrease in input resistance at more negative membrane potentials was shown by a decrease in the slope of the plot of the I/V relationship (Figure 3.4Aii) and was shown to be instantaneous and non-inactivating. This active conductance has been described previously in other neurones of the CNS (Constanti & Galvan, 1983; Tasker & Dudek, 1991) and is called an anomalous inward rectification. These cells had a mean resting membrane potential and input resistance of -46.6 ± 0.5 mV and 1827 ± 115 MΩ, respectively. At a mean membrane potential of -99.4 ± 0.6 mV these cells displayed a reduction in input resistance of 32.3 ± 1.6 % relative to the input resistance near the mean resting membrane potential of -46.6 ± 0.5 mV. The threshold for activation as estimated from current-voltage relationship amounted to -84.4 ± 0.7 mV (range -63.5 to -97.5 mV).

3.2.2.2 I_h - Hyperpolarisation activated inward current

101/ 254 (40%) of Arc neurones displayed a voltage- and time-dependent inward rectification, which presented as a depolarising 'sag' of the membrane potential response when injected with negative current (figure 3.3Aii). This 'sag' becomes more prominent at more negative potentials. This characteristic 'sag' of the inward rectification resembles the previously described hyperpolarisation-activated non-selective cation channel or H–current (Halliwell & Adams, 1982; Akasu *et al.*, 1993; Pape, 1996). These cells had a mean membrane potential and input resistance of -47.7 ± 0.7 mV and 1746 ± 121 MΩ, respectively. To quantify the activation of I_h, the difference between instantaneous and steady state membrane potential during the injection of a rectangular wave negative current step was used (Figure 3.3Aii). At a mean membrane potential of -101.7 ± 1.4 mV the amplitude of the

hyperpolarising sag amounted to 4.9 ± 0.4 mV resulting in a steady-state decrease in input resistance of 11.3 ± 0.7 %. The mean threshold for activation, calculated by averaging the membrane potential of the I/V plot in which the rectification was first apparent, was -69.6 ± 1.1 mV (range -52.0 to 99.9 mV, Figure 3.7Aii).

3.2.2.3 I_a- A-like transient outward rectifier

16/254 (6.3%) of cells displayed a conductance characterised by a delayed return to the resting membrane potential upon termination of a negative current injection (Figure 3.3Aiii). This conductance resembled the A-like transient outward rectifier noted in other neurones and has been previously reported within the Arc (Connor & Stevens, 1971; Miyazaki *et al.*, 1996; van den Top *et al.*, 2004). The magnitude of the membrane hyperpolarisation induced by current injections determined the amplitude of the conductance with the amplitude increasing at more negative membrane potentials. These cells had a mean membrane potential and input resistance of -48.4 ± 1.1 mV and 1237 ± 108 MΩ, respectively. The average inactivation time was 1106 ± 137 ms, measured from the termination of the negative current injection until the return of the membrane potential to baseline/control levels. The amplitude of the conductance was 5.8 ± 0.7 mV calculated at half-decay time.

3.2.2.4 T-type-like calcium conductance

180/254 (71%) of neurones exhibited a rebound depolarisation on termination of negative current injection (Figure 3.3Aiiii). This rebound potential is similar to that described before in the CNS mediated by T-type calcium channels (Llinas & Yarom, 1981). In order to quantify this conductance the amplitude of the rebound depolarisation was measured. This was carried out by calculating the difference in membrane potentials at the peak of the rebound depolarisation and at rest. In some neurones the rebound spiking lasted the duration

of the T-type activation induced depolarisation and were excluded from this study. From a mean resting membrane potential of -49.2 ± 0.6 mV (n=130), the amplitude of the rebound depolarisations amounted to 10.9 ± 0.4 mV (n=130). These cells had a mean membrane potential and input resistance of -46.4 ± 0.5 mV and 1782 ± 82 MΩ, respectively.

3.2.3 Eight electrophysiological distinct neuronal clusters

The above described active conductances were used as parameters to separate and distinguish between potentially different functional neuronal populations. These parameters led to the identification of 8 distinct electrophysiological groups, expressing none or a combination of, one to three, active conductances. The 8 electrophysiologically defined populations were termed clusters (Pennartz *et al.*, 1998). This term is often used to define a group that possess the same or similar features gathered or occurring closely together. An overview of the active conductances expressed by each defined neuronal cluster is shown in Table 3.2.

3.2.3.1 Cluster 1

Cluster 1 neurones were identified by the expression of I_{an} and the absence of any other active conductances used to classify neurones within the present study, resulting in a non-linear I/V relationship (n=23; Figure 3.4). The mean membrane potential and input resistance of the cluster 1 neurones was -47.8 ± 1.4 mV (range -39 to -64 mV) and 1802 ± 201 MΩ (range 556 to 4664 MΩ) respectively. Distribution histograms summarising the passive membrane properties for cluster 1 is shown in Figure 3.4Bi-iii. The tau amounted to 54.4 ± 4.5 ms (range 11.9 to 82.4). All these values are expressed in Figure 3.12 for cluster 1 and all subsequent clusters for clarity and comparison. The membrane potential at which an action potential was generated was termed the absolute spike threshold (Figure 3.1 Bi). In

cluster 1 neurones this was on average -31.3 ± 1.2 mV (n=23). The mean amplitude and duration of the action potential was 94.3 ± 2.4 mV and 2.9 ± 0.2 ms respectively (n=23). The I_{an} accounted for a 29.6 ± 3.5 % reduction in input resistance at a membrane potential of -100.2±1.1 mV relative to the input resistance calculated at rest. The threshold for activation as estimated from current-voltage relationships amounted to -86.0 ± 1.1 mV (range -76.0 to -97.5, Figure 3.4Aii).

3.2.3.2 Cluster 2

Cluster 2 neurones were identified as expressing a visible I_{an} and I_a – like conductance. (n=16; Figure 3.5). This subgroup of neurones has been previously described as Arc pacemaker neurones. They either spontaneously or in the presence of the orexigens orexin/ghrelin show pacemaker activity and are inhibited by leptin, they have been identified as NPY/AgRP neurones (van den Top *et al.*, 2004). The expression of the active conductance I_{an} resulted in a nonlinear I/V relationship (n=16, Figure 3.5Ai-ii). The mean membrane potential and input resistance of the cluster 2 neurones was -47.8 ± 1.2 mV (range -42 to -56 mV) and 1172 ± 95 MΩ (range 590 to 1742 MΩ), respectively. The tau amounted to 38.4 ± 4.4 ms (range 11.9 - 82.4ms). Distribution histograms summarising the passive membrane properties for cluster 2 is shown in Figure 3.5Bi-iii. The mean spike threshold, mean amplitude and duration of the action potential were -30.5 ± 1.1 mV, 93.2 ± 2.7 mV and 3.1 ± 0.2 ms, (n=14), respectively (all values for general membrane properties are expressed in Table 3.3 for cluster 2 and all other clusters). The I_{an} induced a 37.0 ± 4.3 % (n=14) reduction in input resistance at a membrane potential of -93.9 ± 1.1 mV relative to the input resistance calculated at rest. The mean estimated threshold for activation of I_{an} was -82.6 ± 1.7 mV (range -73.4 to -89.6 mV, Figure 3.5Aii,) estimated from the current-voltage relationships. The expression of I_a resulted in a delayed return to baseline following

termination of a negative current injection (Figure 3.3 Aiii). The average inactivation time was 1106 ± 137 ms (n=16), measured from the termination of negative current injection until the return of the membrane potential to baseline/control levels. The amplitude of the conductance was 5.8 ± 0.7 mV calculated at half decay-time as the difference in membrane potentials during activation of the conductance and at rest.

3.2.3.3 Cluster 3

Cluster 3 neurones were characterized by the absence of any obvious subthreshold active conductances (n=13; Figure 3.6Ai). The I/Vs of cluster 3 neurones were therefore linear, showing a directly proportional relationship between injected current and membrane response (Figure 3.6Aii). The mean membrane potential and input resistance of the cluster 3 neurones was -48.9 ± 2.1 mV (range -39 to -61 mV) and 1587 ± 262 MΩ (range 665 to 3412 MΩ), respectively (n=13). The value of tau was 27.3 ± 3.1 ms (range 14 to 49.5 ms; Figure 3.12). The membrane potential at which an action potential was generated was (absolute spike threshold) on average -31.2 ± 1.5 mV (n=13). The mean amplitude and duration of the action potential was 90.5 ± 3.3 mV and 2.9 ± 0.1 ms respectively (Table 3.3).

3.2.3.4 Cluster 4

Neurones that expressed a time- and voltage-dependent inward rectification, visible as a 'sag' (I_h) in the membrane in response to negative current steps were termed cluster 4 neurones (n=22; Figure 3.7). The expression of the I_h resulted in a decrease in the steady state membrane response at negative holding potential resulting in a non-linear I/V relationship relative to the membrane responses at instantaneous (Figure 3.7Aii). The mean membrane potential and input resistance of these neurones was -48.8 ± 1.7 mV (range -38 to -65 mV) and 1407 ± 159 MΩ (range 415 to 3350 MΩ), respectively. The membrane time-

constant amounted to 38.1 ± 6.7 ms (range 11.9 to 138.8; see Figure 3.12). Distribution histograms summarising the passive membrane properties for cluster 4 is shown in Figure 3.7Bi-iii. The mean spike-threshold, mean amplitude and duration of the action potential were -28.4 ± 0.8 mV, 83.8 ± 3.5 mV and 2.9 ±0.1 ms, respectively (Table 3.3). At a mean membrane potential of -104.1 ± 1.1 mV the amplitude of the hyperpolarising sag amounted to 7.4 ± 0.7 mV equivalent to a steady-state decrease in input resistance of 13.6 ± 1.2% (n=22). The mean threshold for activation, calculated by averaging the membrane potential of the current-voltage plot in which the rectification was first apparent, was -69.3 ± 3.1mV (range -57.5 to 99.9 mV, Figure 3.7Aii,).

3.2.3.5 Cluster 5

Cluster 5 neurones were defined as expressing time- and voltage-dependent inward rectification (I_h) and a T-type calcium-like conductance (n=45, Figure 3.8Ai). The mean input resistance and resting membrane potential of these cells was 1767 ± 117 MΩ (range 593 to 4000 MΩ) and 47.1 ± 0.9 mV (range -39 to -66 mV), respectively. Charging of these neurones resulted in a membrane time-constant of 49.9 ± 5.1 ms (range 12.4 to 142.3 ms; Figure 3.12;). Distribution histograms summarising the passive membrane properties for cluster 5 is shown in Figure 3.8Bi-Biii. The absolute threshold for action potential firing was -29.1 ± 0.8 mV with a mean amplitude and duration of 83.3 ± 1.6 mV and 3.3 ± 0.1 ms, respectively (Table 3.3). At a mean membrane potential of -104.8 ± 1.0 mV the amplitude of the hyperpolarising sag amounted to 6.4 ± 0.5 mV equivalent to a steady-state decrease in input resistance of 11.5 ± 0.9 % (n=44). The mean threshold for activation, calculated by averaging the membrane potential of the current-voltage plot in which the rectification was first apparent, was -70.0 ± 0.9 mV (range -52.0 to 86.9 mV, Figure 3.8Aii). The activation of the T-type calcium conductance resulted in a mean membrane depolarisation of 11.7 ± 1.0 mV (range 3.7 to

23.5.9 mV) following negative current injection from a membrane potential of -48.7 ± 1.2 mV (n=35).

3.2.3.6 Cluster 6

Cluster 6 neurones only expressed the T-type like calcium conductance (n=56, Figure 3.9Ai). The average resting membrane potential and input resistance of these neurones was -45.4 ± 0.8 mV (range -38 to -64 mV) and 1523 ± 101 MΩ (range 543 to 3433 MΩ; Figure 3.12). The membrane time-constant for this group of neurones had a mean value of 41.3 ± 3.3 ms (range 7.3 to 125 ms). Distribution histograms summarising the passive membrane properties for cluster 6 is shown in Figure 3.9Bi-iii. The mean spike threshold, mean amplitude and duration of the action potential were -29.9 ±0.6 mV, 87.4 ± 2.0 mV and 3.5 ±0.1 ms, respectively (Table 3.3) The activation of the T-type like calcium conductance induced a mean rebound membrane depolarisation of 9.5 ± 0.6 mV (range 23.1 to 4.1 mV) following the break in negative current injection from a mean resting membrane potential of -49.6 ± 0.9 mV (n=51).

3.2.3.7 Cluster 7

Cluster 7 neurones characteristically expressed the conductances I_{an} and the T-type calcium-like conductance (n=45, Figure 3.10Ai). The average resting membrane potential and input resistance of these neurones was -45.3 ± 0.7 mV (range -36 to -54 mV) and 2036 ± 148 MΩ (range 760 to 6350 MΩ), respectively (Figure 3.12). The mean membrane time-constant for cluster 7 neurones amounted to 54.4 ± 3.6 ms. The threshold for action potential firing was observed at -29.3.± 0.6 mV with an action potential amplitude and duration of 93.4 ± 1.9 mV and 3.2 ± 0.1 ms, respectively (Table 3.3) The I_{an} –induced a 35% reduction in input resistance at a holding potential of -98 ± 0.2 mV relative to the input resistance calculated at

rest. The threshold for activation as estimated from current-voltage relationship amounted to -83.6 ± 0.9 mV (Figure 3.10Aii, range -70.7 to -93.5).The activation of the T-type calcium conductance resulted in a mean rebound membrane depolarisation of 11.4 ± 0.9 mV (range 3.5 to 24.8 mV) following negative current injection from a membrane potential of -50.1 ± 1.0 mV .

3.2.3.8 Cluster 8

The final cluster was characterised as expressing a time- and voltage-dependent inward rectification that was visible as a 'sag' in the membrane in response to negative current injections; ($I_{h)}$ .and the presence of an anomalous inward rectifier (I_{an}) and a T-type-like calcium conductance (n=34, Figure 3.11Ai). Values were taken instantaneously and not at steady- state, thus to avoid contribution from other subthreshold active conductances. The average resting membrane potential and input resistance of these neurones was -46.6 ± 1.2 mV (range -34 to -61 mV) and 1589 ± 146 MΩ (range 676 to 4667 MΩ, n=34,). The membrane time-constant amounted to 66.3 ± 4.9 ms (Figure 3.12; range 24 to 137 ms). The threshold for action potential firing was observed at -29.5 ± 0.8 mV with an action potential amplitude and duration of 95.6 ± 2.3 mV and 2.9 ± 0.1 mV, respectively (Table 3.3). The I_{an} – induced a 32% reduction in input resistance at a holding potential of -100.6 ± 1.1 mV relative to the input resistance calculated at rest. The threshold for activation as estimated from current-voltage relationship amounted to -85.1 ± 1.6 mV (Figure 3.11Aii, range -63.5 to -95.7). At a mean membrane potential of -99.4 ± 1.0 mV the amplitude of the hyperpolarising sag amounted to 3.4 ± 1.4 mV equivalent to a steady-state decrease in input resistance of 9.6 ± 0.9 %. The mean threshold for activation, calculated by averaging the membrane potential of the current-voltage plot in which the rectification was first apparent, was -69.1 ± 2.1 mV (Figure 3.11Aiii, range -52.5 to 94.2 mV). The activation of the T-type calcium-like

conductance resulted in a mean rebound membrane depolarisation of 12.4 ± 1.7 mV (range 3.0 to 24.5 mV) following negative current injection from a membrane potential of -47.0 ± 1.3 mV (n=15). Distribution histograms summarising the passive membrane properties for cluster 8 neurones is shown in Figure 3.11Bi-iii

3.2.4 Statistical comparison of the general membrane properties of the different classified clusters

ANOVAs were carried out to analyse the difference in membrane potentials, input resistance and membrane time-constant between the differential clusters. (Means are shown for each cluster; Figure 3.12). Between cluster 1 and all other clusters there was no significant difference in membrane potential (P=0.2). Cluster 1 neurones varied in mean input resistance significantly to the mean input resistance of cluster 2 neurones (P<0.05). The membrane time constant observed for cluster 1 neurones did not differ significantly from other clusters. Statistical differences between each cluster are summarised in Table 3.5.

Cluster 2 neurones did not differ significantly in mean membrane potentials from other neurones; it did however differ in input resistance and the membrane time constant. Input resistance for cluster 2 neurones differed from the mean input resistance for clusters 1 and 7 (P<0.05). The mean membrane time constant for cluster 2 neurones also varied significantly from cluster 8 neurones (P <0.05).

Statistically significant differences were observed between cluster 3 and clusters 7 and 8. These differences were observed in the membrane time-constant value where clusters 7 and 8 had a significantly longer charging time (P<0.05 and P<0.001, respectively).

There was no significant difference in input resistance or membrane potential between cluster 4 neurones and the other 7 groups of electrophysiological defined clusters.

Cluster 4 neurones varied significantly from cluster 8 neurones in their mean membrane time-constant (P<0.01), cluster 8 neurones having a significantly longer time-constant.

Cluster 6 neurones were significantly different to cluster 8 cells in their Tau value (P<0.001). Cluster 8 neurones had a much longer charging time than cluster 6 cells. Cluster 6 did not vary significantly in its mean membrane potential or input resistance from any other cluster.

Cluster 7 exhibited a significantly larger input resistance then cluster 2 neurones (P<0.05). Cluster 7 neurones also displayed a significantly longer charging time than cluster 3 neurones (P< 0.05) hence giving a larger mean membrane time-constant value.

Statistically significant differences were observed between cluster 8 and clusters 2,3,4,6. The tau was significantly longer than that observed for cluster 2 (P<0.05), cluster 3 (P<0.001), cluster 4 (P<0.01) and cluster 6 (P<0.001).

3.2.5 Morphology- Four distinct morphological groups

A total of 254 Arc neurones were electrophysiologically recorded from the Arc and subsequently processed and visualised for biocytin staining. Figure 3.1 Ai shows a schematic representation of the location of all 254 neurones recorded within the Arc. The neurones were recorded in all areas of the defined 'barrier' of the Arc. Neurones were pictured and analysed for their general features, which included the size of the soma (width and length both measured), origin, projection and length of primary (Figure 3.13). To access the direction in which the Arc neurones were sending their projections (axons) would have been a great insight into which and how Arc neurones interact with other hypothalamic nuclei. Unfortunately this study was unable to reliably visualise axons and thus provide an appropriate functional

context for the properties of axons; this was due to the absence of numbers for defined axons and also axonal trajectory could not be seen clearly on each cell.

There was great variance in morphology of the Arc neurones, origin and direction of projection of primary dendrites showed significant diversity. Some neurones also displayed secondary dendrites. Given such complexity it was necessary to establish an overarching classification. Thus, stained neurones were separated on the basis of the number and origin of primary dendritic projections. Soma size and shape were not used as measures to separate neurones, diversity in size was not significant enough between each neurone to be used as a parameter to separate out neurones, and hence functionality. However in the overall analysis it was noted that some clusters had greater mean membrane time-constants (tau) than others which would theoretically equate to larger cell bodies (cluster 8). Dendritic orientation was also excluded from this study. It was noted however that dendrites projected from the soma in every direction throughout the Arc.

The criteria used resulted in the compilation of 4 distinct morphological groups. Morphology group A, was made up of neurones with a single primary dendrite (Figure 3.17Aii). Group B, included neurones displaying two primary dendrites originating from opposite sides of the soma (bipolar; Figure 3.17Bii.) Group C was made up of neurones with 2 primary dendrites not-originating from opposing sides of the cell body (Figure 3.18Aii). Finally, morphology group D, was made up of neurones that displayed 3 or more primary dendrites (Figure 3.18Bii).

With this criteria in place for each morphological subtype, 58/254 neurones (22.8%) were categorised morphologically as group A (Figure 3.14). The mean width and length of the soma of this group of neurones amounted to 12.4 ± 0.4 µm and 16.9 ± 0.4 µm respectively, giving a mean surface area of 218 ± 14 μm^2. The length of the single primary dendrite

amounted to 202 ± 14 µm (n=58), and the most common site of projection was dorsally (n=35; 60%). Collating the general electrophysiological membrane properties of these neurones gave a mean membrane time-constant, resting membrane potential and input resistance of 44.1 ± 3.3 ms, -46.2 ± 0.8 mV and 1683 ± 97 MΩ (n=58), respectively (summarised in Table 3.4).

The largest group morphologically was group B, comprising 41% (Figure 3.14) of neurones (104/254). The mean soma width and length were 13.1 ± 0.3 µm and 17.7 ± 0.4 µm, respectively giving a mean soma surface area of 240.2 ± 9.6 μm^2. The mean sum of the total bipolar dendritic length amounted to 262 ± 15 µm (n=104). Total dendritic length refers to the sum total of the entire primary dendritic tree, after reconstruction as a 3D image. Neurones most commonly had the combination of dendrites projecting ventrally and dorsally (58.6%). Analysing the passive membrane properties of these neurones gave a membrane time-constant, resting membrane potential and input resistance of 46.9 ± 2.8 ms, -46.7 ± 0.6 mV and 1669 ± 95 MΩ respectively (n=104; Table 3.4).

50/254 neurones (20%) were categorised as group C thus having 2 primary dendrites not projecting from opposite sides of the soma. This group had a mean total dendtric length of 280 ± 20 µm. The mean width and length of the cell bodies of these neurones was 12.8 ± 0.5 µm and 17.4 ± 0.7 µm respectively giving a mean surface area of 234.9 ± 18.2 μm^2. Neurones most commonly had the combination of dendrites projecting dorsally and laterally (66%). The membrane time constant, resting membrane potential and input resistance amounted to 54.9 ± 4.5 ms, -47.7 ± 0.9 mV and 1866 ± 134 MΩ, respectively (n=50; Table 3.4).

Group D neurones compromised 17% of neurones stained and analysed (43/254). The mean width and length of the cell bodies amounted to 14.3 ± 0.6 µm and 18.6 ± 0.7 µm respectively, a mean surface area of 276.7 ± 18.8 μm^2. The mean sum of primary dendrites

amounted to 343 ± 27 µm (n=43). The membrane time-constant, resting membrane potential and input resistance amounted to 51.8 ± 4.2 ms, -46.5 ± 1.0 mV and 1463 ± 105 MΩ, respectively (n=43; Table 3.4)

Performing ANOVAs shows that there was no significant difference in the general properties of these different morphological defined groups. There is no significant difference in membrane potential (P=0.74), membrane resistance (P=0.15) and the membrane time-constant (P=0.20). Although not using soma size as a parameter to separate out neurones it was noted that the mean surface area of those neurones classified as morphology group A were significantly different to those classified as morphology group D (P<0.05). As would be expected comparing the sum of primary dendrites shows that there is significant differences between groups. The difference in monopolar neurones and multipolar neurones is considered extremely significant (P<0.001).

3.2.6 Morphology and electrophysiology

At this point in the study 8 electrophysiological groups have been defined, along with 4 defined morphological groups. The next step was to combine the two sets of data and analyse for any correlation between groups and clusters. Figure 3.15 shows each individual morphology group and how it was made up relative to each electrophysiological cluster as a percentage of all those patched. Figure 3.16 displays each cluster group and what percentages of those neurones are defined in each morphological group. Thus, morphology group A; neurones that were monopolar consisted of a majority of cluster 6 (31.0%) neurones followed closely by cluster 5 (25.9%) neurones. Few cluster 1, (1.7%) or 2 (1.7%), neurones were identified as being monopolar. Group B included all electrophysiological clusters and was the biggest morphological group (n=104). Neurones that were bipolar were most commonly defined as cluster 6/7 (18.4%) neurones. The least electrophysiological cluster

contributing to this morphological group was clusters 2 and 3 (7.8%). Neurones that were composed of 2 primary dendrites most commonly were defined as cluster 5 (24%) and cluster 7 (24%) neurones. There were no cluster 4 neurones making up this group. Group D; multipolar neurones was made up of a majority of cluster 6 neurones (25.6%) and cluster 8 neurones (18.6%). No cluster 3 neurones were identified in this latter morphological group.

Electrophysiologically 8 distinct groups were identified with differential expression of different subthreshold active conductances (Table 3.2). Cluster 1 neurones were predominately made up of bipolar neurones (60.7%; see figure 3.16) thus displaying 2 primary dendrites protruding from opposing ends of the soma. A large number of bipolar neurones were located ventro-medially (Figure 3.19A). These neurones predominately had dendrites projecting in a combination of either medial and lateral (21.4%) or dorsal and ventral (57.1%) orientation (Figure 3.19Bi/Bii). 62.7% neurones were described as having an oval soma. Cluster 1 neurones were also seen to be multipolar (30.4%) located more dorsally than those neurones that were bipolar. Multipolar neurones were typically seen as displaying the primary dendrites projecting dorsally and a third dendrite projecting ventrally, giving a characteristic 'fork' appearance (Figure 3.19Biii). Figure 3.16 shows each individual electrophysiological defined cluster and how it was made up relative to each morphological group as a percentage of all those recorded.

Cluster 2 neurones have been previously been suggested to be a functionally homogenous population with its linear response to orexigens with spontaneous pacemaker-like activity (van den Top *et al.*, 2004). These neurones have predominantly 2 primary dendrites either originating in a bipolar manner or non-bipolar manner. Neurones that had 2 primary dendrites (morphology group B and C) had a majority of dendrites projecting in the combination of dorsally and ventrally (50%; Figure 3.20Bi). Cluster 2 neurones occasionally

appeared multipolar with the most number of dendrites being 3. Despite cluster 2 neurones having neurones in 3 distinct morphological groups (B, C, D) they showed distinct distribution in location within the Arc (Figure 3.20A), all being located in the ventromedial region. As seen in Figure 3.20Bi, these bipolar neurones often showed secondary dendrites (42.8%)

Cluster 3 neurones that display no active subthreshold conductances morphologically showed predominately 2 primary dendrites, again being bipolar or non-bipolar. These neurones typically had dendrites projecting dorsally and ventrally (58.3%) or dendrites projecting medially and ventrally (25%; Figure 3.21Bi/Bii) 33.3% of neurones displayed secondary dendrites. Cluster 3 neurones were not multipolar neurones.

Cluster 4 neurones did not form part of the morphology group C. Cluster 4 neurones were mainly bipolar or monopolar, and were spread throughout the Arc with no distinctive location (Figure 3.22A). Monopolar, cluster 4 neurones had dendrites that projected in 66.6% of cases laterally (Figure 3.22Bi). Those neurones that were bipolar were seen to have at least one dendrite projecting dorsally (Figure 3.22Bii).

Cluster 5 neurones were observed to have a complex morphology. Cluster 5 neurones were found to be monopolar, bipolar, display 2 primary dendrites and be multipolar, and thus were observed in all morphological subgroups. Those cluster 5 neurones that were multipolar were observed to have a relatively lateral location within the Arc, whereas the other groups had no clear topographical differences within the populations. (Figure 3.23A) Multipolar neurones tended to have a large number of branchlets relative to the other groups, with dendrites projecting in every direction (Figure 3.23Biv). Most cluster 5 neurones were observed to be monopolar (33.3%) with dendrites projecting in either a dorsal (53.8 or %) lateral (30.8%) direction originating from primarily an oval soma (Figure 3.23Bi). Neurones that were bipolar made up 31.1% of cluster 5 neurones. 47% of bipolar neurones had

dendrites projecting ventrally and dorsally (Figure 3.23Bii). Neurones that formed part of Group C that were present in cluster 5s showed dendrites commonly projecting dorsally and laterally (61.5%). These neurones typically displayed short secondary dendrites (61.5%) (Figure 3.23Biii).

Cluster 6 neurones were either bipolar (33.9%; Group B) or monopolar (32.1%; Group A). Monopolar neurones exhibited either a single dendrite projecting dorsally (60%) or laterally (40%) originating from an oval soma (70%; Figure 3.24Bi) Neurons that were bipolar were located ventro-medially and all were classified as displaying oval cell bodies (Figure 3.24A). Bipolar neurones commonly had dendrites projecting dorsally and ventrally (65.5%) and often displayed short distal secondary dendrites (30%; Figure 3.24Bii). Cluster 6 neurones that were multipolar were located laterally and displayed 3 primary dendrites (Figure 3.24A/Biv). These neurones commonly had large round cell bodies (58.3%) which formed the origin for multiple dendrites projecting in all directions of the Arc.

Cluster 7 neurones were once again observed in all morphological groups. Those cluster 7 neurones that exhibited 2 primary dendrites were located distinctly medially within the Arc, the other morphological subgroups showed no topographical distinction (Figure 3.25A). Cluster 7 neurones that were monopolar displayed a single dendrite projecting dorsally (100%; Figure 3.25Bi). Bipolar neurones often displayed dendrites projecting either ventrally and dorsally (37.5%) or projecting medially and laterally (41.2%) thus forming two unique groups within cluster 7 bipolar neurones (Figure 3.25Bii). Neurones that displayed 2 primary dendrites often had dendrites projecting dorsally and laterally or medially thus forming almost a right angle (Figure 3.25 Biii). 15.5% of cluster 7 neurones were identified has being multipolar expressing 3 primary dendrites with predominately a round soma (62.5%; Figure 3.25Biv).

Cluster 8 neurones were found to be part of all morphological groups, with homogenous features. They were also dispersed in all areas of the Arc. Monopolar neurones were located more medially (Figure 3.26A) than other groups and predominately had a single dendrite projecting dorsally. These monopolar neurones often (75.0%) displayed secondary dendrites, also projecting dorsally (Figure 3.26Bi). Bipolar neurones were observed to have an oval soma (69.2%) with dendrites projecting commonly ventrally and dorsally (92.0%; Figure 3.26Bii). All cluster 8 cells that had 2 primary dendrites originating from relatively the same side of the soma had their dendrites projecting dorsally and laterally (100%) again forming a right-angle composition (Figure 3.2Biii). Cluster 8 neurones were also observed morphologically as multipolar neurones, possessing 3-5 primary dendrites with often multiple secondary dendrites (Figure 3.26Biv). These neurones were often found more laterally within the Arc (Figure 3.26A).

3.3 Discussion

This study characterised the electrophysiological and morphological properties of hypothalamic Arc neurones, in order to gain an understanding of the cellular properties underlying the contributions to regulating the excitability of these neurones. The principle aim of this study was to initiate the identification of functionally distinct neuronal populations in the Arc by examining the electrophysiological and morphological characteristics, thus to elucidate a link/ correlation between subthreshold active conductance characteristics of individual neurones with their morphology which could be used as a signature ultimately for function. Towards this aim this study combined biocytin labelling techniques with whole cell patch-clamp recordings in hypothalamic slices. Slices containing the recorded neurones were subsequently processed and individual neurones were visualised and where possible were reconstructed in three-dimensions for morphometric analysis. An indication of morphology

gives an idea of the number and level of modulation of synaptic inputs. The patch-clamp technique enables the individual to be able to analyse their recording on-line and thus carry out further experiments with an idea of the neurone recorded. In this study there were slight correlations seen between electrical and morphological parameters within the neurones of the Arc. This study reports heterogeneity in the expression of subthreshold conductances which is what one would expect in regards to the vast expression of neuropeptides within the Arc (Chronwall, 1985).

Focusing on the electrophysiological properties of Arc neurones, this study found the expression of four different subthreshold active conductances that established 8 unique groups (clusters) based on the differential expression of these conductances. These have been previously described and pharmacologically identified with specific blockers for each individual subthreshold active conductance (van den Top, 2002). The differences and the unique properties of the voltage-gated currents were sufficient in identifying unambiguously each cluster type on-line. Active conductances reflect and govern the type of input/output relationship of a neurone as they shape the integration of synaptic inputs and control the patterning of activity that represents the neurones output (Huguenard & Prince, 1994; Pape, 1996; Magee & Johnston, 2005). Thus, it is predicted differentiating neurones based on their active conductances will be the first step in dividing neurones based on functionality and pathways involved in different autonomic processes controlled by the Arc. The wide range of functional properties displayed by CNS neurones largely stems from heterogeneous expression and distribution of channel subtypes and the modulatory systems that regulate them (Magee & Johnston, 2005). An example of where active conductances play a crucial role in integrating an input and determining the patterning of output is within Arc pacemaker NPY/ AgRP neurones (van den Top *et al.*, 2004). These neurones are orexigen sensitive and display distinctive membrane potential oscillations which underlie pacemaker activity that is

dependent on the expression of I_a and a T-type calcium conductance. van den Top *et al.,* (2004) therefore showed that there exists a neuronal subpopulation within the Arc that has a homogenous response to feeding signals related to its unique expression of electrical properties thus functionally similar. Interestingly, here we describe differences in the morphology of these neurones which may represent neurones with the same neuropeptidergic expression and which are functionally similar may contribute to different parts of complex autonomic processes whereby they receive different inputs and have different targets.

The differential expression of one or a combination of subthreshold active conductances led to 8 electrophysiologically distinct groups. The active conductances expressed within the Arc included an anomalous inward rectification (I_{an}), hyperpolarisation-activated non-selective cation conductance (I_h), a transient outward rectification (I_a) and a T-type- like calcium conductance. Morphological analysis revealed the existence of four different populations based on the orientation and number of primary dendrites. Group A was combined of neurones that displayed one primary dendrite. Group B was made up of neurones that were bipolar. Group C was made up of neurones that had 2 primary dendrites not projecting from opposite sides of the cell body. Group D was made up of neurones that were multipolar. Combining both morphology with electrophysiology yielded 32 different neuronal groups. However, the large number of groups precludes statistical analysis of the 32 populations as the power per group is not sufficient. It cannot be ruled out nonetheless that these distinct cell groups are functionally divergent. Previously reported NPY/AgRP neurones (cluster 2) in this study have been separated into three different morphological groups. Cluster 2 neurones are not the only NPY/AgRP neurones within the Arc but represent a small population. At first sight these observations based on stereotypical responses to the orexigens, orexin and ghrelin show that these morphological differences may not appear to indicate differences in the physiological function of these neurones (van den Top *et al.*, 2004).

However, even though the previously described NPY/AgRP cells respond in being excited to orexigens the degree and type of responses may vary (i.e. not all oscillate) thus although these cells express NPY mRNA, responses may not be stereotypical and thus are not only heterogeneous in response but also morphology as this study shows.

The different expression of subthreshold conductances is an indication of the heterogeneity of neuronal cell types seen within the Arc.

T-type: This was the most common of conductances expressed in 180/254 (71%) cells, and was observed in four separate clusters; 5, 6, 7 and 8. It is sensitive to external nickel (van den Top, 2002). On termination of negative current injection this conductance is characterised by a rebound depolarisation, similar to that described in cells activated mediated by T-type calcium channels (Llinas & Yarom, 1981).T-type calcium channels are strongly related to the generation of burst-like firing patterns in neurones of the CNS (Huguenard & Prince, 1994). Indeed, T-type calcium channels are essential for the pacemaker activity in NPY/AgRP pacemaker neurones (van den Top *et al.*, 2004).

I_{an}: I_{an} was expressed by four different clusters, 1, 2, 7 and 8. This conductance is sensitive to external barium (van den Top, 2002). This translated into 118/254 (46%) of cells expressing this conductance and thus representing the second most common. As the name suggests 'rectification' means change of conductance with voltage, and 'anomalous' suggests that this conductance works in the contrary direction to that predicted by the Goldman-Hodgkin- Katz electro-diffusion equation (Goldman, 1943). This conductance is characterised by an instantaneous decrease in input resistance at more negative membrane potentials. Its function within neurones is unclear, it has been suggested to play a role in maintaining the membrane potential of neurones within a functional range (van den Top &

Spanswick, 2006). It may avoid neurones from becoming 'too hyperpolarised' and hence prevent then from being within a readily excitable state (Wilson *et al.*, 2002).

I_h: Clusters 4, 5 and 8 expressed I_h, a total of 101/254 (40%) neurones, that manifested as a depolarising sag during the response to hyperpolarising current injections as seen in other neurones (Halliwell & Adams, 1982; Pape, 1996). This conductance is sensitive to external cesium (van den Top, 2002). It has been suggested that the time-dependent inward rectification has a role in establishing the resting membrane potential of hypothalamic neurones (Akasu *et al.*, 1993). In addition the I_h current together with a T-type calcium conductance work in tandem to generate rhythmic activity in thalamic relay neurones (for review see Huguenard, 1996). It has been reported that this conductance is not found within the Arc of mice which is contrary to this study in the rat (Burdakov & Ashcroft, 2002).

I_a: I_a was only expressed by a small proportion of Arc neurones; 16/254 (16%), termed cluster 2 neurones. This conductance was characterised by a delayed return to the resting membrane potential upon termination of the injection of a negative current and is sensitive to external application of 4-aminopyridine (4-AP). A-like conductances are a common feature of hypothalamic neurones (Bourque, 1988; Tasker & Dudek, 1991; Bouskila & Dudek, 1995). Generally, these conductances are believed to influence spike repolarisation and modulate the frequency of tonically firing neurones (Connor & Stevens, 1971; Kenyon & Gibbons, 1979; Segal *et al.*, 1984). Within NPY/AgRP neurones, I_a was found to be modulating the interval of membrane potential oscillations (van den Top *et al.*, 2004).

The morphology described within this study shows Arc neurones to have a simple cytoarchitecture and dendritic tree, in comparison to other hypothalamic neurones such as the PVN (Stern, 2001). In agreement with previous studies the Arc has generally a small dendritic arborisation and 2 major types of neurones; small soma with 1-2 primary dendrites

(morphology group 1-3) and the second type of neurone that has a slightly larger soma with a greater number of primary dendrites and a greater number of secondary dendrites (morphology group 4; Bodoky & Rethelyi, 1977). Rarely does primary dendritic branching exceed that of 4. The greatest number of primary dendrites witnessed within the Arc was 5; however multipolar neurones were the least prevalent. We might have underestimated their prevalence though as a result of the nature of our experiments; working *in vitro* on hypothalamic slices destroys some of the neurone's projections. Coronal slices were used in this study and therefore dendrites running rostral to caudal to the surface of the slice would have been severed and thus not stained or were hard to see due to it travelling in the plane. The simplicity of the dendritic tree of Arc neurones suggests that the previously described affect of cytoarchitecture of complex and extensive dendritic trees determines the electrotonic properties and consequently the propagation of distal synaptic inputs into the soma may not be so relevant to Arc neurones (Rall, 1962; Stern, 2001; Gulledge *et al.*, 2005; Magee & Johnston, 2005). The sparsely branched dendritic trees of Arc neurones indicate a less extensive membrane area for synaptic contact than in other brain regions such as the cerebellum. However, a subpopulation of cluster 8 neurones were large and multipolar, this also was the cluster that expressed the greater number of active conductances. It could be that the number of active conductances represents to a degree a larger dendritic branching. Multipolar neurones for cluster 5, 6 and 8 were found in the lateral parts of the Arc again in line with previous studies (Bodoky & Rethelyi, 1977).

Although morphology between neuronal clusters and within clusters was seen to be heterogeneous there are common features, for example the majority of monopolar neurones that were identified as cluster 6 neurones projected dorsally. This was a common feature of many monopolar neurones not only in cluster 6 but the whole study. Dendrites projecting dorsally maybe neurones branching to the PVN, which is well known input for Arc neurones.

The PVN and Arc are closely connected by bidirectional monosynaptic neural projections (Tebbe *et al.*, 2003). In particular NPY neurones of the Arc have been shown to have projections to corticotrophin releasing factor neurones in the PVN (Toth & Palkovits, 1998) involved in a number of physiological processes.

Within the clusters looking closely at the tau shows that for cluster 5, 6, 7 and 8 there may well be heterogeneous populations with neurones in the same cluster having different sizes of cell bodies. This may correlate with clusters being made up of a combination of morphological features. The multipolar neurones that were found more laterally within the Arc had an overall larger mean soma surface area than the monopolar neurones. This would give a larger time-constant, in theory the membrane would be larger and hence take longer to charge. This maybe the reason why the frequency histograms of the tau values show heterogeneous populations. Indeed the membrane time constant between clusters does significantly differ (Table 3.5). Cluster 8 neurones have a significantly greater tau then cluster 2,3,4 and 6. Cluster 8 neurones also been identified as large multipolar neurones which may be represented in the large tau value.

In the past other studies have used different parameters to separate out neurones electrophysiologically. For example Pennartz *et al.,* (1998) used the amplitude and rising slope of the spike after-hyperpolarisation potential (AHP) as a denominator for separation. The current study did not look at suprathreshold conductances like the (AHP). The mechanism underlying the AHP is critical for the general speed and efficiency of neuronal processing as well as the more specific functions like controlling transmitter release and repetitive firing. Unfortunately this study has not included the analysis of such conductances, as the experimental design did not allow us to discriminate accurately between the different

components of the AHP i.e. Pennartz *et al.,* (1998) controlled the firing frequency of neurones between a set range. Studying the AHP could be a possible extension of this study.

In summary, this study presents a detailed electrophysiological and morphological characterisation of rat hypothalamic Arc neurons; the data suggests that the Arc is collection of heterogeneous neurones with expression of a combination of subthreshold active conductances. Neurones of the Arc have a complex morphology that does not directly correlate with the neurone's electrical properties.

At present, studies use green fluorescent protein/ immunocytochemistry /PCR to determine the neuropeptidergic expression of neurones, however these all have their limitations. What would be advantageous and a great prospect for the future would be to identify functionally different neuronal subpopulations within the Arc on-line.

The present study provides a biophysical framework for further investigation into the functional heterogeneity of Arc neurones. In order to progress this study future experiments would need to be carried out to identify both the afferent and efferent projections to and from Arc neurones respectively. This could be carried out by stimulation and track tracing experiments to determine neuronal inputs. Determining the chemical phenotype of each neurone and the responsiveness to a broad variety of physiologically relevant stimuli in relation to the clusters would be the next step in progressing with this investigation.

Table 3.2 **Overview of the active conductances expressed by Arc neurones and classified into clusters based on their expression of these conductances.**

Summarises the recognized conductances expressed by the electrophysiologically characterised subtypes of Arc neurones (Cluster 1-8)

Table 3.2 Active conductances expressed by arcuate nucleus neurones								
	Cluster							
	1	2	3	4	5	6	7	8
Conductance								
I_{an}	x	x					x	x
I_a		x						
I_h				x	x			x
T-type					x	x	x	x

Table 3.3 Overview of the general membrane properties of the electrophysiologically categorised clusters within the Arc								
Parameter	**Cluster 1**	**Cluster 2**	**Cluster 3**	**Cluster 4**	**Cluster 5**	**Cluster 6**	**Cluster 7**	**Cluster 8**
Resting Membrane potential (mV)	-47.9 ± 1.5	-47.8 ± 1.2	-48.9 ± 2.1	-48.8 ± 1.7	47.1 ± 0.9	45.4 ± 0.8	45.3 ± 0.7	46.6 ± 1.2
Input resistance (mΩ)	2006 ± 231	1172 ± 95	1587 ± 262	1407 ± 159	1767 ± 117	1523 ± 101	2036 ± 148	1589 ± 146
Membrane time constant (ms)	54.4 ± 4.5	38.4 ± 4.4	27.3 ± 3.1	38.1 ± 6.7	49.9 ± 5.1	41.3 ± 3.3	54.4 ± 3.6	66.3 ± 4.9
n	**23**	**16**	**13**	**22**	**45**	**56**	**45**	**34**
Action potential spike threshold (mV)	-31.3 ± 1.2	-30.5 ± 1.1	-31.2 ± 1.5	-28.4 ± 0.8	-29.1 ± 1.8	-29.9 ± 0.6	-29.3 ± 0.6	-29.5 ± 0.8
Action potential spike amplitude (mV)	94.3 ± 2.4	93.2 ± 2.7	90.5 ± 3.3	83.8 ± 3.5	83.3 ± 1.6	87.4 ± 2.0	93.4 ± 1.9	95.6± 2.3
Action potential spike duration (ms)	2.9 ± 0.2	3.1 ± 0.2	2.9 ± 0.1	2.9 ± 0.1	3.3 ± 0.1	3.5 ± 0.1	3.2 ± 0.1	2.9 ± 0.1
n	**23**	**14**	**13**	**22**	**43**	**51**	**35**	**34**
Whole cell recordings from Arc neurones. Results are expressed as the mean ± SEM								

Table 3.4 Overview of the general membrane properties of the morphologically categorised groups within the Arc				
Parameter	**Group A**	**Group B**	**Group C**	**Group D**
Resting Membrane potential (mV)	-46.0 ± 0.8	-46.7 ± 0.6	47.7 ± 0.9	46.5 ± 0.9
Input resistance (mΩ)	1646 ± 98	1668 ± 95	1876 ± 132	1402 ± 104
Membrane time constant (ms)	44.0 ± 3.3	46.9 ± 2.8	54.9 ± 4.6	51.8± 4.2
n	**57**	**104**	**50**	**43**
Whole cell recordings from 254 Arc neurones that were subsequently analysed for their morphology. Results are expressed as the mean ± SEM				

Table 3.5 **Overview of the statistical comparison of the general membrane properties of the different electrophysiologically classified clusters in the Arc**

ANOVAs were carried out to analyse the difference in membrane potentials, input resistance and membrane time constant between the differential clusters. This graph shows the statistical differences in passive membrane properties of each cluster, for example cluster 1 neurones varied in mean input resistance (as shown by the key) significantly to the mean input resistance of cluster 2 neurones ($p<0.05$).

↓Cluster→	1	2	3	4	5	6	7	8
1		P < 0.05						
2							P< 0.05	
3							P< 0.05	
4								
5								
6								
7			P<0.05					
8		P<0.05	P<0.001	P<0.01		P< 0.001		

KEY: Input Resistance
tau

Figure 3.1 **Identification, characterisation and analysis of electrical properties of Arc neurones**

Ai: A schematic representation of the location of Arc neurones recorded and subsequently processed for biocytin staining.

Bi: Action potential of an Arc neurone. The amplitude of the action potential was calculated as the difference between the membrane potential measured at threshold and the peak of the action potential. The duration of the action potential was measured as the time difference between the crossing of spike threshold between the rising and falling phase of the action potential.

Figure 3.2 **Frequency histograms summarising the distribution of the passive membrane properties characteristic of Arc neurones.**

A: The resting membrane potential of hypothalamic Arc neurones, ranging between -35 to -70 mV, with a distribution slightly skewed towards less negative membrane potentials.

B: The input resistances of Arc neurones, ranging between 400-6000 MΩ, with a distribution slightly skewed towards lower resistances.

C: A graph showing the distribution of the different membrane time-constants (Tau) of Arc neurones. The membrane time-constant was estimated by fitting double exponentials to the membrane voltage charging curves induced by injection of hyperpolarising rectangular- wave current pulses (of variable amplitude and steps). The range of Tau values was 0-150 ms, with a varied distribution, presenting the possibility of 2-3 different populations.

Figure 3.3 **Identification, characterisation and analysis of electrophysiological properties of Arc neurones**

Ai: The activation of the anomalous inward rectifier (I_{an}) gave rise to a decrease in membrane resistance at negative holding potentials. The arrows marked 1 and 2 indicate the amplitude of the membrane response to negative current injection with a ratio of 1:2. Note the fast activation and the lack of inactivation of this conductance.

Aii: Activation of the H-conductance (I_h) induces a time- and voltage-dependent sag in the membrane response to negative current injection. The amplitude of I_h was measured by subtracting the membrane potential at the end of the negative current injection (Upper dotted line, instantaneous) from the membrane potential following steady-state charging of the cellular membrane (lower dotted line).

Aiii: The activation of an A-like conductance (I_a) resulted in a delayed return to baseline following negative current injection. The duration of I_a was measured as the time between the end of current injection (marked by the first vertical dotted line) and the return of the membrane potential to the level prior to the current injection (marked by the second vertical dotted line). The amplitude of the current was measured at half the duration (line marked *).

Aiv: The activation of low threshold T-type like calcium conductance close to the resting membrane potential resulted in the generation of a rebound depolarisation on cessation of negative current injection. The lower dotted line marks the resting membrane potential and the upper dotted line marks the peak of the rebound depolarisation as observed as a plateau following the action potential. The difference between these values was used to quantify the T-type conductance.

Figure 3.4 **Characteristic electrophysiological properties of Arc cluster 1 neurones**

Ai: Characteristic current/voltage (I/V) relationship of a cluster 1 neurone. Superimposed traces of the membrane responses to a range of hyperpolarizing and depolarising rectangular-wave current steps of constant increment. The arrows (1) indicate the decreased membrane response at more hyperpolarized membrane potentials (downward arrow) relative to membrane potentials responses close to rest (upward arrow) as a result of the activation of I_{an}.

Aii: Plot of the current-voltage relationship of the neurone shown in Ai. Note the decreased slope of the plot towards more negative membrane potentials as a result of the activation of I_{an}. The arrow (2) shows the point in the current-voltage relationship at which the slope of the plot decreases used as an estimation for the activation threshold for $I_{an.}$

Bi-Biii: Distribution histograms summarising the passive membrane properties; membrane potential; input resistance; membrane time-constant respectively observed in cluster 1 Arc neurones.

Figure 3.5 **Characteristic electrophysiological properties of Arc cluster 2 neurones**

Ai: Characteristic I/V relationship of a cluster 2 neurone. Arrow (1) indicates the decrease in the peak amplitude of membrane response at negative holding potentials due to activation of I_{an} whilst arrow (2) indicates the delayed return to baseline following negative current injection as a result of I_a activation.

Aii: Plot of the current-voltage relationship of the neurone shown in Ai. The arrow (3) shows the point in the current-voltage relationship at which the slope of the plot decreases. The arrow (3) shows the point in the current-voltage relationship at which the slope of the plot decreases used as an estimation for the activation threshold for I_{an}.

Bi-Biii: Distribution histograms summarising the passive membrane properties; membrane potential; input resistance; membrane time-constant respectively observed in cluster 2 Arc neurones.

Figure 3.6 **Characteristic electrophysiological properties of Arc cluster 3 neurones**

Ai: Membrane responses of a typical cluster 3 neurone to a range of depolarising and hyperpolarizing current steps of constant increment and rectangular waveform. Note the lack of any distinctive subthreshold active membrane conductances and the fast charging of the membrane consistent with a short membrane time-constant.

Aii: Plot of the current-voltage relationship of the neurone shown in Ci. Note the constant slope of the plot as a result of the constant membrane resistance over the range of membrane potentials tested.

Bi-iii Distribution histograms summarising the passive membrane properties; membrane potential; input resistance; membrane time-constant respectively observed in cluster 3 Arc neurones.

Figure 3.7 Characteristic electrophysiological properties of Arc cluster 4 neurones

Ai: Typical I/V relationship of a cluster 4 neurone. Note the sag in the membrane response during negative current injection as a result of the activation of I_h. The distance between the dotted horizontal lines indicates the amplitude of the conductance induced as a result of the activation of I_h. Note the decrease in activation latency (time difference between the two arrowheads) at more negative membrane potentials. Also note the increased amplitude of the voltage sag at more negative membrane potentials. Closed square and open circles mark the position of the traces used to measure the instantaneous and steady-state membrane responses, respectively (see Aii).

Aii: Plot of the instantaneous (closed square) and steady-state (open circle) membrane responses of the neurone shown in Ai. The difference between the curves is indicative of the activation of I_h, which decreases the steady-state membrane response at negative holding potentials resulting in a non-linear current-voltage relationship. The arrow marks the point used to estimate the activation threshold of I_h in Arc neurones.

Bi-Biii: Distribution histograms summarising the passive membrane properties; membrane potential; input resistance; membrane time-constant respectively, observed in cluster 4 Arc neurones.

Figure 3.8 Characteristic electrophysiological properties of Arc cluster 5 neurones

Ai: Typical current-voltage relationship of a cluster 5 neurone. Note the sag in the membrane response during negative current injection as a result of the activation of I_h. The distance between the dotted horizontal lines indicates the amplitude of the conductance induced as a result of the activation of I_h Rebound depolarisations were induced following the release of current injection contributing to the activation of a T-type like calcium conductance (arrow; T-type).

Aii: Plot of the instantaneous (closed square) and steady-state (open circle) membrane responses of the neurone shown in Ai. The difference between the curves is indicative of the activation of I_h, which decreases the steady-state membrane response at negative holding potentials resulting in a non-linear current-voltage relationship. The arrow marks the point used to estimate the activation threshold of I_h in Arc neurones.

Bi-Biii: Distribution histograms summarising the passive membrane properties; membrane potential; input resistance; membrane time-constant respectively observed in cluster 5 Arc neurones. Further inspection of the distribution graphs indicated the potential for more than one population as indicated by the red dotted lines in this, and subsequent figures.

Figure 3.9 **Characteristic electrophysiological properties of Arc cluster 6 neurones**

Ai: Typical current-voltage relationship of a cluster 6 neurone Rebound depolarisations were induced following the release of the hyperpolarising current injection due to the activation of a T-type like calcium conductance (arrow; T-type).

Aii: Plot of the current-voltage relationship of the neurone shown in Ai. Note the linear relationship between injected current and the resulting membrane response, thus the absence of expression of any active conductances, such as I_h or I_{an}.

Bi-Biii: Distribution histograms summarising the passive membrane properties; membrane potential; input resistance; membrane time-constant respectively observed in cluster 6 Arc neurones.

Figure 3.10 Characteristic electrophysiological properties of Arc cluster 7 neurones

Ai: Characteristic I/V relationship of a cluster 7 neurone. The arrows (1) indicate the decreased membrane response at more hyperpolarized membrane potentials (downward arrow) relative to membrane potentials responses close to rest (upward arrow) as a result of the activation of I_{an}. Cluster 7 also expresses a T-type like calcium conductance. Rebound depolarisations were induced following the release of the hyperpolarising current injection contributing to the activation of a T-type like calcium conductance (arrow; T-type).

Aii: Plot of the current-voltage relationship of the neurone shown in Ai. Note the decreased slope of the plot towards more negative membrane potentials as a result of the activation of I_{an}. The arrow (2) shows the point in the current-voltage relationship at which the slope of the plot decreases.

Bi-Biii: Distribution histograms summarising the passive membrane properties; membrane potential; input resistance; membrane time-constant respectively observed in cluster 7 Arc neurones.

Figure 3.11 Characteristic electrophysiological properties of Arc cluster 8 neurones

Ai: Characteristic I/V relationship of a cluster 8 neurone. The arrows (1) indicate the decreased membrane response at more hyperpolarized membrane potentials (downward arrow) relative to membrane potentials responses close to rest (upward arrow) as a result of the activation of $I_{an.}$ Note the sag in the membrane response during negative current injection as a result of the activation of I_h. Cluster 8 also expresses a T-type calcium like conductance that is seen as a rebound depolarisation following the injection of negative current.

Aiii: Plot of the current-voltage relationship of the neurone shown in Ai. Note the decreased slope of the plot towards more negative membrane potentials as a result of the activation of I_{an}. The arrow (2) shows the point in the current-voltage relationship at which the slope of the plot decreases.

Aii: Plot of the instantaneous (closed square) and steady-state (open circle) membrane responses of the neurone shown in Ai. The difference between the curves is indicative of the activation of I_h, which decreases the steady-state membrane response at negative holding potentials resulting in a non-linear current-voltage relationship.

Bi-Biii: Distribution histograms summarising the passive membrane properties; membrane potential; input resistance; membrane time-constant, respectively observed in cluster 8 Arc neurones.

Figure 3.12 **Distribution histograms summarising the distribution of the mean passive membrane properties characteristic of Arc neurones for each electrophysiologically defined cluster**

Ai Distribution-histogram showing the mean membrane potential for each electrophysiological cluster.

Aii Distribution-histogram showing the mean neuronal input resistance for each electrophysiological defined cluster

Aiii Distribution-histogram showing the mean membrane time-constant for each electrophysiological cluster

Note: A statistical comparison of the passive membrane properties of each electrophysiological cluster is represented in table 3.5

Figure 3.13A **A schematic showing the guidelines used in this study in order to classify the length, quantity and orientation of dendrite projection.**

A: The neurone in this schematic was classified as a bipolar neurone with dendrites projecting from an oval shaped soma in a dorsal and lateral direction.

Figure 3.13B **A schematic showing the guidelines used in this study in order to calculate soma surface area and total primary dendritic length.**

B: Schematic shows arrows to origin of primary dendrites from cell body. Here the dendrites originate from opposite sides of the soma, thus this neurone is classified as bipolar. Carl Zeiss vision, axiovision 4.1 programme was used to measure total primary dendritic length online.

Figure 3.14 **A pie chart showing the % of neurones that fall into each morphological group.**

Morphology group A: Monopolar neurones
Morphology group B: Bipolar neurones
Morphology group C: 2 primary dendrites
Morphology group D: Multipolar neurones

Figure 3.15 **Frequency histograms summarising the electrophysiological make-up of each morphological defined group**

Ai: A frequency-histogram showing that Morphological Group A (monopolar neurones) were primarily made up of clusters 5 and 6.

Aii: A frequency-histogram showing that Morphological Group B (bipolar neurones) contained all clusters. Thus, all clusters morphologically had a percentage of neurones that were bipolar.

Aiii. A frequency-histogram showing that Morphological Group C (2 primary dendrites) had no cluster 4 neurones and few cluster 1 neurones.

Aiii. A frequency-histogram showing that Morphological Group D (multipolar neurones) were primarily neurones electrophysiologically classified as cluster 6 neurones. No cluster 3 neurones were mulitpolar.

Figure 3.16 **Shows each individual electrophysiological defined cluster and how it was made up relative to each morphological group as a percentage of all those cells recorded.**

Figure 3.17 **Morphology of Arc nucleus neurones**

Photomicrographs showing the biocytin labelled soma and proximal dendrites of two separate neurones. Images in the higher magnification are made up as result of individual photographs captured in different focal planes and pieced together in order to provide a comprehensive overview of the individual neurone recorded. Orientation arrows are shown for individual neurones. D; dorsal, V; ventral, L; lateral, M; medial

Ai: A representative morphology group A neurone shown at 10x magnification depicting its location within the Arc nucleus. This neurone is located medially within the Arc

Aii: 40x magnification of the neurone shown in Ai. A typical monopolar neurone with its single primary dendrite projecting dorsally from an oval shaped soma. This neurone also displays a short distal secondary dendrite. Note also the faint projection projecting ventrally which is believed to be an axon.

Bi: A representative morphology group B neurone shown at 10x magnification depicting its location within the Arc nucleus. This neurone is located in the dorso-medial.

Bii: 40x magnification of the neurone shown in Bi. A typical bipolar neurone with a single primary dendrite projecting dorsally and another ventro-laterally (classified as ventral) from an oval shaped soma.

Figure 3.18 **Morphology of Arc nucleus neurones**

Photomicrographs capturing the biocytin-labelled soma and proximal dendrites of two separate neurones. Images in the higher magnification are made up as result of individual photographs captured in different focal planes and pieced together in order to provide a comprehensive overview of the individual neurone recorded. Orientation arrows are shown for individual neurones. D; dorsal, V; ventral, L; lateral, M; medial

Ai: A representative morphology group C neurone shown at 10x magnification depicting its location within the Arc nucleus. This neurone is located dorso-medially within the Arc

Aii: 40x magnification of the neurone shown in Ai. A typical 2 primary dendrite projecting neurone from different sides of the pyramidal shaped soma. Note also the faint projection projecting ventrally which is believed to be an axon.

Bi: A representative morphology group D neurone shown at 10x magnification depicting its location within the Arc nucleus. This neurone is located medially with the Arc.

Bii: 40x magnification of the neurone shown in Bi. A typical mulitipolar neurone with 3 primary dendrites originating from a round cell body. Dendrites are projecting dorsally, laterally and ventrally and this neurone displays multiple secondary dendrites.

Figure 3.19 **Schematic of the distribution of cluster 1 neurones throughout the Arc. Schematic drawings of the morphology of cluster 1 neurones**

A: Comparative distribution of cluster 1 neurones separated based on morphological characteristics shown in schematic coronal planes depicting the Arc. An overview of the location of all cluster 1 neurones recorded is shown at the end (overview). The majority of cluster 1 neurones were bipolar and multipolar distributed throughout the Arc with no clear differences based on morphological features.

B: **Drawings of biocytin labelled Arc neurones electrophysiologically classified as cluster 1 neurones (not to scale)**

i: Typical cluster 1 bipolar neurones with a single dendrite projecting medially and another projecting laterally, from an oval shaped soma. These neurones often displayed short distal secondary dendrites. Note the dotted dorsal projection in the 2nd neurone which is thought to be an axon.

ii: Another group of cluster 1 bipolar neurones which displayed a different dendrite orientation from the above. These bipolar neurones had a single dendrite projecting dorsally and a second projecting ventrally, typically from an oval shaped soma.

iii: Representative multipolar cluster 1 neurones displaying a characteristic 'fork' appearance. These neurones often displayed 2 primary dendrites projecting dorsally and another single dendrite projecting ventrally, typically from a round cell body.

Figure 3.20 **Schematic of the distribution of cluster 2 neurones in the Arc. Schematic drawings of the morphology of cluster 2 neurones**

A: Comparative distribution of cluster 2 neurones classified based on morphological characteristics shown in a schematic representation of coronal planes depicting the Arc. An overview of the location of all cluster 2 neurones recorded is shown at the end (overview). The majority of cluster 2 neurones were bipolar distributed closely to the 3rd ventrical and medially within the Arc.

B: **Drawings of biocytin labelled Arc neurones electrophysiologically classified as cluster 2 neurones (not to scale)**

i: Typical cluster 2 bipolar neurones with a single primary dendrite projecting dorsally and another projecting ventrally from an oval shaped soma. These neurones often displayed short proximal secondary dendrites.

ii: Cluster 2 neurones were also monopolar. They displayed a single dendrite projecting dorsally

iii: Representative multipolar cluster 2 neurones.

Figure 3.21 **Schematic of the distribution of cluster 3 neurones in the Arc. Schematic drawings of the morphology of cluster 3 neurones**

A: Comparative distribution of cluster 3 neurones classified based on morphological characteristics shown in a schematic representation of coronal planes depicting the Arc. An overview of the location of all cluster 3 neurones recorded is shown at the end (overview). The majority of cluster 3 neurones were bipolar distributed medially within the Arc and relatively close to the 3rd ventricle. There were no multipolar cluster 3 neurones.

B: **Drawings of biocytin labelled Arc neurones electrophysiologically classified as cluster 3 neurones.**

i: Typical cluster 3 bipolar neurones with a single dendrite projecting ventrally and another projecting dorsally, from a round shaped soma. These neurones often displayed short distal secondary dendrites originating from the primary dendrite projecting dorsally.

ii: Another group of cluster 3 bipolar neurones which displayed a different dendrite orientation from the above. These bipolar neurones had a single dendrite projecting laterally and a second projecting medially, typically from an oval shaped soma.

Figure 3.22 **Schematic of the distribution of cluster 4 neurones in the Arc. Schematic drawings of the morphology of cluster 4 neurones**

A: Comparative distribution of cluster 4 neurones separated out based on morphological characteristics shown in a schematic representation of coronal planes depicting the Arc. An overview of the location of all cluster 4 neurones recorded is shown at the end. The majority of cluster 4 neurones were bipolar distributed medially within the Arc and monopolar neurones located slightly more laterally.

B: **Drawings of biocytin labelled Arc neurones electrophysiologically classified as cluster 4 neurones.**

i: A representative cluster 4 monopolar neurone with a single dendrite projecting laterally originating from a oval shaped soma

ii: Bipolar cluster 4 neurones displaying neurones originating medially and laterally but then projecting dorsally. Note the dotted line which represents what is thought to be an axon.

Figure 3.23 **Schematic of the distribution of cluster 5 neurones in the Arc. Schematic drawings of the morphology of cluster 5 neurones**

A: Comparative distribution of cluster 5 neurones separated out based on morphological characteristics shown in a schematic representation of coronal planes depicting the Arc. An overview of the location of all cluster 4 neurones recorded is shown at the end. Cluster 5 neurones were monopolar, bipolar, had 2 primary dendrites and were also multipolar. Multipolar neurones tended to be located laterally within the Arc

B: **Drawings of biocytin labelled Arc neurones electrophysiologically classified as cluster 5 neurones.**

i: A representative cluster 5 monopolar neurone with a single dendrite projecting laterally or dorsally originating from an oval shaped soma

ii: Typical bipolar cluster 5 neurones displaying dendrites projecting dorsally and ventrally from a pyramidal shaped soma.

iii: Characteristic cluster 5 neurone displaying 2 primary dendrites originating from the same side of the soma. Dendrites typically projected to make a 'right angle'. Orientation of dendritic projection was commonly dorsal and lateral. These neurones also frequently had distal short secondary dendrites.

iv: Cluster 5 neurones were also large multipolar neurones with 3-4 primary dendrites projecting in all orientations throughout the Arc. These neurones commonly had a number of secondary dendrites.

Figure 3.24 **Schematic of the distribution of cluster 6 neurones in the Arc. Schematic drawings of the morphology of cluster 6 neurones**

A: Comparative distribution of cluster 6 neurones separated out based on morphological characteristics shown in a schematic representation of coronal planes depicting the Arc. An overview of the location of all cluster 6 neurones recorded is shown at the end. Cluster 6 neurones were monopolar, bipolar, had 2 primary dendrites and were also multipolar. Bipolar neurones were distinctively found 'clumped' together dorsally within the Arc.

B: **Drawings of biocytin labelled Arc neurones electrophysiologically classified as cluster 6 neurones.**

i: A representative cluster 6 monopolar neurone with a single dendrite projecting laterally or dorsally originating from an oval shaped soma. These neurones commonly had short axons projecting from the opposing side of the soma.

ii: Typical bipolar cluster 6 neurones displaying dendrites projecting dorsally and ventrally from a pyramidal shaped soma. These neurones also typically displayed short distal secondary dendrites

iii. Characteristic cluster 6 neurone displaying 2 primary dendrites originating from same sides of the soma.

iv. Cluster 6 neurones were also large multipolar neurones with 3 primary dendrites projecting in all orientations throughout the Arc. These neurones commonly had a number of secondary dendrites.

Figure 3.25 **Schematic of the distribution of cluster 7 neurones in the Arc. Schematic drawings of the morphology of cluster 7 neurones**

A: Comparative distribution of cluster 7 neurones separated out based on morphological characteristics shown in a schematic representation of coronal planes depicting the Arc. An overview of the location of all cluster 7 neurones recorded is shown at the end. Cluster 7 neurones were monopolar, bipolar, had 2 primary dendrites and were also multipolar. Neurones with 2 primary dendrites were found dorso-medially within the Arc

B: **Drawings of biocytin labelled Arc neurones electrophysiologically classified as cluster 7 neurones.**

i: A representative cluster 7 monopolar neurone with a single dendrite projecting dorsally originating from an oval shaped soma. These neurones commonly had short axons projecting ventrally and typically displayed distal secondary dendrites also projecting dorsally.

ii: Typical bipolar cluster 7 neurones displaying dendrites projecting dorsally and ventrally from an oval shaped soma. Another 'group' of bipolar neurones had dendrites projecting laterally and medially.

iii. Characteristic cluster 7 neurone displaying 2 primary dendrites originating from similar sides of the soma creating a right angle formation. Dendrites commonly projected dorsally and laterally from a round cell body.

iv. Cluster 7 neurones were also multipolar with 3 primary dendrites that projected in all directions in the Arc.

Figure 3.26 **Schematic of the distribution of cluster 8 neurones in the Arc. Schematic drawings of the morphology of cluster 8 neurones**

A: Comparative distribution of cluster 8 neurones separated out based on morphological characteristics shown in a schematic representation of coronal planes depicting the Arc. An overview of the location of all cluster 8 neurones recorded is shown at the end. Cluster 8 neurones were monopolar, bipolar, had 2 primary dendrites and were also multipolar. Monopolar neurones were found lying close to the 3rd ventricle.

B: **Drawings of biocytin labelled Arc neurones electrophysiologically classified as cluster 8 neurones.**

i: A representative cluster 8 monopolar neurone with a single dendrite projecting dorsally originating from an oval/round shaped soma. These neurones commonly had axons projecting ventrally and typically displayed distal secondary dendrites also projecting dorsally.

ii: Typical bipolar cluster 8 neurones displaying dendrites projecting dorsally and ventrally from an oval shaped soma.

iii Characteristic cluster 8 neurone displaying 2 primary dendrites originating from the same sides of the soma creating a right angle formation. Dendrites commonly projected dorsally and laterally from an oval cell body

iv Cluster 8 neurones were also multipolar with 4-5 primary dendrites that projected in all orientations throughout the Arc from large round somas.

Chapter 4

The effects of changes in ambient extracellular glucose levels on the neuronal activity of arcuate neurones *in vitro*

4.1 Introduction

Glucose is a vitally important carbohydrate that provides the brain with its primary fuel source. It is essential for the brains correct functioning and survival (Ritter *et al.*, 2006). Glucose utilisation, storage and mobilisation are meticulously regulated by both neuronal and hormonal mechanisms. The control of glucose by central mechanisms is essential and has been recognised since the classical experiments carried out by Bernard in 1849 (Alquier & Kahn, 2004).

It has been shown that there is direct reciprocal neuronal control from the hypothalamus to the liver and pancreas (Buijs *et al.*, 2001; Buijs *et al.*, 2003). Retrograde transneural viral tracing methods highlight hypothalamic nuclei, including the paraventricular nucleus (PVN), and the lateral hypothalamus (LH) in the regulation of the liver and pancreas via sympathetic and parasympathetic pathways. Furthermore, the PVN integrates information from other hypothalamic nuclei, such as the Arc (Buijs *et al.*, 2003), which is essential for the control of energy homeostasis and initiates an appropriate autonomic control of both the liver and pancreas.

In times of hypoglycaemia activation of the autonomic nervous system (ANS), in particular the sympathetic nervous system (SNS), results in the mobilisation of glucose from storage tissues hence increasing plasma glucose levels. SNS activation results in an increase in neuronal and hormonal noradrenaline (NA) levels (McCaleb *et al.*, 1979; Smythe *et al.*, 1984) and hormonal adrenaline that directly enhance hepatic glucose production by activating both glycogenolysis and gluconeogenesis within the liver. The liver is also directly under the control of hormonal signals such as insulin and glucagon which regulate the levels of glucose within the blood. Thus, in times when blood glucose is high, activation of the parasympathetic nervous system (PNS) leads to the conversion of glucose to glycogen within the liver. Insulin,

released form the pancreas suppresses hepatic glucose production by inhibiting both gluconeogensis and glycogenolysis which ultimately leads to lower plasma glucose levels. Disruption of the tight control of glucose levels within an individual leads to syndromes such as diabetes mellitus, due to defective insulin secretion, resistance to insulin secretion or both. The pathologies related to diabetes include cognitive deficits, diabetic neuropathy and weight loss amongst others (Biessels *et al.*, 2002).

Plasma glucose levels can fluctuate between 4-7 mM within a healthy individual and can become much higher in individuals with diabetes. The levels of glucose to which the brain is exposed is less clear. With a plasma glucose range of 5-8 mM, brain glucose levels are detected to be between 1-2.5 mM (Silver & Erecinska, 1994). With plasma glucose concentrations ranging from pathophysiolological levels of 2-18 mM, the brain has been suggested to detect levels between 0.2 to 4.5 mM, respectively (Silver & Erecinska, 1994). Within the hypothalamus glucose basal levels have been shown to achieve concentrations of around 1.4 mM (de Vries *et al.*, 2003; Mayer *et al.*, 2006). It has been suggested that brain glucose levels range from approximately 10-30 % of blood levels (Silver & Erecinska, 1994; de Vries *et al.*, 2003). However, certain areas of the brain such as the arcuate nucleus (Arc) are well positioned to detect circulating glucose levels due to its close proximity to the median eminence (ME) where the blood-brain-barrier (BBB) is compromised due to its vascularised structure and fenestrated endothelial cells (Ganong, 2000). Thus these areas may be exposed to higher levels of glucose than other parts of the brain; however the exact concentrations are still unknown.

Hypothalamic neurones within the Arc, LH and ventral medial nucleus (VMN) have been identified to use glucose, in a concentration-dependent manner, as a signalling molecule to regulate neuronal electrical excitability (Wang *et al.*, 2004; Burdakov *et al.*, 2005; Ma *et al.*, 2008). These glucose-sensing neurones have been termed glucose-responsive (GR) and

glucose-sensitive (GS; Oomura *et al.*, 1964). GR neurones are those that increase their firing rate as brain glucose levels rise, also termed glucose excited neurones (GE). Conversely, GS neurones decrease their firing rate as glucose levels rise, also termed glucose inhibited (GI) neurones (Song *et al.*, 2001; Wang *et al.*, 2004).

Within the Arc reside two principal populations of neurones that are anatomically adjacent and work in an antagonistic fashion as parallel but opposing pathways to maintain a balanced energy state. Neuropeptide Y/ agouti related peptide (NPY/AgRP) neurones form the main anabolic drive and pre-pro-opiomelanocortin /cocaine and amphetamine regulated transcript (POMC/CART) neurones form the main catabolic drive (Schwartz *et al.*, 1991; Guan *et al.*, 1998b; Lin *et al.*, 2000). Populations of NPY/AgRP neurones are suggested to be GI neurones (Muroya *et al.*, 1999) that are also inhibited by leptin (van den Top *et al.*, 2004), and POMC/CART neurones are suggested to be GE neurones (Ibrahim *et al.*, 2003) that are excited by leptin (Cowley *et al.*, 2001). Glucose sensing in POMC-mut-6.2 mice have disrupted whole body glucose sensing, providing evidence that the ATP-sensitive potassium channels are required for glucose excitation of POMC neurones (Parton *et al*, 2007). Both subsets of neurones have been shown to express functional ATP-sensitive potassium channel (K_{ATP} channels; Ibrahim *et al.*, 2003; van den Top *et al.*, 2007). K_{ATP} is an important ion channel classically suggested to be involved in glucose-sensing. Furthermore, the functioning of this ion channel in the central nervous system (CNS) has been shown to be pivotal for glucose-sensing in the CNS by the use of knock-out studies and specific ion channel blockers (Ashford *et al.*, 1990; Rowe *et al.*, 1996; Spanswick *et al.*, 1997; Lee *et al.*, 1999; Spanswick *et al.*, 2000; Miki *et al.*, 2001). K_{ATP} channels are composed of two different components: pore forming inward rectifier K^+ channel (KIR) and sulfonylurea receptor (SUR) subunits arranged in a 4:4 stoichiometry (Ashcroft & Gribble, 1999). Specifically GE neurons are proposed to use functional K_{ATP} channels to sense glucose much like the pancreatic β-cells

(Ashford *et al.*, 1990; Yang *et al.*, 1999; van den Top *et al.*, 2007). In brief GLUT 3 transporters on the membrane surface of hypothalamic neurones permit glucose influx at a rate dependent on extracellular plasma glucose concentration (Kang *et al.*, 2004). Within the cell glucose is phosphorylated by glucokinase (GK). This step is considered to be the rate-limiting step for glucose metabolism in the pancreatic β cell and is the major mechanism for glucose sensing (Dunn-Meynell *et al.*, 2002). The metabolism of glucose increases the intracellular ATP/ADP ratio causing the K_{ATP} channel to close leading to a membrane depolarisation (Yang *et al.*, 1999; Levin *et al.*, 2001; Dunn-Meynell *et al.*, 2002; Kang *et al.*, 2004). Hypothalamic K_{ATP} channels have also been shown to be crucial in the control of hepatic glucose production whereby their activation lowers blood glucose by inhibiting glucose production, specifically gluconeogenesis within the liver (Pocai *et al.*, 2005). Thus, K_{ATP} channels appear to be essential for integrating signals generated by glucose metabolism and for signal transduction pathways activated via insulin and leptin receptors.

The mechanism by which GS neurones respond to changes in extracellular glucose is unclear. The activation of a hyperpolarising chloride current (Song *et al.*, 2001; Routh, 2002; Fioramonti *et al.*, 2007); and a mechanism involving the reduction in the depolarising activity of the electrogenic Na^+/ K^+ pump within the LH (Oomura *et al.*, 1974) has been suggested.

Together with findings that K_{ATP} channels are essential in the central control of glucose homeostasis these results suggest a link between glucose responsiveness and neurones involved in the control of energy homeostasis (Miki *et al.*, 2001). Hence, glucose responsiveness might be a useful tool to separate functional subsets of Arc neurones involved in the control of specific aspects of energy balance from neurones controlling other aspects of energy balance and autonomic processes.

Previous studies, electrophysiologically characterising the responsiveness of hypothalamic neurones to glucose and other stimuli, have used non-physiological ranges of

glucose; 0-20 mM (Anand *et al.*, 1964; Oomura *et al.*, 1964; Ashford *et al.*, 1990; Spanswick *et al.*, 1997). Under normal physiological conditions neurones within the Arc would never be exposed to 0 mM levels of glucose and rarely would they see glucose levels higher than 5 mM (Silver & Erecinska, 1994) unless under pathological conditions. The levels of extracellular glucose have been shown to be critical in the responsiveness of some neurones. Leptin can either decrease the activity of POMC neurones or increase the activity of POMC neurones in 5 mM and 11 mM glucose, respectively (Ma *et al.*, 2008). Thus, studies carried out under non-physiological ranges of glucose, may need to be re-evaluated. Studies have now looked at using a more physiological range of glucose when conducting experiments (Song *et al.*, 2001; Wang *et al.*, 2004; Burdakov *et al.*, 2005) but none have directly looked at and analysed the differences in expression of subthreshold active conductances in physiological versus non-physiological levels of glucose.

Active and passive membrane properties of a neurone shape its function, integration and computational capability. Subthreshold conductances shape electrical activity, control spontaneous firing and the membrane potential of individual neurones regulate synaptic release of peptides (Dutton & Dyball, 1979; Gulledge *et al.*, 2005; see chapter 3).

This study attempted to mimic two different sets of conditions where ambient levels of extracellular glucose concentrations were maintained at different concentrations to determine the impact of these glucose levels on the electrophysiological function and operation of Arc neurones. Electrophysiological recordings were carried out in 10 mM glucose, thus mimicking a putative hyperglycaemic state and 2 mM (30% of 6mM plasma glucose; Silver & Erecinska, 1994; de Vries *et al.*, 2003) glucose imitating a putative euglycaemic state. Electrophysiological recordings were therefore undertaken in the two differing glucose concentrations and their active and passive membrane properties compared. This electrophysiological comparison included an analysis of subthreshold active conductances,

differentially expressed in Arc neurones, used as a basis of a functional classification of Arc neurones (as described in chapter 3).

4.2 Results

Whole-cell recordings were obtained from a total of 538 neurones within the hypothalamic Arc *in vitro,* defined as the area directly above the median eminence on both sides of the 3rd ventricle. 313 were recorded in an extracellular glucose concentration of 2 mM (osmolarity was compensated with D-mannitol; see methods) and the remainder in a glucose concentration of 10 mM (n=225). Differences in firing rate, passive and active membrane conductances and expression of subthreshold active conductances were compared and analysed in the two different glucose concentrations.

General membrane properties included the resting membrane potential, input resistance and the firing rate of the neurone. Input resistances were calculated at steady-state resting membrane potential from membrane responses to the smallest negative current injection. The firing rate was established by counting the number of action potentials discharged within a one minute period and the frequency of firing expressed in Hertz (Hz). Other electrophysiological properties studied were current/voltage relations (I/V), membrane time-constants (tau) and action potential wave-forms. I/V's were carried out on each individual neurone to explore the active conductances expressed by Arc neurones (See chapter 3). Hypothalamic Arc neurones expressed a range of subthreshold active conductances.

4.2.1 Passive membrane properties of neurones recorded in 10 mM and 2 mM extracellular glucose

For all neurones recorded in 10 mM and 2 mM glucose aCSF, respectively, the membrane potential, input resistance and firing rate were established. Spontaneous firing rate could not be obtained for all neurones. An overall comparison is shown in Table 4.1. Bar charts showing the mean, standard error of the mean and frequency histograms for each passive membrane property in both glucose concentrations are shown in Figures 4.1 and 4.2 respectively.

4.2.1.1 Resting Membrane potential

The average resting membrane potential for neurones recorded in 10 mM glucose and 2 mM glucose was -46.6 ± 0.4 mV (n=225; range -30 to -66 mV) and -45.9 ± 0.3 mV (n=313; range -32 to -66 mV), respectively (Figure 4.1 A; Table 4.1). These data revealed no significant difference between the resting membrane potentials of Arc neurones recorded in 10 and 2 mM extracellular glucose (P=0.13; two-tailed student's t-test). Frequency-histograms plotted for both 10 mM and 2 mM glucose-containing aCSF followed a normal distribution (Figure 4.2 A). However, the modes and therefore peaks of the distributions for each concentration differed. The mode was taken as the bin containing the largest percentage of neurones, -40 to -45 mV (28.9%) for neurones recorded in 10 mM as opposed to - 45 to -50mV (30.4%) for 2 mM glucose. The median value was -46mV for both concentrations of glucose.

4.2.1.2 Neuronal input resistance

The mean neuronal input resistance of neurones recorded in 10 mM glucose was - 1643 ± 68 MΩ (n= 225; range 294 to 4682 MΩ) compared to that observed in 2 mM glucose which amounted to 1493 ± 41 MΩ (n=313; range 170 to 4153 MΩ). There was a significant difference in the neuronal input resistance observed in the two extracellular glucose concentrations, input resistance being significantly higher in neurones recorded in 10 mM glucose ($p>0.05$; Figure 4.1 B). Frequency histograms (Figure 4.2 B) plotted for both 10 mM and 2 mM glucose-containing aCSF for the input resistance were skewed to the right. The modes for each concentration were the same, with the largest percentage of neurones in 10 mM (25.4%) and 2 mM (23.1%) glucose falling within the range of 1200-1600 MΩ. The median values were 1450MΩ and 1347MΩ for 10 mM and 2 mM glucose-containing aCSF, respectively. These data suggest that on average neurones recorded in 10 mM glucose aCSF have a higher input resistance than those recorded in 2 mM glucose aCSF.

4.2.1.3 Firing rate

In neurones recorded in 10 mM extracellular glucose spontaneous action potential firing rate was 1.1 ± 0.1 Hz (n= 105; range 0 to 7.5 Hz) and 1.6 ± 0.1 Hz (n= 267; range 0 to 9.7 Hz) in 2 mM glucose. Spontaneous firing rate was found to be significantly higher in 2 mM compared to 10 mM extracellular glucose ($P<0.01$; see Figures 4.1C and 4.2C). Frequency histograms revealed neurones recorded in 2 mM glucose-containing aCSF had a larger proportion of neurones with a higher firing rate than those recorded in 10 mM. The modes for each concentration were the same, with the largest percentage of neurones in 10 mM (27.6%) and 2 mM (23.6%) glucose having a firing rate between 0-0.5 Hz. There was a also a greater

proportion of neurones recorded in 10 mM aCSF (23.6%) that were silent, showing no spontaneous suprathreshold activity than compared to those observed in 2 mM glucose-containing aCSF (23.6%; see Figure 4.3). The median values were 0.43Hz and 0.8Hz for 10 mM and 2 mM glucose-containing aCSF, respectively, again highlighting the significantly greater degree of spontaneous, suprathreshold activity in 2 mM extracellular glucose.

Table 4.1 **General membrane properties of Arc neurones recorded in 2 mM and 10 mM extracellular glucose**

All neurones			
	10 mM glucose	**2 mM glucose**	**Significance (*P*)**
Membrane potential (mV)	-46.6 ± 0.4 (*n*=225)	-45.9 ± 0.3 (*n*=313)	*P*=0.13 (ns)
Input Resistance (MΩ)	1643 ± 89 (n=225)	1493 ± 41 (*n*=313)	***P* < 0.05**
Firing frequency (Hz)	1.1 ± 0.1 (n=104)	1.6 ± 0.1 (n=267)	***P* < 0.01**

4.2.2 The effects of different ambient extracellular glucose concentrations on subthreshold active conductances expressed in Arc neurones.

In chapter 3 this study described 8 electrophysiologically distinct groups (termed clusters) based on the expression of active conductances commonly observed within the Arc namely, I_h, I_{an}, T-type like calcium conductance and I_a. These clusters were characterised according to their differential expression of one or more of these active conductances. This classification enabled the identification of a specific subset of orexigenic neurones (cluster 2),

that were subsequently identified as orexigen-sensitive NPY/AgRP-expressing conditional pacemaker neurones (van den Top *et al.*, 2004). Other clusters require further clarification of their functional and operational significance. To determine the subthreshold active conductances expressed by each individual neuron, I/V relationships were generated. Hyperpolarising and depolarising current pulses of constant increment (step: amplitude 5-20pA, duration 1200ms, 0.2Hz) were applied to each cell, and subsequent membrane responses recorded.

4.2.2.1 Cluster 1

Cluster 1 neurones were defined as displaying anomalous inward rectification (I_{an}, see chapter 3). The inward rectification was shown as a decrease in input resistance, as seen by reduced voltage deflections to incremental negative current pulses, at hyperpolarised membrane potentials, thus showing distinct membrane potential non-linearity.

The mean resting membrane potential of cluster 1 neurones recorded in 10 mM glucose was -48.4. ± 1.4 mV (n=19; range -38 to -64 mV) and -45.2 ± 1.8 mV (n=21; range -33 to -62 mV) in the presence of 2 mM glucose (Figure 4.4 Ai / Aii). Comparing the mean resting membrane potentials of the two groups showed there was no significant difference between cluster 1 neurones recorded in the presence of 10 mM or 2 mM glucose (P=0.2). Frequency-histograms were (Figure 4.4 Ai) plotted for cluster 1 neurones recorded in 10 mM and 2 mM glucose-containing aCSF. The modes for each concentration differed, with cluster 1 neurones recorded in 10 mM glucose having the highest percentage of neurones with resting membrane potentials between -50 to -55mV (47.4%). In contrast in 2 mM glucose the highest percentage of cluster 1 neurones had more depolarised resting membrane potentials falling between -35 to -45mV. The median values for the resting membrane potentials were -50mV

and -41mV for 10 mM and 2 mM glucose-containing aCSF, respectively. These findings suggest more depolarised resting membrane potentials of cluster 1 neurones recorded in 2 mM glucose. However, increased numbers (n) would need to be obtained to confirm this.

The mean input resistance of cluster 1 neurones amounted to 2039 ± 277 MΩ (range 556 to 4664 MΩ) in 10 mM glucose and 1691 ± 230 MΩ (range 589 to 4115 MΩ) in 2 mM glucose (*P*=0.3; Figure 3.4 Bi/Bii). The modes for each glucose concentration differed with the largest percentage of neurones in 10 mM (33.3%) having an input resistance between 1200-1600 MΩ and neurones in 2 mM (33.3%) commonly having a lower input resistance between 800-1200 MΩ. The median values for the neuronal input resistance was 1626 MΩ and 1270 MΩ for 10 mM and 2 mM glucose-containing aCSF, respectively. Thus, although not reaching statistical significance probably due to the insufficient numbers, the general trend was that input resistance of cluster 1 neurones in 10 mM glucose was higher than that observed in 2 mM glucose.

The firing rate of neurones in 10 mM glucose was 1.16 ± 0.36 Hz (range 0.02 to 2.6Hz; n=8) and in 2 mM a higher firing rate of 2.36 ± 0.53 (range 0 to 9.73 Hz; *P*=0.2; n=21 Figure 3.4 Ci/Cii). Neurones recorded in 10 mM glucose-containing aCSF had a higher percentage of neurones (33.3%) with a firing rate between 0 to 0.5 Hz, compared to the cluster 1 neurones recorded in 2 mM aCSF that had a mode of 1.5 to 2.0Hz (19.1%). Thus again there appeared a trend towards a higher spontaneous firing rate in cluster 1 neurones recorded in 2 mM glucose.

Membrane time-constants (tau) give an indication of the size of somatic and proximal dendritic membrane surface area of a neurone. Membrane time-constants were taken from the charging section (bi-exponential fit) of the voltage transient elicited by weak hyperpolarising current pulses. The membrane time-constant of neurones recorded in 10 mM extracellular glucose was 67.6 ± 8.7 ms and 64.1 ± 10.5 ms in 2 mM glucose, and were

therefore not significantly different (*P*=0.8) suggesting cluster 1 neurones comprised of similar populations of neurones in both concentrations of glucose tested. In the presence of 2 mM glucose there was a slightly prolonged action potential duration (3.1 ± 0.2 ms) compared to that observed in cluster 1 neurones in the presence of 10 mM glucose (2.8 ± 0.1 ms), although this difference was not statistically significant (*P*=0.1). Closer inspection of the anomalous inward rectification observed in cluster 1 neurones revealed no significant differences in this active conductance in the two glucose concentrations. Neurones recorded in 10 mM glucose had a mean relative rectification (input resistance at rest relative to input resistance around -100mV) of 30.3 ± 4.1% at a mean holding potential of -100.4 ± 0.9. The mean holding potential indicating the membrane potential to which the neurone was driven too when carrying out the I/V relationship. Activation of I_{an} in 2 mM glucose amounted to a 31.0 ± 3.3% reduction in input resistance at a holding membrane potential of -100 ± 0.8 mV relative to input resistance at rest. Thus there was no significant difference in the relative strength of this conductance in either concentration of glucose (*P*=0.9).

In summary therefore cluster 1 neurones recorded in 2 mM extracellular glucose, on average, had a lower input resistance and a higher firing rate than the corresponding cluster 1 neurones recorded in 10 mM extracellular glucose. Table 4.2 summarises all data obtained for cluster 1 neurones.

Table 4.2 Passive and active membrane properties of Cluster 1 neurones

Cluster 1			
	10 mM glucose	**2 mM glucose**	***Significance (P)***
Parameter			
Membrane potential (mV)	-48.4 ± 1.4	-45.2 ± 1.8	0.2
Input Resistance (MΩ)	2039 ± 277	1691 ± 230	0.3
Firing frequency (Hz)	1.16 ± 0.36	2.37 ± 0.53	0.2
Membrane time-constant (ms)	67.6 ± 8.7	64.1 ± 10.5	0.8
AP spike duration (ms)	2.8 ± 0.1	3.1 ± 0.2	0.1
Holding potential (mV)	-100.4 ± 0.9	-100 ± 0.8	0.7
I_{an} (%)	30.3 ± 4.1	31.0 ± 3.3	0.9

4.2.2.2 Cluster 2

Cluster 2 neurones were defined as displaying an anomalous inward rectification (I_{an}) and an A-like transient outward conductance (I_a) as described in chapter 3. The I_a manifests as a delayed return to rest of the membrane response to hyperpolarisation following negative current injections. The mean resting membrane potential of cluster 2 neurones recorded in 10 mM extracellular glucose was -45.3 ± 1.5 mV (range -35 to -50 mV; n=10) and -44 ± 1.9 mV (range -35 to -55 mV; n=13) in 2 mM extracellular glucose (*P*=0.6; Figure 4.5 Ai/Aii). Frequency-histograms were plotted for all cluster 2 neurones in both 10 mM and 2 mM glucose-containing aCSF (Figure 4.5 Ai). The modes in each concentration differed, with cluster 2 neurones recorded in 10 mM glucose having the highest percentage of neurones occurring over a wide range of resting membrane potentials (-40 to -45mV, -45 to -50mV and -50 to -55mV; 30%). In contrast in 2 mM glucose-containing aCSF, the highest percentage of neurones were found with resting membrane potentials ranging between -35 to -40 mV (38.4%), and were therefore more depolarised than the corresponding neurones in 10 mM

glucose. The median values for the resting membrane potential were -46mV and -43mV for 10 mM and 2 mM glucose-containing aCSF, respectively.

The mean input resistance of cluster 2 neurones amounted to 1835 ± 359 MΩ (range 1012 to 4682 MΩ) in 10 mM glucose and 1593 ± 129 MΩ (range 1009 to 2671 MΩ) in 2 mM glucose. These differences in input resistance in the two concentrations of glucose were not statistically significant (*P*=0.4; Figure 3.5 Bi/Bii). The mode for input resistance of cluster 2 neurones in both glucose concentrations were the same in 10 mM glucose (50%) and 2 mM glucose (53.8%) having an input resistance ranging between 1200-1600 MΩ. The median values for the neuronal input resistance were 1397 MΩ and 1506 MΩ for 10 mM and 2 mM glucose-containing aCSF, respectively.

The firing rate of cluster 2 neurones in 10 mM glucose was 1.9 ± 0.4 (range 0.1 to 3.7) and in 2 mM a firing rate of 2.19 ± 0.3 Hz (range 0 to 6 Hz; *P*=0.7; Figure 3.5Ci/Cii) was observed. For cluster 2 neurones recorded in both glucose concentrations the mode for firing rate was 1.5-2.0 Hz. The median values for action potential discharge was 1.8 Hz and 1.9 Hz for 10 mM and 2 mM glucose-containing aCSF, respectively.

The membrane time-constant of neurones recorded in 10 mM extracellular glucose was 43.7 ± 7.0 ms and 43.9 ± 10.1 ms in 2 mM glucose, thus not significantly different (*P*=0.9). There was no significant difference in action potential duration (*P*=0.8) at threshold in the two different extracellular glucose concentrations.

Cluster 2 neurones express I_{an} which was relatively stronger in these neurones in 2 mM glucose. Neurones recorded in 10 mM glucose had a mean relative rectification (input resistance change at rest relative to input resistance around -100mV) of 38.3 ± 4.6 % with the corresponding value in 2 mM glucose being 45.5 ± 4.0 % (*P*=0.2). Thus a stronger anomalous inward rectification was seen recorded in cluster 2 neurones in 2 mM glucose aCSF, although this was not statistically significant (*P*=0.2). Properties of I_a were compared in

the two different glucose concentrations, care being taken to compare properties of this conductance at similar membrane potentials to avoid indirect errors reflecting differences in membrane/holding potential. In 2 mM glucose I_a was slightly larger in amplitude indicated by an increase in amplitude at 50% decay-time of 7.3 ± 0.6 mV, the corresponding value in 10 mM glucose-containing aCSF being 6.5 ± 0.6 mV. However this difference did not reach statistical significance (*P*=0.4). The duration of activation of I_a was shorter in the presence of 2 mM (1304 ± 179ms) glucose than in 10 mM glucose (2373 ± 578ms). However, again, these differences in the properties of this conductance did not reach statistical significance (*P*=0.07) probably reflecting the low numbers recorded. Table 4.3 summarises all data obtained for cluster 1 neurones.

Table 4.3 Passive and active membrane properties of Cluster 2 neurones

Cluster 2			
	10 mM glucose	**2 mM glucose**	**Significance (*P*)**
Parameter			
Membrane potential (mV)	-45.3 ± 1.5	-44.0 ± 1.9	0.6
Input Resistance (MΩ)	1835 ± 359	1593 ± 129	0.4
Firing frequency (Hz)	1.94 ± 0.4	2.19 ± 0.4	0.7
Membrane time constant (ms)	43.4 ± 7.0	41.9 ± 9.3	0.9
AP spike duration (ms)	3.2 ± 0.1	3.3 ± 0.2	0.8
Holding potential (mV)	-97.2 ± 1.6	-98.7 ± 0.3	0.3
Ian (%)	38.3 ± 4.6	45.5 ± 3.9	0.2
Ia ½ decay time (mV)	6.5 ± 0.5	7.3 ± 0.7	0.4
Ia duration	2372 ± 578	1304 ± 179	0.07

4.2.2.3 Cluster 3

Cluster 3 neurones were identified on the basis that they expressed no obvious subthreshold active conductances. These neurones in 10 mM glucose had a resting membrane potential of -45.2 ± 3.9 mV (range -30 to -66 mV; n=9), and in 2 mM glucose, -44.0 ± 1.9 mV (range -34 to -56 mV; n=13), thus not statistically significant in the two glucose concentrations (*P*=0.76 Figure 4.6 Ai/Aii). The mode for cluster 3 neurones in both glucose concentrations were the same with the majority of neurones in 10 mM glucose (33.3%) and 2 mM glucose (38.4%) having a resting membrane potential ranging between -35 to -40 mV. The median values for the membrane potential were -42 mV and -39 mV for 10 mM and 2 mM glucose-containing aCSF, respectively.

The mean input resistances of cluster 3 neurones in 10 mM and 2 mM glucose were 1700 ± 315 MΩ (range 694 to 3417 MΩ) and 1379 ± 151MΩ (range 671 to 2587 MΩ), respectively. The input resistance modes for each glucose concentration differed with the largest percentage of neurones in 10 mM glucose being divided equally and ranging between 800-1200 MΩ, 1200-1600 MΩ and 1600-2000 MΩ (22.2%; Figure 4.6 Bi/Bii). However, in 2 mM glucose aCSF, cluster 3 neurones with input resistance ranging between 800-1200 MΩ formed the largest population (38.4%). The median values for the neuronal input resistances of cluster 3 neurones were 1471 MΩ and 1287 MΩ in 10 mM and 2 mM glucose-containing aCSF, respectively. Thus there was a trend for cluster 3 neurones to express a higher neuronal input resistance when exposed to an ambient glucose concentration of 10 mM compared to 2 mM.

The mean spontaneous firing frequency of cluster 3 neurones in 10 mM glucose-containing aCSF was 1.26 ± 0.4 Hz (range 0 to 3.03 Hz) and in 2 mM glucose a slightly higher average spontaneous firing rate of 2.0 ± 0.7 Hz (range 0 to 6.57 Hz) although this

difference did not reach statistical significance (*P*=0.37; see Figures 4.6 Ci/Cii). The majority of neurones in both 2 mM and 10 mM glucose-containing aCSF exhibited firing rates between 0-0.5 Hz.

The membrane time-constant of neurones recorded in 10 mM extracellular glucose was 31.5 ± 8.0 ms, the corresponding value in 2 mM extracellular glucose amounting to 28.1 ± 4.2 ms in 2 mM (*P*=0.73). Action potential duration in 10 mM glucose was 3.4 ± 0.3ms with no significant difference in 2 mM glucose which was associated with a mean duration of 3.3 ± 0.2 ms (*P*=0.84). Table 4.4 summarises all data obtained for cluster 3 neurones.

Table 4.4 Passive and active membrane properties of Cluster 3 neurones

Cluster 3			
	10 mM glucose	**2 mM glucose**	**Significance (*P*)**
Parameter			
Membrane potential (mV)	-45.2 ± 3.9	-44.0 ± 1.9	0.7
Input Resistance (MΩ)	1700 ± 315	1379 ± 151	0.3
Firing frequency (Hz)	1.26 ± 0.4	2.05 ± 0.7	0.3
Membrane time constant (ms)	31.5 ± 8.0	28.1 ± 4.2	0.7
AP spike duration (ms)	3.4 ± 0.3	3.3 ± 0.2	0.8

4.2.2.4 Cluster 4

Cluster 4 neurones displayed a voltage- and time-dependent hyperpolarisation-activated non-selective cation conductance (I_h), which presented as a depolarising 'sag' of the membrane potential response when the cell was injected with negative current. This 'sag' became more prominent at more negative membrane potentials.

In 10 mM glucose, cluster 4 neurones had a mean resting membrane potential of -48.3 ± 1.6 mV (range -38 to -65 mV; n=21) and in 2 mM glucose a value of -47.0 ± 1.7 mV

(range -35 to -60 mV; n=19;) was observed, There was no significant difference in the membrane potentials recorded in 10 mM versus 2 mM extracellular glucose (*P*=0.6; Figure 4.7 Ai/Aii). However the modes observed for each glucose concentration differed with the largest percentage of neurones recorded in 10 mM glucose aCSF (38%) having a membrane potential ranging between -40 to -45 mV. In contrast the mode for neurones recorded in 2 mM glucose aCSF was -50 to -55 mV (26.3%). The median values for the resting membrane potential were -46mV and -48mV in 10 mM and 2 mM glucose-containing aCSF, respectively. Thus there was a trend for the resting membrane potential to sit at more negative values in 2 mM as opposed to 10 mM extracellular glucose.

The mean input resistances of cluster 4 neurones were 1397 ± 167 MΩ (range 294 to 3010 MΩ) and 1684 ± 146 MΩ (range 854 to 2698 MΩ) in 10 mM and 2 mM glucose, respectively (*P*=0.2; Figure 4.7 Bi/Bii). The majority of neurones recorded in 10 mM and 2 mM glucose had an input resistance ranging between 800-1200 MΩ (38% and 39/%, for 10 mM and 2 mM glucose, respectively). The median values for the neuronal input resistance were 1152 MΩ and 1693 MΩ for 10 mM and 2 mM glucose-containing aCSF, respectively.

The mean firing frequency of cluster 4 neurones in 10 mM glucose aCSF was 1.8 ± 0.6 Hz (range 0 to 5.3 Hz) and in 2 mM glucose a slightly lower average of 1.1 ± 0.3 Hz (range 0 to 2.51 Hz) was observed. These differences in spontaneous firing rate were not statistically significant (*P*=0.2; Figure 4.7 Ci/Cii). The majority of neurones in both 2 mM and 10 mM glucose-containing aCSF exhibited firing rates between 0 to 0.5 Hz with median values of 0.8 Hz and 1.5 Hz, respectively.

The membrane time-constant of neurones recorded in 10 mM extracellular glucose was 49.0 ± 10.0 ms and the corresponding value in 2 mM glucose amounting to 31.6 ± 7.7 ms. Thus there was a clear trend toward a reduced membrane time-constant for cluster 4 neurones in 2 mM glucose although this value did not quiet reach statistical significance

(*P*=0.1). Action potential duration in 10 mM was 3.0 ± 0.1ms with no significant difference in 2 mM glucose which gave a mean duration of 3.1 ± 0.2 ms (*P*=0.19).

The change in membrane potential between instantaneous and steady-state responses was used as a measure of the magnitude of I_h. In 10 mM extracellular glucose, the activation of I_h gave rise to depolarising sag of amplitude 7.7 ± 0.7 mV at a mean membrane potential of -102.9 ± 1.1 mV. This is equivalent to a decrease in input resistance of 14.3 % relative to peak input resistance upon activation of I_h indicated in the table below as the input resistance ratio. In contrast in 2 mM glucose the activation of Ih gave rise to a depolarising sag of amplitude 6.5 ± 1.9 mV at a mean membrane potential of -104.4 ± 0.8 mV. This is equivalent to a decrease in input resistance of 24.7% upon activation of I_h. Thus the relative strength of I_h in cluster 4 neurones appears stronger in an extracellular bathing medium of 2 mM.

In summary therefore cluster 4 neurones recorded in 2 mM extracellular glucose, on average, express a higher neuronal input resistance and a lower firing rate than those neurones recorded in 10 mM. Furthermore, in 2 mM glucose-containing aCSF, I_h appears to be relatively 'stronger' although this may also reflect an indirect consequence of the trend for cluster 4 neurones to express a higher neuronal input resistance. Table 4.5 summarises all data obtained for cluster 4 neurones.

Table 4.5 Passive and active membrane properties of Cluster 4 neurones

Cluster 4			
	10 mM glucose	**2 mM glucose**	**Significance (*P*)**
Parameter			
Membrane potential (mV)	-48.3 ± 1.6	-47.0 ± 1.7	0.6
Input Resistance (MΩ)	1397 ± 167	1684 ± 474	0.2
Firing frequency (Hz)	1.8 ± 0.6	1.1 ± 0.3	0.2
Membrane time constant (ms)	49.0 ± 10.0	31.6 ± 7.7	0.1
AP spike duration (ms)	3.0 ± 0.1	3.1 ± 0.2	0.8
Amplitude of I_h (mV)	7.7 ± 0.7	6.5 ± 1.9	0.5
Input resistance ratio (%)	14.3 ± 1.2	24.7 ± 10.0	0.29

4.2.2.5 Cluster 5

Cluster 5 neurones were identified by the expression of a T-type calcium conductance and I_h. In 10 mM glucose cluster 5 neurones had a mean resting membrane potential of -48.1 ± 1.2 mV (range -32 to -66 mV; n=41) and in 2 mM glucose a value of -47.3 ± 0.7 mV was observed (range -34 to -62 mV; n=66). No significant difference between the two glucose concentrations was observed with regard to membrane potential (*P*=0.5; Figure 4.8 Ai/Aii). Frequency histograms followed a normal distribution for all clusters 5 neurones in both 10 mM and 2 mM glucose-containing aCSF. The majority of cluster 5 neurones in both glucose concentrations had a resting membrane potential ranging between -45 to -50 mV. The median

values for the resting membrane potential were -47mV and -47mV in 10 mM and 2 mM glucose-containing aCSF, respectively.

The mean input resistance amounted to 1529 ± 96 MΩ (range 462 to 3582 MΩ) in 10 mM glucose with a corresponding value of 1430 ± 94 MΩ (range 386 to 3466 MΩ) in 2 mM glucose (*P*=0.4; Figure 4.8 Bi/Bii). The modes for each glucose concentration differed with the largest percentage of cluster 5 neurones in 2 mM extracellular glucose ranging between 400-1200 MΩ (22.7%). In 10 mM glucose-containing aCSF, the largest percentage of cluster 5 neurones had input resistances ranging between 1200-1600 MΩ (37.7%). The median values for the neuronal input resistance were 1503 MΩ and 1263 MΩ for 10 mM and 2 mM glucose-containing aCSF, respectively. Thus, cluster 5 neurones displayed a tendency towards higher neuronal input resistances when bathed in extracellular glucose concentrations of 10 mM compared to 2 mM.

The mean spontaneous firing rate of neurones in 10 mM glucose was 0.7 ± 0.2 Hz (n=18; range 0 to 4.4 Hz) with the corresponding value in 2 mM glucose amounting to 0.8 ± 0.2 Hz (n= 59; range 0 to 6.26 Hz), thus not statistically significant (*P*=0.80; Figure 4.8Ci/Cii).

The membrane time-constant of neurones recorded in 10 mM extracellular glucose was 39.3 ± 2.9 ms and 35.2 ± 2.9 ms in 2 mM glucose, and were therefore not significantly different (*P*=0.3).

Action potential duration in 10 mM extracellular glucose was 3.5 ± 0.3 ms with no significant difference in 2 mM glucose, the latter having a mean duration of 3.1 ± 0.1 ms (*P*=0.1).

In 10 mM extracellular glucose, activation of I_h gave rise to a depolarising sag, in response to hyperpolarising current injection, of amplitude 5.9±0.5 mV at a mean membrane potential of -103.9 ± 0.9 mV. This is equivalent to a decrease in input resistance of 10.7 % upon steady-state activation of I_h. In contrast in 2 mM glucose the activation of I_h gave rise to a depolarising sag of amplitude 8.2 ± 0.4 mV at a mean membrane potential of -104.3 ± 0.6

mV. This is equivalent to a decrease in input resistance of 14.5% upon activation of I_h. The decreases in input resistance observed in the two concentrations of glucose-containing aCSF were significantly different ($p < 0.01$). Thus cluster 5 neurones recorded in 2 mM glucose aCSF appear to have a significantly stronger I_h (larger amplitude) than those cluster 5 neurones recorded in 10 mM glucose.

Cluster 5 neurones also exhibit a T-type calcium conductance. Activation of this active conductance in 10 mM glucose gave an average membrane depolarisation of 10.0 ± 1.2mV when activated following hyperpolarisation from a membrane potential of -47.2 ± 1.3mV (n=37). In 2 mM extracellular glucose activation of the T-type conductance gave a mean membrane depolarisation of 10.5 ± 0.7mV when activated by hyperpolarisation from a membrane potential of -47.8 ± 0.7 (n=65). These values for the amplitude of the T-type conductance were not significantly different between the two concentrations of glucose tested. Table 4.6 summarises all data obtained for cluster 5 neurones.

Table 4.6 Passive and active membrane properties of Cluster 5 neurones

Cluster 5			
	10 mM glucose	**2 mM glucose**	**Significance (*P*)**
Parameter			
Membrane potential (mV)	-48.1 ± 1.2	-47.3 ± 0.7	0.5
Input Resistance (MΩ)	1529 ± 96	1430 ± 94	0.4
Firing frequency (Hz)	0.75 ± 0.2	0.85 ± 0.2	0.8
Membrane time constant (ms)	39.3 ± 2.9	35.2 ± 2.9	0.3
AP spike duration (ms)	3.5 ± 0.3	3.1 ± 0.0	0.1
Amplitude of I_h (mV)	5.9 ± 0.5	8.2 ± 0.4	***P* < 0.01**
Input resistance ratio (%)	10.7 ± 0.9	14.4. ± 0.7	***P* < 0.01**
T-type amplitude (mV)	10.0 ± 1.2	10.5 ± 0.7	0.7

4.2.2.6 Cluster 6

Cluster 6 neurones expressed only a T-type calcium conductance, exhibited as a rebound depolarisation on termination of negative current injection. In 10 mM glucose cluster 6 neurones had a mean resting membrane potential of -44.9 ± 0.8 mV (n=59; range -30 to -60 mV) compared to a mean resting membrane potential of -44.7 ± 0.7 mV (n=75; range -32 to -63 mV) for cluster 6 neurones exposed to an extracellular glucose concentration of 2mM. These differences were not statistically significant (*P*=0.8; Figure 4.9 Ai/Aii). Frequency-histograms followed a normal distribution for all clusters 6 neurones in both 10 mM and 2 mM glucose-containing aCSF. The majority of neurones in both glucose concentrations had a membrane potential ranging between -45 to -50mV. The median values for the resting membrane potential for both populations was -45mV in 10 mM and 2 mM glucose-containing aCSF, respectively for neurones identified as cluster 6.

The mean input resistance was 1404 ± 89 MΩ (range 435 to 3433 MΩ) and 1475 ± 70 MΩ (range 170 to 3314 MΩ) in 10 mM and 2 mM glucose, respectively *(P*=0.5; Figure 4.9 Bi/Bii). Input resistances for cluster 6 neurones recorded in 10 mM glucose aCSF when plotted as a frequency histogram were slightly skewed to the left. This indicated that there was a greater proportion of neurones recorded in 10 mM glucose aCSF with a relatively lower input resistance than those recorded in 2 mM glucose-containing aCSF. The greatest proportion of neurones recorded in 10 mM glucose aCSF had an input resistance ranging between 800-1200 MΩ (27.1%). In contrast the largest proportion of neurones recorded in 2 mM glucose-containing aCSF had an input resistance ranging between 1200-1600 MΩ (22.5%). The median values for the neuronal input resistance were 1295 MΩ and 1468 MΩ for 10 mM and 2 mM glucose-containing aCSF, respectively for neurones identified as cluster 6.

Spontaneous firing rates in the two concentrations varied significantly ($p < 0.01$). In 10 mM glucose the mean spontaneous firing rate was 0.39 ± 0.17 Hz (n=28; range 0 to 4.56 Hz). In contrast, in 2 mM glucose, spontaneous firing rate was 1.24 ± 0.19Hz (n= 59; 0 to 5.68 Hz; Figure 4.9 Ci/Cii). Plotting frequency histograms reveals that cluster 6 neurones recorded in 2 mM extracellular glucose-containing aCSF tended to higher firing rates, as shown by the 'tail' in the graph shown in Figure 4.9 Ci.

The membrane time-constant of neurones recorded in 10 mM extracellular glucose was 37.9 ± 2.6 ms and 29.2 ± 2.2 ms in 2 mM extracellular glucose. There was a significant difference in the membrane time-constant of these neurones in the two different extracellular glucose concentrations ($p < 0.05$). Action potential duration in 10 mM glucose was 3.7 ± 0.1 ms and the corresponding value in 2 mM glucose of 3.3± 0.0 ms being significantly lower than that observed in 10 mM ($P < 0.05$).

Activation of the T-type conductance gave a mean membrane depolarisation of 8.4 ± 0.7 mV and 9.2 ± 0.6 mV , following hyperpolarisation from a membrane potential of -47.2 ± 0.9 and -44 .2± 0.7 in 10 mM and 2 mM extracellular glucose, respectively. The differences in the amplitude of the T-type calcium conductance in the two different concentrations of glucose were not statistically significant (P =0.4). Table 4.7 summarises all data obtained for cluster 6 neurones.

Table 4.7 Passive and active membrane properties of Cluster 6 neurones

Cluster 6			
	10 mM glucose	**2 mM glucose**	**Significance (*P*)**
Parameter			
Membrane potential (mV)	-44.9 ± 0.8	-44.7 ± 0.7	0.8
Input Resistance (MΩ)	1404 ± 89	1475 ± 70	0.5
Firing frequency (Hz)	0.39 ± 0.17	1.24 ± 0.19	***P* < 0.01**
Membrane time-constant (ms)	37.9 ± 2.9	29.2 ± 2.2	***P* < 0.05**
AP spike duration (ms)	3.7 ± 0.1	3.3 ± 0.0	***P* < 0.05**
T-type amplitude (mV)	8.4 ± 0.7	9.2 ± 0.6	0.4

4.2.2.7 Cluster 7

Cluster 7 neurones expressed I_{an} and a T-type calcium conductance. The mean resting membrane potential of cluster 7 neurones recorded in 10 mM extracellular glucose was -46.0 ± 0.9 mV (range -39 to -59 mV; n=29) and -45.8 ± 1.3mV (range -33 to -62 mV; n=33; Figure 4.10 Ai/Aii) in the presence of 2 mM extracellular glucose (*P*=0.9). The majority of neurones in both glucose concentrations had resting membrane potentials ranging between -45 to -50 mV. The median values for the resting membrane potential were -45 mV and -45 mV in 10 mM and 2 mM glucose-containing aCSF, respectively for neurones identified as cluster 7.

The mean input resistance amounted to 1781 ± 153 MΩ (range 623 to 3577 MΩ) in 10 mM glucose and 1653 ± 121 MΩ (range 665 to 4323 MΩ) in 2 mM glucose, values that were not significantly different (*P*=0.5; Figure 4.10 Bi/Bii). The modes for each glucose concentration were the same with the largest percentage of neurones in 2 mM and 10 mM glucose-containing aCSF ranging between 1200-1600 MΩ accounting for 39% and 25% of the populations, respectively. The median values for the neuronal input resistance were 1595

MΩ and 1488 MΩ in 10 mM and 2 mM glucose-containing aCSF, respectively for neurones identified falling under cluster 7.

The spontaneous firing rate of neurones in 10 mM glucose-containing aCSF was 2.3 ± 0.8Hz (n=10; range 0 to 7.5 Hz) and in 2 mM a lower firing rate of 1.87 ± 0.3 Hz (n=29; 0 to 6.5 Hz; Figure 4.10 Ci/Cii) although this difference did not reach statistical significance (*P*=0.5).

The membrane time-constant of neurones recorded in 10 mM extracellular glucose was 46.1 ± 3.0 ms with the corresponding value in 2 mM glucose amounting to 43.3 ± 3.2 ms with no statistically significant difference between the two (*P*=0.5). Neurones recorded in 10 mM glucose had a mean relative rectification (input resistance at rest relative to input resistance around -100 mV) of 23.2 ± 2.6 % with the corresponding value in 2 mM glucose-containing aCSF being significantly higher at 30.6 ± 2.6% ($p < 0.05$). Thus a stronger rectification was seen in 2 mM glucose-containing aCSF. Activation of the T-type conductance gave a mean membrane depolarisation of 9.7 ± 1.4mV and 9.6 ± 1.0 mV, following hyperpolarisation from a resting membrane potential of -48.3 ± 1.1mV and -46.1 ± 1.3mV, in 10 mM and 2 mM glucose, respectively. Thus there were no statistically significant differences between the amplitudes of T-type conductances recorded under the two different glucose concentrations. Table 4.8 summarises all data obtained for cluster 7 neurones.

Table 4.8 Passive and active membrane properties of Cluster 7 neurones

Cluster 7			
	10 mM glucose	**2 mM glucose**	**Significance (*P*)**
Parameter			
Membrane potential (mV)	-46.0 ± 0.9	-45.8 ± 1.3	0.9
Input Resistance (MΩ)	1781 ± 153	1653 ± 121	0.5
Firing frequency (Hz)	2.3 ± 0.8	1.8 ± 0.3	0.5
Membrane time-constant (ms)	46.1 ± 3.0	43.3 ± 3.2	0.6
AP spike duration (ms)	3.5 ± 0.2	3.0 ± 0.1	0.1
Holding potential (mV)	-100.7 ± 0.6	-100.8 ± 0.6	0.8
I_{an} (%)	23.2 ± 2.6	30.6 ± 2.6	***P* < 0.05**
T-type amplitude (mV)	9.7 ± 1.4	9.6 ± 1.0	0.9

4.2.2.8 Cluster 8

Cluster 8 neurones were identified by the expression of a T-type calcium conductance, I_h and I_{an}. The mean resting membrane potential of neurones recorded in 10 mM glucose was -46.7 ± 1.4mV (n= 37; range -32 to -62 mV) and -46.6 ± 0.9 mV (n=67; range -32 to -66 mV) in the presence of 2 mM extracellular glucose (Figure 4.11 Ai / Aii). Comparing the membrane potentials of the two groups revealed no significant difference between the two populations of neurones recorded in these concentrations of extracellular glucose (*P*=0.9). Frequency histograms were plotted for cluster 8 neurones in both 10 mM and 2 mM glucose-containing aCSF (see Figure 4.11 Ai). The modes for resting membrane potential for each population exposed to these concentrations of glucose were the same, with all cluster 8 neurones recorded in both 10 mM and 2 mM glucose-containing aCSF having the highest number of neurones with resting membrane potentials ranging between -45 to -50 mV, accounting for 45.5% of the cluster 8 neurones observed in 10 mM extracellular glucose and 23.8% of the population of cluster 8 neurones observed in 2 mM glucose. The median values for the resting

membrane potentials were -46mV and -46mV for 10 mM and 2 mM glucose-containing aCSF, respectively.

The mean input resistance amounted to 1651 ± 113 MΩ (range 500 to 3333 MΩ) in 10 mM glucose and 1385 ± 95 MΩ (range 288 to 3901 MΩ) in 2 mM glucose (*P*=0.08; Figure 4.11Bi/Bii). The median values for the neuronal input resistances were 1575 MΩ and 1220 MΩ in 10 mM and 2 mM glucose-containing aCSF, respectively for neurones identified as cluster 8.

Spontaneous firing rates in the two concentrations varied significantly ($P < 0.05$). In 10 mM glucose the mean firing rate was 1.16 ± 0.3 Hz (range 0 to 5.7 Hz; n=28). In contrast in 2 mM glucose firing rate was higher with a value of 2.2 ± 0.2Hz (0 to 7.5Hz; n= 59; see Figure 4.11 Ci/Cii). Plotting frequency-histograms reveals that cluster 8 neurones recorded in 2 mM glucose aCSF tended to higher firing rates, as suggested by the 'tail' in the distribution plot (Figure 4.11 Ci).

The membrane time-constant of neurones recorded in 10 mM extracellular glucose was 65.5 ± 6.1 ms and 60.0 ± 4.0ms in 2 mM glucose, and were therefore not significantly different (*P*=0.4). Action potential duration in 10 mM extracellular glucose was 3.1 ± 0.1 ms with no significant difference in 2 mM glucose, (*P*=0.4) where the corresponding value amounted to 3.1 ± 0.0 ms.

The difference in peak amplitude between the instantaneous and steady-state membrane potential responses to hyperpolarising current injection was used as a measure of the size of I_h. In 10 mM extracellular glucose, activation of I_h gave rise to depolarising sag of amplitude 5.1 ± 0.4 mV at a mean membrane potential of -101.6 ± 0.8mV. This is equivalent to a decrease in input resistance of 9.7 % upon activation of I_h. In contrast in 2 mM glucose the activation of I_h gave rise to a depolarising sag of amplitude 9.2 ± 0.4 mV at a mean membrane potential of -100.6 ± 0.4mV. This is equivalent to a decrease in input resistance of

25% upon activation of I_h. Thus, again in 2 mM glucose-containing aCSF, I_h appears to be enhanced in cluster 8 neurones compared to Ih observed in these neurones in 2 mM glucose (*P* <0.001).

Neurones recorded in 10 mM glucose had a mean rectification percentage (input resistance at rest relative to input resistance around -100mV) of 34.1 ± 2.6% and in 2 mM extracellular glucose a lower value of 24.8 ± 2.0% was recorded. Thus there was an apparent enhancement of the anomalous inward rectification in the presence of 10 mM compared to 2 mM extracellular glucose (*P*<0.001). Activation of the T-type conductance gave mean rebound membrane depolarisations of 8.1 ± 1.2mV and 8.6 ± 0.8 mV, following membrane hyperpolarisation from resting potentials of -48.7 ± 1.6mV and -47.0 ± 0.8mV in 10 mM and 2 mM glucose, respectively. Thus there was no significant difference in the amplitude of the rebound depolarisation in these two different ambient extracellular glucose concentrations. Table 4.9 summarises all data obtained for cluster 8 neurone

Table 4.9 Passive and active membrane properties of Cluster 8 neurones

	Cluster 8			
		10 mM glucose	**2 mM glucose**	**Significance (*P*)**
	Parameter			
	Membrane potential (mV)	-46.7 ± 1.0	-46.6 ± 0.9	0.9
	Input Resistance (MΩ)	1651 ± 113	1385 ± 95	0.08
	Firing frequency (Hz)	1.16 ± 0.3	2.26 ± 0.2	***P* < 0.05**
	Membrane time-constant (ms)	65.5 ± 6.1	60.0 ± 4.0	0.4
	AP spike duration (ms)	3.1 ± 0.1	3.1 ± 0.0	0.9
I_h	Amplitude of I_h (mV)	5.1 ± 0.4	9.2 ± 0.4	***P* < 0.001**
I_h	Input resistance ratio (%)	9.7 ± 1.0	25.4 ± 1.7	***P* < 0.001**
	T-type amplitude (mV)	8.1 ± 1.2	8.59 ± 0.8	0.7
I_{an}	Holding potential (mV)	-100.7 ± 0.8	-100.6 ± 0.4	0.18
I_{an}	I_{an} (%)	34.1 ± 2.6	24.8 ± 2.0	***P* < 0.001**

4.3 Discussion

The aim of the present study was to investigate the effects of physiologically- and pathophysiologically-relevant glucose concentrations, on the passive and active subthreshold electrophysiological properties of hypothalamic Arc neurones. 2 mM glucose aCSF was used to mimic a putative euglycaemic state and 10 mM glucose aCSF was used to emulate a putative hyperglycaemic state.

Hypothalamic slices were prepared and transferred to a recording chamber in either 10 mM or 2 mM glucose-containing aCSF where they were continually perfused with the same glucose concentration as they were prepared in. The composition of aCSF in *in vitro* slice preparations has been shown to be of fundamental importance as it dictates neuronal excitability and affects protein synthesis (An *et al.*, 2008). Neurones were recorded from the Arc in prescribed euglycaemic (2mM glucose) and hyperglycaemic (10mM glucose) conditions and fundamental electrophysiological properties of the neurones compared in these extracellular glucose levels.

Glucose is essential for the correct functioning of many biological systems and provides the brain with its primary energy source. Neurones within hypothalamic nuclei, in particular the lateral hypothalamus (LH) and ventromedial nucleus (VMN), and more recently the Arc, have been reported to use glucose as a signalling molecule to regulate electrical excitability and neuronal firing (Anand *et al.*, 1964; Oomura *et al.*, 1964; Spanswick *et al.*, 1997; Muroya *et al.*, 1999; Ibrahim *et al.*, 2003; Burdakov *et al.*, 2005). These function-specific glucose-sensing neurones are thought to be crucial for the homeostatic control of glucose levels, effectively forming neural circuits and key components of the counter-regulatory feedback mechanisms and pathways responsible for maintaining glucose levels within narrow limits.

Glucose levels are tightly controlled by multiple homeostatic systems within the body in order to avoid serious pathological conditions such as diabetes. Plasma glucose levels peak and trough after and before meals and are under circadian control (La Fleur *et al.*, 1999). When plasma levels are in the euglycaemic range of 5-8 mM this corresponds to brain glucose levels of 1-2.5 mM (Silver & Erecinska, 1994). In a hyperglycaemic state when plasma levels rise to 15-17 mM, brain glucose levels have been suggested to rise in parallel to as much as 4.5 to 5.5 mM (Silver & Erecinska, 1994). However, the absolute concentrations of glucose that the Arc is exposed to remains unclear. With the hypothalamic Arc being in close proximity to a compromised BBB it has long been suggested that this area of the brain may be exposed too much higher concentrations of glucose than the majority of the rest of the brain. Further work is needed to fully address this issue.

Classic experiments studying glucose-sensing neurones within the hypothalamus used glucose levels outside of the normal physiological range (0-20 mM; Anand *et al.*, 1964; Oomura *et al.*, 1964; Ashford *et al.*, 1990; Spanswick *et al.*, 1997). It has been shown that changes in extracellular concentrations of glucose initiate changes in neuronal excitability of some neurones and hence their functional output (Ma *et al.*, 2008). Certain stimuli can either excite or inhibit neurones depending on the concentration of extracellular glucose. For example, leptin can either decrease or increase the activity of POMC neurones in 5 mM and 11 mM glucose, respectively (Ma *et al.*, 2008).

Artificial CSF with a composition comprised of 10 mM glucose is routinely used in whole-cell electrophysiological recordings from brain slice preparations including the hypothalamic Arc (Spanswick *et al.*, 1997; Ibrahim *et al.*, 2003; van den Top *et al.*, 2004). However, 10 mM may be an excessive amount to expose Arc neurones to, and may even be interpreted as mimicking a hyperglycaemic state (Routh, 2002; de Vries *et al.*, 2003; Mayer *et al.*, 2006). Thus, this study set out to investigate whether there are differences in electrophysiological

properties and the functional operation of Arc neurones and circuits under physiological glucose concentrations (2 mM) versus a putative pathophysiological concentration (10 mM).

The major findings of this study revealed significant differences in some active and passive membrane properties of neurones recorded in 2 mM glucose-containing aCSF and 10 mM glucose-containing aCSF. Specifically, the neuronal input resistance and the firing frequency of neurones significantly differed in each glucose concentration. The neuronal input resistance was significantly higher in Arc neurones recorded in 10 mM compared to 2 mM extracellular glucose whereas the spontaneous firing rate was higher in Arc neurones exposed to 2 mM glucose compared to 10 mM glucose aCSF. However, there was no overall significant change in the resting membrane potential of these neurones. Significant differences in the expression of subthreshold active conductances were also observed, particularly the magnitude of I_h was enhanced and the duration of the A-like transient outward conductance was reduced in 2 mM glucose-containing aCSF compared to 10 mM. The major findings of this study are summarised in Figure 4.11, which shows sample electrophysiological recordings from 'typical' neurones recorded in 10 mM and 2 mM glucose-containing aCSF.

The resting membrane potential was similar for neurones recorded in 10 mM and 2 mM extracellular glucose. These observations are similar to those reported previously by Claret *et al.,* (2007). These investigators reported no significant changes in the resting membrane potential when reducing the glucose concentration from 10 mM to 2 mM in mouse hypothalamic slice preparations.

Neuronal input resistance was significantly different in neurones recorded in the two extracellular glucose concentrations tested in this study. Neurones recorded in 2 mM glucose-containing aCSF had a significantly lower neuronal input resistance than those neurones recorded in 10 mM glucose. These results are in contrast to those found by Fioramonti *et al.*,

(2004) showing that with a higher concentration of glucose (20 mM) there is reduction in input resistance relative to neurones recorded in a more physiological glucose concentration (5 mM). This suggests that neurones recorded in 2 mM glucose may have one or more conductances activated, or relatively more activated than those recorded in 10 mM glucose. A possible ion channel candidate for this role is the K_{ATP} channel which has been strongly implicated in glucose-sensing in the hypothalamus previously (Ashford *et al.*, 1990; Rowe *et al.*, 1996; Spanswick *et al.*, 1997; Lee *et al.*, 1999; Spanswick *et al.*, 2000; Miki *et al.*, 2001). Thus in theory in 2 mM glucose-containing aCSF a larger number of K_{ATP} channels may be open than in 10 mM glucose where more may be closed. Raising levels of extracellular glucose increases the intracellular ATP/ADP ratio causing the K_{ATP} channel to close leading to membrane depolarisation (van den Top *et al.*, 2007). For general review see (Nichols, 2006). However, to fully elucidate if indeed this channel is involved, further work will need to be carried out. For example, comparing the sensitivity of neurones to the sulphonylureas tolbutamide or glibenclamide, both of which would be predicted more effective on neurones at rest, in 2 mM glucose, compared to 10 mM. When looking closely at the electrophysiologically defined clusters, all groups apart from clusters 4 and 6 had a mean overall higher neuronal input resistance in 10 mM glucose compared to their counterparts in 2 mM glucose.

Other possible mechanisms that may be potentially responsible for the observed shift in the input resistance in the two glucose concentrations involve a chloride conductance, and tandem-pore domain, acid-sensitive potassium (TASK) channels (Song *et al.*, 2001; Burdakov *et al.*, 2006; Fioramonti *et al.*, 2007). An increase in extracellular glucose inhibits orexin neurones in the LH through the activation of TASK channels (Burdakov *et al.*, 2006). Another mechanism suggested to be involved in glucose sensing is a chloride conductance whereby elevated glucose levels activate chloride channels within the membrane leading to a

membrane hyperpolarisation (Song *et al.*, 2001; Fioramonti *et al.*, 2007). Which mechanism or combination of mechanisms, if any, relate to observations described here remains to be elucidated and therefore requires further work.

Overall, the mean spontaneous firing rate of neurones recorded in 2 mM extracellular glucose was significantly higher than the corresponding population recorded in 10 mM glucose-containing aCSF. There was also a larger percentage of neurones recorded in 2 mM glucose that were spontaneously active compared to those recorded in 10 mM glucose-containing aCSF. These data are in contradiction to the data obtained for the neuronal input resistance in the differing glucose concentrations. Indeed, a decrease in input resistance in 2mM glucose suggests that there are more ion channels open. However, it is unlikely that this can be accounted for by opening of K_{ATP} channels as this would lead to a membrane hyperpolarisation and a reduction in action potential firing of neurones recorded in 2mM. The results here suggest that it is more than likely that the change in glucose concentrations alters the firing rate and the neuronal input resistance through modulation of other ion channels other than solely K_{ATP} or may involve changes in one or more electrogenic ion pumps or exchangers. It must also been considered that the changes observed maybe due to indirect effects on the cellular membrane, which were not studied in the present investigation.

When characterising neurones based on their expression of subthreshold active conductances, all clusters apart from clusters 4 and 7 displayed an increase in neuronal firing in 2 mM glucose-containing aCSF compared to those recorded in 10 mM glucose-containing aCSF. Thus neurones with similar subthreshold active conductances may behave differently in the presence of different glucose concentrations or under physiological euglycaemic and pathophysiological hyperglycaemic conditions. Glucose-sensing neurones are specialised cells that use glucose as a signalling molecule to alter their action potential frequency in response to changes in ambient glucose levels (Anand *et al.*, 1964; Oomura *et al.*, 1964;

Levin *et al.*, 2004). Whether the neurones recorded within this study are directly glucose sensing is unclear, but the level of suprathreshold spontaneous activity was certainly altered with exposure to different glucose concentrations, with neurones generally being more active when exposed to physiological levels of extracellular glucose. These data therefore cast doubt on the validity of previous studies carried out in 10 mM glucose, a non-physiological or pathophysiological level, and further suggest that a change in extracellular glucose from a non-physiological to a physiological level can shape and change the activity of Arc neurones. Furthermore, if such changes are paralleled at the signalling level, for example at the receptor/transmitter expression level, previous published work undertaken in high levels of extracellular glucose, may require a major re-evaluation.

Another passive membrane property that was considered was the membrane time-constant (tau). Tau is given by the product of the membrane resistance and membrane capacitance hence it reflects the size of the neuronal membrane surface area. For the majority of neuronal clusters classified, the tau value did not dramatically change between the two glucose concentrations. This data suggests that these recordings may have been taken from a similar population of neurones and morphology did not significantly change. However, neurones classified as cluster 4 and cluster 6 were two groups of neurones that were close to or had significantly different tau values when compared between the two glucose concentrations. In 2 mM glucose, clusters 4 and 6 had significantly smaller tau values in comparison to the corresponding clusters recorded in 10mM glucose. These groups of neurones were also the only neurones that exhibited an increase in neuronal input resistance in 2 mM compared to 10 mM extracellular glucose. These results are in accordance with the general consensus that neurones which have a smaller tau value and hence a smaller membrane surface area would be associated with a higher neuronal input resistance, reflecting a smaller sized neurone compared to a large neurone. A possible explanation for

the change in tau values within these clusters is that the change in glucose concentrations may alter the expression of intrinsic conductances to such an extent that they subsequently classify to another cluster. For example extrinsic factors such as NA can activate subthreshold active conductances (I_{an}; See chapter 6). Thus in the presence of NA, an instantaneous inwardly rectifying potassium conductance is activated giving the appearance of a neurone electrophysiologically defined as another cluster. Therefore, in 2 mM glucose where we see a difference in tau values compared to the same electrophysiological phenotype in 10 mM glucose, it may be that we actually recorded from a different population of neurones that shifted or changed expression of active conductances in response to the extrinsic factor, in this case, glucose. Another point to mention is that in chapter 3 we discussed the possibility that clusters do not constitute a morphologically homogeneous group. It maybe that the tau values appear different due to selective recording from a different subset of the same cluster that exhibits different morphological features which is reflected in the tau value. Alternatively, previous studies have suggested considerable synaptic plasticity within the Arc in the regulation of energy homeostasis, and that under pathological conditions synaptic plasticity is impaired (Pinto *et al.*, 2004). The frequency of inputs of both EPSCs and IPSPs differs on fundamental Arc neurones involved in the control of energy balance in leptin-deficient mice (ob/ob) compared to their wild type litter mates. This altered synaptic profile in ob/ob mice is shifted towards wild type values with subsequent administration of leptin (Pinto *et al.*, 2004). Therefore, leptin has the ability to rapidly affect the wiring of key Arc neurones with inputs being suggested to be physically inserted and retracted depending on energy status. Thus, the alteration in glucose levels may modulate synaptic inputs, whereby neurones can retract and rewire in an apparent functional manner. The change in the number of projections and synaptic inputs of a neurone may be reflected in the tau value, whereby for example an

increase in synaptic inputs and projections of a neurone, increases membrane surface area, equating to a larger tau value.

Unfortunately a direct comparison of the clusters in each glucose concentration could not be made, as numbers were made up so to include similar numbers in each group. Therefore a comparison in this case would not be useful as it would not indicate which cluster we would observe more frequently in each concentration.

Neurones expressing I_h revealed an apparent enhancement of this conductance when recorded in 2 mM as opposed to 10 mM extracellular glucose, as shown for clusters 4, 5, and 8. This characteristic 'sag' typical of this time- and voltage-dependent inward rectification resembles the previously described hyperpolarisation-activated non-selective cation conductance or H–current (Halliwell & Adams, 1982; Akasu *et al.*, 1993; Pape, 1996). This apparent sag in the membrane response to hyperpolarising current injection was more prominent in neurones recorded in 2 mM glucose-containing aCSF compared to those recorded in 10 mM glucose. It has been suggested that the time-dependent inward rectification has a role in establishing the resting membrane potential of hypothalamic neurones (Akasu *et al.*, 1993) and contributes to burst-like patterns of firing (van Welie *et al.*, 2006). The apparent enhancement of I_h in 2 mM extracellular glucose could have important functional consequences for these neurones in terms of their ability to integrate synaptic inputs. For example synaptic inputs such as those mediated by GABA can trigger rebound excitations which are mediated through the activation of I_h (Huguenard & Prince, 1994; Whyment *et al.*, 2004). I_h also may have a role in shaping and modulating the output of these neurones such as generating intrinsic oscillations and burst firing patterns of activity, the latter being suggested key for neuropeptide release from neurones (Dutton & Dyball, 1979; Bicknell & Leng, 1981; van Welie *et al.*, 2006).

Another subthreshold active conductance that appeared to change functionally was the A-like transient outward conductance, expressed by cluster 2 neurones. This conductance was characterised by a delayed return to the resting membrane potential following membrane hyperpolarisation induced in response to injection of a negative current. A-like conductances are a common feature of hypothalamic neurones (Bourque, 1988; Tasker & Dudek, 1991; Bouskila & Dudek, 1995). Generally, these conductances are believed to influence spike repolarisation and modulate the frequency of tonically firing neurones (Connor & Stevens, 1971; Kenyon & Gibbons, 1979; Segal *et al.*, 1984). The size and the duration of the A-like conductance were shown to be larger in amplitude and shorter in duration in 2 mM glucose-containing aCSF. These particular neurones have a unique expression of subthreshold active conductances within the Arc and have been previously characterised as NPY/AgRP conditional pacemakers that exhibit burst firing patterns of activity (van den Top *et al.*, 2004). The release of neuropeptides from the Arc could be dependent upon the pattern and properties of the electrical activity of these neurones as described for the release of vasopressin from hypothalamic magnocellular neurones (Dutton & Dyball, 1979). A shorter duration A-current, as observed in 2 mM glucose, could increase the frequency of burst firing in these neurones and thus modulate neuropeptide release. In contrast, in 10 mM glucose, a longer duration A-current could lead to a decrease in burst firing and to differential neuropeptide release compared to that observed in lower glucose levels. Although this study did not directly report the occurrence of burst firing, cluster 2 neurones did exhibit an increase in firing frequency in 2 mM glucose-containing aCSF although not reaching statistical significance, consistent with a shorter duration A-like conductance. The lack of apparent burst firing patterns of activity may reflect the need for the presence of an orexigenic signal, previous work suggesting cluster 2 neurones to be conditional pacemaker neurons requiring an orexigen such as ghrelin for initiation of pacemaker activity (van den Top *et al.*, 2004).

Further work using detailed voltage-clamp recordings are required to clarify exactly what properties of this conductance are changed in the different glucose concentrations.

I_{an} was also expressed by Arc neurones, namely those classified into clusters 1, 2, 7 and 8. This conductance is characterised by an instantaneous decrease in input resistance at more negative membrane potentials. Its function is unclear but its suggested role is to maintain neurones within a functional range to prevent them from becoming 'too' hyperpolarised (Wilson *et al.*, 2002; van den Top & Spanswick, 2006). There was a stronger rectification seen in clusters 1, 2 and 7 in 2mM glucose which may reflect opening of K_{ATP} channels in this lower glucose concentration compared to 10mM glucose, as K_{ATP}-mediated conductances are well documented as weak inward rectifiers (Nichols, 2006). Therefore K_{ATP} channels may contribute to the difference in strength of I_{an} under the different glucose concentrations. However further studies utilising blockers of this channel (such as tolbutamide) are needed to clarify this. One exception to this rule was cluster 8 neurones which exhibited a weaker I_{an} in 2mM glucose than in 10mM glucose. This may be due to the fact that cluster 8 neurones also express I_h, which was significantly stronger in 2mM glucose and may have countered or masked the true effect on the instantaneous rectification, as both conductances were apparent over similar membrane potential ranges.

In summary, observations described in this chapter strongly suggest that there is a need for us to re-evaluate studies that have conducted experiments in non-physiological levels of glucose. The significant alterations in both passive and active subthreshold electrophysiological properties seen in physiological compared to non-physiological glucose suggests that whole networks may behave differently in these two different levels of glucose. The type and properties of these active conductances can change depending on the extracellular glucose concentration ultimately dictating the final integrative properties of Arc neurones. Thus, clusters are not defined and discrete, but show considerable plasticity and

therefore the classification of Arc neurones represent the spectrum of electrophysiological neuronal populations present within this nucleus. The differences in expression of ion channels and neuronal activity have been shown to change in physiological and pathophysiological states which may also be reflected in alterations in receptor, transmitter and peptide expression, the latter requiring investigation. Possible extensions to this project are changing glucose concentrations from 2 mM to 10 mM online whilst recording from the same neurone. This will give us a clearer idea of the plasticity of the Arc on exposure to differing glucose concentrations and how easily the neuronal system can be manipulated. Is it possible for there to be a transition from one cluster to another on exposure to different concentrations of glucose? Chapter 5/6 has shown that NA can active an anomalous inward rectifying conductance, thus changing fundamental properties. If differing glucose concentrations can manipulate the electrophysiological expression of Arc neurones then one must be also aware of other factors that may change the expression of active conductances; such as the time of day of recording and temperature which have been shown to alter protein synthesis and receptor expression.

Figure 4.1 **Mean passive membrane properties of neurones recorded in 2 mM and 10 mM glucose containing aCSF**

A: A Bar-chart comparing the mean membrane potentials of neurones recorded in 10 mM glucose-containing aCSF (Green bar) and 2 mM glucose-containing aCSF (Black bar). A total of 225 neurones were recorded in 10 mM glucose aCSF and 313 neurones were recorded in 2 mM glucose aCSF.

B: A Bar-chart comparing the mean input resistance of neurones recorded in 10 mM glucose-containing aCSF (Green bar) and 2 mM glucose-containing aCSF (Black bar). The * denotes that the mean input resistances recorded in each glucose concentration are significantly different. Neurones recorded in 2 mM glucose aCSF had a significantly lower input resistance than those neurones recorded in 10 mM glucose aCSF.

C: A Bar-chart comparing the mean firing frequency of neurones recorded in 10 mM glucose-containing aCSF (Green bar) and 2 mM glucose-containing aCSF (Black bar). The * denotes that the mean firing frequencies recorded in each glucose concentration are significantly different. Neurones recorded in 2 mM glucose aCSF had a significantly higher firing rate than those neurones recorded in 10 mM glucose aCSF at the resting membrane potential.

Figure 4.2 **Frequency histograms comparing the passive membrane properties of neurones recorded in 2 mM and 10 mM glucose containing aCSF**

A: Frequency distribution plots comparing the membrane potentials of neurones recorded in 10 mM glucose-containing aCSF (Green bars) and 2 mM glucose-containing aCSF (Black bars). A total of 225 neurones were recorded in 10 mM glucose aCSF and 313 neurones were recorded in 2 mM glucose aCSF, and were placed in each appropriate bin size and plotted as a percentage of the totals. The median and mode for both groups of neurones in each glucose concentration is indicated above the frequency distributions, in this figure and subsequent figures.

B: Frequency distribution plots comparing the input resistances of neurones recorded in 10 mM glucose-containing aCSF (Green bars) and 2 mM glucose-containing aCSF (Black bars). A total of 225 neurones were recorded in 10 mM glucose aCSF and 313 neurones were recorded in 2 mM glucose aCSF, and were placed in each appropriate bin size for their neuronal input resistance and plotted as a percentage of the totals.

C: Frequency distribution plots comparing the firing rates of neurones recorded in 10 mM glucose-containing aCSF (Green bars) and 2 mM glucose-containing aCSF (Black bars). A total of 105 neurones were recorded in 10 mM glucose aCSF and 267 neurones were recorded in 2 mM glucose aCSF, and were placed in each appropriate bin size for their neuronal input resistance and plotted as a percentage of the totals.

Figure 4.3 **A comparison of the percentage of spontaneously active and silent neurones recorded in 10 mM and 2 mM glucose aCSF.**

A: A Bar-chart comparing the proportion of active and silent neurones recorded in 10 mM glucose aCSF and 2 mM glucose-containing aCSF. Note the increase in the proportion of spontaneously active cells in 2 mM glucose aCSF compared to those recorded in 10 mM glucose aCSF.

Figure 4.4 **Mean passive membrane properties and frequency distribution plots of Cluster 1 neurones recorded in 2 mM and 10 mM glucose containing aCSF**

Ai: Frequency distribution plots comparing the membrane potentials of neurones characterised as cluster 1 neurones recorded in 10 mM glucose-containing aCSF (Green bars) and 2 mM glucose-containing aCSF (Black bars). A total of 19 neurones were recorded in 10 mM glucose aCSF and 21 neurones were recorded in 2 mM glucose aCSF, and were placed in each appropriate bin size and plotted as a percentage of the totals. The median and mode (most common bin size) for both groups of neurones in each glucose concentration is indicated above the frequency distributions, in this figure and subsequent figures

Aii: A Bar-chart comparing the mean membrane potentials of cluster 1 neurones recorded in 10 mM glucose-containing aCSF (Green bar) and 2 mM glucose-containing aCSF (Black bar).

Bi: Frequency distribution plots comparing the input resistances of neurones recorded in 10 mM glucose-containing aCSF (Green bars) and 2 mM glucose-containing aCSF (Black bars). A total of 19 neurones were recorded in 10 mM glucose aCSF and 21 neurones were recorded in 2 mM glucose aCSF, and were placed in each appropriate bin size for their neuronal input resistance and plotted as a percentage of the totals.

Bii: A Bar-chart comparing the mean neuronal input resistance of cluster 1 neurones recorded in 10 mM glucose-containing aCSF (Green bar) and 2 mM glucose-containing aCSF (Black bar).

Ci: Frequency distribution plots comparing the firing rates of cluster 1 neurones recorded in 10 mM glucose-containing aCSF (Green bars) and 2 mM glucose-containing aCSF (Black bars). A total of 8 neurones were recorded in 10 mM glucose aCSF and 21 neurones were recorded in 2 mM glucose aCSF, and were placed in each appropriate bin size for their firing frequency and plotted as a percentage of the totals.

Cii: A Bar-chart comparing the mean firing frequency of cluster 1 neurones recorded in 10 mM glucose-containing aCSF (Green bar) and 2 mM glucose-containing aCSF (Black bar).

Figure 4.5 **Mean passive membrane properties and frequency distribution plots of Cluster 2 neurones recorded in 2 mM and 10 mM glucose containing aCSF**

Ai: Frequency distribution plots comparing the membrane potentials of neurones characterised as cluster 2 neurones recorded in 10 mM glucose-containing aCSF (Green bars) and 2 mM glucose-containing aCSF (Black bars). A total of 10 neurones were recorded in 10 mM glucose aCSF and 13 neurones were recorded in 2 mM glucose aCSF, and were placed in each appropriate bin size and plotted as a percentage of the totals. The median and mode (most common bin size) for both groups of neurones in each glucose concentration is indicated above the frequency distributions, in this figure and subsequent figures

Aii: A Bar-chart comparing the mean membrane potentials of cluster 2 neurones recorded in 10 mM glucose-containing aCSF (Green bar) and 2 mM glucose-containing aCSF (Black bar).

Bi: Frequency distribution plots comparing the input resistances of cluster 2 neurones recorded in 10 mM glucose-containing aCSF (Green bars) and 2 mM glucose-containing aCSF (Black bars). A total of 10 neurones were recorded in 10 mM glucose aCSF and 13 neurones were recorded in 2 mM glucose aCSF, and were placed in each appropriate bin size for their neuronal input resistance and plotted as a percentage of the totals.

Bii: A Bar-chart comparing the mean neuronal input resistance of cluster 2 neurones recorded in 10 mM glucose-containing aCSF (Green bar) and 2 mM glucose-containing aCSF (Black bar).

Ci: Frequency distribution plots comparing the firing rates of cluster 2 neurones recorded in 10 mM glucose-containing aCSF (Green bars) and 2 mM glucose-containing aCSF (Black bars). A total of 10 neurones were recorded in 10 mM glucose aCSF and 13 neurones were recorded in 2 mM glucose aCSF, and were placed in each appropriate bin size for their firing frequency and plotted as a percentage of the totals.

Cii: A Bar-chart comparing the mean firing frequency of cluster 2 neurones recorded in 10 mM glucose-containing aCSF (Green bar) and 2 mM glucose-containing aCSF (Black bar).

Figure 4.6 **Mean passive membrane properties and frequency distribution plots of Cluster 3 neurones recorded in 2 mM and 10 mM glucose containing aCSF**

Ai: Frequency distribution plots comparing the membrane potentials of neurones characterised as cluster 3 neurones recorded in 10 mM glucose-containing aCSF (Green bars) and 2 mM glucose-containing aCSF (Black bars). A total of 9 neurones were recorded in 10 mM glucose aCSF and 13 neurones were recorded in 2 mM glucose aCSF, and were placed in each appropriate bin size and plotted as a percentage of the totals. The median and mode (most common bin size) for both groups of neurones in each glucose concentration is indicated above the frequency distributions, in this figure and subsequent figures.

Aii: A Bar-chart comparing the mean membrane potentials of cluster 3 neurones recorded in 10 mM glucose-containing aCSF (Green bar) and 2 mM glucose-containing aCSF (Black bar).

Bi: Frequency distribution plots comparing the input resistances of cluster 3 neurones recorded in 10 mM glucose-containing aCSF (Green bars) and 2 mM glucose-containing aCSF (Black bars). Neurones were recorded in 2 mM glucose aCSF, and were placed in each appropriate bin size for their neuronal input resistance and plotted as a percentage of the totals.

Bii: A Bar-chart comparing the mean neuronal input resistance of cluster 3 neurones recorded in 10 mM glucose-containing aCSF (Green bar) and 2 mM glucose-containing aCSF (Black bar).

Ci: Frequency distribution plots comparing the firing rates of cluster 3 neurones recorded in 10 mM glucose-containing aCSF (Green bars) and 2 mM glucose-containing aCSF (Black bars). A total of 9 neurones were recorded in 10 mM glucose aCSF and 13 neurones were recorded in 2 mM glucose aCSF, and were placed in each appropriate bin size for their firing frequency and plotted as a percentage of the totals.

Cii: A Bar-chart comparing the mean firing frequency of cluster 3 neurones recorded in 10 mM glucose-containing aCSF (Green bar) and 2 mM glucose-containing aCSF (Black bar).

Figure 4.7 **Mean passive membrane properties and frequency distribution plots of Cluster 4 neurones recorded in 2 mM and 10 mM glucose containing aCSF**

Ai: Frequency distribution plots comparing the membrane potentials of neurones characterised as cluster 4 neurones recorded in 10 mM glucose-containing aCSF (Green bars) and 2 mM glucose-containing aCSF (Black bars). A total of 21 neurones were recorded in 10 mM glucose aCSF and 19 neurones were recorded in 2 mM glucose aCSF, and were placed in each appropriate bin size and plotted as a percentage of the totals. The median and mode (most common bin size) for both groups of neurones in each glucose concentration is indicated above the frequency distributions, in this figure and subsequent figures

Aii: A Bar-chart comparing the mean membrane potentials of cluster 4 neurones recorded in 10 mM glucose-containing aCSF (Green bar) and 2 mM glucose-containing aCSF (Black bar).

Bi: Frequency distribution plots comparing the input resistances of cluster 4 neurones recorded in 10 mM glucose-containing aCSF (Green bars) and 2 mM glucose-containing aCSF (Black bars). Neurones were recorded in 2 mM glucose aCSF, and were placed in each appropriate bin size for their neuronal input resistance and plotted as a percentage of the totals.

Bii: A Bar-chart comparing the mean neuronal input resistance of cluster 4 neurones recorded in 10 mM glucose-containing aCSF (Green bar) and 2 mM glucose-containing aCSF (Black bar).

Ci: Frequency distribution plots comparing the firing rates of cluster 4 neurones recorded in 10 mM glucose-containing aCSF (Green bars) and 2 mM glucose-containing aCSF (Black bars).Neurones were recorded in 2 mM glucose aCSF, and were placed in each appropriate bin size for their firing frequency and plotted as a percentage of the totals.

Cii: A Bar-chart comparing the mean firing frequency of cluster 4 neurones recorded in 10 mM glucose-containing aCSF (Green bar) and 2 mM glucose-containing aCSF (Black bar).

Figure 4.8 **Mean passive membrane properties and frequency distribution plots of Cluster 5 neurones recorded in 2 mM and 10 mM glucose containing aCSF**

Ai: Frequency distribution plots comparing the membrane potentials of neurones characterised as cluster 5 neurones recorded in 10 mM glucose-containing aCSF (Green bars) and 2 mM glucose-containing aCSF (Black bars). A total of 41 neurones were recorded in 10 mM glucose aCSF and 66 neurones were recorded in 2 mM glucose aCSF, and were placed in each appropriate bin size and plotted as a percentage of the totals. The median and mode (most common bin size) for both groups of neurones in each glucose concentration is indicated above the frequency distributions, in this figure and subsequent figures

Aii: A Bar-chart comparing the mean membrane potentials of cluster 5 neurones recorded in 10 mM glucose-containing aCSF (Green bar) and 2 mM glucose-containing aCSF (Black bar).

Bi: Frequency distribution plots comparing the input resistances of cluster 5 neurones recorded in 10 mM glucose-containing aCSF (Green bars) and 2 mM glucose-containing aCSF (Black bars). Neurones were recorded in 2 mM glucose aCSF, and were placed in each appropriate bin size for their neuronal input resistance and plotted as a percentage of the totals.

Bii: A Bar-chart comparing the mean neuronal input resistance of cluster 5 neurones recorded in 10 mM glucose-containing aCSF (Green bar) and 2 mM glucose-containing aCSF (Black bar).

Ci: Frequency distribution plots comparing the firing rates of cluster 5 neurones recorded in 10 mM glucose-containing aCSF (Green bars) and 2 mM glucose-containing aCSF (Black bars). A total of 18 neurones were recorded in 10 mM glucose aCSF and 56 neurones were recorded in 2 mM glucose aCSF, and were placed in each appropriate bin size for their firing frequency and plotted as a percentage of the totals.

Cii: A Bar-chart comparing the mean firing frequency of cluster 5 neurones recorded in 10 mM glucose-containing aCSF (Green bar) and 2 mM glucose-containing aCSF (Black bar).

Figure 4.9 **Mean passive membrane properties and frequency distribution plots of Cluster 6 neurones recorded in 2 mM and 10 mM glucose containing aCSF**

Ai: Frequency distribution plots comparing the membrane potentials of neurones characterised as cluster 6 neurones recorded in 10 mM glucose-containing aCSF (Green bars) and 2 mM glucose-containing aCSF (Black bars). A total of 59 neurones were recorded in 10 mM glucose aCSF and 75 neurones were recorded in 2 mM glucose aCSF, and were placed in each appropriate bin size and plotted as a percentage of the totals. The median and mode (most common bin size) for both groups of neurones in each glucose concentration is indicated above the frequency distributions, in this figure and subsequent figures

Aii: A Bar-chart comparing the mean membrane potentials of cluster 6 neurones recorded in 10 mM glucose-containing aCSF (Green bar) and 2 mM glucose-containing aCSF (Black bar).

Bi: Frequency distribution plots comparing the input resistances of cluster 6 neurones recorded in 10 mM glucose-containing aCSF (Green bars) and 2 mM glucose-containing aCSF (Black bars). Neurones were recorded in 2 mM glucose aCSF, and were placed in each appropriate bin size for their neuronal input resistance and plotted as a percentage of the totals.

Bii: A Bar-chart comparing the mean neuronal input resistance of cluster 6 neurones recorded in 10 mM glucose-containing aCSF (Green bar) and 2 mM glucose-containing aCSF (Black bar).

Ci: Frequency distribution plots comparing the firing rates of cluster 6 neurones recorded in 10 mM glucose-containing aCSF (Green bars) and 2 mM glucose-containing aCSF (Black bars). A total of 28 neurones were recorded in 10 mM glucose aCSF and 59 neurones were recorded in 2 mM glucose aCSF, and were placed in each appropriate bin size for their firing frequency and plotted as a percentage of the totals.

Cii: A Bar-chart comparing the mean firing frequency of cluster 6 neurones recorded in 10 mM glucose-containing aCSF (Green bar) and 2 mM glucose-containing aCSF (Black bar). The * denotes that the mean firing frequencies recorded in each glucose concentration are significantly different. Neurones recorded in 2 mM glucose aCSF had a significantly higher firing rate than those neurones recorded in 10 mM glucose aCSF at the resting membrane potential.

Figure 4.10 **Mean passive membrane properties and frequency distribution plots of Cluster 7 neurones recorded in 2 mM and 10 mM glucose containing aCSF**

Ai: Frequency distribution plots comparing the membrane potentials of neurones characterised as cluster 7 neurones recorded in 10 mM glucose-containing aCSF (Green bars) and 2 mM glucose-containing aCSF (Black bars). A total of 29 neurones were recorded in 10 mM glucose aCSF and 33 neurones were recorded in 2 mM glucose aCSF, and were placed in each appropriate bin size and plotted as a percentage of the totals. The median and mode (most common bin size) for both groups of neurones in each glucose concentration is indicated above the frequency distributions, in this figure and subsequent figures

Aii: A Bar-chart comparing the mean membrane potentials of cluster 7 neurones recorded in 10 mM glucose-containing aCSF (Green bar) and 2 mM glucose-containing aCSF (Black bar).

Bi: Frequency distribution plots comparing the input resistances of cluster 7 neurones recorded in 10 mM glucose-containing aCSF (Green bars) and 2 mM glucose-containing aCSF (Black bars). Neurones were recorded in 2 mM glucose aCSF, and were placed in each appropriate bin size for their neuronal input resistance and plotted as a percentage of the totals.

Bii: A Bar-chart comparing the mean neuronal input resistance of cluster 7 neurones recorded in 10 mM glucose-containing aCSF (Green bar) and 2 mM glucose-containing aCSF (Black bar).

Ci: Frequency distribution plots comparing the firing rates of cluster 7 neurones recorded in 10 mM glucose-containing aCSF (Green bars) and 2 mM glucose-containing aCSF (Black bars). A total of 10 neurones were recorded in 10 mM glucose aCSF and 29 neurones were recorded in 2 mM glucose aCSF, and were placed in each appropriate bin size for their firing frequency and plotted as a percentage of the totals.

Cii: A Bar-chart comparing the mean firing frequency of cluster 7 neurones recorded in 10 mM glucose-containing aCSF (Green bar) and 2 mM glucose-containing aCSF (Black bar).

Figure 4.11 **Mean passive membrane properties and frequency distribution plots of Cluster 8 neurones recorded in 2 mM and 10 mM glucose containing aCSF**

Ai: Frequency distribution plots comparing the membrane potentials of neurones characterised as cluster 8 neurones recorded in 10 mM glucose-containing aCSF (Green bars) and 2 mM glucose-containing aCSF (Black bars). A total of 37 neurones were recorded in 10 mM glucose aCSF and 67 neurones were recorded in 2 mM glucose aCSF, and were placed in each appropriate bin size and plotted as a percentage of the totals. The median and mode (most common bin size) for both groups of neurones in each glucose concentration is indicated above the frequency distributions, in this figure and subsequent figures

Aii: A Bar-chart comparing the mean membrane potentials of cluster 8 neurones recorded in 10 mM glucose-containing aCSF (Green bar) and 2 mM glucose-containing aCSF (Black bar).

Bi: Frequency distribution plots comparing the input resistances of cluster 8 neurones recorded in 10 mM glucose-containing aCSF (Green bars) and 2 mM glucose-containing aCSF (Black bars). Neurones were recorded in 2 mM glucose aCSF, and were placed in each appropriate bin size for their neuronal input resistance and plotted as a percentage of the totals.

Bii: A Bar-chart comparing the mean neuronal input resistance of cluster 8 neurones recorded in 10 mM glucose-containing aCSF (Green bar) and 2 mM glucose-containing aCSF (Black bar).

Ci: Frequency distribution plots comparing the firing rates of cluster neurones recorded in 10 mM glucose-containing aCSF (Green bars) and 2 mM glucose-containing aCSF (Black bars). A total of 28 neurones were recorded in 10 mM glucose aCSF and 59 neurones were recorded in 2 mM glucose aCSF, and were placed in each appropriate bin size for their firing frequency and plotted as a percentage of the totals.

Cii: A Bar-chart comparing the mean firing frequency of cluster 8 neurones recorded in 10 mM glucose-containing aCSF (Green bar) and 2 mM glucose-containing aCSF (Black bar). The * denotes that the mean firing frequencies recorded in each glucose concentration are significantly different. Neurones recorded in 2 mM glucose aCSF had a significantly higher firing rate than those neurones recorded in 10 mM glucose aCSF at the resting membrane potential.

Figure 4.12 **Typical electrophysiological differences of neurones recorded in 10 mM and 2 mM glucose containing aCSF**

A: Continuous current clamp recordings of two separate neurones recorded in 10 mM and 2 mM glucose containing aCSF, respectively. Note the increase in firing rate of the neurone recorded in 2 mM glucose compared to the neurones recorded in 10 mM containing aCSF.

B: The activation of an A-like conductance (I_a) resulted in a delayed return to baseline following negative current injection. The duration of I_a was measured as the time between the end of current injection (marked by the first vertical dotted line) and the return of the membrane potential to the level prior to the current injection (marked by the second vertical dotted line). The amplitude of the current was measured at half the duration (line marked *). Note in 2 mM glucose the activation of the A-like conductance was shorter in duration than in 10 mM glucose aCSF.

C: Activation of the H-conductance (I_h) induces a time- and voltage-dependent sag in the membrane response to negative current injection. The amplitude of I_h was measured by subtracting the membrane potential at the end of the negative current injection (Upper dotted line) from the membrane potential following steady-state charging of the cellular membrane (lower dotted line). Note in 2 mM glucose I_h increased in amplitude compared to the activation of I_h in 10 mM glucose aCSF.

Chapter 5

The excitatory effects of noradrenaline on rat hypothalamic arcuate nucleus neurones *in vitro*

5.1 Introduction

The noradrenergic system represents one of four major aminergic systems within the mammalian brain. These systems are unique in that their projections cover the majority of the brain and thus play an important role in modulating numerous aspects of neuronal function including higher functions and autonomic and neuroendocrine modes of homeostatic control (Sawchenko & Swanson, 1981; Brown *et al.*, 2001). Noradrenergic cell bodies, present within brain-stem nuclei are predominately found in the locus coeruleus (LC; A6); a bilateral pontine structure with a uniquely wide-spread terminal network reaching throughout the neuroaxis (Svensson, 1987). These neurones play a major part in a number of physiological processes, including the control of energy homeostasis, arousal and mood (Leibowitz *et al.*, 1983a; Svensson, 1984; Berridge, 2008).

The use of noradrenaline (NA) reuptake inhibitors, and serotonin reuptake inhibitors, such as sibutramine are commonly used today as anti-obesity drugs, thus demonstrating the importance of this neurotransmitter in the control of energy homeostasis. Sibutramine has been shown to reduce food intake and increase thermogenesis, effects that are completely or partially reversed with pre-treatment of NA antagonists (Heal *et al.*, 1998). Prazosin, a selective α_1-adrenoceptor (AR) antagonist, has been shown to block the decrease in food intake induced by sibutramine (Jackson *et al.*, 1997).

Noradrenergic receptors are found differentially expressed throughout the brain with an abundance of α- AR subtypes expressed in diverse areas (Young & Kuhar, 1979). The hypothalamus, and in particular the paraventicular nucleus (PVN), has been found to be an important nucleus involved in the control of energy balance, and is a target for NA. Central injections of NA directly into the PVN have resulted in stimulation of feeding in fully satiated rats (Grossman, 1962; Leibowitz, 1978). NA is thought to increase feeding within the PVN by disinhibiting descending satiety signals through activation of α_2- ARs (Goldman *et al.*, 1985;

Wellman *et al.*, 1993). Conversely, activation of the α_1- ARs induces excitatory effects, which may inhibit food intake.

NA application at the level of the rat lateral perifornical hypothalamus (PFA) has suppressive effects on feeding behaviour (Margules, 1970; Leibowitz *et al.*, 1983b), thus showing the complexity of this catecholamine in the control of energy homeostasis. NA has the ability to either increase or decrease feeding/consumption depending on the site of application within the brain.

NA infusions at the level of the hypothalamus not only increases feeding but also affects other physiological and metabolic processes. It is suggested that NA's stimulatory effect on feeding within the hypothalamus is secondary to autonomic influences on the viscera. NA infusions into the hypothalamus have been shown to increase vasodilation (Carmona & Slangen, 1976), gastric acid secretion (Carmona & Slangen, 1973), insulin secretion (Moltz & McDonald, 1985) and bradycardia (Li *et al.*, 1996). These processes are thought to be activated partly through the vagus nerve, as complete vagotomy eliminates eating elicited by noradrenergic stimulation of the hypothalamus (Sawchenko *et al.*, 1981). Futhermore the vagal efferent pathway has also be shown to be an important route for conveying peripheral orexigenic ghrelin signals to the hindbrain which in turn transmits signals through the noradrenergic pathway to the hypothalamus, in particular to the arcuate nucleus (Arc; Date *et al.*, 2006).

The Arc of the hypothalamus is a heterogeneous structure comprising of an array of different neuronal populations (Chronwall, 1985) and forms the site for convergence of central and peripheral signals indicating the status of energy stores (Cone *et al.*, 2001). Within the Arc these neurones work together to maintain energy balance between narrow limits. Inputs to and outputs from the Arc are complex and multiple (Chronwall, 1985). The Arc receives afferent inputs from the periphery, brain-stem and other hypothalamic nuclei (Horvath *et al.*,

2004). Neurones of the hypothalamic Arc are innervated by noradrenergic fibres originating in the nucleus tractus solitarius (NTS; A2) and the LC (Sawchenko & Swanson, 1981). It has been shown that NPY neurones of the Arc are impinged upon by noradrenergic neurones arising from the hindbrain (Date *et al.*, 2006). NPY neurones are colocalised with AgRP and are powerful stimulators of food intake (Hahn *et al.*, 1998). It has been suggested that ghrelin induces c-fos expression in NPY/AgRP neurones in a NA-dependent manner through the activation of α_1 and β ARs (Date *et al.*, 2006), although central ghrelin does also act through it own receptor, the growth hormone secretagogue receptor in the Arc (GHS-R; Kojima & Kangawa, 2005). This data suggests NA excites NPY neurones within the hypothalamic arcuate nucleus.

5.1.1 α_1 –Adrenoceptors

NA is an endogenous ligand for the G- protein coupled adrenoceptors- α_1, α_2, β_1, β_2 (Hein, 2006). None of these receptors constitute homogenous groups, and therefore can be further divided into subtypes.

After the first pharmacological differentiation of the adrenoceptors by Alquist in 1948 (Nicholas *et al.*, 1993), it was not until the mid/late 1980s that the α_1- AR subgroup was divided into subtypes ($\alpha_{1A/1C}$,α_{1B} and α_{1d}) isolated by molecular cloning techniques (Voigt *et al.*, 1990; Lomasney *et al.*, 1991; Perez *et al.*, 1994). A non-selective agonist and antagonist, phenylephrine and prazosin, respectively, are now commonly used to probe for the α_1-AR (Langer, 1998), as all 3 subtypes exhibit similar affinity for these compounds.

The signal transduction mechanisms involved in the activation of the α_1- ARs involves the release of internal calcium stores. α_1- ARs are coupled to the $G_{q/11}$- signalling pathway, which involves the activation of phospholipase C (PLC), generation of the second messengers

inositol triphosphate (IP3) and diacylglycerol (DAG), and thus the mobilisation of intracellular calcium stores (Zhong & Minneman, 1999; Koshimizu *et al.*, 2007).

Within the Arc, light microscopic studies have shown the presence of α_1-ARs and their differential distribution compared to that of the α_2- ARs (Young & Kuhar, 1979). α_1- ARs have been shown to be located more laterally than α_2- ARs within the hypothalamus. The α_1- AR subtypes have also show a differential distribution within the brain. For example, the α_{1a}- AR in the Arc is the most abundant AR subtype, whereas the α_{1d}- AR is undetectable in the Arc, as determined by in situ hybridization studies (Day *et al.*, 1997).

The α_1- ARs are the most abundant ARs in the brain, and are thought to be postsynaptic and stimulatory in character; and like other postsynaptic receptors in the brain they can cause the release of neurotransmitters (Tanoue *et al.*, 2002). α_1- ARs are also present in glial cells and therefore may affect brain functions by means of non-neuronal mechanisms.

It has been shown that tissue that contains both the α_1- AR and α_2- AR subtypes can show an antagonistic organisation, in which activation of one subtype results in a particular physiological effect, whereas the activation of the other subtype results in the opposite physiological effect (Wellman, 2000). This has been characterised in the PVN where the activation of the α_1- AR results in a reduction in feeding and the activation of the α_2- ARs results in an increase in feeding (Wellman *et al.*, 1993). Thus, even within a single hypothalamic nucleus the effect of NA on functional output is complex.

NA has multiple effects in regards to feeding within the CNS; however its effects at the cellular level in the Arc of the hypothalamus remain poorly understood. Infusion of NA within different nuclei of the hypothalamus produces differential results. At present the role of NA within the Arc has not yet been explored for its effects involved in the central control of food intake and energy homeostasis.

In the present study, the aim was to investigate the cellular mechanisms by which NA regulates neuronal excitability within the Arc using whole-cell patch clamp recording techniques in isolated hypothalamic slice preparations.

5.2 Results

In the present study the effects of NA (1-2 minutes; 40 µM) on the electrophysiological activity of 172 Arc neurones in slice preparations were studied using whole-cell patch recordings *in vitro*. The mean resting membrane potential of these neurones was -48.6 ± 0.6 mV associated with a mean input resistance of 1397 ± 51 MΩ (n=172).

5.2.1 NA- depolarises hypothalamic Arc neurones

88/172 (51.2%) neurones exposed to 40 µm NA responded with an excitation, observed as an increase in suprathreshold activity. Bath application of NA to the slice by superfusion for 60-120 s induced an increase in mean spontaneous firing rate from a control level of 0.5 ± 0.1 Hz to 2.1 ± 0.2 Hz (339%; $P < 0.001$; n=88), effects that were reversible with a return to a firing rate of 0.4 ± 0.1 Hz following the wash of NA from the bath (Figure 5.1A).

The excitation was associated with a reversible membrane depolarisation which returned to resting levels approximately 15 minutes following the wash of NA from the bath. NA application induced a membrane depolarisation from a mean resting membrane potential of -48.9 ± 0.9 mV (n=88) to -41.6 ± 0.8 mV, resulting in a mean peak membrane depolarisation of 7.2 ± 0.6 mV (n=88). Performing an ANOVA revealed a highly significant difference in the membrane potential between the control and the neurone in the presence of NA ($P < 0.001$) and no significant difference between the control and wash ($P = 0.97$).

In voltage-clamp at a holding potential of -50 mV, application of NA in the presence of tetrodotoxin (TTX) to the slice by superfusion for 60-120 s (40 μM, n=12) induced an inward current, with a mean peak amplitude of 16.1 ± 1.6 pA (Figure 5.4 A).

Bath application of NA resulted in a 17.8 ± 2.8% (*P*=0.38) increase in neuronal input resistance from 1292 ± 68 MΩ at rest to 1500 ± 84 MΩ in the presence of NA returning to 1210 ± 61.0 MΩ (n=88) following the wash of NA from the bath.

TTX was used to block activity-dependent synaptic transmission and hence investigate whether NA-induced excitation was mediated via a direct post-synaptic mechanism on the recorded neurones. NA-induced membrane depolarisation and associated increase in input resistance persisted in the presence of 1 μm TTX (Figure 5.2 A), thus indicating a direct post-synaptic effect on Arc neurones. NA application in the presence of TTX induced a membrane depolarisation from a resting membrane potential of -46.7 ± 2.5 mV to -35.4 ± 2.3 mV resulting in a mean peak membrane depolarisation of 11.3 ± 1.5 mV (n=12). Following wash of NA the membrane potential returned to -46.4 ± 3.3 mV, near to control values. The membrane depolarisation in the presence of TTX was associated with an increase in input resistance of 8.0 ± 2.5 % (n= 12), from a mean resting input resistance of 1250 ± 149 MΩ to 1325 ± 212 MΩ.

5.2.2 Ionic mechanism underlying the NA-induced depolarisation

To determine the ionic mechanism underlying the NA-induced excitation, current-voltage (I/V) relationships were obtained in control conditions and at the peak of the NA-induced depolarisation in 24 neurones. Plotting I/V relations revealed more than one mechanism/ component contributing to the NA-induced excitation. NA induced depolarisation

was associated with either an increase (n=7), decrease (n=5) or no change in input resistance (n=10).

10/22 neurones displayed no significant change in neuronal input resistance in response to NA. These neurones had mean neuronal input resistance of 1118 ± 168 MΩ at rest and 1154 ± 183 MΩ in the presence of NA. I/V relationships plotted for this group displayed a parallel shift (Figure 5.1B/C). The parallel shift suggests the NA-induced excitation may in part be mediated through modulation of electrogenic ion pumps or an ion exchanger mechanism. However, a slight change in the slope of the I/V indicates the activation/inhibition of a conductance, thus the parallel shift may indicate a combination of multiple conductances activated by NA that effectively offset each other.

7/22 neurones displayed a clear reversal potential amounting to -84.1 ± 5.3 mV (Figure 5.2B/C), close to the predicted reversal potential for potassium under our recording conditions. The reversal potential was taken from the point at which the plots of the two I/V relations intersected. These neurones showed an increase in input resistance of 33.8 ± 8.2 %, increasing from 1104 ± 157 MΩ at rest to 1511 ± 292 MΩ in NA in the presence of NA. The mean peak membrane depolarisation of these neurones was 11.1 ± 2.7 mV from a mean membrane potential of -54.7 ± 3.5 mV in control to -43.5 ± 2.5 mV in the presence of NA. This suggests that the NA-induced excitation in these neurones is mediated through the closure of one or more resting potassium conductances.

22.8% of neurones revealed the extrapolated point of intersection of the two I/V curves (control and response) amounted to -24.3 ± 2.9 mV suggesting the activation of a non-selective cation channel (NSCC) underlies the NA-induced excitation in some hypothalamic arcuate neurones (Figure 5.3 B/C). These neurones showed a significant decrease in input resistance of -22.6 ± 1.7 %, from 1300 ± 310 MΩ at rest to 1029 ± 301 MΩ in the presence of NA.

Voltage-clamp ramps from -130 to 30mV / -110 to -30 at a rate of 10 $mV.s^{-1}$, were applied in control conditions and at the peak of the NA-induced response in TTX to further investigate the ionic mechanism underlying the NA-induced current. Again plotting the ramps revealed that more than one mechanism contributed to the NA-induced excitation.

Predominately when plotting the NA ramps there was no change in neuronal input resistance in the presence of NA thus currents were presented as parallel shifts (n=8; Figure 5.4B). NA-induced inward currents that did show a change in resistance had a mean reversal potential of -88 ± 9 mV (n=2; Figure 5.4 C), close to the reversal potential for potassium under our recording conditions.

5.2.3 NA- induced indirect effects on hypothalamic Arc neurones

NA application resulted in an increase or induction of spontaneous synaptic events including both excitatory post-synaptic potentials (EPSPs; n=6) and inhibitory post-synaptic currents (IPSCs; n=4). Spontaneous EPSPs at rest were observed at a frequency of 0.1 ± 0.0 Hz, increasing to 0.8 ± 0.1 Hz (n=6) in the presence of NA before returning close to control levels (0.1 ± 0.0 Hz; n=3) following wash. Thus the frequency of EPSPs in the presence of NA increased by 236.0 ± 63.5 % ($P<0.01$; Figure 5.5) and returned to around 9.2 ± 5.1 % of control after washout of NA. To establish that these spontaneous synaptic events induced in response to NA were indeed EPSPs, the effects of the glutamatergic non-NMDA receptor antagonist 2,3-dihydroxy-6-nitro-7-sulfamoyl-benzo[f]quinoxaline-2,3-dione (NBQX; 10 μM) were tested. NA-induced EPSPs were completely blocked in the presence of this antagonist (n=4).

NA-induced or increased the frequency of spontaneous inhibitory post-synaptic potentials (IPSCs) in a subset of Arc neurones. The mean frequency of spontaneous IPSCs at

rest was 0.2 ± 0.0 Hz and increased to 0.5 ± 0.0 Hz (n=4) in the presence of NA, returning to 0.1 ± 0.0 Hz (n=3) following washout of the drug. Thus the frequency of IPSCs increased by 165.5 ± 65.3% ($p<0.05$) in the presence of NA. The polarity of these IPSCs were reversed between -60 to -70 mV suggesting the involvement of $GABA_A$ channels (Figure 5.6A). Indeed the NA-induced IPSCs were completely blocked in the presence of the $GABA_A$ receptor antagonist bicuculline (10 μM; Figure 5.6B).

Both the frequency of EPSPs and IPSPs increased in the presence of NA, thus suggesting that the catecholamine modulates neuronal excitability at the level of the Arc, at least in part, via both post- and pre-synaptic sites of action.

5.2.4 NA-induced membrane potential oscillations

5 neurones exposed to 40 μM NA displayed a significant membrane depolarisation which when injected with negative current to clamp the membrane potential close to the pre-NA resting value revealed a burst-firing pattern of activity (Figure 5.7Ai). NA-induced membrane potential oscillations consisted of a biphasic waveform, which presented itself as a rapid depolarising phase with regular bursts of action potential firing followed by a slower hyperpolarising component (Figure 5.7Aii). The mean peak amplitude of the membrane potential oscillations amounted to 18.3 ± 5.7 mV (n=5). The mean number of action potentials per burst was 21.6 ± 5.8 giving a mean peak frequency of 2.0 ± 0.7 Hz.

5.2.5 The effects of NA receptor agonists on Arc neurones

To determine the noradrenergic receptor subtype involved in mediating the NA-induced depolarisation a range of agonists and antagonists were subsequently tested.

Phenylephrine (10 μM), a selective α_1 AR agonist was bath applied for 1-2 minutes to a total of 20 neurones, 13 of which had previously been exposed to NA (40 μM). 14 neurones responded to the application of phenylephrine with a membrane depolarisation and/or increase in spontaneous action potential firing (Figure 5.8A) and/or an increase in spontaneous synaptic events. Application of phenylephrine induced a reversible membrane depolarisation (n= 12) from a mean resting potential of -46.3 ± 1.5 mV to -42.7 ± 1.5 mV in the presence of NA, amounting to a mean peak membrane depolarisation of 3.6 ± 0.7mV. The phenylephrine-induced depolarisation was associated with an increase in neuronal input resistance from a mean resting input resistance of 1036 ± 107 MΩ to 1245 ± 152 MΩ in the presence of NA (n=12). In the presence of 1μm TTX, phenylephrine-induced membrane depolarisation and associated increase in neuronal input resistance persisted, indicating a direct effect of the agonist on the recorded neurone (n=4; Figure 5.8A).

5.2.6 Ionic mechanism underlying the phenylephrine-induced depolarisation

It was possible to gain I/V relationships for 5 hypothalamic arcuate neurones in the presence and absence of phenylephrine. Phenylephrine induced an increase in neuronal input resistance from a mean resting input resistance of 1005 ±111 MΩ to 1104 ± 130 MΩ (n=5) in the presence of phenylephrine, amounting to a 12.5 ± 13.2 % in input resistance in the presence of this agonist. The response was associated with a mean peak membrane potential depolarisation of 5.8 ± 1.7 mV, from a mean resting membrane potential of -44.2 ±

2.1 mV to -38.4 ± 2.0 mV in the presence of phenylephrine. Plotting the I/V relations before and during the application of phenylephrine (4/5) including in the presence of TTX (3/5) revealed a parallel shift (Figure 5.8 B/C). This suggests that the phenylephrine induced excitation in part, is mediated through modulation of one or more ion pumps. However the slight change in input resistance suggests that the phenylephrine excitation could involve the combination of multiple conductances being activated and thus offset each other.

5.2.7 The effects of adrenoceptor antagonists on Arc neurones

In order to further clarify and determine the AR subtype (s) mediating the NA- induced excitation, the effects of prazosin, a selective α_1- AR antagonist, were tested on NA-induced excitation. Prazosin blocked the NA- induced excitation in a concentration-dependent manner (Figures 5.9C).

Application of NA (40 μM), for 60 to 120s, in the absence of prazosin induced a membrane depolarisation and an increase in spontaneous action potential firing frequency, an effect that was reversible on washout of NA (Figure 5.9A). Neurones were subsequently exposed to the α_1-AR antagonist, prazosin for 240-300 s, a time-course of application sufficient to ensure saturation of the recording chamber with the required concentration of antagonist. The NA-induced depolarisation was blocked in a concentration-dependent manner with prazosin (Figure 5.9C). In the presence of 300 nM prazosin, NA failed to induce a membrane depolarisation and increase in spontaneous action potential firing, thus completely abolishing the NA-induced excitation. The complete block of NA-induced excitation with prazosin suggests that α_1-ARs mediate the depolarisation induced by NA.

NA in the presence of the α_1- AR antagonist (300 nM) in 18.8% of neurones that responded with an excitation blocked the NA-induced excitation and revealed an NA-induced

hyperpolarisation of the membrane potential. NA, in the presence of prazosin, induced a hyperpolarisation of the membrane potential from a mean of -50.3 ± 4.6 mV to -56.2 ± 5.1 mV in the presence of the agonist and decreased the firing frequency by 51.8 ± 19.4 % (Figure 5.9 B). The block of one receptor mediating the NA-induced excitation therefore unmasked a NA-induced hyperpolarisation. Thus NA is capable of inducing differential cellular membrane effects on the same Arc neurone.

5.2.8 NA-induced depolarisation is mediated differentially through α_{1A} ARs and α_{1B} ARs

As NA-induced excitation appeared mediated through α_1-ARs, this study subsequently followed on to determine the α_1- AR subtype(s) involved in mediating NA-induced excitation. To achieve this, the α_{1A} -AR antagonist RS100329 hydrochloride and the α_{1B}- AR antagonist 02484100, were tested on NA-induced excitation.

Application of NA (40 μM), for 60 to 120 s, alone induced a membrane depolarisation and an increase in spontaneous action potential firing, a response that was partially reduced in the presence of RS100329 (10 nM). In the presence of RS100329 hydrochloride (10 nM; 240-300 s), the peak amplitude of the NA-induced membrane depolarisation was reduced to 5.6 ± 1.6 mV from a peak amplitude 9.5 ± 1.3 mV in NA alone, amounting to a 40.3% decrease in the response to NA in the presence of 10 nM RS100329.

The effects of higher concentrations of RS100329 were subsequently tested. In the presence of 100 nM RS100329 hydrochloride, the peak amplitude of the membrane depolarisation induced by NA was reduced to 3.4 ± 0.8 mV from a peak amplitude of 9.1 ± 1.0 mV, in NA alone, amounting to a 62.5% decrease in the response to NA in the presence of 100 nM RS100329. The NA-induced increase in firing was reduced by 89% in

the presence of 100 nM RS100329 hydrochloride thus suggesting that the α_{1A}- AR is in part responsible for the NA-induced depolarisation observed in Arc neurones (Figure 5.10A/B).

The application of a selective α_{1A}- AR antagonist did not fully block the NA-induced depolarisation, and therefore this study also investigated the effects of a selective α_{1B}- AR antagonist, 02484100 (Figure 5.11). In the presence 100 nM 02484100 (n=5) the mean peak amplitude of the depolarisation induced by NA was 7.8 ± 1.0 mV compared to a control peak amplitude of 7.1 ± 1.0 mV, in NA alone, amounting to a 11.4% increase in the response to NA in the presence of this antagonist (*P*=0.2). Although 02484100 had little effect on the amplitude of the NA-induced depolarisation, it did have an effect on the NA-induced increase in spontaneous firing rate. Spontaneous firing rate decreased in the presence of 100 nM 02484100. NA alone induced an increase in firing rate of 2.1 ± 0.5 Hz relative to control levels, whereas in the presence of 02484100, NA caused an increase in firing rate of only 0.8 ± 0.3 Hz, amounting to a 61.6% decrease in NA-induced increases in firing rate in the presence of this selective α_{1B}- AR antagonist, thus suggesting that the α_{1B}- AR also plays a part in mediating NA-induced excitation.

5.2.9 β-adrenoceptor agonist has no effect on NA-induced excitation of hypothalamic Arc neurones

It has been shown previously that both β- and α_{1}- AR receptors mediate mainly excitatory effects within the CNS (Kang et al, 2000). Therefore the possible involvement of the β AR was investigated. Application of isoproterenol (10 μM; β AR agonist) for 60 to 120 s to hypothalamic slices did not affect the membrane potential of all Arc neurones tested (n=3). Isoproterenol had no significant effect on membrane potential (*P*=0.18) or input resistance

(*P*=0.26). This preliminary data suggests that the NA-induced excitation of Arc neurones is not mediated through β- ARs.

5.2.10 NA- induced depolarisation in NPY/AgRP pacemaker neurones

We have subsequently shown that NA directly excites a subpopulation of Arc neurones through α_1-ARs. However the chemical phenotype of these neurones and putative function remains unclear. Previously we have used electrophysiological recording techniques in combination with single-cell RT-PCR to characterise a subpopulation of Arc NPY/AgRP neurones (van den Top *et al.*, 2004). These neurones are identified electrophysiologically upon their unique expression of active conductances (anomalous inward rectification and a transient outward rectifying conductance; van den Top et al., 2004). In the present study a total of 9 neurones were characterised as Arc NPY/AgRP pacemaker neurones. Bath application of NA (40 μM), for 60-120 s, induced a reversible membrane depolarisation in all NPY/AgRP neurones tested (n=9). NA-induced depolarisation in these neurones from a resting membrane potential of 47.1 ± 2.4 mV with a mean peak amplitude of 5.9 ± 1.3 mV (Figure 5.12A). The response was associated with an increase in neuronal input resistance from a resting input resistance of 1474 ± 195 MΩ to 1763 ± 308 MΩ in the presence of NA (n=9; Figure 5.12C/D). This amounted to a 19.1± 9.2 % increase in neuronal input resistance in the presence of NA. With the NA-induced membrane depolarisation there was a concomitant increase in mean spontaneous firing rate from 0.49 ± 0.2 Hz to 2 ± 0.6 Hz in the presence of NA ($P<0.05$;n=6; student's *t*-test), returning to a firing rate of 0.3 ± 0.1 Hz following wash of NA (n=6). This amounted to a 410% increase in firing rate in NPY/AgRP neurones in the presence of NA. The NA-induced membrane depolarisation and increase in

neuronal input resistance persisted in the presence of 1 µm TTX (Figure 5.12B; n=3), indicating a postsynaptic effect of NA on the NPY/AgRP Arc neurones.

5.2.11 NA differentially regulates excitability of CART-expressing neurones

CART is an anorexigenic peptide that co-localises with POMC (Elias *et al.*, 1998). Thus to test if NA-induced responses were mediated through anorexigenic neurones, a double-labelling technique with a dye (Alexa 633; 100 µM) introduced from the recording electrode combined with subsequent immunohistochemistal labelling for CART 55-102, was undertaken to identify anorexigenic CART-expressing neurones. Alexa 633 (100 µM) was introduced to the intracellular solution, which diffuses into the neurone and allows the recorded neurone to be visualised retrospectively. Subsequently slices were stained for CART to enable double-labelling of recorded neurones and CART expression. NA-induced an excitation in 5/12 recorded neurones that were also co-stained for CART (Figure 5.13). 4/12 neurones responded in a NA-induced inhibition (see chapter 6). 1 neurone responded in a biphasic response and the remaining 2 CART positive neurones did not respond to bath application of NA. 12/26 neurones that were CART negative responded to NA with an increase in spontaneous firing rate and a depolarisation of the membrane (Figure 5.14).

5.3 Discussion

The correct functioning of a number of hypothalamic neuronal networks, including those for the release of corticosterone, vasopressin (Vp) and glucose (Benetos *et al.*, 1986; Chafetz *et al.*, 1986) require essential noradrenergic inputs from the brain-stem. However, how NA modulates these and other neuronal networks remains at present unclear. Little is known about the central effects of NA on hypothalamic Arc neuronal activity. In the present

study, whole-cell patch-clamp recording techniques were employed to investigate the role of NA within the Arc and more specifically, in neurones involved in the maintenance of energy homeostasis.

NA had an effect on the neuronal excitability of 74% of Arc neurones recorded, in excess of 50% of which responded with an increase in firing rate and/or membrane depolarisation. The remaining responded with a membrane hyperpolarisation and a decrease in firing rate to bath application of NA (22.7%; see chapter 6). NA-induced an excitation in a subpopulation of hypothalamic Arc neurones that was associated with an increase, decrease or no change in input resistance mediated through the α_{1}- ARs. NA's excitatory effects were directly post-synaptic as shown in this study by the persistence of the response in TTX and in other studies following lowering extracellular Ca^{2+} (Kang *et al.*, 2000). In addition NA also produced indirect effects on Arc neurones as shown by the induction or increase in spontaneous excitatory or inhibitory synaptic events.

This study used 40μM NA and saturated the whole slice when carrying out electrophysiological recordings. NA is subject to reuptake and therefore a slightly higher dose of NA was used then produced the maximum response. Limitations with the technique in reference to the dose response curve means that one can not be aware of the exact concentration of ligand that saturates the slice at any one time, and in particular what concentration is reaching our recorded neurone. This study also assumed that once the response was recovered to the resting membrane potential before the drug was applied the drug was washed off and had left the bath. There may be potential problems with not knowing the exact time course of the drug action. This may lead to false responses due to receptor desensitisation. Thus, there are limitations in the frequency of drug application.

The Arc is a complex nucleus. With its heterogeneity of neuronal inputs, targets and chemical phenotypes, it forms a series of function-specific intricate neuronal networks. It has a

major role in the central neuronal responses to changes in energy balance. Within the Arc there are subpopulations of neurones containing neuropeptide Y (NPY) and agouti-related protein (AgRP), a subpopulation of which are reported conditional pacemakers. These are activated by orexigens (orexin) and inhibited by the anorexigens such as leptin (van den Top *et al.*, 2004). This subpopulation of NPY/AgRP neurones can be identified electrophysiologically on the basis of their expression of a unique combination of subthreshold active conductances; an anomalous inward rectification (I_{an}) and a transient outward rectifying conductance (I_a; van den Top *et al.*, 2004). This subpopulation of NPY/AgRP neurones upon exposure to NA responded with a membrane depolarisation and an increase in firing rate, suggesting an orexigenic role for NA at the level of the Arc NPY/AgRP pacemaker neurone. NPY neurones have been shown to be stimulated in states of energy deficit and fat loss (Williams *et al.*, 2001), and therefore NA may play a part in exciting these neurones to promote food intake and fat conservation. However, these conclusions may not apply to every Npy/AgRP neurone. This study showed that the NA-induced excitation is mediated through α_1-ARs. Therefore NA excites a subpopulation of NPY/AgRP neurones via α_1-ARs. These results suggest an opposing role for NA in the Arc to those observed in the PVN. NA reduces food intake following activation of α_1-ARs (Wellman *et al.*, 1993) and increases food intake through the activation of α_2-ARs (Leibowitz, 1988) within the PVN.

Firing patterns of single neurones have been shown to be important in the differential release of neurotransmitters and neuropeptides (Dutton & Dyball, 1979; Bicknell & Leng, 1981). Interestingly burst firing was not induced by application of NA in the previously described NPY/AgRP pacemaker neurones. An explanation for the observations seen in this study may be the difference in extracellular glucose used. This study has conducted experiments in 2 mM aCSF, a physiological range of glucose (see chapter 4), unlike the experiments carried out by van den Top *et al.,* (2004) that had carried out their recording in 10

mM glucose (a non-physiological concentration of glucose). Chapter 4 described that with the change in extracellular glucose levels there are significant changes in both passive and subthreshold active conductances. This may be a factor contributing to the identified NPY/AgRP neurones not bursting. The change in the patterning of firing may result in the release of other peptides/ neurotransmitters expressed by the same population of neurones.

NA did induce burst firing in a subpopulation of Arc neurones of which the phenotype is unknown. Bursts of action potentials were accompanied by membrane potential oscillations, a pattern of activity that has previously been shown associated with the regulation and release of neuropeptides from neurones (Dutton & Dyball, 1979; Bicknell & Leng, 1981). This has been shown in magnocellular neurones where burst-firing-like activity and action potential discharge facilitates the release of Vp. Further work needs to be carried out to establish the functional significance of the NA-induced burst firing in the Arc.

To further investigate the role of NA and its role in Arc neural circuits and control of energy homeostasis, immunohistochemical studies were carried out that labelled CART-containing neurones, used as an indicator for anorexigenic POMC/CART neurones. NA excited or inhibited (see chapter 6) subpopulations of CART-containing neurones, suggesting that NA may have multiple effects within the Arc at the level of these neurones. The NA-induced excitation of CART-containing neurones suggests an anorexigenic role within the Arc whilst their inhibition suggests an orexigenic role (see chapter 6). Consequently we have identified NA to play both a putative orexigenic and anorexigenic role within the Arc at the level of POMC/CART neurones. The overall net effect of NA within the Arc in relation to feeding requires further clarification. However, POMC neurones do not constitute a functionally homogenous group. POMC neurones form the precursor for a number of peptides, including adrenocorticotrophic hormone (ACTH), α- melanocyte stimulating hormone (α-MSH) and β-endorphin which are implicated in a number of physiological functions including the

control of metabolic homeostasis, heart rate, blood pressure, growth hormone release and fluid balance (Li *et al.*, 1996; Mountjoy & Wong, 1997; Ibrahim *et al.*, 2003; Raffin-Sanson *et al.*, 2003). Thus NA may excite POMC neurones that function in roles independent of those associated with the control of energy homeostasis, but may be involved in other physiological processes at the level of the Arc. NA also excited neurones that were CART negative and were not identified as NPY/AgRP neurones. These neurones may be other subpopulations of NPY/AgRP neurones or of another chemical phenotype such as dopamine, somatostatin-, galanin- or dynorphin-containing neurones, all of which are found localised with origins in the Arc.

The NA-induced depolarisation was suggested to be attributable to a number of neuronal mechanisms. 31.8% of neurones that were excited by application of NA responded with an increase in input resistance. I/V relationships revealed a reversal potential of -84.1 ± 5.3 mV suggestive of the closure of one or more resting potassium conductances in the neuronal membrane. 22.7% of neurones responded with a decrease in input resistance with a mean extrapolated reversal potential of -24.3 ± 2.9 mV suggesting that the NA induced depolarisation is in part mediated through activation of one or more non-selective cation channels. 45.5% of neurones responded with no change in neuronal input resistance suggestive of the activation of one or more membrane ion pumps or the combination of closure of one or more potassium conductances and the activation of a non-selective cation conductance.

The majority of studies have commonly reported a decrease in potassium conductance for the ionic mechanism underlying the NA-induced depolarisation (Freedman & Aghajanian, 1987; McCormick & Prince, 1988; Inokuchi *et al.*, 1992; Akasu *et al.*, 1993; Pan *et al.*, 1994) but there are reports of NA acting on various other conductances (Pan *et al.*, 1994). Yamanaka *et al.*, (2006) found with the use of electrophysiological experiments, that

NA activated non-selective cation channels mediated by α_1 -ARs in orexin-expressing neurones. Results presented here suggest that both of these cellular signal-transduction mechanisms may operate at the level of the Arc. The difference in ionic mechanisms underlying the excitation seen by NA may also reflect the extent of dialysis of the neurone with the recording solution, which may significantly alter the electrophysiological characteristics of the neurone over the recording period (Velumian *et al.*, 1997) hence the time from going whole-cell and application of NA may be crucial. With the whole-cell recording there is a possibility of wash-out or wash-in of a factor that may prevent the observation of a reversal potential (Pan *et al.*, 1994). Maybe an alternative method of patch-clamp should be considered such as perforated patch-clamp. This method of patch-clamping has advantages in reducing dialysis of the cell. Further work using selective pump and ion exchanger inhibitors and ion substitution experiments are required to fully clarify the mechanisms underlying these differential effects of NA on Arc neurones.

Bath application of NA also induced indirect effects on Arc neurones. Similar indirect effects of NA through changes in spontaneous synaptic transmission have been shown to occur on orexin-expressing neurones in the lateral hypothalamus (Li & van den Pol, 2005; Yamanaka *et al.*, 2006). NA-induced a significant increase in the frequency of EPSPs, an effect subsequently blocked by NBQX. This is indicative of NA stimulating glutamatergic neurones presynaptic to the recorded neurone (Daftary *et al.*, 2000). NA was also found to induce or increase the frequency of spontaneous IPSPs, an effect reversed on wash out of NA. The IPSPs reversed around -65 mV and were sensitive to bicuculline showing them to be mediated through the activation of $GABA_A$ channels. This response is indicative of NA activating on GABAergic neurones presynaptic to the recorded neurone. Han *et al.*, (2002) found that NA excites and inhibits GABAergic transmission in parvocellular neurones of the rat hypothalamus through modulation of α_1- AR and the α_2- ARs, respectively. To further this study

the next step would be to investigate NA effects on miniature EPSPs and IPSPs in order to address whether NA increases excitability of presynaptic glutamatergic and GABAergic neurones at the level of the presynaptic terminal or elsewhere on the presynaptic cell. Furthermore, stimulation studies with stimulating electrodes located in other hypothalamic areas such as the LH, which directly innervates Arc neurones, may help to clarify the nature of the origins of these synaptic inputs.

Phenylephrine, a α_{1-} AR agonist mimicked the NA-induced depolarisation, and prazosin, a α_{1-} AR antagonist, blocked the response, suggesting NA-induced excitation through activation of α_{1-} ARs. NA-induced excitation through activation of α_{1-} ARs has been previously reported in other areas of the CNS (Lewis & Coote, 1990; Pan *et al.*, 1994; Daftary *et al.*, 2000; Yamanaka *et al.*, 2006).

Subsequent studies to clarify further the subtypes of α_{1-} ARs involved were undertaken. The results suggest that the α_{1A-} AR has a significant role to play in the NA-induced depolarisation and increase in firing rate with a smaller contribution from α_{1B-} ARs. This is in accordance with studies using *in situ* hybridisation to examine the expression of α_{1-} AR subtypes in the CNS. These studies revealed expression of α_{1B-} ARs was extremely low compared to low/ moderate levels of α_{1A-} AR expression at the level of the Arc (Day *et al.*, 1997). The differential expression of these α_{1-} AR subtypes could also explain the variation in ionic mechanisms observed underlying NA-induced depolarisation in Arc neurones. The different α_{1-} AR subtypes could be associated with the different cellular mechanisms found within this study i.e. the subtypes differentially link up with potassium channels, non-selective cation channels or pump in the cellular membrane. Further studies investigating ionic mechanisms underlying NA-induced depolarisation in the presence of selective antagonists are required to clarify this possibility.

In contrast to previous studies we did not find a role for β ARs in mediating an excitation within the Arc (Kang *et al.*, 2000). Application of the β-agonist, isoproterenol, had no affect on hypothalamic Arc neurones. However, our data is only preliminary and therefore we would need a larger (n) number to clarify these results. We also carried out recordings in 2 mM glucose. This is in contrast to Kang *et al*, 2000 who carried out extracellular recordings in 10 mM glucose. The differences observed between the two studies could potentially be due to the change in glucose. The current study has previously described (chapter 4) that changes in extracellular glucose can significantly change subthreshold active conductances which are ultimately involved in synaptic integration and forming the neurone's output.

In studies described here, application of NA in the presence of the antagonist, prazosin, blocked the NA-induced depolarisation in a concentration dependent manner, revealing NA-induced hyperpolarisation. A similar but opposing set of observations were made with the α_{2}- AR antagonist Idazoxan, which blocked the NA-induced α_{2}- AR-mediated hyperpolarisation and uncovered a NA-induced depolarisation and increase in spontaneous firing (see chapter 6; Nakamura *et al.*, 1984; Yamanaka *et al.*, 2006). This suggests that Arc neurones express multiple receptors that mediate opposing effects. In this case α_{1}- ARs mediate an excitation and α_{2}- AR mediate inhibition (Nakamura *et al.*, 1984; Yamanaka *et al.*, 2006). The antagonist therefore unmasks hitherto hidden effects. These differential effects might reflect differential expression of these receptors, the type of response to NA being dependant on the relative density and distribution of AR subtypes present on the postsynaptic membrane. The NA-induced depolarisation may dominate in neurones where α_{1}- ARs are present in high densities proximal to the recording site at the soma or proximal dendrites, and α_{2}- ARs are expressed distal. Whereas the inverse may be true in neurones where block of inhibition uncovers NA-induced excitation, the latter scenario reflecting a higher level of expression of α_{2}- ARs proximal to the recording site. Such an arrangement of receptors may

have functional significance whereby pathway- and function-specific noradrenergic inputs are differentially activated at different times and / or under different physiological circumstances.

Orexin neurones, exclusively located in the lateral hypothalamus (LH), are implicated in the regulation of sleep and energy homeostasis and have been found to have complex responses to NA (Li & van den Pol, 2005). Orexin neurons project to all parts of the brain including the Arc. They are orexigenic and have been found to be inhibited by NA, thus suggesting that NA may be anorexigenic at the level of the LH (Li & van den Pol, 2005). However, Bayer *et al*., (2005) has reported that orexin neurones can be excited by NA within the LH thus indicating that NA can have differential effects on orexin neurones within the LH. Furthermore, orexin neurones are activated by NA but inhibited when rats are sleep deprived, supporting the notion of a function-specific organisation and plasticity associated with noradrenergic inputs to hypothalamic neurones (Yamanaka *et al.*, 2006). Whether NA responsiveness of Arc neurones changes depending on levels of arousal or energy status requires further study and clarification.

5.3.1 Future studies

To further this study, c-fos experiments combined with CART staining would be an efficient and productive way to clarify the role of NA and anorexigenic circuits in regulating excitability of Arc neurones and their role in controlling energy homeostasis.

Further double-labelling experiments would be an efficient method to characterise other peptide-expressing Arc neurones present within the Arc. This study could be extended to incorporate NA effects within the Arc in other homeostatic processes other than energy homeostasis.

Further pharmacological and ion substitution experiments could be carried out in order to identify the specific ionic mechanism underlying the NA-induced depolarisation. It would be of interest also to determine if each of the different ionic mechanisms mediating the NA-induced depolarisation is mediated through different α_1- AR subtypes.

5.3.2 Conclusion

This study has shown that NA excites hypothalamic Arc neurones through the activation of α_{1-} ARs, partially through α_{1A-} ARs and to a lesser extent through α_{1B-} ARs. This includes a subpopulation of orexigenic NPY/AgRP-expressing neurones and a subpopulation of identified putative anorexigenic CART-expressing neurones. Multiple mechanisms are involved in mediating the NA-induced depolarisation including: the inhibition of one or more resting potassium conductances, activation of one or more non-selective cation conductances or a combination of the two, or possibly through activation of an electrogenic pump within the membrane. In the presence of α_{1-} AR antagonists, NA induced a hyperpolarisation suggesting multiple receptor subtypes are localised to the same neurone but producing opposite effects. Further studies are required to clarify the functional significance of these differential NA inputs.

Figure 5.1 **NA-induced a depolarisation in hypothalamic Arc neurones**

A: A continuous current- clamp recording of an Arc neurone showing the effect 40 μM NA bath applied for approximately 1 minute. The line above the recording indicates the application time and duration of NA. The / / indicates a break within the trace of approximately 2 minutes, during which time a current/ voltage relationship (I/V) was generated. The regular negative membrane potential responses are evoked as a result of rectangular- wave negative current injections (5-20 pA, 1.2s, 1/5Hz), enabling the input resistance to be monitored. Application of NA induced a membrane potential depolarisation and increased firing rate, which the effects were reversible within approximately 15 minutes from the time of wash out of NA.

B: I/V relationships obtained from a different neurone than that shown in (A) in the absence and presence of NA respectively. The traces shown are superimposed samples of a continuous whole-cell current- clamp recording showing membrane responses to a series of hyperpolarising and depolarising current injections of constant increment.

C: A graph plotting the current- voltage relationship obtained from the traces shown in (B), obtained by plotting the current injected into the cell (x-axis) against the resulting membrane holding potentials (y-axis). The symbols ▪ and o indicate the current-voltage relationships in the absence and presence of NA, respectively. Note the parallel shift which maybe indicative of the activation of an electrogenic pump within the membrane, or the activation of multiple conductances that off-set each other.

Figure 5.2 **NA excites hypothalamic arcuate neurones in the presence of TTX**

A: A trace from a continuous current- clamp recording of an Arc neurone in the presence of 1 μM TTX showing the direct action of NA on ARC neurones. The regular negative membrane potential responses are evoked as a result of rectangular- wave negative current injections (5-20 pA, 1.2 s, 1/5 Hz), enabling the input resistance to be monitored. The / / indicates a break within the trace of approximately 2 minutes where an I/V relationship was generated. The line above the recording marked NA indicates the time course of application of 40 μM NA. * denotes the manual injection of negative current in order to clamp back the membrane to the resting membrane in order to monitor the input resistance in the presence of NA excluding the activation of other active conductances. In this case NA causes an increase in input resistance. Application of NA induced a membrane depolarisation was reversible within approximately 15 minutes following the wash of NA from the bath.

B: IV relationships obtained from a different neurone than that shown in (A) in the presence of TTX (1 μM). Recordings were taken before and during the application of NA (40 μM).The traces shown are superimposed samples of a continuous whole-cell current- clamp recording showing membrane responses to a series of hyperpolarising and depolarising current injections of constant increment. Note the activation of a rebound depolarisation spike in the presence of NA

C: A plot of the current-voltage relationship of the neurone shown in B. The symbols ▪ and ○ indicate the current- voltage relationships in the absence and presence of NA, respectively. Note the increase in slope of the I/V relationship in the presence of NA which is suggesting an increase in neuronal input resistance. The two lines intersect around -100 mV which indicates a reversal potential close to that of potassium under our recording conditions.

Figure 5.3 **NA-induces a depolarisation through the activation of a Non selective cat-ion channel**

A: A trace from a continuous current-clamp recording of a NA responsive arcuate neurone. The regular negative membrane potential responses are evoked as a result of rectangular-wave current injections in order to monitor the input resistance. The line above the recording marked NA indicates the time course of application of 40 µM NA. The application of NA induced a membrane depolarisation and an increase in firing that was seen to be reversible within approximately 15 minutes following the wash of NA from the bath. The // in the recording marks a break of approximately 3 minutes in which an I/V relationship was generated.

B: IV relationships obtained from the neurone shown in (A) before and during the application of NA. The traces shown are superimposed samples of a continuous whole-cell current-clamp recording showing the membrane responses to a series of hyperpolarising and depolarising current injections of constant increment.

C: A graph plotting the current-voltage relationship obtained from the traces shown in B, obtained by plotting the current injected into the cell (x-axis) against the resulting membrane holding potentials (y-axis). The symbols ▪ and ○ indicate the current-voltage relationships in the absence and presence of NA, respectively. Note, that the IV lines have been extrapolated to determine point of intersection. In this case they cross at approximately -25 mV suggesting the activation of a non-selective cation (NSCC).

Figure 5.4 **NA-induces an inward current in Arc neurones**

A: Trace showing a continuous recording from an Arc neurone in Voltage clamp mode. Application NA (40 µM) at a holding potential of -50 mV induced a reversible inward current.

B: Current responses obtained in voltage-clamp in the presence (green trace) and absence (black trace) of NA. The currents were obtained from ramp protocols that drove the holding potential from -100 mV to -30 mV, at a rate of 10 mV per second. These responses are mostly parallel.

C: Current response obtained in voltage-clamp in the presence (green trace) and absence (black trace) of NA, from a separate neurone from that shown in A and B. The currents were obtained from a ramp protocol that drove the holding potential from -130 mV to -30 mV, at a rate of 10 mV per second. The resulting graph showed a reversal potential for the NA-induced current close to the K^+ reversal potential under our recording conditions.

Figure 5.5 **NA- induced indirect effects on hypothalamic Arc neurones**

A: 3 samples of a continuous current clamp, showing before, during and after the application of NA respectively. Application of NA (40 µM) induces an increase in spontaneous synaptic (excitatory postsynaptic potentials, EPSPs) transmission in addition to a membrane depolarisation. The third section shows the neurone in the presence of NBQX (10 µM) a blocker of non-NMDA glutamatergic synaptic transmission, thus confirming the synaptics to be EPSPs. Below are further sections that have then been shown at a faster time base thus showing a minor proportion of the recording in more detail. The resting membrane of this neurone is at -48 mV, and was slightly active.

.

Figure 5.6 **Application of NA on hypothalamic Arc neurones IPSCs**

A: A continuous voltage-clamp recording showing the effects of changing the holding potential on IPSCs. Below, sections are shown on a faster time-scale showing the polarity of IPSCs reversed at membrane potential more negative than -70 mV.

B: A continuous voltage-clamp recording of a single Arc neurone exposed to NA (40 Mm) that induces a slight outward current and induces IPSCs. IPSCs are subsequently blocked with 10 μM bicuculline, a selective $GABA_A$ antagonist.

Figure 5.7 **NA induces membrane potential oscillations and burst-like pattern of firing in a population of Arc neurones**

Ai: Sample of a continuous whole-cell current-clamp recording from an Arc neurone showing a NA-induced depolarisation (40 μM). With a holding current of -16 pA, bursting of action potentials and membrane oscillations are seen.

Aii: Expanded region from the neurone shown in Ai at a faster time scale, showing membrane potential oscillations with associated bursts of action potentials.

Figure 5.8 **α_1 AR agonist depolarises hypothalamic Arc neurones**

A: A trace from a continuous current- clamp recording from an Arc neurone exposed to 10 μM phenylephrine. The regular downward deflections are constant negative current injections of constant amplitude enabling the input resistance to be monitored (5-20 pA, 1.2 s, 1/5 Hz). The / / indicates a break within the recording of approximately 2 minutes, this is in order to carry out a current/ voltage relationship. The line above the recording marked phenylephrine indicates the time course of application of 10 μM phenylephrine in the presence of TTX (1 μM) also shown in the figure. The application of phenylephrine caused a pronounced membrane depolarisation that was reversible within approximately 4 minutes following the wash of phenylephrine from the bath.

B: IV relationships obtained from the neurone shown in (A) in the presence of TTX (1 μM). Recordings were taken before and during the application of phenylephrine (10 μM).The traces shown are superimposed samples of a continuous whole-cell current- clamp recording showing membrane responses to a series of hyperpolarising and depolarising current injections of constant increment. Note again the activation of a rebound depolarisation spike in the presence of NA

C: A graph plotting the current- voltage relationship obtained from the traces shown in B obtained by plotting the current injected into the cell (x-axis) against the resulting membrane holding potentials (y-axis). The symbols ▪ and ○ indicate the current-voltage relationships in the absence and presence of phenylephrine, respectively. Note the parallel shift which maybe indicative of a pump within the membrane, or the activation of multiple conductances that off-set each other.

Figure 5.9 **NA-induced excitation is blocked by a α_1. AR antagonist in a concentration dependant manner**

A: Samples of a continuous current- clamp recording from an Arc neurone showing exposure to 40 µM NA, which induced a reversible membrane depolarisation and increase in action potential firing. The application of the α_1-AR antagonist, prazosin at 300 nM blocked the NA induced response. The regular negative membrane potential responses are the result of evoked rectangular- wave negative current injections enabling the input resistance to be monitored (5-20 pA, 1.2 s, 1/5 Hz). The lines above the recording indicates the time course to NA and prazosin.

B: A trace from a neurone (different to the neurone shown in A) that has been exposed to 40 µM NA that has also induced a membrane depolarisation and increase in firing rate. Application of 300 nM prazosin blocked the NA induced depolarisation, and revealed a NA induced inhibition.

C: A dose response curve, showing the effects of differential concentrations of prazosin in blocking the NA induced response.

Figure 5.10 NA induced excitation is (partially) blocked by a α_{1A}-AR antagonist

A: A trace from a neurone that has been exposed to 40 μM NA that has also induced a membrane depolarisation and increase in firing rate. Application of 10 nM RS100329 HCL does not completely abolish the NA induced excitation, however the response lasts a shorter period of time. Application of NA in the presence of 100 nM RS100329 blocks the NA-induced increase in firing rate. On wash out of the α_{1A}-AR antagonist, further application of NA induces an increase in firing rate and a larger depolarisation of the membrane, thus suggesting that there is little receptor desensitisation to NA application and that the α_{1A}-AR contributes partially to the NA-induced excitation. The regular negative membrane potential responses are the result of evoked rectangular-wave negative current injections enabling the input resistance to be monitored (5-20 pA, 1.2 s, 1/5 Hz).The lines above the recording indicates the time course to NA and RS100329 HCL. // represent breaks within the recording to carry out I/V relationships.

B: Sample of a continuous current-clamp recording from an Arc neurone showing exposure to 40 μM NA, which induced a reversible membrane depolarisation and increase in action potential firing The application of the α_{1A}-AR antagonist; RS100329 HCL at 100 nM blocked the NA induced response. The regular negative membrane potential responses are the result of evoked rectangular- wave negative current injections enabling the input resistance to be monitored (5-20 pA, 1.2 s, 1/5 Hz). The lines above the recording indicates the time course of NA and RS100329 HCL.

Figure 5.11 **NA induced excitation is (partially) blocked by the α_{1b}- AR antagonist-02484100**

A: Samples of a continuous current-clamp recording from an Arc neurone showing exposure to 40 μM NA, which induced a reversible membrane depolarisation and increase in action potential firing. The application of the α_{1b}-AR antagonist; 02484100 at 100 nM partially blocks the NA- induced response. NA still induced a depolarisation of the membrane but fails to induce a significant increase in firing rate in the presence of the antagonist. The regular negative membrane potential responses are the result of evoked rectangular- wave negative current injections enabling the input resistance to be monitored (5-20 pA, 1.2 s, 1/5 Hz). The lines above the recording indicate the time course to NA and 02484100.

Figure 5.12 NPY/AgRP pacemaker neurones are excited by NA

A: A continuous current clamp recording of a NPY/AgRP neurone exposed to 40 μM NA. The regular negative membrane potential responses are evoked as a result of rectangular- wave negative current injections enabling the input resistance to be monitored (5-20 pA, 1.2 s, 1/5 Hz). The / / indicates a break within the recording of approximately 2 minutes, during which time a current/ voltage relationship (I/V) was generated. The line above the recording marked NA indicated the time application of this drug. Application of NA induced a reversible membrane depolarisation and a reversible increase in firing rate.

B: A continuous current clamp recording of a NPY/AgRP neurone exposed to NA in the presence of TTX. In the presence of TTX, NA still induced a membrane depolarisation, thus showing that NA acts directly upon the NPY/AgRP arcuate neurone.

C: IV relationships obtained from a neurone in the presence and absence of NA and TTX. The traces shown are superimposed samples of a continuous whole-cell current clamp recording showing membrane responses to a series of hyperpolarising and depolarising current injections of constant increment.

D: A graph plotting the current/voltage relationship obtained from the traces shown in C, obtained from plotting the current injected to the cell (x-axis) against the resulting membrane holding potentials (y-axis). The symbols ▪ and ○ indicate the current voltage relationships in the absence and presence of NA, respectively. Note, the point of intersection between to the I/V curves, that is close to the reversal potential of potassium under our recording conditions.

Figure 5.13 **NA-induced an excitation in CART positive neurones**

Ai: Confocal images showing the staining of CART within the Arc (Green). Aii: A single neurone labelled with Alexa (633) during recording that was shown to be excited by NA. Aiii. Shows the two images in Ai, Aii superimposed, and subsequently confirming that the neurone recorded from was a CART-expressing neurone.

Figure 5.14 **NA-induced an excitation in CART negative neurons**

Ai: Confocal images showing the staining of CART within the Arc (Green). Aii: A single neurone labelled with Alexa (633) during recording that was shown to be excited by NA. Aiii. Shows the two images in Ai, Aii superimposed, and subsequently confirming that the neurone recorded from was not a CART-expressing neurone.

Chapter 6

The inhibitory effects of noradrenaline on rat hypothalamic arcuate nucleus neurones *in vitro*

6.1 Introduction

The arcuate nucleus (Arc) plays a fundamental role in a variety of circuits functionally dedicated to controlling autonomic processes, and is crucial for the regulation of energy homeostasis. It forms a key site for the integration of peripheral and central signals regarding the energy stores of the body (Beck *et al.*, 2001; Williams *et al.*, 2001). It receives a number of afferent inputs and is equally diverse with regards to its target efferents. Of particular interest to this study is the noradrenergic input Arc neurones receive from brainstem nuclei (Sawchenko & Swanson, 1981).

The endogenous catecholamine, noradrenaline (NA) activates a family of G-protein-coupled receptors (GPCRs) to transmit signals across the plasma membrane (Hein, 2006). The adrenergic receptors can be divided into two different classes, the α-adrenoceptors (ARs) and the β- ARs, which are distributed differentially within the CNS (Nicholas *et al.*, 1993; Day *et al.*, 1997) and throughout the periphery (Zhong & Minneman, 1999). The α- AR subfamily can be further subdivided into the α_{1-} AR and α_{2-} AR, which have both been reported to be widely distributed within the hypothalamus (Young & Kuhar, 1980). α_{2-} ARs have been found to be abundant in the Arc and the paraventricular nucleus (PVN), whereas α_{1-} ARs are found more laterally within these nuclei (Young & Kuhar, 1980; Unnerstall *et al.*, 1984).

α_2- ARs can be divided into 3 separate subtypes; $_{2A, 2B}$ and $_{2C.}$ All three subtypes appear to couple to the same signalling systems, the G_i-mediated pathway, which involves inhibition of adenylyl cyclase, activation of receptor-operated potassium channels and inhibition of voltage-gated Ca^{2+} channels (Rogawski & Aghajanian, 1982; Limbird, 1988). α_2-AR are located both pre- and post-synaptically. Postsynaptic α_2- ARs are directly inhibitory or presynaptic α_{2-} AR provide negative feedback which inhibits presynaptic release of NA

(Rogawski & Aghajanian, 1982; Wellman *et al.*, 1993) and thus function as inhibitory autoreceptors.

The functioning of the noradrenergic system on Arc neurones has previously been described in POMC neurones, which are abundant within the Arc and are implicated in the control of energy homeostasis, and mediate anorexigenic effects. α_2- ARs present on POMC neurones have been shown to cause bradycardia and hypotension (Li *et al.*, 1996) thus showing the complexity of the roles of these receptors in multiple cellular functions that have not yet been fully explored.

Application of the α_2- AR agonist clonidine, or NA, into the PVN elicits feeding. These receptors seem postsynaptic in nature, since their sensitivity to noradrenergic stimulation is unaffected or even enhanced by drug manipulations that destroy the presynaptic terminals or block neurotransmitter synthesis (Goldman *et al.*, 1985).

Insulin, a well known long-term adiposity signal exerts its effects, in part, via actions on specific neurones of the hypothalamus to produce an overall anorexigenic effect (Benoit *et al.*, 2002). Brain α- ARs exhibit considerable plasticity in situations where plasma insulin levels fluctuate as a function of diet and obesity (Levin & Hamm, 1994). Insulin importantly has been reported to directly regulate noradrenergic responsive neurones within the Arc via effects mediated through the α_2- AR (Levin *et al.*, 1998). Thus, studies suggest that the noradrenergic system is involved in the central control of energy homeostasis. However, the precise role of NA in regulating energy balance at the level of the hypothalamic Arc remains unclear.

The previous chapter has focused on the excitatory effects of NA within the Arc. Bath application of NA depolarises a population of Arc neurones through the activation of α_1- ARs. In the present study, the aim was to investigate the cellular mechanisms by which NA induced an inhibition and hyperpolarisation of Arc neurones and to determine the AR and the neuronal

cell type associated with mediating these effects, using whole-cell patch clamp recording techniques and immunohistochemistry in hypothalamic slice preparations.

6.2 Results

Whole-cell patch clamp recordings *in vitro* were obtained from a total of 172 neurones that were exposed to bath application of NA (40 μm; 1-2 minutes). These neurones exhibited a mean resting membrane potential of -48.6 ± 0.6 mV, associated with a mean neuronal input resistance of 1397 ± 51 MΩ. Neurones responded to NA with either a depolarisation (51.2%), hyperpolarisation (22.7%) or no response (26.1%) to the membrane.

6.2.1 NA-induced a hyperpolarisation of hypothalamic Arc neurones

39/172 (22.7%) neurones exposed to 40 μM NA responded with an inhibition, observed as a decrease in suprathreshold activity and hyperpolarisation of the membrane potential. Bath application of NA induced a decrease in spontaneous firing rate from a control level of 1.1 ± 0.2 Hz to 0.0 ± 0.0 Hz ($P < 0.001$; student's *t*-test), the effects of which were reversible following the wash of NA from the bath, spontaneous firing rate recovering to 1.3 ± 0.2 Hz (n=25; Figure 6.1A).

The NA-induced inhibition was associated with a reversible membrane hyperpolarisation. The membrane potential recovered to control levels within approximately 5-7 minutes following the wash of NA from the bath. NA application induced a membrane hyperpolarisation from a mean resting membrane potential of -45.9 ± 1.2 mV to -59.9 ± 1.7 mV ($P < 0.001$ for control versus NA; ANOVA), amounting to a mean peak membrane hyperpolarisation amplitude of 14.1 ± 1.2 mV (n=39). Performing an ANOVA revealed a highly

significant difference in the membrane potential between the control and the neurone in presence of NA. The membrane potential returned to a mean resting potential of -44.3 ± 1.4 mV on washout of NA from the bath (*P*=0.38; control compared to wash). Neurones that were silent at rest, displaying no suprathreshold activity, were also inhibited by NA indicating that NA-induced hyperpolarisation was not exclusive to 'active' cells (see Figure 6.1B).

The NA- induced membrane hyperpolarisation was associated with a decrease in neuronal input resistance from a mean resting neuronal input resistance of 1467 ± 119 MΩ to 1023 ± 81 MΩ (*P*<0.001; student's *t*-test) in the presence of NA, amounting to a mean 23.2 ± 5.2 % decrease in neuronal input resistance in the presence of NA. The effects were reversible following the wash of NA from the bath, with the input resistance recovering to 1545 ± 234 MΩ.

NA-induced hyperpolarisation and decrease in neuronal input resistance persisted in the presence of TTX (1 μM, n=3; see Figure 6.2 A), thus indicating a direct post-synaptic effect of NA on Arc neurones. NA application in the presence of TTX induced a membrane hyperpolarisation from a mean resting membrane potential of -49.7 ± 3.0 mV to -65.7 ± 2.0 mV amounting to a mean peak membrane hyperpolarisation amplitude of 16.0 ± 5.0 mV (n=3). This response to NA, in the presence of TTX, was associated with a decrease in input resistance of 50.0 ± 10.4 %, from a mean resting input resistance of 1965 ± 624 MΩ to 888 ± 114 MΩ in NA (n=3).

In voltage-clamp at a holding potential of -50 mV, application of NA (40 μM, n=10) in the presence of TTX, induced an outward current, with a mean peak amplitude of 14.1 ± 1.4 pA (Figure 6.3A).

6.2.2 NA-induced hyperpolarisation was concentration-dependent.

The magnitude of the NA-induced hyperpolarisation was dependent upon the concentration of NA applied (see Figure 6.4). NA at a concentration of 0.1 μM (1-2 minutes) had no effect on the membrane potential of the neurone; 40 μM induced a maximal membrane hyperpolarisation. The higher concentrations of NA induced membrane hyperpolarisations that were more prolonged in time-course. All NA-induced hyperpolarisations were reversible within approximately 5 minutes of washing the drug from the bath.

6.2.3 Ionic mechanism underlying the NA-induced hyperpolarisation.

The NA-induced hyperpolarisation was associated with a decrease in neuronal input resistance or an increase in membrane conductance. To determine the ionic mechanism underlying the NA-induced hyperpolarisation, current-voltage (I/V) relationships were obtained in control conditions and at the peak of the NA-induced hyperpolarisation in 13 neurones (Figure 6.1 C/D). In 13/13 neurones it was possible to determine a clear mechanism underlying the hyperpolarisation. The NA-induced inhibition revealed a clear reversible potential amounting to -82.6 ± 1.6 mV, close to the predicted reversible potential for potassium under our recording conditions. The reversal potential was taken from the point at which the plots of the two I/V relations intersected. These neurones showed a decrease in input resistance from 1269 ± 103 MΩ at rest to 794 ± 69 MΩ in NA with a mean peak amplitude membrane hyperpolarisation of 17.6 ± 2.0 mV. This indicates that the NA-induced hyperpolarisation is at least in part mediated through the opening of one or more potassium conductances.

In voltage-clamp at a holding potential of -50 mV, application of NA (n=10) induced an outward current, with a mean peak amplitude of 14.1 ± 1.4 pA .Voltage-clamp ramps from -110 to -30 mV at a rate of 10 mVs^{-1} were applied in control conditions and at the peak of the NA-induced response to investigate the ionic mechanism and reversal potential of the NA-induced current. NA-induced outward currents had a mean reversal potential of -93.6 ± 2.2 mV, close to the reversal potential of potassium under our recording conditions (n=6; Figure 6.3B)

A further feature of the NA-induced hyperpolarisation was an apparent "transformation" of the current-voltage relations characterised by the presence of an inwardly rectifying conductance observed at more negative membrane potentials in the presence of NA. The conductance was similar in characteristics to the inwardly rectifying potassium conductance described in chapters 3 and 4.

6.2.4 NA activates an inwardly rectifying potassium channel

Hypothalamic Arc neurones express a number of subthreshold active conductances (see Chapter 3). A population of neurones express an anomalous inward rectifying channel (I_{an};Figure 6.5). As the name suggests 'rectification' means change of conductance with voltage, and 'anomalous' suggests that this conductance works in the contrary direction to that predicted by the Goldman-Hodgkin- Katz electro-diffusion equation (Goldman, 1943). This conductance is characterised by an instantaneous decrease in input resistance at more negative membrane potentials. The NA induced membrane hyperpolarisation was associated with the enhancement or appearance of inward rectification at negative membrane potentials. Thus there was a notable enhanced decrease in input resistance at more negative membrane potentials in the presence of NA. The expression of this inward rectification amounted to a

30.9 ± 4.0 % (n=7) reduction in input resistance at a membrane potential of -99.2 ± 1.5 mV relative to the steady-state input resistance calculated at rest in the absence of NA. In contrast, I/V relationships carried out in the presence of NA revealed a 40.9 ± 5.7 % (n=7) reduction in input resistance at a membrane potential of -100.4 ± 4.5 mV, amounting to an overall 10.1 ± 5.7 % increase in inward rectification in the presence of NA.

6.2.5 The effects of Ba^{2+} on NA-induced hyperpolarisation and activation of inward rectification.

Barium (applied in these studies as the chloride salt; $BaCl_2$) is a non-selective potassium channel blocker; frequently used as a blocker I_{an} at a concentration around 100 μM (Rudy, 1988; van den Top *et al.*, 2004). Thus Ba^{2+} was used to further characterise the inward rectification associated with NA-induced hyperpolarisation. Bath application of $BaCl_2$ (300 μM, n=5) significantly blocked the NA induced hyperpolarisation (Figure 6.6). Upon wash of $BaCl_2$ subsequent application of NA induced a response similar to the NA-induced hyperpolarisation of the membrane observed in the absence of the blocker. Thus this data suggests the involvement of one or more barium-sensitive potassium conductances in mediating the NA-induced hyperpolarisation.

6.2.6 The pharmacological profile of receptors mediating NA-induced inhibition: effects of adrenoceptor agonists on Arc neurones

UK-14,304 (10 μM; 1-2 minutes), a specific α_{2}- AR agonist, was bath applied to a total of 12 hypothalamic Arc neurones, 7 of which had previously been exposed to NA (40 μM). A total of 9 (75%) neurones responded with a hyperpolarisation of the membrane potential and

a decrease in input resistance in the presence of UK-14, 304. Application of UK-14, 304 induced a reversible membrane hyperpolarisation from a mean resting potential of -46.6 ± 2.2 mV to -54.4 ± 2.6 mV, a mean peak membrane hyperpolarisation of 7.9 ±1.1 mV (n=9; Figure 6.7A). Neuronal input resistance decreased overall, giving a percentage decrease of 14.6 ± 8.1% from a mean input resistance at rest of 1296 ± 159 MΩ to 1092 ± 176 MΩ in the presence of the α_{2-} AR agonist (n=9). Firing frequency also decreased by 91.7 ± 4.2% in the presence of the α_{2-} AR agonist, from a mean spontaneous firing frequency of 0.9 ± 0.2 Hz in control to 0.0 ± 0.0 Hz in the presence of UK-14,304 (n=6). UK-14,304 was also applied to neurones in the presence of TTX (n=4). The UK-14,304 -induced hyperpolarisation persisted in the presence of TTX thus indicating a direct post-synaptic effect on Arc neurones.

6.2.7 Ionic mechanism underlying the UK-14, 304 induced hyperpolarisation

The α_{2-} AR agonist, UK-14,304 mimicked the hyperpolarisation induced by NA. To deduce the ionic mechanism underlying the decrease in membrane potential, I/V relationships were taken in control conditions and at the peak of the UK-14, 304-induced hyperpolarisation in 4 neurones. 75% of neurones displayed a clear reversal potential amounting to -83.3 ± 7.3mV (Figure 6.7 B/C) close to the predicated reversible potential for potassium ions under our recording conditions. The point of intersection indicated the reversal potential. Thus, NA and UK-14, 304 induce hyperpolarisation of hypothalamic Arc neurones through similar mechanisms, specifically via opening of one or more potassium conductances. Again in the presence of UK- 14,304 there was a stronger I_{an} than in the absence of (see Figure 6.7 C) suggesting that UK-14,304 activates an inward rectifying potassium channel(s).

6.2.8 The pharmacological profile of receptors mediating NA-induced inhibition: effects of adrenoceptor antagonists on Arc neurones

In order to further determine the AR mediating the NA- induced inhibition, the effects of NA in the presence of the α_{2}- AR antagonist, Idazoxan, were examined under current-clamp conditions.

Application of 40 μM NA alone caused a membrane hyperpolarisation and a reduction in action potential firing, a response that was partially blocked (n=2) or completely abolished by pre-treatment of the slice with 200 nM Idazoxan (n=2). Overall, in the presence of Idazoxan, the mean peak amplitude of the hyperpolarisation induced by NA was reduced to 6.0 ± 4.6 mV from 17.2 ±3.2mV, in NA alone, amounting to a 187 % decrease in responsiveness to NA in the presence of Idazoxan. This data suggests that α_2 ARs are at least partially responsible for mediating the inhibition induced by NA (Figure 6.8).

Furthermore, in the presence of Idazoxan, application of NA revealed a NA-induced depolarisation in some neurones and an associated increase in action potential firing frequency from 0.8 ± 0.2 Hz at rest (in presence of Idazoxan) to 2.9 ± 0.7 Hz in response to NA in the presence of idazoxan (n=3 ;Figure 6.8). NA in the presence of Idazoxan depolarised the membrane potential from a mean of -50.0 ± 2.5 mV to -44.0 ± 2.8 mV. This data suggests that block of α_2- ARs with Idazoxan suppresses NA–induced hyperpolarisation of the membrane potential, and reveals a NA-induced excitation. Thus, hypothalamic Arc neurones are capable of expressing more than one type of AR which mediate differential responses. A hyperpolarisation followed by a return to the resting membrane potential and then a subsequent depolarisation and increase in firing rate was observed in 13/39 neurones. This was termed a biphasic response and further substantiated the concept that Arc neurones can express both α_{1}- ARs and α_2-ARs (see Figure 6.9). NA induced a hyperpolarisation of the

membrane potential, a response that was blocked by idazoxan and revealed a depolarisation of the membrane potential. To determine whether the depolarisation was via a direct postsynaptic site of action, the effects of TTX were investigated on NA-induced responses in the presence of idazoxan. In the presence of TTX and idazoxan, the NA-induced depolarisation persisted, thus indicating that NA acts directly on the recorded neurone. To clarify the potential involvement of α_1 ARs in mediating this effect, actions of phenylephrine were tested (see chapter 4). Application of phenylephrine similarly induced a membrane depolarisation, thus further suggesting that both α_1 ARs and α_2 ARs receptors can be functionally expressed in the same neurone and yield opposing effects.

Application of idazoxan alone induced an increase in firing rate suggesting that Arc neurones may be under tonic inhibition by endogenous α_2- AR ligands (n=2; Figure 6.10).

6.2.9 NA differentially regulates excitability of CART-expressing neurones

In order to address the functional significance of these differential responses to NA, the effects of NA were tested on neurones in which the chemical phenotype was determined. Alexa 633 (100 μM) was used in the recording pipette to allow for the identification of the recorded neurones, retrospectively. Slices were subsequently processed immunohistochemically for CART 55-102, using a high affinity antibody. CART has been recognised as an anorectic peptide that co-localises with POMC within the Arc and that is directly up-regulated by leptin (Elias *et al.*, 2001). Thus CART immunohistochemistry was used as a marker to identify anorexigenic neurones and double-labelling with Alexa 633 used to confirm that recordings were made from CART-expressing neurones. 4/12 CART positive neurones responded to NA with membrane hyperpolarisation (Figure 6.11). One neurone identified as a CART-positive cell responded with a biphasic response to application of NA.

NA induced firstly a relatively rapid hyperpolarisation of the membrane potential followed by a depolarisation associated with an increase in action potential firing. 5/12 CART- positive neurones responded in a NA-induced excitation. 8/26 neurones that were CART-negative responded to NA with an inhibition of spontaneous firing and a hyperpolarisation of the membrane potential (Figure 6.12).

6.2.10 The effects of NA on neurones classified according to electrophysiological phenotype.

Chapter 3 in this study classified neurones based on their differential expression of subthreshold active conductances and were subsequently termed clusters. This classification was formed as a basis for further experiments to be carried out in order to identify neurones, based upon their electrophysiological characteristics. The hypothesis driving this initiative is that neurones with different electrophysiological conductances within the Arc are elements controlling different pathways and functional processes. Differential responses to NA over the clusters are to be expected if they form functionally distinct populations. Here the effects of NA were tested on the different electrophysiological subtypes. Figure 6.13 shows a summary histogram showing the responsiveness of each cluster to NA; separated into excitation, inhibition or no response to NA.

Neurones identified as cluster 1 (expressed I_{an}) responded to NA with membrane depolarisation in 53% of neurones; membrane hyperpolarisation in 20% of neurones and did not respond in 27% of cluster 1 neurones (n=15).

Cluster 2 neurones (expressed I_{an} and I_a – like conductance) responded to NA with membrane potential depolarisation in all neurones tested (n=9; 100%). These neurones have previously been identified as Arc NPY/AgRP pacemaker neurones (van den Top *et al.*, 2004).

Thus NA induced excitation of a subpopulation of NPY/AgRP neurones suggesting a potential orexigenic role for NA at the level of the Arc.

Cluster 3 neurones (express no obvious sub-threshold active conductances; n=8) responded to NA with membrane depolarisation (50%) or NA failed to have any significant effect (50%).

The majority (66.6%) of cluster 4 neurones (express a time- and voltage-dependent inward rectification; I_h) failed to respond to NA, this lack of effect being the greatest number across clusters (n=9).

Cluster 5 neurones (express I_h and a T-type-like calcium conductance) responded to application of NA with membrane potential depolarisation in 54% of neurones. 26% of neurones did not respond to NA, the remaining cluster 5 neurones responding in a membrane hyperpolarisation (n=35).

Cluster 6 neurones (express T-type-like calcium conductance) responded to NA with membrane depolarisation in 47% of neurones. No response was obtained to NA in 31% and NA induced a membrane potential hyperpolarisation in 22% of cluster 6 neurones (n=36).

Cluster 7 neurones (express I_{an} and a T-type-like calcium conductance; n=19) responded to application of NA with membrane depolarisation (42%), membrane hyperpolarisation (32%) or no effect (26%).

Finally cluster 8 neurones (express I_h, I_{an} and a T-type-like calcium conductance; n=41) were the group that were most responsive to application of NA with a total of 80% of neurones responding to bath application of NA. Cluster 8 neurones responded to application of NA with membrane depolarisation (51%), hyperpolarisation (23%) or no effects (26%).

6.2.11 Indirect effects of NA on electrophysiologically -defined cell types.

22.7% of neurones responded with a hyperpolarisation of the membrane potential in the presence of NA. 20.5 % (n=8) of neurones that responded with an inhibition to NA also responded with an induction of spontaneous EPSPs (Figure 6.14A). Both the frequency and amplitude of EPSPs/EPSCs increased in the presence of NA. EPSCs increased in frequency from a mean of 0.1 ± 0.0 Hz at rest to 1.6 ± 0.4 Hz in the presence of NA amounting to a 741 ± 351 % increase in frequency of EPSCs in the presence of NA. NA-induced EPSCs, were completely blocked in the presence of NBQX (10μM), a glutamatergic non-NMDA receptor antagonist (n=4; see Figure 6.15). These indirect effects of NA on Arc neurones through glutamatergic synaptic transmission were restricted to specific electrophysiologically defined clusters: 6/8 responding neurones were defined as cluster 8 (Figure 6.14B) and 2/8 neurones were identified as cluster 5 neurones.

NA also induced/increased the frequency of spontaneously evoked IPSPs in a subset of Arc neurones. The frequency of IPSPs increased from a mean of 0.2 ± 0.0 Hz at rest to 0.4 ± 0.0 Hz in the presence of NA amounting to a 165.5 ± 65.3 % ($p<0.05$; n=4) increase in frequency of IPSPs in the presence of NA (Figure 6.16 A). NA-induced IPSPs and IPSCs were completely blocked by the $GABA_A$ antagonist, bicuculline (10μM).

In a further subset of neurones, application of NA suppressed spontaneously evoked IPSPs (n=3), an effect reversible upon washout of NA. These neurones were all subsequently identified as cluster 5 neurones (Figure 6.16 B).

6.3 Discussion

Little is known of the central effects of NA on hypothalamic Arc neurones. This study was carried out to characterise the electrophysiological actions of NA on Arc neurones and the cellular mechanisms underlying these responses. NA induced differential effects on neuronal excitability of Arc neurones including depolarisation (51.2%; see chapter 4) and hyperpolarisation in 22.7% of neurones recorded.

NA-induced a direct hyperpolarisation in a population of CART-expressing neurones mediated most likely through α_{2-} ARs through activation of one or more potassium conductances. Staining for the anorexigenic peptide CART was carried out to identify the chemical phenotype of the neurone and correlated with the electrophysiological properties and responsiveness to NA. NA inhibited a population of Arc neurones that expressed CART, suggesting that NA has an orexigenic role at the level of the Arc. However, as stated earlier (see also chapter 4) POMC/CART-expressing neurones are heterogeneous in function and therefore it cannot be assumed that NA's only function within the Arc is restricted to effects related to energy balance. The overall net effect of NA in relation to feeding therefore requires further work. However, observations described here of NA inducing inhibition of Arc neurones, together with results described in the previous chapter of NA inducing excitation of identified pacemaker NPY/AgRP neurones, are consistent with an orexigenic, anabolic role for NA at the level of the Arc.

NA induced a direct hyperpolarisation of Arc neurones, as revealed by the persistence of the response in TTX, indicating NA acts postsynaptically to inhibit some Arc neurones. This hyperpolarisation was mimicked by the α_{2-} AR agonist, UK-14,304, and blocked by the α_{2-} AR antagonist, Idazoxan, thus verifying that the NA hyperpolarisation is most likely mediated through α_{2-} ARs, observations consistent with other studies in the CNS

showing an inhibitory role for these receptors (Nakamura *et al.*, 1984; Akasu *et al.*, 1985; Arima *et al.*, 1998; Li & van den Pol, 2005; Yamanaka *et al.*, 2006). The significance of NA inducing a membrane hyperpolarisation through α_{2-} AR reported here is in contradiction to previous studies in the Arc. Kang *et al*., (2000) reported that there was no α_{2-} AR within the Arc, and that Arc neurones only responded with an excitation on application of NA through the α_{1-} AR and the β receptor. They reported that the NA-induced inhibition observed was indirect and was completely abolished by low Ca^{2+}- high Mg^{2+}–containing bathing medium. The inhibition seen in the study by Kang *et al*., (2000) may be due to the activation of α_1 and/or β ARs on local inhibitory interneurons, leading to Ca^{2+} dependent release of an inhibitory transmitter such as GABA which then acts to inhibit the recorded neurone. Indeed we do find an increase in IPSPs in a subpopulation of neurones. However this affect does not mediate the NA-induced inhibition. The results of this study contradict observations see by Kang *et al*., (2000) and clearly demonstrates a direct post-synaptic site of action for NA.

The mechanism mediating the NA-induced hyperpolarisation was a consequence of activating one or more potassium conductances, established as a result of plotting I/V relationships before and in the presence of the NA, revealing a reversal potential around -83 mV in current clamp and -93 mV from voltage-clamp ramp data. This value is near the equilibrium potential for potassium under our recording conditions. The NA-induced hyperpolarisation was associated with a decrease in neuronal input resistance thus the activation of α_{2-} ARs resulted in the opening of one or more potassium conductances, a notion further supported by the block of NA-induced inhibition with the potassium channel blocker barium (Akasu *et al.*, 1985; Li & van den Pol, 2005).

UK-14,304, the selective α_{2-} AR agonist induced a membrane hyperpolarisation associated with a decrease in neuronal input resistance that exhibited a reversal potential

close to the reversal potential for potassium under our recording conditions. This is consistent with effects being mediated by the opening of one or more potassium-selective conductances.

In the presence of idazoxan, the application of NA induced a depolarisation and increase in firing frequency. Interestingly, in the absence of NA, idazoxan alone increased firing frequency in some neurones, suggesting that Arc neurones may be under the control of a tonic inhibition by endogenous α_{2-} AR ligands such as NA (Li & van den Pol, 2005). Idazoxan blocked the α_{2-} AR induced hyperpolarisation and unmasked a NA-induced depolarisation. This suggests the presence of other adrenergic receptors mediating other responses previously masked by activation of the α_{2-} ARs (Nakamura *et al.*, 1984; Yamanaka *et al.*, 2006). It has previously been shown that neurones can express more than one subtype of the α-AR and can have opposing actions (Nakamura *et al.*, 1984; Yamanaka *et al.*, 2006). Depending on the receptor subtype expressed, NA has the capacity to either stimulate or depress neuronal activity. The ratio of α_{2-} AR/ α_{1-} AR expressed in any given neurone at a given time can determine its intrinsic responsiveness to NA. The relative levels of expression of α_2 –AR numbers have the ability to change with the circadian cycle so that expression has been shown to peak at the onset of the nocturnal cycle in the rat (Jhanwar-Uniyal *et al.*, 1986; Stanley *et al.*, 1989). It is at this time that these rodents are most active and their feeding behaviour is at its highest, levels decreasing in the light phase when feeding is at its lowest level of activity (Date *et al.*, 2006). The prevalence of NA inducing a depolarisation of the membrane was more than twice that of NA-induced inhibition. This study has concluded that NA excites Arc neurones through activation of α_{1-} ARs and induces a hyperpolaristion though activation of α_{2-} AR. As mentioned above the α_{2-} AR density /expression increases at the beginning of the dark phase when activity and feeding behaviour is at its highest in rats (Jhanwar-Uniyal *et al.*, 1986; Stanley *et al.*, 1989). We began conducting our experiments on average at 10.00am GMT which is during the early light phase and when rats are less active

and feeding is low. The frequency of inhibition seen could relate to the fact that α_{2-} AR expression is at its lowest. In order to determine if the light/dark cycle has an effect on NA responsiveness of Arc neurones further studies are required on slices in the "dark-phase" to determine if responsiveness to NA shifts.

Arc neurones have been shown to express a variety of active conductances (Burdakov & Ashcroft, 2002), one such conductance being an 'anomalous inward rectification' I_{an} (Tasker & Dudek, 1991). These neurones show a decrease in the membrane response relative to the predicted responses in the absence of active conductances. It shows a decrease in input resistance at more negative membrane potentials. In the presence of NA, cells previously either devoid of I_{an} or displaying $I_{an,}$ exhibited this conductance or an enhanced expression of inward rectification in the presence of NA. Thus the mechanism of action of NA-induced inhibition appears, at least in part, to be mediated through activation of an inward rectifying K^+ (IRK) current as shown previously in other areas of the brain by NA (Jeong & Ikeda, 1998; Ishimatsu *et al.*, 2002; Li & van den Pol, 2005). Thus this study has shown that NA activates potassium conductances, including inwardly rectifying conductances. Further work is required to determine the type of α_{2-} AR that mediates the response. It has been shown that α_{2-} AR are coupled to $G_{i/o}$- signalling pathways thus it is tempting to speculate here that NA activates G-protein inward rectifying K^+ (GIRK) currents. GIRK channels are distributed in the pancreas, heart and brain and play a crucial role in controlling insulin release, neuronal signalling and membrane excitability (Sadja *et al.*, 2003). To further investigate if GIRK channels mediate the NA-induced hyperpolarisation described here, further work will need to be carried out. For example, the effects of tertiapin Q, which selectively blocks GIRK channels (Kanjhan *et al.*, 2005), should be investigated. This study does not address whether the NA activation of the inwardly rectifying K^+ conductance is through a second messenger pathway, i.e. the inhibition of adenylate cyclase and thus the

reduction of cAMP. Previous studies by Aghajanian & Wang, (1986) found with the use of pertussis toxin and cAMP analogues, that within the locus coeruleus α_{2}- AR agonists hyperpolarise the membrane potential by inhibiting adenylate cyclase through a guanine nucleotide regulatory protein (G_i). This is in contrast to the findings of Arima *et al*., (1998) who found, that membrane permeant dibutyryl-cAMP analogues and other compounds acting on the second messenger pathway, failed to have any effect on the inward rectifying K^+ current. These investigators indicated a direct interaction between the G-protein-coupled receptor and ion channel and not through cytoplasmic diffusible second messengers. The study described here is yet to elucidate which of these, if any, are relevant to α_{2}- AR-mediated signalling in the Arc.

Arc neurones have been shown to receive both glutamatergic and GABAergic inputs, the origins of which have not been fully determined (Kiss *et al.*, 2005). NA has been shown to increase the activity of spontaneous EPSPs in a subpopulation of neurones that express a unique combination of active conductances (see chapter 3). Synaptic integration in an individual neurone is critically affected by how active conductances are distributed over the dendrites (Takashima & Takahata, 2008). In these neurones NA directly inhibits the neurone and stimulates a presynaptic glutamatergic neurone, resulting in glutamate release acting on the recorded neurone. A possible glutamatergic input could be from the LH and specifically orexin-containing neurones where reciprocal connection to and from the Arc have been revealed and in which NA directly excites orexin neurones (Chronwall, 1985; Cone *et al.*, 2001; Williams *et al.*, 2001; Rosin *et al.*, 2003; Bayer *et al.*, 2005). Another possible glutamatergic source could be from the VMH, whereby a strong excitatory synaptic input from the medial VMH to the POMC neurones of the Arc have been reported (Sternson *et al.*, 2005). A possible GABAergic input could be from nearby NPY/AgRP neurones present within the Arc which have been shown to co-exist with the amino acid transmitter GABA (Horvath *et al.*, 1997).

Interactions such as this have previously been reported within the Arc, where POMC neurones receive a GABAergic input from NPY neurones (Cowley *et al.*, 2001). Thus, it is possible that when we are recording from a POMC neurone the application of NA activates NPY neurones to increase GABA release on to the POMC neurones thereby inhibiting it. Further work is required to fully elucidate the origins of these glutamatergic and GABAergic synaptic inputs.

NA has also been shown to markedly reduce the frequency of IPSPs in a subset of Arc neurones. This implies that the neurones recorded from received a tonic input from GABAergic presynaptic neurones, which NA subsequently suppressed. As these experiments were not undertaken in TTX, the precise location of these adrenoceptors mediating presynaptic inhibition is uncertain. It may be that presynaptic GABAergic neurones are directly inhibited by NA at the level of the soma or dendrites, thus suppressing release. Alternatively this may reflect activation of presynaptic ARs acting to suppress neurotransmitter release. In relation to this, NA has been shown previously in a number of studies to act via presynaptic α_2- ARs to suppress neurotransmitter release. For example, NA has been shown to have similar effects in rat supraoptic neurones (SON) through the modulation of presynaptic α_2- ARs (Wang *et al.*, 1998).

6.3.1 Conclusion and future studies

NA has been shown to inhibit spontaneous action potential firing and induces hyperpolarisation of the membrane potential. This effect may be mediated through a mechanism involving the activation of a GIRK current via α_2- ARs. To investigate the potential involvement of GIRK channels further experiments need to be carried out. For example, using GTP-γ-S (a nonhydrolyzable GTP analog) to clarify the activation of a G-protein underlies NA-

mediated effects and the use of second-messenger inhibitors, for example adenylyl cyclase inhibitors, to identify the role of signal transduction mechanism in mediating the response.

It has been suggested that α_{2}- AR are located on POMC neurones within the Arc (Li *et al.*, 1996). Results shown here support this notion and the fact that identified pacemaker NPY/AgRP neurones that represent a subpopulation of NPY/AgRP neurones are excited by NA further indicates a possible orexigenic and anabolic role for NA at the level of the Arc.

Studies have shown that ghrelin, an orexigenic peptide whose plasma concentrations increase in response to fasting and fall after meal consumption, signal via the vagus nerve and act on noradrenergic neurones present within brainstem nuclei, which in turn increases NA release in the Arc to stimulate feeding through α_{1}- ARs (Date *et al.*, 2006). It may be that in a fasted state there would be a greater release of ghrelin and thus a greater release of NA at the level of the Arc (Date *et al.*, 2006). Also, the ratio of α_1/α_2 may also be subject to modulation, as discussed earlier. Thus it would be of interest to study the extent of involvement of the circadian cycle and fasted versus fed states in regulating the responsiveness of Arc neurones to NA and the regulation of ARs.

Of interest also would be to determine the specific subtype of α_{2}- ARs involved in mediating the NA-induced inhibition, this could be carried out with the use of more specific agonists and antagonists, single-cell RT-PCR and in situ hybridisation techniques.

Figure 6.1 **NA-induced a hyperpolarisation in hypothalamic Arc neurones**

A: A continuous current clamp recording of a NA (40 μM) sensitive neurone. The line above the recording indicates the application time and duration of NA. The regular negative membrane potential responses are the result of evoked rectangular- wave negative current injections (5-20 pA, 1.2s, 1/5 Hz), enabling the input resistance to be monitored. Application of NA on the active neurone induced a membrane potential hyperpolarisation and decreased activity/ firing. The effects were reversible within approximately 4 minutes from the time of wash out of NA.

B: A trace of a current clamp recording showing the effects of 40 μM NA. Again, hyperpolarising current was injected to monitor input resistance (5-20 pA, 1.2s, 1/5 Hz). The larger downward deflections are a result of injecting increasing amounts of hyperpolarising currents to obtain a current-voltage (I/V) relationship. Application of NA to a silent cell induced a membrane potential hyperpolarisation, again the effects were reversible and the cell returned to its resting membrane potential on washout of NA from the bath. The arrows on the diagram within the recording show expanded regions of the trace shown below which indicate changes in synaptic activity. The first enlargement shows the presence of IPSPs before the application of NA. The second expanded section enlarges the trace in the presence of NA that hyperpolarises the membrane and, and reduces the amplitude and reverses the inhibitory post-synaptic potentials (IPSPs).

C: I/V relationships obtained from the neurone shown in (B) in the absence and presence of NA respectively. The traces shown are superimposed samples of a continuous whole-cell current- clamp recording showing membrane responses to a series of hyperpolarising and depolarising current injections of constant increment.

D: Plot of the I/V relationship of the neurone shown in C. The symbols ▪ and ○ indicate the current- voltage relationships in the absence and presence of NA, respectively. Note the slight decrease in slope of the I/V relationship in the presence of NA which is indicating a decrease in neuronal input resistance. The two lines intersect just above -100 mV which indicates a reversal potential close to the reversal potential of potassium under our recording conditions. Note the decreased slope of the plot towards more negative membrane potentials in the presence of NA as a result of the activation of an inward rectifier.

Figure 6.2 NA inhibits hypothalamic arcuate neurones in the presence of TTX

A: A trace from a continuous current clamp recording of an Arc neurone in the presence of 1μM TTX showing the direct inhibitory action of NA (1-2 minutes; 40 μM) on Arc neurones. The regular negative membrane potential responses are the result of evoked rectangular- wave negative current injections to monitor the changes in input resistance (5-20 pA, 1.2 s, 1/5 Hz). Application of NA induced a membrane hyperpolarisation that was shown to be reversible upon wash of NA from the bath.

B: I/V relationships obtained from a different neurone than that shown in (A) in the presence of TTX (1 μM). Recordings were taken before and during the application of NA (40 μM).The traces shown are superimposed samples of a continuous whole-cell current- clamp recording showing membrane responses to a series of hyperpolarising and depolarising current injections of constant increment.

C: A plot of the current-voltage relationship of the neurone shown in B. The symbols ▪ and ○ indicate the current- voltage relationships in the absence and presence of NA, respectively. Note the decrease in slope of the I/V relationship in the presence of NA which is indicating a decrease in neuronal input resistance. The two lines intersect above -85 mV which indicates a reversal potential close to that of potassium under our recording conditions.

Figure 6. 3 NA induces an outward current in Arc neurones

A: Trace showing samples of a continuous recording of an Arc neurone in voltage-clamp mode at a holding potential of -50 mV. Application NA (40 μM) induced a reversible outward current. The / / indicates a break within the trace of approximately 2 minutes, during which time voltage ramp was generated.

B: Current response obtained in voltage-clamp in the presence (green trace) and absence (black trace) of NA, from a separate neurone from that shown in A. The currents were obtained from a ramp protocol that drove the holding potential from -130 mV to -30 mV, at a rate of 10 mV per second. The resulting graph showed a reversal potential for the NA-induced current close to the K^+ reversal potential under our recording conditions.

Figure 6.4 **Concentration dependence of NA-induced hyperpolarisation**

A: A trace from a continuous current clamp recording of a single Arc neurone exposed to increasing concentrations of NA that induce significant hyperpolarisations of the membrane. 40 μM induces a maximal hyperpolarisation.

Figure 6.5 **NA activates an inwardly rectifying potassium channel**

A: I/V relationships obtained from a neurone in the absence and presence of NA (40 μM) respectively. The traces shown are superimposed samples of a continuous whole-cell current- clamp recording showing membrane responses to a series of hyperpolarising and depolarising current injections of constant increment. With application of NA the neurone was hyperpolarised and when carrying out a I/V relationship it is apparent that NA activated an inwardly rectifying channel (steps are seen closer together).
The arrows (1) indicate the decreased membrane response at more hyperpolarized membrane potentials (downward arrow) relative to membrane potentials responses close to rest (upward arrow) as a result of the activation of a anomalous inward rectification (I_{an})

B: A plot of the current-voltage relationship of the neurone shown in A. The symbols ▪ and ○ indicate the current- voltage relationships in the absence and presence of NA, respectively. Note the decrease in slope of the I/V relationship in the presence of NA which is indicating a decrease in neuronal input resistance and the activation of I_{an} . The two lines intersect just above -100 mV which indicates a reversal potential close to the reversal potential of potassium under our recording conditions.

Figure 6.6 **NA induced hyperpolarisation, in part, is barium sensitive**

A Trace from a continuous current clamp recording of a single Arc neurone exposed to 40 μM NA (1-2 minutes) that induces a significant hyperpolarisation of the membrane with a reduction in firing. Application of barium significantly reduces the NA induced hyperpolarisation and reduction in firing rate. Upon wash of barium a further application of NA revealed a response similar to the control response.

Figure 6.7 **α_2. AR agonist hyperpolarises hypothalamic Arc neurones**

A: A trace from a continuous current clamp recording of an Arc neurone superfused with 10 μM UK-13,304 for 1-2 minutes. The regular negative membrane potential responses are the result of evoked rectangular- wave negative current injections (5-20 pA, 1.2 s, 1/5 Hz), enabling the input resistance to be monitored. The / / indicates a break within the recording of approximately 2 minutes, this is in order to generate a I/V relationship. The line above the recording marked UK-13,304 indicates the time course of application of 10 μM UK-13,304 which induced a pronounced membrane hyperpolarisation that was reversible in approximately 4 minutes from wash out of the agonist from the bath.

B: I/V relationships obtained from the neurone shown in (A) .Recordings were taken before and during the application of UK-13,304 (10 μM).The traces shown are superimposed samples of a continuous whole-cell current- clamp recording showing membrane responses to a series of hyperpolarising and depolarising current injections of constant increment.

C: A graph plotting the current- voltage relationship obtained from the traces shown in Bi, obtained by plotting the current injected into the cell (x-axis) against the resulting membrane holding potentials (y-axis). The symbols ▪ and ○ indicate the I/V relationships in the absence and presence of UK-13,304, respectively. Note the decrease in slope of the I/V relationship in the presence of NA which is indicating a decrease in neuronal input resistance. The two lines intersect just above -90 mV which indicates a reversal potential close to that of potassium under our recording conditions.

Figure 6.8 **NA induced inhibition is blocked by the α_2- AR antagonist; Idazoxan in a concentration dependent manner**

A: A trace from a continuous current clamp recording of an Arc neurone superfused with 40 μm NA for 1-2 minutes induces a reversible membrane hyperpolarisation and a reversible decrease in action potential firing. The regular negative membrane potential responses are the result of evoked rectangular wave negative injection to monitor the input resistance (5-20 pA, 1.2 s, 1/5 Hz). The lines above the recording indicate the time course of NA.

B: Same neurones as above exposed to 200 nM Idazoxan. Application of 40 μM NA blocked the NA induced hyperpolarisation and revealed a slight NA-induced membrane potential depolarisation with a increase in firing. This has been shown more clearly with the expanded sections beneath the recording.

Figure 6.9 **Arcuate nucleus neurones express both α_{1}- AR and α_{2}- ARs**

A: Samples of a continuous current clamp recording of a neurone exposed to bath application of 40 μM NA (1-2 minutes) that induced initially a hyperpolarisation of the membrane. The red dotted line shows that the membrane comes back to the original membrane potential, but becomes more depolarised than before suggesting multiple effects of NA.
Application of idazoxan blocks the NA induced hyperpolarisation revealing a NA-induced depolarisation of the membrane which is shown to be direct with the subsequent application of TTX. Application of phenylephrine to the neurone induces a depolarisation of the membrane suggesting that NA acts through α_{1}- ARs to induce this effect. This experiment suggests that Arc neurones can express both α_{1} and α_{2}- ARs that have opposing effects on the membrane potential.

Figure 6.10 **Idazoxan, a α_{2-}AR antagonist induces an increase in firing**

A: A trace from a continuous current clamp recording of an Arc neurone superfused with 200 nM Idazoxan. Application of idazoxan only induces an increase in action potential firing. This has been shown more clearly with the expanded sections beneath the recording. These data suggest that Arc neurones undergo tonic inhibition by endogenous α_{2-}AR ligands.

Figure 6.11 **NA-induced an inhibition in CART positive neurones**

Ai: Confocal images showing the staining of CART within the Arc (Green). **Aii**: A single neurone labelled with Alexa (633) during recording that was shown to be inhibited by NA. **Aiii**. Shows the two images in Ai, Aii superimposed, and subsequently confirms that the neurone recorded from was a CART-expressing neurone.

Figure 6.12 **NA-induced an inhibition in CART negative neurones**

Ai: Confocal images showing the staining of CART within the Arc (Green). **Aii**: A single neurone labelled with Alexa (633) during recording that was shown to be inhibited by NA. **Aiii**. Shows the two images in Ai, Aii superimposed, and subsequently confirms that the neurone recorded from was not a CART-expressing neurone.

Figure 6.13 **Electrophysiological classification of Arc neurones and their responsiveness to NA**

A: A histogram showing the responsiveness of electrophysiologically defined groups of neurones within the Arc (See chapter 3).

Figure 6.14 **NA induces a hyperpolarisation with a simultaneous increase in EPSPs in neurones predominately termed cluster 8s.**

A: Samples of a continuous current clamp recording of an Arc neurone exposed to 40 μM NA that induced a hyperpolarisation of the membrane and a significant increase in spontaneous EPSPS. Below sections of the current clamp recording are shown on a faster time base, to illustrate the induction of EPSPs more clearly. The regular negative membrane potential responses are the result of evoked rectangular wave negative injection to monitor the input resistance. These were ceased in the middle of the recording in order to monitor the induction of EPSPs more clearly.

B: IV relationships obtained from the neuron shown in (A) before and during the application of NA. The traces shown are superimposed samples of a continuous whole-cell current-clamp recording showing the membrane responses to a series of hyperpolarising and depolarising current injections of constant increment. The neurone is termed a cluster 8 neurones (see chapter 3) based on it expression of $I_{h.,}$ I_{an}, and a T-type like calcium conductance.

Figure 6.15 **NA induces an outward current with a simultaneous increase in EPSCs**

A: Trace showing a continuous recording of an Arc neurone in Voltage clamp mode at a holding potential of -50 mV. Application NA (40 μM) induced a small reversible outward current with an increase in frequency and amplitude of EPSCs. EPSCs were subsequently blocked with application of NBQX. Below sections are expanded at a faster time base, to illustrate the induction of EPSCs more clearly.

Figure 6.16 **NA induces IPSPs/IPSCs**

A: Trace showing a continuous recording of an Arc neurone in Voltage clamp mode at a holding potential of -50 mV. Application NA (40 μM) induced an increase in frequency and amplitude of IPSCs. IPSCs were subsequently blocked with application of Bicuculline (10 μM). This neurone was termed a cluster 5 neurone due to its expression of time- and voltage-dependent inward rectification (I_h) and a T-type like calcium-like conductance

B: A trace from a continuous current clamp recording of an Arc neurone exposed to 40 μM NA that induces a significant decrease/ block in spontaneous IPSPS. Below sections of the current clamp recording are shown on a faster time base, to illustrate the decrease in IPSPs more clearly.

Chapter 7

The effects of histamine on rat hypothalamic arcuate nucleus neurones *in vitro*

7.1 Introduction

Histamine (β-imidazolylethylamine) is an endogenous biogenic amine that is synthesised in the brain from L-histidine by the enzyme L-histidine decarboxylase (HDC). The central histaminergic system has been reported to regulate numerous physiological functions, including energy homeostasis (Ookuma *et al.*, 1993), the sleep-wake cycle (Haas & Panula, 2003) and memory (Brown *et al.*, 2001). Histamine is widely distributed throughout the CNS in both neurones and mast cells (Garbarg *et al.*, 1976). In 1984, the origins and projections of the brain neuronal histaminergic system were identified (Panula *et al.*, 1984; Watanabe *et al.*, 1984). These studies revealed histamine neurones to be restricted to the tubermammillary nucleus (TM) of the posterior hypothalamus, from which efferent fibres project and terminate to almost all parts of the brain, including the hypothalamic Arc (Haas *et al.*, 1989).

Histamine exerts its effects through four G-protein-coupled receptors designated histamine receptor H_1, H_2, H_3, and H_4 (Parsons & Ganellin, 2006). Three of the four identified histamine receptors (H_1-H_3) are expressed in the CNS, whereas the fourth (H_4) receptor is detected predominately within the periphery, for example in bone marrow and leukocytes (Liu *et al.*, 2001; Oda & Matsumoto, 2001; Shin *et al.*, 2002).

The H_1 receptor is associated with the $G_{q/11}$ GTP hydrolysing protein which when activated stimulates activity of phospholipase C, and ultimately the release of calcium from internal calcium stores. Electrophysiological studies have shown that stimulation of the H_1 receptor results in depolarisation and an increase in firing (McCormick & Williamson, 1991; Reiner & Kamondi, 1994; Whyment *et al.*, 2006; Haas, 1992) through a mechanism involving inhibition of a leak potassium conductance. H_1-knockout mice have been shown to develop diet-induced and aging-related obesity (Masaki *et al.*, 2001; Masaki *et al.*, 2004). Infusion of H_1 antagonists significantly increases feeding (Sakata *et al.*, 1988) thus leading to the

hypothesis that hypothalamic neuronal histamine is important in the control of energy homeostasis and may tonically suppress food intake through the histamine H_1 receptor.

H_2 receptors are coupled to the G-protein G_S and adenylyl cyclase and generally have excitatory actions on neuronal membranes and have similar physiological functions within the brain as H_1 (Yanai & Tashiro, 2007). H_3 receptors are thought to be auto-receptors that regulate the release and synthesis of histamine. They act in an inhibitory manner at the presynaptic terminal and are coupled to $G_{i/o}$ and ultimately high voltage-activated Ca^{2+} channels (Haas & Panula, 2003). In relation to feeding, the application of the H_3 antagonist thioperamide suppresses feeding (Cohn *et al.*, 1973; Machidori *et al.*, 1992; Lecklin *et al.*, 1998). The signal transduction pathways of the recently cloned H_4 receptor (Nakamura *et al.*, 2000; Nguyen *et al.*, 2001) are as yet unclear, although, like the H_3 receptor, the H_4 receptor seems to couple to $G_{i/o}$ (Hough, 2001).

It has been previously reported that neuronal histamine has a physiological role in the regulation of food intake, specifically acting to suppress feeding through H_1 receptors in the VMH and the PVN, two hypothalamic nuclei that are known to be involved in the control of feeding (Sakata *et al.*, 1990). The Arc, also within the hypothalamus, is an essential component of the central neural aspects dedicated to controlling energy homeostasis, and consists of a heterogeneous population of neurones that synthesise numerous neurotransmitters and neuropeptides (Chronwall, 1985; Schwartz *et al.*, 2000).

In the present study, the aim was to undertake a preliminary investigation of the cellular mechanisms by which histamine regulates the neuronal excitability of key hypothalamic neurones in the Arc using whole-cell patch clamp recording techniques in isolated slice preparations.

7.2 Results

In the present study the effects of bath application of histamine (10 μM; 1-2 minutes) on the electrophysiological properties and activity of single hypothalamic Arc neurones in a slice preparation were studied using whole-cell patch clamp recording techniques *in vitro*. A total of 46 neurones were included in this study. The mean resting membrane potential of these neurones was -50.7 ± 1.3 mV and the corresponding input resistance of these neurones was 1320 ± 101 MΩ.

7.2.1 Histamine depolarises hypothalamic Arc neurones

30/46 (65%) neurones exposed to a brief application of histamine (10 μM, 1-2 minutes) responded with an excitation, observed as membrane potential depolarisation and/or an increase in suprathreshold electrical activity. Bath application of histamine to the slice by superfusion for 1-2 minutes induced an increase in mean firing rate from a control level of 0.09 ± 0.05 Hz to 1.13 ± 0.22 Hz (190%; $P<0.001$; n=18). These effects of histamine were reversible within around 10 minutes following the wash of histamine from the bath (Figure 7.1A).

Histamine induced a significant membrane depolarisation from a mean resting membrane potential of -51.8 ± 1.6 mV (n=30) to -43.5 ± 1.5 mV, resulting in a mean peak membrane depolarisation amplitude of 8.3 ± 0.9 mV (n=30; paired students T-test; $P<0.001$; Figure 7.1A).

The histamine-induced depolarisation was also seen in a subpopulation of NPY/AgRP neurones (n=2; van den Top *et al.*, 2004). However, these data are as yet preliminary and further work will need to be carried out (results not shown).

Bath application of histamine induced a non-significant (*P*=0.24) increase in neuronal input resistance (n=30). Application of the monoamine increased neuronal input resistance from a mean of 1331 ± 116 MΩ at rest to 1473 ± 134 MΩ in the presence of histamine, amounting to a 10.6 % increase in neuronal input resistance in the presence of histamine.

Application of histamine (n= 5) in the presence of 1 μm TTX (Figure 7.1B) induced a membrane depolarisation, thus indicating a direct post-synaptic effect on Arc neurones. Histamine induced a depolarisation in the presence of TTX, from a mean resting membrane potential of -54.8 ± 3.1 mV to -40.6 ± 3.6 mV amounting to a mean peak membrane depolarisation amplitude of 14.2 ± 2.0 mV (n=5). The histamine-induced membrane depolarisation in the presence of TTX was associated with a non-significant decrease in neuronal input resistance of -2.9 % (*P*=0.7; n= 5), from a mean resting input resistance of 1346 ± 177 MΩ to 1300 ± 155 MΩ in histamine.

7.2.2 Ionic mechanism underlying histamine-induced depolarisation

In order to determine the ionic mechanism underlying the histamine-induced membrane depolarisation and increase in firing rate, current-voltage (I/V) relationships were acquired in the absence and at the peak of the histamine-induced response in 11 neurones. I/V relationships were not clamped back to the resting membrane potential in the presence of the drug which would have given us a clearer idea of the mechanism(s) involved.

Plots of these I/V relationships suggested more than one mechanism/component contributing to the histamine-induced excitation (Figure 7.2). Histamine-induced depolarisation was associated with either an increase or no change in input resistance, as indicated above.

6/11 neurones displayed no change in neuronal input resistance in response to histamine. These neurones had a mean neuronal input resistance of 1183 ± 180 MΩ at rest and 1298 ± 114 MΩ in the presence of histamine, amounting to a 9.7 % increase, from a resting membrane potential of -46.5 ± 3.5 mV to -37.2 ± 1.9 MΩ in the presence of histamine. Plots of I/V relationships indicated a parallel shift (Figure 7.2B). The parallel shift suggests the histamine-induced excitation may in part be mediated through modulation of electrogenic ion pumps or an ion exchanger mechanism. However the slight increase in input resistance may indicate the involvement of other ionic mechanisms, for example activation and inhibition of two conductances leading to no net change in input resistance but a net membrane depolarisation.

5/11 neurones displayed a clear reversal potential amounting to -83.4 ± 4.9 mV (Figure 7.2D), close to the predicted reversal potential for potassium under our recording conditions. The reversal potential was taken from the point at which the plots of the two current-voltage relations intersected. These neurones showed an increase in input resistance of 31.8 % (915 ± 114 MΩ at rest to 1207 ± 122 MΩ in histamine) in the presence of histamine with a mean peak amplitude depolarisation of 10.2 ± 2.4 mV, from a resting membrane potential of -48.0 ± 2.3 mV to -37.8 ± 2.8 MΩ in the presence of histamine. This indicates that the histamine-induced excitation, at least in-part is mediated through the closure of one or more potassium conductances.

In voltage-clamp at a holding potential of -50 mV, application of histamine (10 μM, n=6) for 1-2 minutes, in the presence of TTX, induced an outward current, with a mean peak amplitude of 17.4 ± 3.5 pA (Figure 7.3A).

Voltage ramps from -110 to -30 at a rate of 10 mVs^{-1} were applied in control conditions and at the peak of the histamine-induced response, in TTX, to further investigate the ionic mechanism underlying the histamine-induced current. These responses to voltage-

clamp ramps revealed no obvious change in membrane conductance in the presence of histamine, thus presented as parallel shifts (n=5; figure 7.3B)

7.2.3 The effects of histamine receptor agonists on Arc neurones

All three histaminergic receptor subtypes (H_1, H_2 & H_3) have been shown to be present within the hypothalamus (Brown *et al.*, 2001; Schwartz *et al.*, 1991) with high densities of the H_1 receptors within the Arc. To investigate the nature of the receptor(s) mediating the observed histamine-induced effects, the effects of the H_1 agonist, histamine trifluoromethyl toluidide (HTMT;10 μM; 1-2 minutes), H_2 agonist, dimiprit (10 μM; 1-2 minutes) and the H_3 agonist, imetit (10 μM; 1-2 minutes) were investigated. A total of 6 Arc neurones were exposed to HTMT, of which only 2 responded with a relatively small increase in suprathreshold activity (Figure 7.4). Firing rate increased from 0.7 ± 0.3 Hz to 0.8 ± 0.3 Hz in the presence of HTMT. Application of HTMT induced a membrane depolarisation from a resting membrane potential of -48.2 ± 7.6 mV to -47.0 ± 6.4 mV in the presence of the agonist. Application of dimiprit (n=4) and imetit (n=3) had no significant effect on membrane potential or input resistance. This data suggests that the histamine induced excitation of Arc neurones is not mediated through the H_2 or H_3 receptor, but at least in part is mediated through the H_1 receptor.

7.2.4 Histamine depolarises Arc neurones via an action at H1 receptors

In order to further characterise the likely receptor(s) mediating the histamine- induced excitation, the effects of the H_1 antagonist, mepyramine maleate (300 nm) were tested on histamine-induced responses under current clamp conditions. Application of 10 μM histamine

alone caused a membrane depolarisation and an increase in action potential firing, a response that was partially blocked or completely abolished in the presence of 300 nM mepyramine maleate (n=6). Application of 10 µm histamine alone induced a membrane depolarisation from -51.6 ± 1.8 mV in control to 45.2 ± 1.8 mV in the presence of histamine, a mean peak amplitude depolarisation of 6.4 ± 0.8 mV (n=8). It also induced an increase in firing rate from 0.0 ± 0.0 Hz at control to 1.2 ± 0.3 Hz in the presence of histamine. In contrast, histamine application in the presence of the H1-receptor antagonist was greatly reduced by up to 82.5 %, the mean peak depolarisation amplitude response to histamine being reduced from 6.4 ± 0.8 mV in the absence to 1.1 ± 0.9 mV in the presence of the antagonist (n=8). The histamine-induced increase in firing rate was also reduced by 86 %. These results suggest H_1 receptors are likely to be responsible for mediating the histamine-induced excitation (Figure 7.5).

7.2.5 Histamine- induced indirect effects on hypothalamic Arc neurones

Preliminary observations suggest that histamine application induced an increase in spontaneous IPSPs (n=4). The mean frequency of IPSPs increased from 0.1 ± 0.0 Hz at rest to 1.3 ± 0.3 Hz in the presence of histamine (n=4). This equated to an increase in frequency of IPSPs in the presence of histamine by 358 % (P<0.01; Figure 7.6). Further work will need to be carried out in order to clarify the nature of these induced synaptics. The increase in IPSP frequency in the presence of histamine suggests that the monoamine regulates activity of Arc neurones at least in part via sites located pre-synaptic to Arc neurones.

7.3 Discussion

The Arc is innervated by histamine-containing projections originating from the tubermammillary (TM) nucleus of the posterior hypothalamic region (Panula *et al.*, 1984). This interaction provides Arc neurones with its major source of histamine although a second source available to the Arc may exist in the form of histamine secreted by mast cells originating within the median eminence (Pollard *et al.*, 1976; Panula *et al.*, 1984). This study found that bath application of histamine induced a membrane depolarisation that was associated with an increase or no change in neuronal input resistance in around 65 % of neurones. Histamine-induced excitatory effects were directly post-synaptic within the Arc as shown in this study by the persistence of the response in the presence of TTX and in other studies with the use of low extracellular calcium and high magnesium-containing bathing medium to reduce influence from indirect pre-synaptic sources (Jorgenson *et al.*, 1989). Post-synaptic actions of histamine have been reported in other areas of the brain and spinal cord such as the suprachiasmatic nucleus (Stehle, 1991) and the supraoptic nucleus (Li & Hatton, 1996). In addition to direct postsynaptic effects of histamine on Arc neurones, histamine also produced indirect effects manifest as the induction or modulation of spontaneous on-going GABAergic synaptic activity. The histamine-induced excitation was mimicked, in-part, by the highly selective H_1 receptor agonist, HTMT and blocked by the potent and selective H_1 antagonist, mepyramine maleate confirming the presence of functional, postsynaptic H_1 receptors in some Arc neurones that most likely mediated the direct postsynaptic effects observed here. This study reported very weak or no histamine receptor agonist responses. Due to time constraints, higher doses of the agonists were not used, but this may be a suggestion for future work for this project. Figure 7.4 shows the HTMT response which induces a non-significant increase in firing frequency and depolarisation. Further analysis is

required of these results which may require binning of spikes. It must also be noted that Figure 7.5 that represents the histamine response being blocked by a selective H1 antagonist may also require further work. The first application of histamine may induce desensitisation and therefore the antagonist effect may be spurious. A longer wash-off and a repeated application of histamine after the antagonist is required to clarify the involvement of the H_1 receptor in the histamine induced depolarisation.

Preliminary data suggests that histamine may excite a subpopulation of Arc NPY/AgRP neurones, previously characterised by this lab and readily identified based upon their unique expression of subthreshold active conductances (van den Top *et al.*, 2004). However little can be concluded from these results due the lack of (n) numbers. Previous studies have shown that histamine injected into the PVN and VMH reduced food intake and injections of H1 antagonists into these sites has been shown to increase food intake (Ookuma *et al.*, 1989). The role of histamine at the level of the Arc in relation to feeding can not yet be concluded from the results of this study.

H_1 receptors mediated the histamine-induced excitation within the Arc, an effect similar to that previously reported for histamine in the Arc, other hypothalamic areas and other parts of the CNS (Haas & Wolf, 1977; Geller, 1981; Armstrong & Sladek, 1985; Jorgenson *et al.*, 1989; Bell *et al.*, 2000; Whyment *et al.*, 2006). H_2 and H_3 receptor agonists were without effect on Arc neurones suggesting a lack of functional roles for these receptors at the level of the Arc. Studies previously carried out on Arc and its responsiveness to histamine have also observed and reported a role for H_2 receptors in mediating the histamine-induced excitation (Jorgenson *et al.*, 1989). H_2 receptors have been shown to mediate excitatory actions of histamine on hippocampal pyramidal cells, dentate granule cells and brainstem medullary neurones (Jones *et al.*, 1985; Haas & Greene, 1986; Greene *et al.*, 1989; Haas & Panula, 2003; Yanai & Tashiro, 2007). H_2 receptors have also been shown to mediate histamine-

induced neuronal inhibition in the CNS (Haas & Bucher, 1975; Haas & Wolf, 1977). This study did not observe a histamine induced hyperpolarisation of the neuronal membrane or a decrease in suprathreshold activity, observations consistent with those findings reported by (Jorgenson *et al.*, 1989) who found that only 1/177 neurones within the Arc responded to histamine with an inhibition. This may reflect a lack of expression of functional H_2 receptors in the hypothalamus (Brown *et al.*, 2001). However, an indirect inhibition of Arc neurones was observed in a subpopulation of neurones where histamine induced the discharge or an increase in spontaneous IPSPs. This data suggests histamine activates inhibitory neurones located presynaptic to the recorded Arc neurones. Further work is required to identify the receptors involved in this response mediating both the discharge of IPSPs, presumably GABAergic, and the increased excitability of these neurones induced by histamine. Furthermore, whether these histamine receptors are located on the presynaptic terminals to modulate GABA release or elsewhere on the presynaptic neurones, such as the soma and/or dendrites, to increase neuronal excitability requires further clarification.

Histamine-induced membrane depolarisation and associated increase in neuronal input resistance, exhibited a reversal potential close to the reversal potential for potassium ions under our recording conditions, consistent with the effect of histamine being mediated by closure of one or more potassium-selective conductances. This data is similar to that reported previously for effects of histamine in other parts of the CNS (McCormick & Williamson, 1991; Reiner & Kamondi, 1994; Whyment *et al.*, 2006).

Histamine binds to the H_1 receptor leading to increased activity of phospholipase C (PLC) through the activation of the $G_{q/11}$ G protein which subsequently leads to the formation of two second messengers, diacylglycerol (DAG) and IP_3. IP_3 releases Ca^{2+} from internal stores subsequently leading to activation of a number of other processes, which include not only a block in leak potassium conductances (discussed above) but also includes the opening

of a cation channel and the activation of a Na^{+}- Ca^{2+} exchanger to induce a membrane depolarisation (Gorelova & Reiner, 1996; Bell *et al.*, 2000; Brown *et al.*, 2001). It is the latter that this study considers may also be involved in the histamine induced excitation in Arc neurones. The histamine-induced membrane depolarisation was also associated with no measurable change in neuronal input resistance, revealed from current-clamp and voltage-clamp ramp studies. These results suggest that the histamine-induced excitation could be in part mediated through modulation of electrogenic ion pumps or an ion exchanger mechanism. Similar findings have been reported in cholinergic neurones of the rat striatum and medial septum (Gorelova & Reiner, 1996; Bell *et al.*, 2000) whereby multiple mechanisms are involved in the histamine-induced excitation. To further clarify the involvement of an ion exchanger mechanism mediating the histamine induced excitation further work will need to be carried out with the use of specific blockers and ion substitution approaches.

In summary this study provides preliminary data observing the effects of histamine on Arc neurones. Histamine excites a population of Arc neurones mediated through the H1 receptor coupled to the closure of one or more potassium conductances or via the activation of a pump/exchanger within the membrane.

Further work will need to be carried out to determine the role of histamine in the control of energy homeostasis which was the initial focus of this study. Preliminary data suggests that histamine may have an orexigenic role within feeding, but further work will need to be carried out which could involve the use of electrophysiological recordings to identify a subpopulation of NPY/AgRP neurones. To extend this project further we should carry out double labelling in order to identify CART expressing neurones. CART is a well known anorexigenic peptide that could be an effective way of identifying the phenotype of histamine-responsive neurones. Single-cell RT-PCR could also be used to determine histamine responsive neurones within the Arc.

Figure 7.1 **Histamine directly excites hypothalamic Arc neurones**

A: A continuous current- clamp recording of an Arc neurone showing the effects of histamine (10 μM) bath applied for approximately 2 minutes. The line above the recording indicates the application time and duration of application of histamine. Application of histamine induced a membrane potential depolarisation and induced suprathreshold activity, effects that were reversible within approximately 10 minutes from the time of wash out of histamine.

B: A trace from a continuous current- clamp recording of an Arc neurone in the presence of 1 μM TTX showing the persistence of the histamine-induced response in the presence of the toxin, thus indicating a direct effect of histamine on these neurones. The regular evoked negative membrane potential responses are the result rectangular- wave negative current injections enabling the input resistance to be monitored (5-20 pA, 1.2 s, 1/5 Hz). The / / indicates a break within the trace of approximately 2 minutes where an I/V relationship was generated. The line above the recording marked histamine indicates the time-course of application of 10 μM histamine. Application of histamine induced a membrane depolarisation, associated with an increase in input resistance indicated by the increase in amplitude of the induced electronic potential (downward deflections). The effect being reversible within approximately 10 minutes following the wash of histamine from the bath.

Figure 7.2 **Ionic mechanism underlying the histamine-induced excitation**

A: IV relationships obtained from a neurone before and during the application of histamine (10 μM). The traces shown are superimposed samples of a continuous whole-cell current-clamp recording showing the membrane responses to a series of hyperpolarising and depolarising current injections of constant increment .

B: A graph plotting the current- voltage relationship obtained from the traces shown in (A), obtained by plotting the current injected into the cell (x-axis) against the resulting membrane potentials (y-axis). The symbols ▪ and o indicate the current- voltage relationships in the absence and presence of histamine, respectively. Note the parallel shift which maybe indicative of a pump within the membrane, or the activation of multiple conductances that off-set each other.

C: IV relationships obtained from another neurone before and during the application of histamine. The traces shown are superimposed samples of a continuous whole-cell current-clamp recording showing the membrane responses to a series of hyperpolarising and depolarising current injections of constant increment.

D: A plot of the current-voltage relationship of the neurone shown in C. The symbols ▪ and ○ indicate the current- voltage relationships in the absence and presence of histamine, respectively. Note the increase in slope of the IV relationship in the presence of histamine which indicates an increase in neuronal input resistance. The two lines intersect around -85 mV which indicates a reversal potential close to that of potassium under our recording conditions.

Figure 7.3 **Histamine-induces an inward current in Arc neurones**

A: Trace showing a continuous recording from an Arc neurone in Voltage clamp mode at a holding potential of -50 mV. Application histamine (10 μM) induced a reversible inward current.

B: Current responses obtained in voltage-clamp in the presence (green trace) and absence (black trace) of histamine. The wash out of histamine is shown by the orange trace. The currents were obtained from ramp protocols that drove the holding potential from -110 mV to -30 mV, at a rate of 10 mV per second.

Figure 7.4 **The H_1 agonist HTMT induced a depolarisation in hypothalamic Arc neurones**

A: A trace from a continuous current- clamp recording from an Arc neurone exposed to 10 μM HTMT. The line above the recording marked HTMT indicates the time course of application of 10 μM HTMT. The application of HTMT caused a slight membrane depolarisation and increase in firing rate; shown at a faster time base below (B). The increase in firing rate was reversible within approximately 4 minutes following the wash of HTMT from the bath.

Figure 7.5 **Histamine-induced excitation is blocked by a H1 antagonist mepyramine maleate**

A: Samples of a continuous current- clamp recording from an Arc neurone showing exposure to histamine (10 μM) induced a reversible membrane depolarisation and increase in action potential firing. The application of the H_1 antagonist, mepyramine maleate 300 nM blocked the histamine induced response. The regular negative membrane potential responses are the result of evoked rectangular- wave negative current injections enabling the input resistance to be monitored (5-20 pA, 1.2 s, 1/5 Hz).The lines above the recording indicates the time-course of application of histamine and mepyramine maleate.

Figure 7.6 **Histamine induces indirect effects on hypothalamic Arc neurones**

A: A sample of a continuous current clamp, showing the effects of bath application of histamine (10 μM; 2 minutes). Application of histamine induces an increase in spontaneous inhibitory postsynaptic potentials (IPSPs) in addition to an increase in firing rate.

B: Samples of the current clamp recording of the neurone shown in A at a faster time base, showing the induction of synaptic transmission, IPSPs, by histamine more clearly.

Chapter 8

General Discussion

Energy stores are regulated and maintained through a balance between food intake and energy expenditure and requires co-operation and integration between interconnected central and peripheral networks dedicated to maintaining energy status (Cone *et al.*, 2001). The hypothalamic Arcuate nucleus (Arc) is believed to be essential in the maintenance of energy balance. The Arc, being situated close to a compromised blood brain barrier at the median eminence, is susceptible to circulating factors relaying information regarding energy stores and status from the periphery (Ganong, 2000). Receptors for all the main humoral and central transmitters involved in the regulation of energy homeostasis are expressed in the Arc. The Arc is innervated by multiple afferent and neurotransmitter inputs from hypothalamic, brainstem and higher centres (Sawchenko & Swanson, 1981; Chronwall, 1985; Elias *et al.*, 1998; Hentges *et al.*, 2004; Horvath *et al.*, 2004). The Arc efferent outputs are equally as diverse and neuropeptidergic expression within the Arc reflects multiple chemical phenotypes (Chronwall, 1985; Baker & Herkenham, 1995; Melander *et al.*, 1986; Koylu *et al.*, 1997; Reyes *et al.*, 2001; Lu *et al.*, 2002), the best described of which being the orexigenic NPY/AgRP and anorexigenic POMC/CART expressing neurones. How communicating factors including hormones, nutrients and transmitters of central origin are integrated at the level of the Arc, transduced into electrical codes and electrical output generated to bring about appropriate counterregulatory responses and behavioural change, remains to a large extent unclear. The present study aimed to begin to address these issues by investigating intrinsic factors regulating electrical excitability of Arc neurones and how electrical excitability is subject to modification and modulation by extrinsic factors related to energy status, specifically glucose, and factors of central origin, noradrenaline and histamine, implicated in regulating energy homeostasis at the level of the Arc.

8.1 The electrophysiological and morphological characterisation of Arc neurones

Active and passive electrophysiological membrane properties of a neurone are fundamental to their functional processing, integrative and computational capability. Thus recognising these properties along with their morphological characteristics is fundamental to understanding the functional organisation and operation of Arc neurones and their associated circuits. Thus, this study attempted to characterise Arc neurones based upon their elecctrophysiological and morphological properties.

The main subthreshold active conductances expressed by Arc neurones were used as criteria to classify neurones electrophysiologically with 8 groups (clusters) being identified based on the differential expression of these conductances. The active conductances expressed within the Arc used as parameters to classify neurones included an anomalous inward rectification (I_{an}), hyperpolarisation-activated non-selective cation conductance (I_h), a transient outward rectification (I_a) and a T-type- like calcium conductance. Cluster 1 neurones were defined by expressing $I_{an;}$ cluster 2 neurones expressed I_a and I_{an}; cluster 3 expressed no obvious subthreshold active conductance; cluster 4 expressed I_h; cluster 5 expresses I_h and T-type-like calcium conductance; cluster 6 expressed only a T-type-like calcium conductance; cluster 7 expressed I_{an} and T-type conductance and finally cluster 8 neurones expressed $I_{an,}$ I_h and a T-type like conductance. The fact that 8 distinct electrophysiological subtypes, based upon differential expression of active conductances is at odds with previous electrophysiological studies in mice where 3 electrophysiological subtypes were proposed based on differential expression of an A-like current (Type A and C) and a T-type calcium current (Type B). Type A and C where distinguished from each other based on the differential time- and voltage-dependence of the A-like current expressed (Burdakov & Ashcroft, 2002). This classification was proposed to have functional significance based on the fact that orexin only affected Type C cells (Burdakov *et al.*, 2003). However, a more recent study in mice

suggested 5 subtypes of neurones exist in the Arc based on their differential expression of active conductances and at least 4 subtypes of neurone exist in the Arc based entirely on their sensitivity to glucose (Fioramonti *et al.*, 2004; Fioramonti *et al.*, 2007). Fioramonti observed the same 3 phenotypes as Burdakov & Ashcroft and identified two others that expressed I_h and I_h and T-type like conductance. The I_h conductance that was previously reported not to be expressed within the Arc (Burdakov & Ashcroft, 2002). One obvious explanation for the discrepancies between these studies and data described here may simply be species variation, rats being used in the present study as opposed to mice in the studies indicated above (Burdakov *et al.*, 2003; Fioramonti *et al.*, 2004). However, given the diversity of chemical and functional phenotype of neurones in the Arc and their diverse projections, it is difficult to reconcile that only 3 electrophysiological phenotypes can have any functional significance. Furthermore, recent studies on mice from our lab (Spanswick, van den Top and Cowley, unpublished observations) suggest POMC neurones alone constitute a morphologically and electrophysiologically diverse subgroup. Further work is required to fully understand the functional significance of the 8 electrophysiological clusters described here.

Morphologically, neurones manifest as 4 distinct groups, separated based upon the number of primary dendrites and their origin from the soma. Thus, group A neurones were monopolar; group B neurones were bipolar; group C neurones displayed two primary dendrites projecting from the same side of the soma; group D neurones were multipolar neurones.

After combining both the electrophysiological and morphological properties of Arc neurones this study could not correlate the two. There was considerable heterogeneity of morphology between neuronal clusters and within clusters. Ultimately, further work will now need to be carried out to identify the chemical phenotype of these neurones which is as yet unknown, with the exception of neurones classified as cluster 2 neurones which are

identified as a subpopulation of NPY/AgRP neurones (van den Top *et al*., 2004). This study provides a framework on which to build a functional classification of Arc neurones. Future work investigating both the afferent and efferent projections of Arc neurones will give an insight in to their physiological function. Examining the receptor expression of Arc neurones and their responsiveness to a variety of extrinsic factors (such as noradrenaline; chapters 5 & 6) could potentially be a tool in order to separate functionally divergent neuronal groups. In relation to this latter point, studies of the differential effects of NA on Arc neurones revealed cluster-specific responses to this catecholamine. Thus, a response to NA characterised by membrane hyperpolarisation and a concomitant increase in the discharge of spontaneous EPSP's was almost exclusively observed in cluster 8 neurones. Furthermore, NA induced inhibition of spontaneous IPSP's was only observed in a subset of cluster 5 neurones and cluster 2 neurones, previously identified as NPY/AgRP neurones (van den Top *et al*., 2004), responded in all instances with excitation upon exposure to NA. Taken together, these data suggest that the electrophysiological classification has functional significance. However, at present it remains a framework in its infancy and requires further investigation before its functional significance in relation to the operation of Arc neural circuits and their role in controlling energy balance can be recognised.

8.2 Effect of glucose on electrophysiological properties of Arc neurones

Glucose provides the brain with its primary fuel source and is essential for the brains correct functioning and survival (Ritter *et al*., 2006). Thus circulating and CSF glucose levels are tightly controlled, failure to do so leading to serious pathological complications such as diabetes. To achieve this, a complex homeostatic feedback system comprised of aspects of the periphery and CNS, function to maintain glucose levels within narrow limits. Of the central

effector pathways involved in maintaining glucose homeostasis, aspects of the hypothalamus are crucial. Historically the ventromedial nucleus (VMN) and lateral hypothalamus have been revealed as key glucose-sensing areas of the hypothalamus (Anand *et al.*, 1964; Oomura *et al.*, 1974), but more recently aspects of the Arc have been implicated in glucose sensing and glucose homeostasis. The glucose-sensing neurones can be separated into two groups according to their responsiveness to changes in extracellular glucose (for review see Levin *et al.*, 2004). GE neurones are those that increase their firing rate as brain glucose levels rise. Conversely, GI neurones decrease their firing rate as glucose levels rise (Oomura *et al.*, 1964, for review see Burdakov & Gonzalez, 2008). The physiological changes in glucose to which the brain is exposed are as yet unclear. With a plasma glucose range of 5-8 mM, brain glucose levels are detected to be between 1-2.5 mM (Silver & Erecinska, 1994) with baseline hypothalamic glucose levels being shown to achieve concentrations of around 1.4 mM (de Vries *et al.*, 2003; Mayer *et al.*, 2006).

Previous studies, attempting to characterise the responsiveness of hypothalamic neurones to glucose and other stimuli, have used non-physiological ranges of glucose (0 - 20 mM; (Anand *et al.*, 1964; Oomura *et al.*, 1964; Ashford *et al.*, 1990; Spanswick *et al.*, 1997) and glucose concentrations used generally for *in vitro* brain slice studies are of the order of 10 mM. Brain tissues, including the Arc, are never exposed to such extremes of glucose concentrations. Thus, this study attempted to address this issue by comparing fundamental electrophysiological properties of Arc neurones in physiological levels of glucose (2 mM) with Arc neurones recorded in classic "*in vitro*" aCSF levels of glucose (10 mM), the latter more likely to reflect a diabetic, hyperglycaemic state.

Key observations within this study included finding significant differences in both the active and passive membrane properties of neurones recorded in euglycaemic (2 mM glucose-containing aCSF) and hyperglycaemic (10 mM glucose-containing aCSF) conditions.

The neuronal input resistance was significantly higher in Arc neurones recorded in 10 mM compared to 2 mM extracellular glucose, suggesting that neurones recorded in 2 mM glucose may have one or more conductances activated, or relatively more activated than those recorded in 10 mM glucose. The observed increase in input resistance at higher glucose concentrations may be attributable to the closure of K_{ATP} channels that have been shown to be important in glucose-sensing networks in the hypothalamus, including the Arc (Ashford *et al.*, 1990; Rowe *et al.*, 1996; Spanswick *et al.*, 1997; Lee *et al.*, 1999; Spanswick *et al.*, 2000; Miki *et al.*, 2001).

Spontaneous firing rate was higher in Arc neurones exposed to 2 mM glucose compared to 10 mM glucose-containing aCSF, and the membrane time-constant (tau), used as measure of the size of the neurone, dramatically changed in subpopulations of neurones. These changes may reflect changes in expression of intrinsic conductances in different glucose concentrations. This notion is supported by the fact that significant differences in the expression of subthreshold active conductances were observed; particularly the apparent magnitude of I_h was enhanced in neurones recorded in 2 mM glucose-containing aCSF. I_h modulates the output of neurones such as generating oscillations and burst firing patterns of activity, the latter being suggested to be important for neuropeptide release (Dutton & Dyball, 1979; Bicknell & Leng, 1981; Pape, 1996; van Welie *et al.*, 2006). Furthermore, the duration of the A-like transient outward conductance was reduced in 2 mM glucose-containing aCSF compared to 10 mM. As these conductances are believed to influence spike repolarisation and modulate the frequency of tonically firing neurones (Connor & Stevens, 1971; Kenyon & Gibbons, 1979; Segal *et al.*, 1984) the change in size of the A-like transient current may potentially lead to differences in firing of these neurones. Taken together, these observations suggest neurones with specific expression patterns of subthreshold active conductances behave differently in different glucose concentrations.

Overall the results from this study strongly suggest that there is a need for us to re-evaluate past studies that have conducted experiments in non-physiological levels of glucose. The significant difference in both passive and active subthreshold electrophysiological properties seen in physiological and non-physiological glucose levels suggest that whole networks may behave differently in these two different levels of glucose. Further work investigating changes in expression of receptors, ion channels, and responsiveness to extrinsic factors in hyperglycaemic and euglycaemic glucose concentrations should be undertaken in glucose-sensing areas such as those of the hypothalamus. For example, when levels of CNS glucose are low, NA levels increase within the hypothalamus which subsequently increases circulating blood glucose levels (McCaleb *et al.*, 1979; Smythe *et al.*, 1984) via direct action of the ANS enhancing glucose production through activation of glycogenolysis and gluconeogenesis. Similar investigations should also be undertaken in other areas of the CNS, such studies potentially shedding light on the need to re-evaluate functional studies in *in vitro* preparations which almost without exception are undertaken in non-physiological glucose concentrations.

8.3 The differential effects of NA on hypothalamic Arc neurones

The noradrenergic system originating from brainstem nuclei projects throughout the neuroaxis and plays a major role in many physiological processes (Leibowitz *et al.*, 1983; Svensson, 1984; Berridge, 2008). The noradrenergic system has been heavily implicated in the control of energy homeostasis (Wellman *et al.*, 1993) and several noradrenergic agents have been explored for the treatment of obesity (Jackson *et al.*, 1997).

The effects of NA at the cellular level in the Arc of the hypothalamus remains poorly understood. In the present study NA was shown to induce direct postsynaptic membrane

depolarisation, hyperpolarisation or had no effect on the cellular membrane of Arc neurones. NA-induced excitation was indicated to be mediated via closure of one or more resting potassium conductances in a subpopulation of Arc neurones and via activation of a non-selective cation conductance in a further subset of neurones. Neurones that responded with no change in neuronal input resistance upon application of NA were suggestive of the activation of one or more membrane ion pumps or differential effects on a combination of ionic conductances. NA-induced depolarisation was mediated primarily through the α_{1A}- AR, with a smaller contribution from α_{1B}- ARs. Further work will need to be carried out determine if a particular α-AR subtype is associated with a specific ionic mechanism and different downstream signalling pathways involved.

NA-induced hyperpolarisation and/or decrease in firing rate was mediated via α_2- ARs and associated with a concurrent decrease in neuronal input resistance likely to be mediated by the activation of one or more potassium-selective conductances. Current-voltage relationships in the presence of NA revealed an enhancement or appearance of an inward rectifier therefore at least in part, the NA-induced inhibition is mediated through activation of an inward rectifying K^+ conductance (IRK). Further studies will need to be carried out to investigate whether GIRK channels are involved in mediating the NA-induced hyperpolarisation, utilising specific blockers for this channel (Kanjhan *et al.*, 2005). A subset of Arc neurones expressed more than one subtype of AR that mediated opposing actions on the cellular membrane. This arrangement of receptors may have a functional significance whereby pathway- and function-specific noradrenergic inputs are differentially activated at different times and / or under different physiological circumstances. This is reflected in the ability of α_2- AR expression to change in numbers with the circadian cycle (Jhanwar-Uniyal *et al.*, 1986; Stanley *et al.*, 1989). Thus, depending on the receptor subtype activated, NA has

the capacity to either stimulate or depress neuronal activity on a given neurone (Nakamura *et al.*, 1984; Yamanaka *et al.*, 2006).

The functional significance of these differential effects of NA on Arc neurones was investigated further by correlating NA responsiveness with chemical phenotype. A subpopulation of orexigenic NPY/AgRP neurones, identified by their expression of a unique combination of active conductances (van den Top *et al.*, 2004) were excited by NA whereas anorexigenic POMC/CART expressing neurones were differentially regulated by NA being both excited and inhibited. The differential effects of NA on POMC/CART neurones suggests NA is involved in multiple functions, as POMC/CART neurones do not constitute a functionally homogenous group. However, together with results that NA excites a subpopulation of NPY/AgRP neurones and an inhibition of a population of POMC/CART neurones suggest a primarily an orexigenic role for NA at the level of the Arc. Further work is now required in order to clarify NA's net effect and role in the control of energy balance at the level of the Arc. Additional immunohistochemistry, *insitu* hybridisation and single-cell RT-PCR could be potentially utilised in order to identify NA's effects on other neuronal cell types within the Arc. What would of also be of interest is it study the differential effects of NA under differing glucose concentrations, which as been shown to be important in the expression of both the passive and active conductances of Arc neurones. Figure 8.1 shows a schematic illustration of the functional organisation of adrenoceptors at the level of the Arc.

Figure 8.1: **Hypothetical functional organisation of adrenoceptors at the level of the Arc based on data generated in this project.**

A schematic illustrating the proposed functional organisation of adrenoceptors on Arc neurones. NA excites NPY/AgRP neurones via multiple mechanisms: closing of one or more potassium conductances, through a pump-dependent mechanism within the membrane or the activation of a non-selective cation conductance, mediated through α_{1-} ARs. NA also inhibits a subpopulation of POMC/CART through the opening of one or more potassium conductances mediated through α_{2-} ARs. Multiple subtypes of noradrenergic receptors can also be present on the same neurone, this being true for a subpopulation of POMC neurones where NA can either induce an excitation or inhibition.

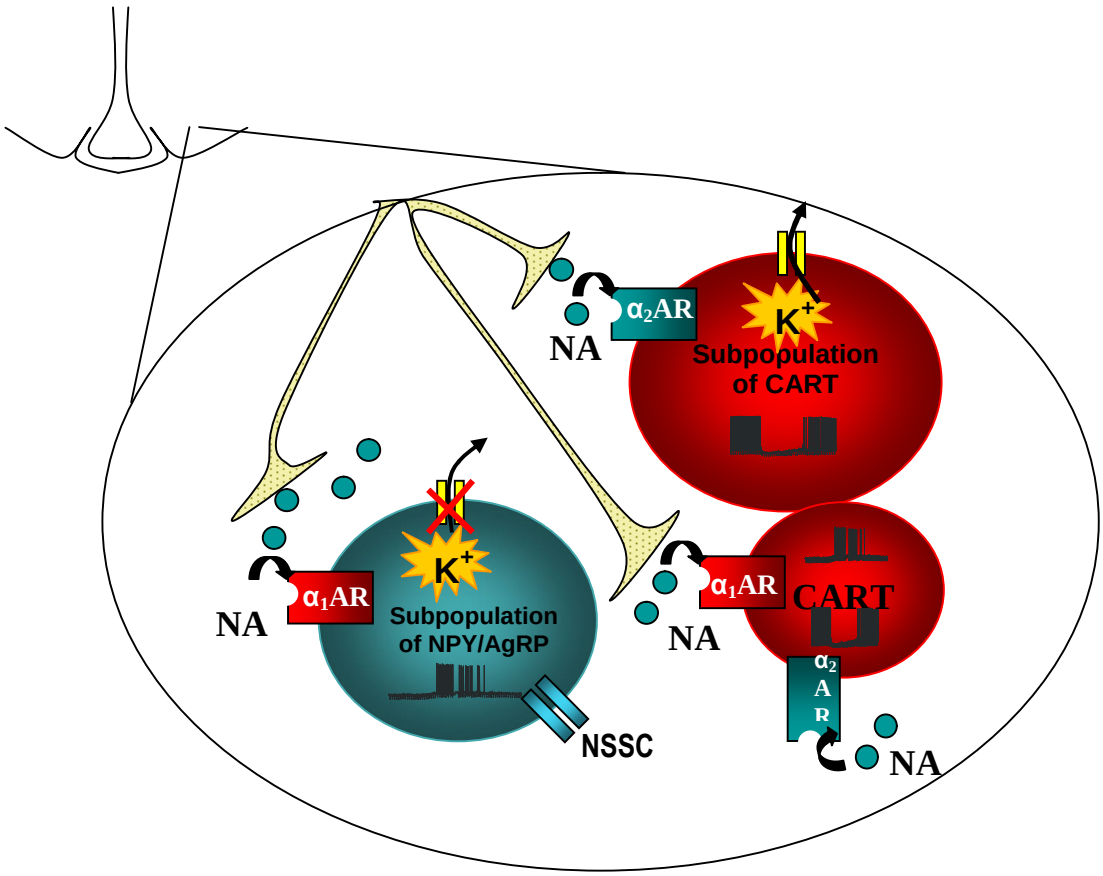
α2AR
NA
K+
Subpopulation
of CART
α1AR
NA
K+
Subpopulation
of NPY/AgRP
NSSC
α1AR
NA
CART
α2
A
R
NA

8.4 The effects of histamine on hypothalamic Arc neurones

Histamine has been previously reported to have a physiological role in the regulation of food intake, whereby hypothalamic neuronal histamine may tonically suppress food intake through the histamine H_1 receptor (Sakata *et al.*, 1988; Masaki *et al.*, 2001; Masaki *et al.*, 2004). How histamine regulates the neuronal excitability of Arc neurones at the cellular level however remains unclear. Here histamine was observed to induce a depolarisation and increase in firing in a subpopulation of neurones which was associated with an increase or no change in neuronal input resistance, the latter suggesting a mechanism mediated through closure of one or more selective potassium conductances and/or the involvement of an electrogenic pump. The pharmacological profile of the receptor mediating these effects was consistent with a role for H_1 receptors. However, due to time constraints this study reports only preliminary findings. Further works will need to be carried out using higher concentrations of both agonists and antagonists. Preliminary data does suggest that histamine may have an orexigenic role at the level of the Arc, but further work will need to be carried out to clarify the chemical phenotype(s) of neurones mediating these effects of histamine.

In summary therefore, the present study provides first evidence that hypothalamic Arc neurones are heterogeneous in both their electrophysiological features and morphological phenotype. The study provides a descriptive electrophysiological and morphological review of Arc neurones and how extrinsic factors such as glucose, NA and histamine differentially regulate Arc neurones and have the capacity to alter fundamental intrinsic electrophysiological properties. This suggests that there is considerable plasticity within the Arc and that electrophysiological clusters are not defined groups of neurones but may alter their intrinsic properties in relation to exposure of different extrinsic circumstances.

Chapter 9

References

Adachi A. (1981). Electrophysiological study of hepatic vagal projection to the medulla. *Neuroscience letters* **24,** 19-23.

Adachi A, Shimizu N, Oomura Y & Kobashi M. (1984). Convergence of hepatoportal glucose-sensitive afferent signals to glucose-sensitive units within the nucleus of the solitary tract. *Neuroscience letters* **46,** 215-218.

Adan RA & Kas MJ. (2003). Inverse agonism gains weight. *Trends in pharmacological sciences* **24,** 315-321.

Adrian TE, Allen JM, Bloom SR, Ghatei MA, Rossor MN, Roberts GW, Crow TJ, Tatemoto K & Polak JM. (1983). Neuropeptide Y distribution in human brain. *Nature* **306,** 584-586.

Aghajanian GK & Wang YY. (1986). Pertussis toxin blocks the outward currents evoked by opiate and alpha 2-agonists in locus coeruleus neurons. *Brain Res* **371,** 390-394.

Akabayashi A, Zaia CT, Silva I, Chae HJ & Leibowitz SF. (1993). Neuropeptide Y in the arcuate nucleus is modulated by alterations in glucose utilization. *Brain Res* **621,** 343-348.

Akasu T, Gallagher JP, Nakamura T, Shinnick-Gallagher P & Yoshimura M. (1985). Noradrenaline hyperpolarization and depolarization in cat vesical parasympathetic neurones. *J Physiol* **361,** 165-184.

Akasu T, Shoji S & Hasuo H. (1993). Inward rectifier and low-threshold calcium currents contribute to the spontaneous firing mechanism in neurons of the rat suprachiasmatic nucleus. *Pflugers Arch* **425,** 109-116.

Allen YS, Bloom SR & Polak JM. (1986). The neuropeptide Y-immunoreactive neuronal system: discovery, anatomy and involvement in neurodegenerative disease. *Hum Neurobiol* **5,** 227-234.

Altman JD, Trendelenburg AU, MacMillan L, Bernstein D, Limbird L, Starke K, Kobilka BK & Hein L. (1999). Abnormal regulation of the sympathetic nervous system in alpha2A-adrenergic receptor knockout mice. *Mol Pharmacol* **56,** 154-161.

Alquier T & Kahn BB. (2004). Peripheral signals set the tone for central regulation of metabolism. *Endocrinology* **145,** 4022-4024.

An JH, Su Y, Radman T & Bikson M. (2008). Effects of glucose and glutamine concentration in the formulation of the artificial cerebrospinal fluid (ACSF). *Brain Res* **1218,** 77-86.

Anand BK & Brobeck JR. (1951). Localization of a "feeding center" in the hypothalamus of the rat. *Proc Soc Exp Biol Med* **77,** 323-324.

Anand BK, Chhina GS, Sharma KN, Dua S & Singh B. (1964). Activity of Single Neurons in the Hypothalamic Feeding Centers: Effect of Glucose. *Am J Physiol* **207,** 1146-1154.

Arima J, Kubo C, Ishibashi H & Akaike N. (1998). alpha2-Adrenoceptor-mediated potassium currents in acutely dissociated rat locus coeruleus neurones. *J Physiol* **508 (Pt 1),** 57-66.

Armstrong WE. (1995). Morphological and electrophysiological classification of hypothalamic supraoptic neurons. *Prog Neurobiol* **47,** 291-339.

Armstrong WE & Sladek CD. (1985). Evidence for excitatory actions of histamine on supraoptic neurons in vitro: mediation by an H1-type receptor. *Neuroscience* **16,** 307-322.

Arora S & Anubhuti. (2006). Role of neuropeptides in appetite regulation and obesity--a review. *Neuropeptides* **40,** 375-401.

Arrang JM, Garbarg M & Schwartz JC. (1983). Auto-inhibition of brain histamine release mediated by a novel class (H3) of histamine receptor. *Nature* **302,** 832-837.

Ashcroft FM. (2005). ATP-sensitive potassium channelopathies: focus on insulin secretion. *J Clin Invest* **115,** 2047-2058.

Ashcroft FM & Gribble FM. (1999). ATP-sensitive K+ channels and insulin secretion: their role in health and disease. *Diabetologia* **42,** 903-919.

Ashford ML, Boden PR & Treherne JM. (1990). Glucose-induced excitation of hypothalamic neurones is mediated by ATP-sensitive K+ channels. *Pflugers Arch* **415,** 479-483.

Bady I, Marty N, Dallaporta M, Emery M, Gyger J, Tarussio D, Foretz M & Thorens B. (2006). Evidence from glut2-null mice that glucose is a critical physiological regulator of feeding. *Diabetes* **55,** 988-995.

Bagdade JD, Porte D, Jr. & Bierman EL. (1967). Diabetic lipemia. A form of acquired fat-induced lipemia. *N Engl J Med* **276,** 427-433.

Bagnol D, Lu XY, Kaelin CB, Day HE, Ollmann M, Gantz I, Akil H, Barsh GS & Watson SJ. (1999). Anatomy of an endogenous antagonist: relationship between Agouti-related protein and proopiomelanocortin in brain. *J Neurosci* **19,** RC26.

Baker RA & Herkenham M. (1995). Arcuate nucleus neurons that project to the hypothalamic paraventricular nucleus: neuropeptidergic identity and consequences of adrenalectomy on mRNA levels in the rat. *The Journal of comparative neurology* **358,** 518-530.

Banks WA, Kastin AJ, Huang W, Jaspan JB & Maness LM. (1996). Leptin enters the brain by a saturable system independent of insulin. *Peptides* **17,** 305-311.

Baskin DG, Wilcox BJ, Figlewicz DP & Dorsa DM. (1988). Insulin and insulin-like growth factors in the CNS. *Trends Neurosci* **11,** 107-111.

Batterham RL, Cowley MA, Small CJ, Herzog H, Cohen MA, Dakin CL, Wren AM, Brynes AE, Low MJ, Ghatei MA, Cone RD & Bloom SR. (2002). Gut hormone PYY(3-36) physiologically inhibits food intake. *Nature* **418,** 650-654.

Bayer L, Eggermann E, Serafin M, Grivel J, Machard D, Muhlethaler M & Jones BE. (2005). Opposite effects of noradrenaline and acetylcholine upon hypocretin/orexin versus melanin concentrating hormone neurons in rat hypothalamic slices. *Neuroscience* **130,** 807-811.

Beales PL & Kopelman PG. (1996). Obesity genes. *Clin Endocrinol (Oxf)* **45,** 373-378.

Beck B, Richy S, Dimitrov T & Stricker-Krongrad A. (2001). Opposite regulation of hypothalamic orexin and neuropeptide Y receptors and peptide expressions in obese Zucker rats. *Biochem Biophys Res Commun* **286,** 518-523.

Beck B, Stricker-Krongrad A, Burlet A, Cumin F & Burlet C. (2001). Plasma leptin and hypothalamic neuropeptide Y and galanin levels in Long-Evans rats with marked dietary preferences. *Nutr Neurosci* **4,** 39-50.

Bell ME, Bhatnagar S, Akana SF, Choi S & Dallman MF. (2000). Disruption of arcuate/paraventricular nucleus connections changes body energy balance and response to acute stress. *J Neurosci* **20,** 6707-6713.

Bell MI, Richardson PJ & Lee K. (2000). Histamine depolarizes cholinergic interneurones in the rat striatum via a H(1)-receptor mediated action. *Br J Pharmacol* **131,** 1135-1142.

Benetos A, Gavras I & Gavras H. (1986b). Norepinephrine applied in the paraventricular hypothalamic nucleus stimulates vasopressin release. *Brain Res* **381,** 322-326.

Bennett PA, Thomas GB, Howard AD, Feighner SD, van der Ploeg LH, Smith RG & Robinson IC. (1997). Hypothalamic growth hormone secretagogue-receptor (GHS-R) expression is regulated by growth hormone in the rat. *Endocrinology* **138,** 4552-4557.

Benoit SC, Air EL, Coolen LM, Strauss R, Jackman A, Clegg DJ, Seeley RJ & Woods SC. (2002). The catabolic action of insulin in the brain is mediated by melanocortins. *J Neurosci* **22,** 9048-9052.

Berridge CW. (2008). Noradrenergic modulation of arousal. *Brain Res Rev* **58,** 1-17.

Bicknell RJ & Leng G. (1981). Relative efficiency of neural firing patterns for vasopressin release in vitro. *Neuroendocrinology* **33,** 295-299.

Biessels GJ, van der Heide LP, Kamal A, Bleys RL & Gispen WH. (2002). Ageing and diabetes: implications for brain function. *European journal of pharmacology* **441,** 1-14.

Billington CJ, Briggs JE, Harker S, Grace M & Levine AS. (1994). Neuropeptide Y in hypothalamic paraventricular nucleus: a center coordinating energy metabolism. *Am J Physiol* **266,** R1765-1770.

Bloch B, Bugnon C, Fellmann D & Lenys D. (1978). [Antigenic determinants of beta-LPH, beta-MSH, alpha-endorphin, ACTH and alpha-MSH revealed by anti-beta-endorphin in neurons of the human infundibular nucleus]. *C R Acad Sci Hebd Seances Acad Sci D* **287,** 1019-1022.

Bloom FE, Rossier J, Battenberg EL, Bayon A, French E, Henriksen SJ, Siggins GR, Segal D, Browne R, Ling N & Guillemin R. (1978). beta-endorphin: cellular localization, electrophysiological and behavioral effects. *Adv Biochem Psychopharmacol* **18,** 89-109.

Bodoky M & Rethelyi M. (1977). Dendritis arborization and axon trajectory of neurons in the hypothalamic arcuate nucleus of the rat. *Exp Brain Res* **28,** 543-555.

Bouret SG, Draper SJ & Simerly RB. (2004). Formation of projection pathways from the arcuate nucleus of the hypothalamus to hypothalamic regions implicated in the neural control of feeding behavior in mice. *J Neurosci* **24,** 2797-2805.

Bourque CW. (1988). Transient calcium-dependent potassium current in magnocellular neurosecretory cells of the rat supraoptic nucleus. *J Physiol* **397,** 331-347.

Bouskila Y & Dudek FE. (1995). A rapidly activating type of outward rectifier K+ current and A-current in rat suprachiasmatic nucleus neurones. *J Physiol* **488 (Pt 2),** 339-350.

Broadwell RD, Balin BJ, Salcman M & Kaplan RS. (1983). Brain-blood barrier? Yes and no. *Proceedings of the National Academy of Sciences of the United States of America* **80,** 7352-7356.

Broberger C. (1999). Hypothalamic cocaine- and amphetamine-regulated transcript (CART) neurons: histochemical relationship to thyrotropin-releasing hormone, melanin-concentrating hormone, orexin/hypocretin and neuropeptide Y. *Brain Res* **848,** 101-113.

Broberger C, Johansen J, Johansson C, Schalling M & Hokfelt T. (1998). The neuropeptide Y/agouti gene-related protein (AGRP) brain circuitry in normal, anorectic, and monosodium glutamate-treated mice. *Proceedings of the National Academy of Sciences of the United States of America* **95,** 15043-15048.

Broberger C, Landry M, Wong H, Walsh JN & Hokfelt T. (1997). Subtypes Y1 and Y2 of the neuropeptide Y receptor are respectively expressed in pro-opiomelanocortin- and neuropeptide-Y-containing neurons of the rat hypothalamic arcuate nucleus. *Neuroendocrinology* **66,** 393-408.

Brown RE & Reymann KG. (1996). Histamine H3 receptor-mediated depression of synaptic transmission in the dentate gyrus of the rat in vitro. *J Physiol* **496 (Pt 1),** 175-184.

Brown RE, Stevens DR & Haas HL. (2001). The physiology of brain histamine. *Prog Neurobiol* **63,** 637-672.

Brunetti L, Michelotto B, Orlando G & Vacca M. (1999). Leptin inhibits norepinephrine and dopamine release from rat hypothalamic neuronal endings. *European journal of pharmacology* **372,** 237-240.

Brunetti L, Recinella L, Orlando G, Michelotto B, Di Nisio C & Vacca M. (2002). Effects of ghrelin and amylin on dopamine, norepinephrine and serotonin release in the hypothalamus. *European journal of pharmacology* **454,** 189-192.

Bucheler MM, Hadamek K & Hein L. (2002). Two alpha(2)-adrenergic receptor subtypes, alpha(2A) and alpha(2C), inhibit transmitter release in the brain of gene-targeted mice. *Neuroscience* **109,** 819-826.

Buijs RM, Chun SJ, Niijima A, Romijn HJ & Nagai K. (2001). Parasympathetic and sympathetic control of the pancreas: a role for the suprachiasmatic nucleus and other hypothalamic centers that are involved in the regulation of food intake. *The Journal of comparative neurology* **431,** 405-423.

Buijs RM, la Fleur SE, Wortel J, Van Heyningen C, Zuiddam L, Mettenleiter TC, Kalsbeek A, Nagai K & Niijima A. (2003). The suprachiasmatic nucleus balances sympathetic and parasympathetic output to peripheral organs through separate preautonomic neurons. *The Journal of comparative neurology* **464,** 36-48.

Burdakov D & Ashcroft FM. (2002). Cholecystokinin tunes firing of an electrically distinct subset of arcuate nucleus neurons by activating A-Type potassium channels. *J Neurosci* **22,** 6380-6387.

Burdakov D, Liss B & Ashcroft FM. (2003). Orexin excites GABAergic neurons of the arcuate nucleus by activating the sodium--calcium exchanger. *J Neurosci* **23,** 4951-4957.

Burdakov D & Alexopoulos H. (2005). Metabolic state signalling through central hypocretin/orexin neurons. *J Cell Mol Med* **9,** 795-803

Burdakov D, Gerasimenko O & Verkhratsky A. (2005). Physiological changes in glucose differentially modulate the excitability of hypothalamic melanin-concentrating hormone and orexin neurons in situ. *J Neurosci* **25,** 2429-2433.

Burdakov D, Jensen LT, Alexopoulos H, Williams RH, Fearon IM, O'Kelly I, Gerasimenko O, Fugger L & Verkhratsky A. (2006). Tandem-pore K+ channels mediate inhibition of orexin neurons by glucose. *Neuron* **50,** 711-722.

Burdakov D & Gonzalez JA. (2008). Physiological functions of glucose-inhibited neurones. *Acta Physiol (Oxf)* **195,** 71-78.

Burks DJ, Font de Mora J, Schubert M, Withers DJ, Myers MG, Towery HH, Altamuro SL, Flint CL & White MF. (2000). IRS-2 pathways integrate female reproduction and energy homeostasis. *Nature* **407,** 377-382.

Bylund DB, Blaxall HS, Iversen LJ, Caron MG, Lefkowitz RJ & Lomasney JW. (1992). Pharmacological characteristics of alpha 2-adrenergic receptors: comparison of pharmacologically defined subtypes with subtypes identified by molecular cloning. *Mol Pharmacol* **42,** 1-5.

Bylund DB, Eikenberg DC, Hieble JP, Langer SZ, Lefkowitz RJ, Minneman KP, Molinoff PB, Ruffolo RR, Jr. & Trendelenburg U. (1994). International Union of Pharmacology nomenclature of adrenoceptors. *Pharmacol Rev* **46,** 121-136.

Carmona A & Slangen J. (1973). Effects of chemical stimulation of the hypothalamus upon gastric secretion. *Physiol Behav* **10,** 657-661.

Carmona A & Slangen J. (1976). Hypothalamic chemostimulation and autonomic changes in curarized rats. *Psychopharmacology (Berl)* **47,** 105-110.

Chafetz MD, Parko K, Diaz S & Leibowitz SF. (1986). Relationships between medial hypothalamic alpha 2-receptor binding, norepinephrine, and circulating glucose. *Brain Res* **384,** 404-408.

Chang GQ, Karatayev O, Davydova Z, Wortley K & Leibowitz SF. (2005). Glucose injection reduces neuropeptide Y and agouti-related protein expression in the arcuate nucleus: a possible physiological role in eating behavior. *Brain research* **135,** 69-80.

Cheung CC, Clifton DK & Steiner RA. (1997). Proopiomelanocortin neurons are direct targets for leptin in the hypothalamus. *Endocrinology* **138,** 4489-4492.

Chronwall BM. (1985). Anatomy and physiology of the neuroendocrine arcuate nucleus. *Peptides* **6 Suppl 2,** 1-11.

Chronwall BM, Chase TN & O'Donohue TL. (1984). Coexistence of neuropeptide Y and somatostatin in rat and human cortical and rat hypothalamic neurons. *Neuroscience letters* **52,** 213-217.

Claret M, Smith MA, Batterham RL, Selman C, Choudhury AI, Fryer LG, Clements M, Al-Qassab H, Heffron H, Xu AW, Speakman JR, Barsh GS, Viollet B, Vaulont S, Ashford ML, Carling D & Withers DJ. (2007). AMPK is essential for energy homeostasis regulation and glucose sensing by POMC and AgRP neurons. *J Clin Invest* **117,** 2325-2336.

Cohn CK, Ball GG & Hirsch J. (1973). Histamine: effect on self-stimulation. *Science* **180,** 757-758.

Coleman DL. (1973). Effects of parabiosis of obese with diabetes and normal mice. *Diabetologia* **9,** 294-298.

Cone RD. (1999). The Central Melanocortin System and Energy Homeostasis. *Trends Endocrinol Metab* **10,** 211-216.

Cone RD, Cowley MA, Butler AA, Fan W, Marks DL & Low MJ. (2001). The arcuate nucleus as a conduit for diverse signals relevant to energy homeostasis. *Int J Obes Relat Metab Disord* **25 Suppl 5,** S63-67.

Connor JA & Stevens CF. (1971). Voltage clamp studies of a transient outward membrane current in gastropod neural somata. *J Physiol* **213,** 21-30.

Constanti A & Galvan M. (1983). Fast inward-rectifying current accounts for anomalous rectification in olfactory cortex neurones. *J Physiol* **335,** 153-178.

Cotecchia S, Scheer A, Diviani D, Fanelli F & De Benedetti PG. (1998). Molecular mechanisms involved in the activation and regulation of the alpha 1-adrenergic receptor subtypes. *Farmaco* **53,** 273-277.

Cowley MA, Pronchuk N, Fan W, Dinulescu DM, Colmers WF & Cone RD. (1999). Integration of NPY, AGRP, and melanocortin signals in the hypothalamic paraventricular nucleus: evidence of a cellular basis for the adipostat. *Neuron* **24,** 155-163.

Cowley MA, Smart JL, Rubinstein M, Cerdan MG, Diano S, Horvath TL, Cone RD & Low MJ. (2001). Leptin activates anorexigenic POMC neurons through a neural network in the arcuate nucleus. *Nature* **411,** 480-484.

Cummings DE, Purnell JQ, Frayo RS, Schmidova K, Wisse BE & Weigle DS. (2001). A preprandial rise in plasma ghrelin levels suggests a role in meal initiation in humans. *Diabetes* **50,** 1714-1719.

Currie PJ, Mirza A, Fuld R, Park D & Vasselli JR. (2005). Ghrelin is an orexigenic and metabolic signaling peptide in the arcuate and paraventricular nuclei. *Am J Physiol Regul Integr Comp Physiol* **289,** R353-R358.

Cvetkovic V, Brischoux F, Griffond B, Bernard G, Jacquemard C, Fellmann D & Risold PY. (2003). Evidence of melanin-concentrating hormone-containing neurons supplying both cortical and neuroendocrine projections. *Neuroscience* **116,** 31-35.

Daftary SS, Boudaba C & Tasker JG. (2000). Noradrenergic regulation of parvocellular neurons in the rat hypothalamic paraventricular nucleus. *Neuroscience* **96,** 743-751.

Dahlstrom A & Fuxe K. (1964). Localization of monoamines in the lower brain stem. *Experientia* **20,** 398-399.

Date Y, Shimbara T, Koda S, Toshinai K, Ida T, Murakami N, Miyazato M, Kokame K, Ishizuka Y, Ishida Y, Kageyama H, Shioda S, Kangawa K & Nakazato M. (2006). Peripheral ghrelin transmits orexigenic signals through the noradrenergic pathway from the hindbrain to the hypothalamus. *Cell Metab* **4,** 323-331.

Date Y, Ueta Y, Yamashita H, Yamaguchi H, Matsukura S, Kangawa K, Sakurai T, Yanagisawa M & Nakazato M. (1999). Orexins, orexigenic hypothalamic peptides, interact with autonomic, neuroendocrine and neuroregulatory systems. *Proceedings of the National Academy of Sciences of the United States of America* **96,** 748-753.

Day HE, Campeau S, Watson SJ, Jr. & Akil H. (1997). Distribution of alpha 1a-, alpha 1b- and alpha 1d-adrenergic receptor mRNA in the rat brain and spinal cord. *J Chem Neuroanat* **13,** 115-139.

de Vries MG, Arseneau LM, Lawson ME & Beverly JL. (2003). Extracellular glucose in rat ventromedial hypothalamus during acute and recurrent hypoglycemia. *Diabetes* **52,** 2767-2773.

Doi T, Sakata T, Yoshimatsu H, Machidori H, Kurokawa M, Jayasekara LA & Niki N. (1994). Hypothalamic neuronal histamine regulates feeding circadian rhythm in rats. *Brain Res* **641,** 311-318.

Drouin C, Darracq L, Trovero F, Blanc G, Glowinski J, Cotecchia S & Tassin JP. (2002). Alpha1b-adrenergic receptors control locomotor and rewarding effects of psychostimulants and opiates. *J Neurosci* **22,** 2873-2884.

Dun NJ, Dun SL, Wong PY, Yang J, Chang J (2000). Cocaine-and amphetamine-regulated transcript peptide in the rat epididymis:an immunohistochemical and electrophysiological study. *Biol Reprod* 63 (5), 1518-24

Dunn-Meynell AA, Routh VH, Kang L, Gaspers L & Levin BE. (2002). Glucokinase is the likely mediator of glucosensing in both glucose-excited and glucose-inhibited central neurons. *Diabetes* **51,** 2056-2065.

Dutton A & Dyball RE. (1979). Phasic firing enhances vasopressin release from the rat neurohypophysis. *J Physiol* **290,** 433-440.

Egawa M, Yoshimatsu H & Bray GA. (1991). Neuropeptide Y suppresses sympathetic activity to interscapular brown adipose tissue in rats. *Am J Physiol* **260,** R328-334.

Elias CF, Kelly JF, Lee CE, Ahima RS, Drucker DJ, Saper CB & Elmquist JK. (2000). Chemical characterization of leptin-activated neurons in the rat brain. *The Journal of comparative neurology* **423,** 261-281.

Elias CF, Lee C, Kelly J, Aschkenasi C, Ahima RS, Couceyro PR, Kuhar MJ, Saper CB & Elmquist JK. (1998). Leptin activates hypothalamic CART neurons projecting to the spinal cord. *Neuron* **21,** 1375-1385.

Elias CF, Lee CE, Kelly JF, Ahima RS, Kuhar M, Saper CB & Elmquist JK. (2001). Characterization of CART neurons in the rat and human hypothalamus. *The Journal of comparative neurology* **432,** 1-19.

Elias CF, Saper CB, Maratos-Flier E, Tritos NA, Lee C, Kelly J, Tatro JB, Hoffman GE, Ollmann MM, Barsh GS, Sakurai T, Yanagisawa M & Elmquist JK. (1998). Chemically defined projections linking the mediobasal hypothalamus and the lateral hypothalamic area. *The Journal of comparative neurology* **402,** 442-459.

Elmquist JK, Maratos-Flier E, Saper CB & Flier JS. (1998). Unraveling the central nervous system pathways underlying responses to leptin. *Nature neuroscience* **1,** 445-450.

Erickson JC, Hollopeter G & Palmiter RD. (1996). Attenuation of the obesity syndrome of ob/ob mice by the loss of neuropeptide Y. *Science* **274,** 1704-1707.

Eriksson KS, Sergeeva O, Brown RE & Haas HL. (2001). Orexin/hypocretin excites the histaminergic neurons of the tuberomammillary nucleus. *J Neurosci* **21,** 9273-9279.

Esbenshade TA, Fox GB & Cowart MD. (2006). Histamine H3 receptor antagonists: preclinical promise for treating obesity and cognitive disorders. *Mol Interv* **6,** 77-88, 59.

Fan W, Boston BA, Kesterson RA, Hruby VJ & Cone RD. (1997). Role of melanocortinergic neurons in feeding and the agouti obesity syndrome. *Nature* **385,** 165-168.

Faulconbridge LF, Cummings DE, Kaplan JM & Grill HJ. (2003). Hyperphagic effects of brainstem ghrelin administration. *Diabetes* **52,** 2260-2265.

Fioramonti X, Contie S, Song Z, Routh VH, Lorsignol A & Penicaud L. (2007). Characterization of glucosensing neuron subpopulations in the arcuate nucleus: integration in neuropeptide Y and pro-opio melanocortin networks? *Diabetes* **56,** 1219-1227.

Fioramonti X, Lorsignol A, Taupignon A & Penicaud L. (2004). A new ATP-sensitive K+ channel-independent mechanism is involved in glucose-excited neurons of mouse arcuate nucleus. *Diabetes* **53,** 2767-2775.

Freedman JE & Aghajanian GK. (1987). Role of phosphoinositide metabolites in the prolongation of afterhyperpolarizations by alpha 1-adrenoceptors in rat dorsal raphe neurons. *J Neurosci* **7,** 3897-3906.

Friedman JM & Halaas JL. (1998). Leptin and the regulation of body weight in mammals. *Nature* **395,** 763-770.

Fruhbeck G. (2006). Intracellular signalling pathways activated by leptin. *Biochem J* **393,** 7-20.

Ganong WF. (2000). Circumventricular organs: definition and role in the regulation of endocrine and autonomic function. *Clin Exp Pharmacol Physiol* **27,** 422-427.

Gao Q & Horvath TL. (2007). Neurobiology of feeding and energy expenditure. *Annu Rev Neurosci* **30,** 367-398.

Garbarg M, Barbin G, Bischoff S, Pollard H & Schwartz JC. (1976). Dual localization of histamine in an ascending neuronal pathway and in non-neuronal cells evidenced by lesions in the lateral hypothalamic area. *Brain Res* **106,** 333-348.

Garcia de Yebenes E, Li S, Fournier A, St-Pierre S & Pelletier G. (1995). Regulation of proopiomelanocortin gene expression by neuropeptide Y in the rat arcuate nucleus. *Brain Res* **674,** 112-116.

Garcia M, Floran B, Arias-Montano JA, Young JM & Aceves J. (1997). Histamine H3 receptor activation selectively inhibits dopamine D1 receptor-dependent [3H]GABA release from depolarization-stimulated slices of rat substantia nigra pars reticulata. *Neuroscience* **80,** 241-249.

Geller HM. (1981). Histamine actions on activity of cultured hypothalamic neurons: evidence for mediation by H1- and H2-histamine receptors. *Brain Res* **227,** 89-101.

Goldman CK, Marino L & Leibowitz SF. (1985). Postsynaptic alpha 2-noradrenergic receptors mediate feeding induced by paraventricular nucleus injection of norepinephrine and clonidine. *European journal of pharmacology* **115,** 11-19.

Goldman DE. (1943). Potential, impedance, and rectification in membranes. *The journal of general physiology* **27,** 37-60.

Gorelova N & Reiner PB. (1996). Histamine depolarizes cholinergic septal neurons. *J Neurophysiol* **75,** 707-714.

Gottsch ML, Clifton DK & Steiner RA. (2004). Galanin-like peptide as a link in the integration of metabolism and reproduction. *Trends Endocrinol Metab* **15,** 215-221.

Greene RW, Haas HL, Gerber U & McCarley RW. (1989). Cholinergic activation of medial pontine reticular formation neurons in vitro. *Exs* **57,** 123-137.

Gropp E, Shanabrough M, Borok E, Xu AW, Janoschek R, Buch T, Plum L, Balthasar N, Hampel B, Waisman A, Barsh GS, Horvath TL & Bruning JC. (2005). Agouti-related peptide-expressing neurons are mandatory for feeding. *Nature neuroscience* **8,** 1289-1291.

Grossman SP. (1962). Direct adrenergic and cholinergic stimulation of hypothalamic mechanisms. *Am J Physiol* **202,** 872-882.

Guan XM, Hess JF, Yu H, Hey PJ & van der Ploeg LH. (1997a). Differential expression of mRNA for leptin receptor isoforms in the rat brain. *Mol Cell Endocrinol* **133,** 1-7.

Guan XM, Yu H, Palyha OC, McKee KK, Feighner SD, Sirinathsinghji DJ, Smith RG, Van der Ploeg LH & Howard AD. (1997b). Distribution of mRNA encoding the growth hormone secretagogue receptor in brain and peripheral tissues. *Brain research* **48,** 23-29.

Guan XM, Yu H, Trumbauer M, Frazier E, Van der Ploeg LH & Chen H. (1998a). Induction of neuropeptide Y expression in dorsomedial hypothalamus of diet-induced obese mice. *Neuroreport* **9,** 3415-3419.

Guan XM, Yu H & Van der Ploeg LH. (1998b). Evidence of altered hypothalamic pro-opiomelanocortin/ neuropeptide Y mRNA expression in tubby mice. *Brain research* **59,** 273-279.

Gulledge AT, Kampa BM & Stuart GJ. (2005). Synaptic integration in dendritic trees. *J*

Neurobiol **64,** 75-90.

Guyton A & Hall J. (2006). Behavioral and motivational mechanisms of the brain- The limbic system and the hypothalamus. *Textbook of medical physiolology* **11,** 728-738.

Haas H & Panula P. (2003). The role of histamine and the tuberomamillary nucleus in the nervous system. *Nature reviews* **4,** 121-130.

Haas HL. (1992). Electrophysiology of histamine receptors. *The histamine receptor, Wiley-Liss, New York***,** 161-171.

Haas HL & Bucher UM. (1975). Histamine H2-receptors on single central neurones. *Nature* **255,** 634-635.

Haas HL & Greene RW. (1986). Effects of histamine on hippocampal pyramidal cells of the rat in vitro. *Exp Brain Res* **62,** 123-130.

Haas HL, Greene RW & Reiner PB. (1989). The brain histamine system in vitro. *J Neurosci Methods* **28,** 71-75.

Haas HL & Wolf P. (1977). Central actions of histamine: microelectrophoretic studies. *Brain Res* **122,** 269-279.

Hagan MM, Castaneda E, Sumaya IC, Fleming SM, Galloway J & Moss DE. (1998). The effect of hypothalamic peptide YY on hippocampal acetylcholine release in vivo: implications for limbic function in binge-eating behavior. *Brain Res* **805,** 20-28.

Hahn TM, Breininger JF, Baskin DG & Schwartz MW. (1998). Coexpression of Agrp and NPY in fasting-activated hypothalamic neurons. *Nature neuroscience* **1,** 271-272.

Halliwell JV & Adams PR. (1982). Voltage-clamp analysis of muscarinic excitation in hippocampal neurons. *Brain Res* **250,** 71-92.

Han SK, Chong W, Li LH, Lee IS, Murase K & Ryu PD. (2002). Noradrenaline excites and inhibits GABAergic transmission in parvocellular neurons of rat hypothalamic paraventricular nucleus. *J Neurophysiol* **87,** 2287-2296.

Hanson ES & Dallman MF. (1995). Neuropeptide Y (NPY) may integrate responses of hypothalamic feeding systems and the hypothalamo-pituitary-adrenal axis. *J Neuroendocrinol* **7,** 273-279.

Hara J, Beuckmann CT, Nambu T, Willie JT, Chemelli RM, Sinton CM, Sugiyama F, Yagami K, Goto K, Yanagisawa M & Sakurai T. (2001). Genetic ablation of orexin neurons in mice results in narcolepsy, hypophagia, and obesity. *Neuron* **30,** 345-354.

Harrold JA, Widdowson PS & Williams G. (1999). Altered energy balance causes selective changes in melanocortin-4(MC4-R), but not melanocortin-3 (MC3-R), receptors in specific hypothalamic regions: further evidence that activation of MC4-R is a physiological inhibitor of feeding. *Diabetes* **48,** 267-271.

Hastings JA, Pavia JM & Morris MJ. (1997). Neuropeptide Y and [Leu31,Pro34]neuropeptide Y potentiate potassium-induced noradrenaline release in the paraventricular nucleus of the aged rat. *Brain Res* **750,** 301-304.

Hausberger FX. (1959). Behavior of transplanted adipose tissue of hereditarily obese mice. *Anat Rec* **135,** 109-113.

Heal DJ, Aspley S, Prow MR, Jackson HC, Martin KF & Cheetham SC. (1998). Sibutramine: a novel anti-obesity drug. A review of the pharmacological evidence to differentiate it from d-amphetamine and d-fenfluramine. *Int J Obes Relat Metab Disord* **22 Suppl 1,** S18-28; discussion S29.

Hein L. (2006). Adrenoceptors and signal transduction in neurons. *Cell Tissue Res* **326,** 541-551.

Hentges ST, Nishiyama M, Overstreet LS, Stenzel-Poore M, Williams JT & Low MJ. (2004). GABA release from proopiomelanocortin neurons. *J Neurosci* **24,** 1578-1583.

Hervey GR. (1959). The effects of lesions in the hypothalamus in parabiotic rats. *J Physiol* **145,** 336-352.

Hetherington A & Ranson SW. (1940). Hypothalamic lesions and adiposity in the rat. **78,** 149-172.

Hill JW, Williams KW, Ye C, Luo J, Balthasar N, Coppari R, Cowley MA, Cantley LC, Lowell BB & Elmquist JK. (2008). Acute effects of leptin require PI3K signaling in hypothalamic proopiomelanocortin neurons in mice. *J Clin Invest* **118,** 1796-1805.

Hill SJ, Ganellin CR, Timmerman H, Schwartz JC, Shankley NP, Young JM, Schunack W, Levi R & Haas HL. (1997). International Union of Pharmacology. XIII. Classification of histamine receptors. *Pharmacol Rev* **49,** 253-278.

Hill SJ & Young M. (1978). Antagonism of central histamine H1 receptors by antipsychotic drugs. *European journal of pharmacology* **52,** 397-399.

Hoffman RP, Hausberg M, Sinkey CA & Anderson EA. (1999). Hyperglycemia without hyperinsulinemia produces both sympathetic neural activation and vasodilation in normal humans. *J Diabetes Complications* **13,** 17-22.

Hoggard N, Hunter L, Duncan JS & Rayner DV. (2004a). Regulation of adipose tissue leptin secretion by alpha-melanocyte-stimulating hormone and agouti-related protein: further evidence of an interaction between leptin and the melanocortin signalling system. *J Mol Endocrinol* **32,** 145-153.

Hoggard N, Johnstone AM, Faber P, Gibney ER, Elia M, Lobley G, Rayner V, Horgan G, Hunter L, Bashir S & Stubbs RJ. (2004b). Plasma concentrations of alpha-MSH, AgRP and leptin in lean and obese men and their relationship to differing states of energy balance perturbation. *Clin Endocrinol (Oxf)* **61,** 31-39.

Honda K, Bailey AR, Bull PM, Macdonald LP, Dickson SL & Leng G. (1999). An electrophysiological and morphological investigation of the projections of growth hormone-releasing peptide-6-responsive neurons in the rat arcuate nucleus to the median eminence and to the paraventricular nucleus. *Neuroscience* **90,** 875-883.

Horvath TL, Bechmann I, Naftolin F, Kalra SP & Leranth C. (1997). Heterogeneity in the neuropeptide Y-containing neurons of the rat arcuate nucleus: GABAergic and non-GABAergic subpopulations. *Brain Res* **756,** 283-286.

Horvath TL, Diano S & Tschop M. (2004). Brain circuits regulating energy homeostasis. *Neuroscientist* **10,** 235-246.

Hough LB. (2001). Genomics meets histamine receptors: new subtypes, new receptors. *Mol Pharmacol* **59,** 415-419.

Howard AD, Wang R, Pong SS, Mellin TN, Strack A, Guan XM, Zeng Z, Williams DL, Jr., Feighner SD, Nunes CN, Murphy B, Stair JN, Yu H, Jiang Q, Clements MK, Tan CP, McKee KK, Hreniuk DL, McDonald TP, Lynch KR, Evans JF, Austin CP, Caskey CT, Van der Ploeg LH & Liu Q. (2000). Identification of receptors for neuromedin U and its role in feeding. *Nature* **406,** 70-74.

Huang ZL, Qu WM, Li WD, Mochizuki T, Eguchi N, Watanabe T, Urade Y & Hayaishi O. (2001). Arousal effect of orexin A depends on activation of the histaminergic system. *Proceedings of the National Academy of Sciences of the United States of America* **98,** 9965-9970.

Huguenard JR & Prince DA. (1994). Intrathalamic rhythmicity studied in vitro: nominal T-current modulation causes robust antioscillatory effects. *J Neurosci* **14,** 5485-5502.

Hunter JC, Fontana DJ, Hedley LR, Jasper JR, Lewis R, Link RE, Secchi R, Sutton J & Eglen RM. (1997). Assessment of the role of alpha2-adrenoceptor subtypes in the antinociceptive, sedative and hypothermic action of dexmedetomidine in transgenic mice. *Br J Pharmacol* **122,** 1339-1344.

Huszar D, Lynch CA, Fairchild-Huntress V, Dunmore JH, Fang Q, Berkemeier LR, Gu W, Kesterson RA, Boston BA, Cone RD, Smith FJ, Campfield LA, Burn P & Lee F. (1997). Targeted disruption of the melanocortin-4 receptor results in obesity in mice. *Cell* **88,** 131-141.

Ibrahim N, Bosch MA, Smart JL, Qiu J, Rubinstein M, Ronnekleiv OK, Low MJ & Kelly MJ. (2003). Hypothalamic proopiomelanocortin neurons are glucose responsive and express K(ATP) channels. *Endocrinology* **144,** 1331-1340.

Inagaki N, Miura T, Nagai H, Ono Y & Koda A. (1988). Inhibition of vascular permeability increase in mice. An additional anti-allergic mechanism of glucocorticoids. *Int Arch Allergy Appl Immunol* **87,** 254-259.

Inokuchi H, Yoshimura M, Polosa C & Nishi S. (1992). Adrenergic receptors (alpha 1 and alpha 2) modulate different potassium conductances in sympathetic preganglionic neurons. *Can J Physiol Pharmacol* **70 Suppl,** S92-97.

Ishimatsu M, Kidani Y, Tsuda A & Akasu T. (2002). Effects of methylphenidate on the membrane potential and current in neurons of the rat locus coeruleus. *J Neurophysiol* **87,** 1206-1212.

Ishizuka T, Nomura S, Hosoda H, Kangawa K, Watanabe T & Yamatodani A. (2006). A role of the histaminergic system for the control of feeding by orexigenic peptides. *Physiol Behav* **89,** 295-300.

Ito C, Shen H, Toyota H, Kubota Y, Sakurai E, Watanabe T & Sato M. (1999). Effects of the acute and chronic restraint stresses on the central histaminergic neuron system of Fischer rat. *Neuroscience letters* **262,** 143-145.

Jackson HC, Bearham MC, Hutchins LJ, Mazurkiewicz SE, Needham AM & Heal DJ. (1997). Investigation of the mechanisms underlying the hypophagic effects of the 5-HT and noradrenaline reuptake inhibitor, sibutramine, in the rat. *Br J Pharmacol* **121,** 1613-1618.

Jacobowitz DM & O'Donohue TL. (1978). alpha-Melanocyte stimulating hormone: immunohistochemical identification and mapping in neurons of rat brain. *Proceedings of the National Academy of Sciences of the United States of America* **75,** 6300-6304.

Jeong SW & Ikeda SR. (1998). G protein alpha subunit G alpha z couples neurotransmitter receptors to ion channels in sympathetic neurons. *Neuron* **21,** 1201-1212.

Jhanwar-Uniyal M, Papamichael MJ & Leibowitz SF. (1988). Glucose-dependent changes in alpha 2-noradrenergic receptors in hypothalamic nuclei. *Physiol Behav* **44,** 611-617.

Jhanwar-Uniyal M, Roland CR & Leibowitz SF. (1986). Diurnal rhythm of alpha 2-noradrenergic receptors in the paraventricular nucleus and other brain areas: relation to circulating corticosterone and feeding behavior. *Life Sci* **38,** 473-482.

Jones H, Bradley PB & Roberts F. (1985). Histamine-induced excitation of spontaneously active medullary neurones in the rat brain is mediated by H2-receptors. A microiontophoretic study using H1- and H2-agonists and antagonists. *Neuropharmacology* **24,** 1231-1239.

Jorgenson KL, Kow LM & Pfaff DW. (1989). Histamine excites arcuate neurons in vitro through H1 receptors. *Brain Res* **502,** 171-179.

Kalucy RS. (1980). Drug-induced weight gain. *Drugs* **19,** 268-278.

Kamegai J, Tamura H, Shimizu T, Ishii S, Sugihara H & Wakabayashi I. (2000). Central effect of ghrelin, an endogenous growth hormone secretagogue, on hypothalamic peptide gene expression. *Endocrinology* **141,** 4797-4800.

Kamegai J, Tamura H, Shimizu T, Ishii S, Sugihara H & Wakabayashi I. (2001). Chronic central infusion of ghrelin increases hypothalamic neuropeptide Y and Agouti-related protein mRNA levels and body weight in rats. *Diabetes* **50,** 2438-2443.

Kang L, Routh VH, Kuzhikandathil EV, Gaspers LD & Levin BE. (2004). Physiological and molecular characteristics of rat hypothalamic ventromedial nucleus glucosensing neurons. *Diabetes* **53,** 549-559.

Kang YM, Ouyang W, Chen JY, Qiao JT & Dafny N. (2000). Norepinephrine modulates single hypothalamic arcuate neurons via alpha(1)and beta adrenergic receptors. *Brain Res* **869,** 146-157.

Kanjhan R, Coulson EJ, Adams DJ & Bellingham MC. (2005). Tertiapin-Q blocks recombinant and native large conductance K+ channels in a use-dependent manner. *J Pharmacol Exp Ther* **314,** 1353-1361.

Keire DA, Bowers CW, Solomon TE & Reeve JR, Jr. (2002). Structure and receptor binding of PYY analogs. *Peptides* **23,** 305-321.

Keire DA, Mannon P, Kobayashi M, Walsh JH, Solomon TE & Reeve JR, Jr. (2000). Primary structures of PYY, [Pro(34)]PYY, and PYY-(3-36) confer different conformations and receptor selectivity. *Am J Physiol Gastrointest Liver Physiol* **279,** G126-131.

Kennedy GC. (1953). The role of depot fat in the hypothalamic control of food intake in the rat. *Proc R Soc Lond B Biol Sci* **140,** 578-596.

Kenyon JL & Gibbons WR. (1979). 4-Aminopyridine and the early outward current of sheep cardiac Purkinje fibers. *J Gen Physiol* **73,** 139-157.

Kiss J, Csaba Z, Csaki A & Halasz B. (2005). Glutamatergic innervation of neuropeptide Y and pro-opiomelanocortin-containing neurons in the hypothalamic arcuate nucleus of the rat. *Eur J Neurosci* **21,** 2111-2119.

Kiyono S, Seo ML, Shibagaki M, Watanabe T, Maeyama K & Wada H. (1985). Effects of alpha-fluoromethylhistidine on sleep-waking parameters in rats. *Physiol Behav* **34,** 615-617.

Knauf C, Cani PD, Kim DH, Iglesias MA, Chabo C, Waget A, Colom A, Rastrelli S, Delzenne NM, Drucker DJ, Seeley RJ & Burcelin R. (2008). Role of central nervous system glucagon-like Peptide-1 receptors in enteric glucose sensing. *Diabetes* **57,** 2603-2612.

Knowles F & Bern HA. (1966). Function of neurosecretion in endocrine regulation. *Nature* **210,** 271-272.

Kojima M, Hosoda H, Date Y, Nakazato M, Matsuo H & Kangawa K. (1999). Ghrelin is a growth-hormone-releasing acylated peptide from stomach. *Nature* **402,** 656-660.

Kojima M & Kangawa K. (2005). Ghrelin: structure and function. *Physiol Rev* **85,** 495-522.

Kokkotou EG, Tritos NA, Mastaitis JW, Slieker L & Maratos-Flier E. (2001). Melanin-concentrating hormone receptor is a target of leptin action in the mouse brain. *Endocrinology* **142,** 680-686.

Koshimizu TA, Tanoue A & Tsujimoto G. (2007). Clinical implications from studies of alpha1 adrenergic receptor knockout mice. *Biochem Pharmacol* **73,** 1107-1112.

Kostic VS. (1992). [Beta blockers in the treatment of neurological disorders]. *Srp Arh Celok Lek* **120 Suppl 4,** 54-58.

Kow LM & Pfaff DW. (1987). Responses of ventromedial hypothalamic neurons in vitro to norepinephrine: dependence on dose and receptor type. *Brain Res* **413,** 220-228.

Koylu EO, Couceyro PR, Lambert PD, Ling NC, DeSouza EB & Kuhar MJ. (1997). Immunohistochemical localization of novel CART peptides in rat hypothalamus, pituitary and adrenal gland. *J Neuroendocrinol* **9,** 823-833.

Krahn DD, Gosnell BA, Levine AS & Morley JE. (1988). Behavioral effects of corticotropin-releasing factor: localization and characterization of central effects. *Brain Res* **443,** 63-69.

Kristensen P, Judge ME, Thim L, Ribel U, Christjansen KN, Wulff BS, Clausen JT, Jensen PB, Madsen OD, Vrang N, Larsen PJ & Hastrup S. (1998). Hypothalamic CART is a new anorectic peptide regulated by leptin. *Nature* **393,** 72-76.

La Fleur SE, Kalsbeek A, Wortel J & Buijs RM. (1999). A suprachiasmatic nucleus generated rhythm in basal glucose concentrations. *J Neuroendocrinol* **11,** 643-652.

Langer SZ. (1974). Presynaptic regulation of catecholamine release. *Biochem Pharmacol* **23,** 1793-1800.

Langer SZ. (1998). Nomenclature and state of the art on alpha1-adrenoceptors. *Eur Urol* **33 Suppl 2,** 2-6.

Larue-Achagiotis C & Le Magnen J. (1983). Fast-induced changes in plasma glucose, insulin and free fatty acid concentration compared in rats during the night and day. *Physiol Behav* **30,** 93-96.

Lawrence CB, Snape AC, Baudoin FM & Luckman SM. (2002). Acute central ghrelin and GH secretagogues induce feeding and activate brain appetite centers. *Endocrinology* **143,** 155-162.

Lecklin A, Etu-Seppala P, Stark H & Tuomisto L. (1998). Effects of intracerebroventricularly infused histamine and selective H1, H2 and H3 agonists on food and water intake and urine flow in Wistar rats. *Brain Res* **793,** 279-288.

Lecklin A & Tuomisto L. (1998). The blockade of H1 receptors attenuates the suppression of feeding and diuresis induced by inhibition of histamine catabolism. *Pharmacol Biochem Behav* **59,** 753-758.

LeDoux JE, Iwata J, Cicchetti P & Reis DJ. (1988). Different projections of the central amygdaloid nucleus mediate autonomic and behavioral correlates of conditioned fear. *J Neurosci* **8,** 2517-2529.

Lee GH, Proenca R, Montez JM, Carroll KM, Darvishzadeh JG, Lee JI & Friedman JM. (1996). Abnormal splicing of the leptin receptor in diabetic mice. *Nature* **379,** 632-635.

Lee K, Dixon AK, Richardson PJ & Pinnock RD. (1999). Glucose-receptive neurones in the rat ventromedial hypothalamus express KATP channels composed of Kir6.1 and SUR1 subunits. *J Physiol* **515 (Pt 2),** 439-452.

Leibowitz SF. (1973). Histamine: a stimulatory effect on drinking behavior in the rat. *Brain Res* **63,** 440-444.

Leibowitz SF. (1978). Paraventricular nucleus: a primary site mediating adrenergic stimulation of feeding and drinking. *Pharmacol Biochem Behav* **8,** 163-175.

Leibowitz SF. (1988). Hypothalamic paraventricular nucleus: interaction between alpha 2-noradrenergic system and circulating hormones and nutrients in relation to energy balance. *Neurosci Biobehav Rev* **12,** 101-109.

Leibowitz SF & Brown LL. (1980). Histochemical and pharmacological analysis of noradrenergic projections to the paraventricular hypothalamus in relation to feeding stimulation. *Brain Res* **201,** 289-314.

Leibowitz SF, Diaz S & Tempel D. (1989). Norepinephrine in the paraventricular nucleus stimulates corticosterone release. *Brain Res* **496,** 219-227.

Leibowitz SF, Hammer NJ & Chang K. (1983a). Feeding behavior induced by central norepinephrine injection is attenuated by discrete lesions in the hypothalamic paraventricular nucleus. *Pharmacol Biochem Behav* **19,** 945-950.

Leibowitz SF, Jhanwar-Uniyal M & Levin BE. (1983b). Effects of amphetamine on catecholamine levels and turnover in discrete hypothalamic areas. *Brain Res* **266,** 348-354.

Leibowitz SF, Sladek C, Spencer L & Tempel D. (1988). Neuropeptide Y, epinephrine and norepinephrine in the paraventricular nucleus: stimulation of feeding and the release of corticosterone, vasopressin and glucose. *Brain Res Bull* **21,** 905-912.

Levin BE. (2001). Glucosensing neurons do more than just sense glucose. *Int J Obes Relat Metab Disord* **25 Suppl 5,** S68-72.

Levin BE, Brown KL & Dunn-Meynell AA. (1996). Differential effects of diet and obesity on high and low affinity sulfonylurea binding sites in the rat brain. *Brain Res* **739,** 293-300.

Levin BE, Dunn-Meynell AA & Routh VH. (2001). Brain glucosensing and the K(ATP) channel. *Nature neuroscience* **4,** 459-460.

Levin BE, Govek EK & Dunn-Meynell AA. (1998). Reduced glucose-induced neuronal activation in the hypothalamus of diet-induced obese rats. *Brain Res* **808,** 317-319.

Levin BE & Hamm MW. (1994). Plasticity of brain alpha-adrenoceptors during the development of diet-induced obesity in the rat. *Obes Res* **2,** 230-238.

Levin BE, Israel P & Lattemann DP. (1998). Insulin selectively downregulates alpha2-adrenoceptors in the arcuate and dorsomedial nucleus. *Brain Res Bull* **45,** 179-181.

Levin BE & Planas B. (1993). Defective glucoregulation of brain alpha 2-adrenoceptors in obesity-prone rats. *Am J Physiol* **264,** R305-311.

Levin BE, Routh VH, Kang L, Sanders NM & Dunn-Meynell AA. (2004). Neuronal glucosensing: what do we know after 50 years? *Diabetes* **53,** 2521-2528.

Levine AS, Rogers B, Kneip J, Grace M & Morley JE. (1983). Effect of centrally administered corticotropin releasing factor (CRF) on multiple feeding paradigms. *Neuropharmacology* **22,** 337-339.

Lewis DI & Coote JH. (1990). Excitation and inhibition of rat sympathetic preganglionic neurones by catecholamines. *Brain Res* **530,** 229-234.

Li SJ, Scanlon MN, Jarai Z, Varga K, Gantenberg NS, Lazar-Wesley E & Kunos G. (1996). alpha-2-Adrenergic activation of proopiomelanocortin-containing neurons in the arcuate nucleus causes opioid-mediated hypotension and bradycardia. *Neuroendocrinology* **63,** 275-283.

Li Y & van den Pol AN. (2005). Direct and indirect inhibition by catecholamines of hypocretin/orexin neurons. *J Neurosci* **25,** 173-183.

Li Z & Hatton GI. (1996). Histamine-induced prolonged depolarization in rat supraoptic neurons: G-protein-mediated, Ca(2+)-independent suppression of K+ leakage conductance. *Neuroscience* **70,** 145-158.

Liggett SB & Raymond JR. (1993). Pharmacology and molecular biology of adrenergic receptors. *Baillieres Clin Endocrinol Metab* **7,** 279-306.

Limbird LE. (1988). Receptors linked to inhibition of adenylate cyclase: additional signaling mechanisms. *Faseb J* **2,** 2686-2695.

Lin S, Storlien LH & Huang XF. (2000). Leptin receptor, NPY, POMC mRNA expression in the diet-induced obese mouse brain. *Brain Res* **875,** 89-95.

Liu C, Ma X, Jiang X, Wilson SJ, Hofstra CL, Blevitt J, Pyati J, Li X, Chai W, Carruthers N & Lovenberg TW. (2001). Cloning and pharmacological characterization of a fourth histamine receptor (H(4)) expressed in bone marrow. *Mol Pharmacol* **59,** 420-426.

Llinas R & Yarom Y. (1981). Electrophysiology of mammalian inferior olivary neurones in vitro. Different types of voltage-dependent ionic conductances. *J Physiol* **315,** 549-567.

Loewy AD. (1990). Anatomy of the autonomic nervous system: An overview. In central regulation of autonomic functions. *Oxford University press*, 3-16.

Lomasney JW, Cotecchia S, Lefkowitz RJ & Caron MG. (1991). Molecular biology of alpha-adrenergic receptors: implications for receptor classification and for structure-function relationships. *Biochim Biophys Acta* **1095,** 127-139.

Lowell BB & Bachman ES. (2003). Beta-Adrenergic receptors, diet-induced thermogenesis, and obesity. *J Biol Chem* **278,** 29385-29388.

Lu S, Guan JL, Wang QP, Uehara K, Yamada S, Goto N, Date Y, Nakazato M, Kojima M, Kangawa K & Shioda S. (2002). Immunocytochemical observation of ghrelin-containing neurons in the rat arcuate nucleus. *Neuroscience letters* **321,** 157-160.

Luquet S, Perez FA, Hnasko TS & Palmiter RD. (2005). NPY/AgRP neurons are essential for feeding in adult mice but can be ablated in neonates. *Science* **310,** 683-685.

Luquet S, Phillips CT & Palmiter RD. (2007). NPY/AgRP neurons are not essential for feeding responses to glucoprivation. *Peptides* **28,** 214-225.

Ma X, Zubcevic L & Ashcroft FM. (2008). Glucose regulates the effects of leptin on hypothalamic POMC neurons. *Proceedings of the National Academy of Sciences of the United States of America* **105,** 9811-9816.

Ma X, Zubcevic L, Bruning JC, Ashcroft FM & Burdakov D. (2007). Electrical inhibition of identified anorexigenic POMC neurons by orexin/hypocretin. *J Neurosci* **27,** 1529-1533.

Machidori H, Sakata T, Yoshimatsu H, Ookuma K, Fujimoto K, Kurokawa M, Yamatodani A & Wada H. (1992). Zucker obese rats: defect in brain histamine control of feeding. *Brain Res* **590,** 180-186.

Magee JC & Johnston D. (2005). Plasticity of dendritic function. *Curr Opin Neurobiol* **15,** 334-342.

Magrani J, de Castro e Silva E, Varjao B, Duarte G, Ramos AC, Athanazio R, Barbetta M, Luz P & Fregoneze JB. (2004). Histaminergic H1 and H2 receptors located within the ventromedial hypothalamus regulate food and water intake in rats. *Pharmacol Biochem Behav* **79,** 189-198.

Marcus JN, Aschkenasi CJ, Lee CE, Chemelli RM, Saper CB, Yanagisawa M & Elmquist JK. (2001). Differential expression of orexin receptors 1 and 2 in the rat brain. *The Journal of comparative neurology* **435,** 6-25.

Marek GJ & Aghajanian GK. (1999). 5-HT2A receptor or alpha1-adrenoceptor activation induces excitatory postsynaptic currents in layer V pyramidal cells of the medial prefrontal cortex. *European journal of pharmacology* **367,** 197-206.

Margules DL. (1970). Alpha-adrenergic receptors in hypothalamus for the suppression of feeding behavior by satiety. *J Comp Physiol Psychol* **73,** 1-12.

Masaki T, Chiba S, Yasuda T, Noguchi H, Kakuma T, Watanabe T, Sakata T & Yoshimatsu H. (2004). Involvement of hypothalamic histamine H1 receptor in the regulation of feeding rhythm and obesity. *Diabetes* **53,** 2250-2260.

Masaki T & Yoshimatsu H. (2006). The hypothalamic H1 receptor: a novel therapeutic target for disrupting diurnal feeding rhythm and obesity. *Trends in pharmacological sciences* **27,** 279-284.

Masaki T, Yoshimatsu H, Chiba S, Watanabe T & Sakata T. (2001a). Central infusion of histamine reduces fat accumulation and upregulates UCP family in leptin-resistant obese mice. *Diabetes* **50,** 376-384.

Masaki T, Yoshimatsu H, Chiba S, Watanabe T & Sakata T. (2001b). Targeted disruption of histamine H1-receptor attenuates regulatory effects of leptin on feeding, adiposity, and UCP family in mice. *Diabetes* **50,** 385-391.

Mayer CH, Fink H, Rex A & Voigt JP. (2006). Changes in extracellular hypothalamic glucose in relation to feeding. *Eur J Neurosci* **24,** 1695-1701.

Mayer J. (1953). Glucostatic mechanism of regulation of food intake. *N Engl J Med* **249,** 13-16.

Mayer J. (1955). Regulation of energy intake and the body weight: the glucostatic theory and the lipostatic hypothesis. *Ann N Y Acad Sci* **63,** 15-43.

McCaleb ML, Myers RD, Singer G & Willis G. (1979). Hypothalamic norepinephrine in the rat during feeding and push-pull perfusion with glucose, 2-DG, or insulin. *Am J Physiol* **236,** R312-321.

McCormick DA & Prince DA. (1988). Noradrenergic modulation of firing pattern in guinea pig and cat thalamic neurons, in vitro. *J Neurophysiol* **59,** 978-996.

McCormick DA & Williamson A. (1991). Modulation of neuronal firing mode in cat and guinea pig LGNd by histamine: possible cellular mechanisms of histaminergic control of arousal. *J Neurosci* **11,** 3188-3199.

Melander T, Hokfelt T & Rokaeus A. (1986). Distribution of galaninlike immunoreactivity in the rat central nervous system. *The Journal of comparative neurology* **248,** 475-517.

Menendez JA, McGregor IS, Healey PA, Atrens DM & Leibowitz SF. (1990). Metabolic effects of neuropeptide Y injections into the paraventricular nucleus of the hypothalamus. *Brain Res* **516,** 8-14.

Mercer JG, Hoggard N, Williams LM, Lawrence CB, Hannah LT, Morgan PJ & Trayhurn P. (1996a). Coexpression of leptin receptor and preproneuropeptide Y mRNA in arcuate nucleus of mouse hypothalamus. *J Neuroendocrinol* **8,** 733-735.

Mercer JG, Hoggard N, Williams LM, Lawrence CB, Hannah LT & Trayhurn P. (1996b). Localization of leptin receptor mRNA and the long form splice variant (Ob-Rb) in mouse hypothalamus and adjacent brain regions by in situ hybridization. *FEBS Lett* **387,** 113-116.

Miki T, Liss B, Minami K, Shiuchi T, Saraya A, Kashima Y, Horiuchi M, Ashcroft F, Minokoshi Y, Roeper J & Seino S. (2001). ATP-sensitive K+ channels in the hypothalamus are essential for the maintenance of glucose homeostasis. *Nature neuroscience* **4,** 507-512.

Miller MW, Duhl DM, Vrieling H, Cordes SP, Ollmann MM, Winkes BM & Barsh GS. (1993). Cloning of the mouse agouti gene predicts a secreted protein ubiquitously expressed in mice carrying the lethal yellow mutation. *Genes Dev* **7,** 454-467.

Miyazaki T, Dun NJ, Kobayashi H & Tosaka T. (1996). Voltage-dependent potassium currents of sympathetic preganglionic neurons in neonatal rat spinal cord thin slices. *Brain Res* **743,** 1-10.

Molinoff PB. (1984). Alpha- and beta-adrenergic receptor subtypes properties, distribution and regulation. *Drugs* **28 Suppl 2,** 1-15.

Moltz JH & McDonald JK. (1985). Neuropeptide Y: direct and indirect action on insulin secretion in the rat. *Peptides* **6,** 1155-1159.

Morimoto T, Yamamoto Y, Mobarakeh JI, Yanai K, Watanabe T, Watanabe T & Yamatodani A. (1999). Involvement of the histaminergic system in leptin-induced suppression of food intake. *Physiol Behav* **67,** 679-683.

Morimoto T, Yamamoto Y & Yamatodani A. (2000). Leptin facilitates histamine release from the hypothalamus in rats. *Brain Res* **868,** 367-369.

Mountjoy KG, Mortrud MT, Low MJ, Simerly RB & Cone RD. (1994). Localization of the melanocortin-4 receptor (MC4-R) in neuroendocrine and autonomic control circuits in the brain. *Mol Endocrinol* **8,** 1298-1308.

Mountjoy KG & Wong J. (1997). Obesity, diabetes and functions for proopiomelanocortin-derived peptides. *Mol Cell Endocrinol* **128,** 171-177.

Mouradian RD, Sessler FM & Waterhouse BD. (1991). Noradrenergic potentiation of excitatory transmitter action in cerebrocortical slices: evidence for mediation by an alpha 1 receptor-linked second messenger pathway. *Brain Res* **546,** 83-95.

Murakami DM, Horwitz BA & Fuller CA. (1995). Circadian rhythms of temperature and activity in obese and lean Zucker rats. *Am J Physiol* **269,** R1038-1043.

Muroya S, Funahashi H, Yamanaka A, Kohno D, Uramura K, Nambu T, Shibahara M, Kuramochi M, Takigawa M, Yanagisawa M, Sakurai T, Shioda S & Yada T. (2004). Orexins (hypocretins) directly interact with neuropeptide Y, POMC and glucose-responsive neurons to regulate Ca 2+ signaling in a reciprocal manner to leptin: orexigenic neuronal pathways in the mediobasal hypothalamus. *Eur J Neurosci* **19,** 1524-1534.

Muroya S, Yada T, Shioda S & Takigawa M. (1999). Glucose-sensitive neurons in the rat arcuate nucleus contain neuropeptide Y. *Neuroscience letters* **264,** 113-116.

Nakamura T, Itadani H, Hidaka Y, Ohta M & Tanaka K. (2000). Molecular cloning and characterization of a new human histamine receptor, HH4R. *Biochem Biophys Res Commun* **279,** 615-620.

Nakamura T, Yoshimura M, Shinnick-Gallagher P, Gallagher JP & Akasu T. (1984). alpha 2 and alpha 1-Adrenoceptors mediate opposing actions on parasympathetic neurons. *Brain Res* **323,** 349-353.

Nakazato M, Murakami N, Date Y, Kojima M, Matsuo H, Kangawa K & Matsukura S. (2001). A role for ghrelin in the central regulation of feeding. *Nature* **409,** 194-198.

Neary NM, Goldstone AP & Bloom SR. (2004). Appetite regulation: from the gut to the hypothalamus. *Clin Endocrinol (Oxf)* **60,** 153-160.

Nguyen T, Shapiro DA, George SR, Setola V, Lee DK, Cheng R, Rauser L, Lee SP, Lynch KR, Roth BL & O'Dowd BF. (2001). Discovery of a novel member of the histamine receptor family. *Mol Pharmacol* **59,** 427-433.

Nicholas AP, Pieribone VA & Hokfelt T. (1993). Cellular localization of messenger RNA for beta-1 and beta-2 adrenergic receptors in rat brain: an in situ hybridization study. *Neuroscience* **56,** 1023-1039.

Nichols CG. (2006). KATP channels as molecular sensors of cellular metabolism. *Nature* **440,** 470-476.

Niswender KD, Gallis B, Blevins JE, Corson MA, Schwartz MW & Baskin DG. (2003). Immunocytochemical detection of phosphatidylinositol 3-kinase activation by insulin and leptin. *J Histochem Cytochem* **51,** 275-283.

Niswender KD & Schwartz MW. (2003). Insulin and leptin revisited: adiposity signals with overlapping physiological and intracellular signaling capabilities. *Front Neuroendocrinol* **24,** 1-10.

Oda T & Matsumoto S. (2001). [Identification and characterization of histamine H4 receptor]. *Nippon Yakurigaku Zasshi* **118,** 36-42.

Ookuma K, Sakata T & Fujimoto K. (1990). Evidence for feeding elicited through antihistaminergic effects of tricyclic antidepressants in the rat hypothalamus. *Psychopharmacology (Berl)* **101,** 481-485.

Ookuma K, Sakata T, Fukagawa K, Yoshimatsu H, Kurokawa M, Machidori H & Fujimoto K. (1993). Neuronal histamine in the hypothalamus suppresses food intake in rats. *Brain Res* **628,** 235-242.

Ookuma K, Yoshimatsu H, Sakata T, Fujimoto K & Fukagawa F. (1989). Hypothalamic sites of neuronal histamine action on food intake by rats. *Brain Res* **490,** 268-275.

Oomura Y, Kimura K, Ooyama H, Maeno T, Iki M & Kuniyoshi M. (1964). Reciprocal Activities of the Ventromedial and Lateral Hypothalamic Areas of Cats. *Science* **143,** 484-485.

Oomura Y, Ooyama H, Sugimori M, Nakamura T & Yamada Y. (1974). Glucose inhibition of the glucose-sensitive neurone in the rat lateral hypothalamus. *Nature* **247,** 284-286.

Orr E & Quay WB. (1975). Hypothalamic 24-hour rhythms in histamine, histidine, decarboxylase and histamine-N-methyltransferase. *Endocrinology* **96,** 941-945.

Owen OE, Morgan AP, Kemp HG, Sullivan JM, Herrera MG & Cahill GF, Jr. (1967). Brain metabolism during fasting. *J Clin Invest* **46,** 1589-1595.

Palacios JM, Wamsley JK & Kuhar MJ. (1981). The distribution of histamine H1-receptors in the rat brain: an autoradiographic study. *Neuroscience* **6,** 15-37.

Pan ZZ, Grudt TJ & Williams JT. (1994). Alpha 1-adrenoceptors in rat dorsal raphe neurons: regulation of two potassium conductances. *J Physiol* **478 Pt 3,** 437-447.

Panula P, Yang HY & Costa E. (1984). Histamine-containing neurons in the rat hypothalamus. *Proceedings of the National Academy of Sciences of the United States of America* **81,** 2572-2576.

Papay R, Gaivin R, Jha A, McCune DF, McGrath JC, Rodrigo MC, Simpson PC, Doze VA & Perez DM. (2006). Localization of the mouse alpha1A-adrenergic receptor (AR) in the brain: alpha1AAR is expressed in neurons, GABAergic interneurons, and NG2 oligodendrocyte progenitors. *The Journal of comparative neurology* **497,** 209-222.

Pape HC. (1996). Queer current and pacemaker: the hyperpolarization-activated cation current in neurons. *Annu Rev Physiol* **58,** 299-327.

Pape HC & McCormick DA. (1989). Noradrenaline and serotonin selectively modulate thalamic burst firing by enhancing a hyperpolarization-activated cation current. *Nature* **340,** 715-718.

Parsons ME & Ganellin CR. (2006). Histamine and its receptors. *Br J Pharmacol* **147 Suppl 1,** S127-135.

Parton LE, Ye CP, Coppari R, Enriori PJ, Choi B, Zhang CY, Xu C, Vianna CR, Balthasar N, Lee CE, Elmquist JK, Cowley MA, Lowell BB (2007). Gluocse sensing by POMC neurones regulates glucose homeostasis and is impaired in obesity. *Nature* Sep 13;449(7159):228-32

Pennartz CM, De Jeu MT, Geurtsen AM, Sluiter AA & Hermes ML. (1998). Electrophysiological and morphological heterogeneity of neurons in slices of rat suprachiasmatic nucleus. *J Physiol* **506 (Pt 3),** 775-793.

Perez DM, Piascik MT, Malik N, Gaivin R & Graham RM. (1994). Cloning, expression, and tissue distribution of the rat homolog of the bovine alpha 1C-adrenergic receptor provide evidence for its classification as the alpha 1A subtype. *Mol Pharmacol* **46,** 823-831.

Pessin JE & Bell GI. (1992). Mammalian facilitative glucose transporter family: structure and molecular regulation. *Annu Rev Physiol* **54,** 911-930.

Peyron C, Tighe DK, van den Pol AN, de Lecea L, Heller HC, Sutcliffe JG & Kilduff TS. (1998). Neurons containing hypocretin (orexin) project to multiple neuronal systems. *J Neurosci* **18,** 9996-10015.

Piascik MT & Perez DM. (2001). Alpha1-adrenergic receptors: new insights and directions. *J Pharmacol Exp Ther* **298,** 403-410.

Pinto S, Roseberry AG, Liu H, Diano S, Shanabrough M, Cai X, Friedman JM & Horvath TL. (2004). Rapid rewiring of arcuate nucleus feeding circuits by leptin. *Science* **304,** 110-115.

Pollard H, Bischoff S, Llorens-Cortes C & Schwartz JC. (1976). Histidine decarboxylase and histamine in discrete nuclei of rat hypothalamus and the evidence for mast-cells in the median eminence. *Brain Res* **118,** 509-513.

Qu D, Ludwig DS, Gammeltoft S, Piper M, Pelleymounter MA, Cullen MJ, Mathes WF, Przypek R, Kanarek R & Maratos-Flier E. (1996). A role for melanin-concentrating hormone in the central regulation of feeding behaviour. *Nature* **380,** 243-247.

Raffin-Sanson ML, de Keyzer Y & Bertagna X. (2003). Proopiomelanocortin, a polypeptide precursor with multiple functions: from physiology to pathological conditions. *Eur J Endocrinol* **149,** 79-90.

Rall W. (1962). Theory of physiological properties of dendrites. *Ann N Y Acad Sci* **96,** 1071-1092.

Ramon-Moliner E. (1967). [Morphologic differentiation of neurons]. *Archives italiennes de biologie* **105,** 149-188.

Reiner PB & Kamondi A. (1994). Mechanisms of antihistamine-induced sedation in the human brain: H1 receptor activation reduces a background leakage potassium current. *Neuroscience* **59,** 579-588.

Reyes TM, Lewis K, Perrin MH, Kunitake KS, Vaughan J, Arias CA, Hogenesch JB, Gulyas J, Rivier J, Vale WW & Sawchenko PE. (2001). Urocortin II: a member of the corticotropin-releasing factor (CRF) neuropeptide family that is selectively bound by type 2 CRF receptors. *Proceedings of the National Academy of Sciences of the United States of America* **98,** 2843-2848.

Rink TJ. (1994). Genetics. In search of a satiety factor. *Nature* **372,** 406-407.

Ritter S, Dinh TT & Li AJ. (2006). Hindbrain catecholamine neurons control multiple glucoregulatory responses. *Physiol Behav* **89,** 490-500.

Rogawski MA & Aghajanian GK. (1982). Activation of lateral geniculate neurons by locus coeruleus or dorsal noradrenergic bundle stimulation: selective blockade by the alpha 1-adrenoceptor antagonist prazosin. *Brain Res* **250,** 31-39.

Rolls ET. (1984). The neurophysiology of feeding. *Int J Obes* **8 Suppl 1,** 139-150.

Roseberry AG, Liu H, Jackson AC, Cai X & Friedman JM. (2004). Neuropeptide Y-mediated inhibition of proopiomelanocortin neurons in the arcuate nucleus shows enhanced desensitization in ob/ob mice. *Neuron* **41,** 711-722.

Roselli-Rehfuss L, Mountjoy KG, Robbins LS, Mortrud MT, Low MJ, Tatro JB, Entwistle ML, Simerly RB & Cone RD. (1993). Identification of a receptor for gamma melanotropin and other proopiomelanocortin peptides in the hypothalamus and limbic system. *Proceedings of the National Academy of Sciences of the United States of America* **90,** 8856-8860.

Rosin DL, Weston MC, Sevigny CP, Stornetta RL & Guyenet PG. (2003). Hypothalamic orexin (hypocretin) neurons express vesicular glutamate transporters VGLUT1 or VGLUT2. *The Journal of comparative neurology* **465,** 593-603.

Rossi M, Kim MS, Morgan DG, Small CJ, Edwards CM, Sunter D, Abusnana S, Goldstone AP, Russell SH, Stanley SA, Smith DM, Yagaloff K, Ghatei MA & Bloom SR. (1998). A C-terminal fragment of Agouti-related protein increases feeding and antagonizes the effect of alpha-melanocyte stimulating hormone in vivo. *Endocrinology* **139,** 4428-4431.

Rother E, Konner AC & Bruning JC. (2008). Neurocircuits integrating hormone and nutrient signaling in control of glucose metabolism. *Am J Physiol Endocrinol Metab* **294,** E810-816.

Rothwell NJ & Stock MJ. (1978). A paradox in the control of energy intake in the rat. *Nature* **273,** 146-147.

Routh VH. (2002). Glucose-sensing neurons: are they physiologically relevant? *Physiol Behav* **76,** 403-413.

Rowe IC, Treherne JM & Ashford ML. (1996). Activation by intracellular ATP of a potassium channel in neurones from rat basomedial hypothalamus. *J Physiol* **490 (Pt 1),** 97-113.

Rubio MA, Gargallo M, Isabel Millan A & Moreno B. (2007). Drugs in the treatment of obesity: sibutramine, orlistat and rimonabant. *Public Health Nutr* **10,** 1200-1205.

Rudy B. (1988). Diversity and ubiquity of K channels. *Neuroscience* **25,** 729-749.

Sadja R, Alagem N & Reuveny E. (2003). Gating of GIRK channels: details of an intricate, membrane-delimited signaling complex. *Neuron* **39,** 9-12.

Sahu A, Kalra SP, Crowley WR & Kalra PS. (1988). Evidence that NPY-containing neurons in the brainstem project into selected hypothalamic nuclei: implication in feeding behavior. *Brain Res* **457,** 376-378.

Sakaguchi T & Bray GA. (1987). The effect of intrahypothalamic injections of glucose on sympathetic efferent firing rate. *Brain Res Bull* **18,** 591-595.

Sakata T, Fukagawa K, Fujimoto K, Yoshimatsu H, Shiraishi T & Wada H. (1988a). Feeding induced by blockade of histamine H1-receptor in rat brain. *Experientia* **44,** 216-218.

Sakata T, Fukagawa K, Ookuma K, Fujimoto K, Yoshimatsu H, Yamatodani A & Wada H. (1988b). Modulation of neuronal histamine in control of food intake. *Physiol Behav* **44,** 539-543.

Sakata T, Fukagawa K, Ookuma K, Fujimoto K, Yoshimatsu H, Yamatodani A & Wada H. (1990). Hypothalamic neuronal histamine modulates ad libitum feeding by rats. *Brain Res* **537,** 303-306.

Sakata T, Ookuma K, Fujimoto K, Fukagawa K & Yoshimatsu H. (1991). Histaminergic control of energy balance in rats. *Brain Res Bull* **27,** 371-375.

Sakurai T. (2003). Orexin: a link between energy homeostasis and adaptive behaviour. *Curr Opin Clin Nutr Metab Care* **6,** 353-360.

Sakurai T, Amemiya A, Ishii M, Matsuzaki I, Chemelli RM, Tanaka H, Williams SC, Richarson JA, Kozlowski GP, Wilson S, Arch JR, Buckingham RE, Haynes AC, Carr SA, Annan RS, McNulty DE, Liu WS, Terrett JA, Elshourbagy NA, Bergsma DJ & Yanagisawa M. (1998). Orexins and orexin receptors: a family of hypothalamic neuropeptides and G protein-coupled receptors that regulate feeding behavior. *Cell* **92,** 1 page following 696.

Sawchenko PE. (1998). Toward a new neurobiology of energy balance, appetite, and obesity: the anatomists weigh in. *The Journal of comparative neurology* **402,** 435-441.

Sawchenko PE, Gold RM & Leibowitz SF. (1981). Evidence for vagal involvement in the eating elicited by adrenergic stimulation of the paraventricular nucleus. *Brain Res* **225,** 249-269.

Sawchenko PE & Swanson LW. (1981). Central noradrenergic pathways for the integration of hypothalamic neuroendocrine and autonomic responses. *Science* **214,** 685-687.

Scheibner J, Trendelenburg AU, Hein L & Starke K. (2001). Alpha2-adrenoceptors modulating neuronal serotonin release: a study in alpha2-adrenoceptor subtype-deficient mice. *Br J Pharmacol* **132,** 925-933.

Schlicker E, Betz R & Gothert M. (1988). Histamine H3 receptor-mediated inhibition of serotonin release in the rat brain cortex. *Naunyn-Schmiedeberg's archives of pharmacology* **337,** 588-590.

Schlicker E, Fink K, Hinterthaner M & Gothert M. (1989). Inhibition of noradrenaline release in the rat brain cortex via presynaptic H3 receptors. *Naunyn-Schmiedeberg's archives of pharmacology* **340,** 633-638.

Schwartz JC, Arrang JM, Garbarg M, Pollard H & Ruat M. (1991a). Histaminergic transmission in the mammalian brain. *Physiol Rev* **71,** 1-51.

Schwartz MW, Baskin DG, Kaiyala KJ & Woods SC. (1999). Model for the regulation of energy balance and adiposity by the central nervous system. *Am J Clin Nutr* **69,** 584-596.

Schwartz MW, Marks JL, Sipols AJ, Baskin DG, Woods SC, Kahn SE & Porte D, Jr. (1991b). Central insulin administration reduces neuropeptide Y mRNA expression in the arcuate nucleus of food-deprived lean (Fa/Fa) but not obese (fa/fa) Zucker rats. *Endocrinology* **128,** 2645-2647.

Schwartz MW, Sipols AJ, Marks JL, Sanacora G, White JD, Scheurink A, Kahn SE, Baskin DG, Woods SC, Figlewicz DP & et al. (1992). Inhibition of hypothalamic neuropeptide Y gene expression by insulin. *Endocrinology* **130,** 3608-3616.

Schwartz MW, Woods SC, Porte D, Jr., Seeley RJ & Baskin DG. (2000). Central nervous system control of food intake. *Nature* **404,** 661-671.

Segal M, Rogawski MA & Barker JL. (1984). A transient potassium conductance regulates the excitability of cultured hippocampal and spinal neurons. *J Neurosci* **4,** 604-609.

Shimada M, Tritos NA, Lowell BB, Flier JS & Maratos-Flier E. (1998). Mice lacking melanin-concentrating hormone are hypophagic and lean. *Nature* **396,** 670-674.

Shin N, Coates E, Murgolo NJ, Morse KL, Bayne M, Strader CD & Monsma FJ, Jr. (2002). Molecular modeling and site-specific mutagenesis of the histamine-binding site of the histamine H4 receptor. *Mol Pharmacol* **62,** 38-47.

Shintani M, Ogawa Y, Ebihara K, Aizawa-Abe M, Miyanaga F, Takaya K, Hayashi T, Inoue G, Hosoda K, Kojima M, Kangawa K & Nakao K. (2001). Ghrelin, an endogenous growth hormone secretagogue, is a novel orexigenic peptide that antagonizes leptin action through the activation of hypothalamic neuropeptide Y/Y1 receptor pathway. *Diabetes* **50,** 227-232.

Shyng S & Nichols CG. (1997). Octameric stoichiometry of the KATP channel complex. *J Gen Physiol* **110,** 655-664.

Silver IA & Erecinska M. (1994). Extracellular glucose concentration in mammalian brain: continuous monitoring of changes during increased neuronal activity and upon limitation in oxygen supply in normo-, hypo-, and hyperglycemic animals. *J Neurosci* **14,** 5068-5076.

Siviy SM, Kritikos A, Atrens DM & Shepherd A. (1989). Effects of norepinephrine infused in the paraventricular hypothalamus on energy expenditure in the rat. *Brain Res* **487,** 79-88.

Smith FJ, Campfield LA, Moschera JA, Bailon PS & Burn P. (1998). Brain administration of OB protein (leptin) inhibits neuropeptide-Y-induced feeding in ob/ob mice. *Regul Pept* **75-76,** 433-439.

Smythe GA, Grunstein HS, Bradshaw JE, Nicholson MV & Compton PJ. (1984). Relationships between brain noradrenergic activity and blood glucose. *Nature* **308,** 65-67.

Song Z, Levin BE, McArdle JJ, Bakhos N & Routh VH. (2001). Convergence of pre- and postsynaptic influences on glucosensing neurons in the ventromedial hypothalamic nucleus. *Diabetes* **50,** 2673-2681.

Spanswick D, Smith MA, Groppi VE, Logan SD & Ashford ML. (1997). Leptin inhibits hypothalamic neurons by activation of ATP-sensitive potassium channels. *Nature* **390,** 521-525.

Spanswick D, Smith MA, Mirshamsi S, Routh VH & Ashford ML. (2000). Insulin activates ATP-sensitive K+ channels in hypothalamic neurons of lean, but not obese rats. *Nature neuroscience* **3,** 757-758.

Spiegelman BM & Flier JS. (2001). Obesity and the regulation of energy balance. *Cell* **104,** 531-543.

Spreng M, Cotecchia S & Schenk F. (2001). A behavioral study of alpha-1b adrenergic receptor knockout mice: increased reaction to novelty and selectively reduced learning capacities. *Neurobiol Learn Mem* **75,** 214-229.

Stanley BG, Daniel DR, Chin AS & Leibowitz SF. (1985). Paraventricular nucleus injections of peptide YY and neuropeptide Y preferentially enhance carbohydrate ingestion. *Peptides* **6,** 1205-1211.

Stanley BG, Kyrkouli SE, Lampert S & Leibowitz SF. (1986). Neuropeptide Y chronically injected into the hypothalamus: a powerful neurochemical inducer of hyperphagia and obesity. *Peptides* **7,** 1189-1192.

Stanley BG, Magdalin W, Seirafi A, Thomas WJ & Leibowitz SF. (1993). The perifornical area: the major focus of (a) patchily distributed hypothalamic neuropeptide Y-sensitive feeding system(s). *Brain Res* **604,** 304-317.

Stanley BG, Schwartz DH, Hernandez L, Hoebel BG & Leibowitz SF. (1989). Patterns of extracellular norepinephrine in the paraventricular hypothalamus: relationship to circadian rhythm and deprivation-induced eating behavior. *Life Sci* **45,** 275-282.

Stanley S, Wynne K, McGowan B & Bloom S. (2005). Hormonal regulation of food intake. *Physiol Rev* **85,** 1131-1158.

Steffens AB, Scheurink AJ, Luiten PG & Bohus B. (1988). Hypothalamic food intake regulating areas are involved in the homeostasis of blood glucose and plasma FFA levels. *Physiol Behav* **44,** 581-589.

Stehle J. (1991). Effects of histamine on spontaneous electrical activity of neurons in rat suprachiasmatic nucleus. *Neuroscience letters* **130,** 217-220.

Stern JE. (2001). Electrophysiological and morphological properties of pre-autonomic neurones in the rat hypothalamic paraventricular nucleus. *J Physiol* **537,** 161-177.

Sternson SM, Shepherd GM & Friedman JM. (2005). Topographic mapping of VMH --> arcuate nucleus microcircuits and their reorganization by fasting. *Nature neuroscience* **8,** 1356-1363.

Svensson TH. (1984). Central alpha-adrenoceptors and the mechanisms of action of antidepressant drugs. *Adv Biochem Psychopharmacol* **39,** 241-248.

Svensson TH. (1987). Peripheral, autonomic regulation of locus coeruleus noradrenergic neurons in brain: putative implications for psychiatry and psychopharmacology. *Psychopharmacology (Berl)* **92,** 1-7.

Swanson LW & Sawchenko PE. (1980). Paraventricular nucleus: a site for the integration of neuroendocrine and autonomic mechanisms. *Neuroendocrinology* **31,** 410-417.

Swanson LW & Sawchenko PE. (1983). Hypothalamic integration: organization of the paraventricular and supraoptic nuclei. *Annu Rev Neurosci* **6,** 269-324.

Szafarczyk A, Alonso G, Ixart G, Malaval F & Assenmacher I. (1985). Diurnal-stimulated and stress-induced ACTH release in rats is mediated by ventral noradrenergic bundle. *Am J Physiol* **249,** E219-226.

Taheri S, Zeitzer JM & Mignot E. (2002). The role of hypocretins (orexins) in sleep regulation and narcolepsy. *Annu Rev Neurosci* **25,** 283-313.

Takahashi K, Suwa H, Ishikawa T & Kotani H. (2002). Targeted disruption of H3 receptors results in changes in brain histamine tone leading to an obese phenotype. *J Clin Invest* **110,** 1791-1799.

Takashima A & Takahata M. (2008). Effects of active conductance distribution over dendrites on the synaptic integration in an identified nonspiking interneuron. *PLoS ONE* **3,** e2217.

Takeshita Y, Watanabe T, Sakata T, Munakata M, Ishibashi H & Akaike N. (1998). Histamine modulates high-voltage-activated calcium channels in neurons dissociated from the rat tuberomammillary nucleus. *Neuroscience* **87,** 797-805.

Tanoue A, Koshimizu TA & Tsujimoto G. (2002). Transgenic studies of alpha(1)-adrenergic receptor subtype function. *Life Sci* **71,** 2207-2215.

Tartaglia LA, Dembski M, Weng X, Deng N, Culpepper J, Devos R, Richards GJ, Campfield LA, Clark FT, Deeds J, Muir C, Sanker S, Moriarty A, Moore KJ, Smutko JS, Mays GG, Wool EA, Monroe CA & Tepper RI. (1995). Identification and expression cloning of a leptin receptor, OB-R. *Cell* **83,** 1263-1271.

Tasker JG & Dudek FE. (1991). Electrophysiological properties of neurones in the region of the paraventricular nucleus in slices of rat hypothalamus. *J Physiol* **434,** 271-293.

Tebbe JJ, Mronga S, Schafer MK, Ruter J, Kobelt P & Monnikes H. (2003). Stimulation of neurons in rat ARC inhibits gastric acid secretion via hypothalamic CRF1/2- and NPY-Y1 receptors. *Am J Physiol Gastrointest Liver Physiol* **285,** G1075-1083.

Teuscher C, Subramanian M, Noubade R, Gao JF, Offner H, Zachary JF & Blankenhorn EP. (2007). Central histamine H3 receptor signaling negatively regulates susceptibility to autoimmune inflammatory disease of the CNS. *Proceedings of the National Academy of Sciences of the United States of America* **104,** 10146-10151.

Thomzig A, Laube G, Pruss H & Veh RW. (2005). Pore-forming subunits of K-ATP channels, Kir6.1 and Kir6.2, display prominent differences in regional and cellular distribution in the rat brain. *The Journal of comparative neurology* **484,** 313-330.

Toftegaard CL, Knigge U, Kjaer A & Warberg J. (2003). The role of hypothalamic histamine in leptin-induced suppression of short-term food intake in fasted rats. *Regul Pept* **111,** 83-90.

Tokita S, Takahashi K & Kotani H. (2006). Recent advances in molecular pharmacology of the histamine systems: physiology and pharmacology of histamine H3 receptor: roles in feeding regulation and therapeutic potential for metabolic disorders. *Journal of pharmacological sciences* **101,** 12-18.

Toth ZE & Palkovits M. (1998). Distributions of periventricular projections of the paraventricular nucleus to the median eminence and arcuate nucleus. *Brain Res* **802,** 294-297.

Trapp S, Tucker SJ & Ashcroft FM. (1997). Activation and inhibition of K-ATP currents by guanine nucleotides is mediated by different channel subunits. *Proceedings of the National Academy of Sciences of the United States of America* **94,** 8872-8877.

Tschop M, Smiley DL & Heiman ML. (2000). Ghrelin induces adiposity in rodents. *Nature* **407,** 908-913.

Turner P. (1984). Beta-blocking drugs in migraine. *Postgrad Med J* **60 Suppl 2,** 51-55.

Unnerstall JR, Kopajtic TA & Kuhar MJ. (1984). Distribution of alpha 2 agonist binding sites in the rat and human central nervous system: analysis of some functional, anatomic correlates of the pharmacologic effects of clonidine and related adrenergic agents. *Brain Res* **319,** 69-101.

U'Prichard DC & Snyder SH. (1979). Distinct alpha-noradrenergic receptors differentiated by binding and physiological relationships. *Life Sci* **24,** 79-88.

van den Pol AN & Cassidy JR. (1982). The hypothalamic arcuate nucleus of rat--a quantitative Golgi analysis. *The Journal of comparative neurology* **204,** 65-98.

van den Top M. (2002). Neuropeptide and hormonal signalling in mammalian central autonomic neurones. University of Warwick, Coventry.

van den Top M, Lee K, Whyment AD, Blanks AM & Spanswick D. (2004). Orexigen-sensitive NPY/AgRP pacemaker neurons in the hypothalamic arcuate nucleus. *Nature neuroscience* **7,** 493-494.

van den Top M, Lyons DJ, Lee K, Coderre E, Renaud LP & Spanswick D. (2007). Pharmacological and molecular characterization of ATP-sensitive K(+) conductances in CART and NPY/AgRP expressing neurons of the hypothalamic arcuate nucleus. *Neuroscience* **144,** 815-824.

van den Top M & Spanswick D. (2006). Integration of metabolic stimuli in the hypothalamic arcuate nucleus. *Prog Brain Res* **153,** 141-154.

van Houten M, Posner BI, Kopriwa BM & Brawer JR. (1980). Insulin binding sites localized to nerve terminals in rat median eminence and arcuate nucleus. *Science* **207,** 1081-1083.

van Welie I, Remme MW, van Hooft JA & Wadman WJ. (2006). Different levels of Ih determine distinct temporal integration in bursting and regular-spiking neurons in rat subiculum. *J Physiol* **576,** 203-214.

Velumian AA, Zhang L, Pennefather P & Carlen PL. (1997). Reversible inhibition of IK, IAHP, Ih and ICa currents by internally applied gluconate in rat hippocampal pyramidal neurones. *Pflugers Arch* **433,** 343-350.

Voigt MM, Kispert J & Chin HM. (1990). Sequence of a rat brain cDNA encoding an alpha-1B adrenergic receptor. *Nucleic Acids Res* **18,** 1053.

Wada H, Inagaki N, Itowi N & Yamatodani A. (1991). Histaminergic neuron system in the brain: distribution and possible functions. *Brain Res Bull* **27,** 367-370.

Wada H, Inagaki N, Itowi N & Yamatodani A. (1991). Histaminergic neuron system: morphological features and possible functions. *Agents and actions* **33,** 11-27.

Wang L, Saint-Pierre DH & Tache Y. (2002). Peripheral ghrelin selectively increases Fos expression in neuropeptide Y - synthesizing neurons in mouse hypothalamic arcuate nucleus. *Neuroscience letters* **325,** 47-51.

Wang R, Liu X, Hentges ST, Dunn-Meynell AA, Levin BE, Wang W & Routh VH. (2004). The regulation of glucose-excited neurons in the hypothalamic arcuate nucleus by glucose and feeding-relevant peptides. *Diabetes* **53,** 1959-1965.

Wang YF, Shibuya I, Kabashima N, Setiadji VS, Isse T, Ueta Y & Yamashita H. (1998). Inhibition of spontaneous inhibitory postsynaptic currents (IPSC) by noradrenaline in rat supraoptic neurons through presynaptic alpha2-adrenoceptors. *Brain Res* **807,** 61-69.

Watanabe T, Taguchi Y, Shiosaka S, Tanaka J, Kubota H, Terano Y, Tohyama M & Wada H. (1984). Distribution of the histaminergic neuron system in the central nervous system of rats; a fluorescent immunohistochemical analysis with histidine decarboxylase as a marker. *Brain Res* **295,** 13-25.

Watson SJ & Akil H. (1979). The presence of two alpha-MSH positive cell groups in rat hypothalamus. *European journal of pharmacology* **58,** 101-103.

Wellman PJ. (2000). Norepinephrine and the control of food intake. *Nutrition* **16,** 837-842.

Wellman PJ, Davies BT, Morien A & McMahon L. (1993). Modulation of feeding by hypothalamic paraventricular nucleus alpha 1- and alpha 2-adrenergic receptors. *Life Sci* **53,** 669-679.

Whyment AD, Blanks AM, Lee K, Renaud LP & Spanswick D. (2006). Histamine excites neonatal rat sympathetic preganglionic neurons in vitro via activation of H1 receptors. *J Neurophysiol* **95,** 2492-2500.

Whyment AD, Wilson JM, Renaud LP & Spanswick D. (2004). Activation and integration of bilateral GABA-mediated synaptic inputs in neonatal rat sympathetic preganglionic neurones in vitro. *J Physiol* **555,** 189-203.

Willesen MG, Kristensen P & Romer J. (1999). Co-localization of growth hormone secretagogue receptor and NPY mRNA in the arcuate nucleus of the rat. *Neuroendocrinology* **70,** 306-316.

Williams G, Bing C, Cai XJ, Harrold JA, King PJ & Liu XH. (2001). The hypothalamus and the control of energy homeostasis: different circuits, different purposes. *Physiol Behav* **74,** 683-701.

Williams G, Harrold JA & Cutler DJ. (2000). The hypothalamus and the regulation of energy homeostasis: lifting the lid on a black box. *Proc Nutr Soc* **59,** 385-396.

Willie JT, Chemelli RM, Sinton CM & Yanagisawa M. (2001). To eat or to sleep? Orexin in the regulation of feeding and wakefulness. *Annu Rev Neurosci* **24,** 429-458.

Wilson JM, Coderre E, Renaud LP & Spanswick D. (2002). Active and passive membrane properties of rat sympathetic preganglionic neurones innervating the adrenal medulla. *J Physiol* **545,** 945-960.

Woods SC, Decke E & Vasselli JR. (1974). Metabolic hormones and regulation of body weight. *Psychol Rev* **81,** 26-43.

Wren AM, Seal LJ, Cohen MA, Brynes AE, Frost GS, Murphy KG, Dhillo WS, Ghatei MA & Bloom SR. (2001a). Ghrelin enhances appetite and increases food intake in humans. *J Clin Endocrinol Metab* **86,** 5992.

Wren AM, Small CJ, Abbott CR, Dhillo WS, Seal LJ, Cohen MA, Batterham RL, Taheri S, Stanley SA, Ghatei MA & Bloom SR. (2001b). Ghrelin causes hyperphagia and obesity in rats. *Diabetes* **50,** 2540-2547.

Yamanaka A, Beuckmann CT, Willie JT, Hara J, Tsujino N, Mieda M, Tominaga M, Yagami K, Sugiyama F, Goto K, Yanagisawa M & Sakurai T. (2003). Hypothalamic orexin neurons regulate arousal according to energy balance in mice. *Neuron* **38,** 701-713.

Yamanaka A, Muraki Y, Ichiki K, Tsujino N, Kilduff TS, Goto K & Sakurai T. (2006). Orexin neurons are directly and indirectly regulated by catecholamines in a complex manner. *J Neurophysiol* **96,** 284-298.

Yanai K & Tashiro M. (2007). The physiological and pathophysiological roles of neuronal histamine: an insight from human positron emission tomography studies. *Pharmacology & therapeutics* **113,** 1-15.

Yang XJ, Kow LM, Funabashi T & Mobbs CV. (1999). Hypothalamic glucose sensor: similarities to and differences from pancreatic beta-cell mechanisms. *Diabetes* **48,** 1763-1772.

Yang XJ, Mastaitis J, Mizuno T & Mobbs CV. (2007). Glucokinase regulates reproductive function, glucocorticoid secretion, food intake, and hypothalamic gene expression. *Endocrinology* **148,** 1928-1932.

Yeo GS, Farooqi IS, Aminian S, Halsall DJ, Stanhope RG & O'Rahilly S. (1998). A frameshift mutation in MC4R associated with dominantly inherited human obesity. *Nature genetics* **20,** 111-112.

Yoshimatsu H. (2006). The neuronal histamine H(1) and pro-opiomelanocortin-melanocortin 4 receptors: independent regulation of food intake and energy expenditure. *Peptides* **27,** 326-332.

Young WS, 3rd & Kuhar MJ. (1979). Noradrenergic alpha 1 and alpha 2 receptors: autoradiographic visualization. *European journal of pharmacology* **59,** 317-319.

Young WS, 3rd & Kuhar MJ. (1980). Noradrenergic alpha 1 and alpha 2 receptors: light microscopic autoradiographic localization. *Proceedings of the National Academy of Sciences of the United States of America* **77,** 1696-1700.

Zhang Y, Proenca R, Maffei M, Barone M, Leopold L & Friedman JM. (1994). Positional cloning of the mouse obese gene and its human homologue. *Nature* **372,** 425-432.

Zhong H & Minneman KP. (1999). Alpha1-adrenoceptor subtypes. *European journal of pharmacology* **375,** 261-276.

Zigman JM, Jones JE, Lee CE, Saper CB & Elmquist JK. (2006). Expression of ghrelin receptor mRNA in the rat and the mouse brain. *The Journal of comparative neurology* **494,** 528-548.